Model Based Analysis of the Operation and Control of Falling Film Evaporators

James Winchester
September, 2000

A Thesis presented for the Degree of Doctor of Philosophy
in Technology and Engineering.

Massey University.
Palmerston North, New Zealand.

Summary

Falling film evaporators are a widely used process in the New Zealand dairy industry. They are well suited for the removal of water and are most commonly used as the first stage of the milk powder production process. In New Zealand milk powders are a major export product, so the falling film evaporator is an important part of the Dairy industry. However, there appears to be very little understanding of the design, operation and control of falling film evaporators. The work discussed in this thesis aims to overcome this problem.

This work will derive, develop and analyse a model of the Evaporator A plant at Kiwi Co-op Dairies Ltd. The purpose of developing the evaporator model is to analyse the optimisation and controllability of the plant. A steady state model for the plant will be developed specifically for the optimisation studies and a linear dynamic model for the controllability studies.

The production of milk powders is a two stage process. Falling film evaporators are used to remove approximately 80 % of the water contained in the milk. This produces a highly viscous milk concentrate that cannot be further concentrated using evaporators. The remaining water is removed using spray dryers, which can be operated to produce special powder properties. The powder is easy to transport and relatively free from potential bacterial attack.

Evaporation is an energy intensive process and it is advantageous to minimise its energy requirements. This is the aim of the evaporator optimisation studies. Falling film evaporators are more energy efficient than spray dryers and many evaporator plants also use two stages, with different energy efficiencies. So, the total evaporation cost depends on the process operating conditions. However, there are various operating constraints, which restrict the evaporator capacities. These constraints will be determined and used to develop the constrained optimisation method.

In this thesis the optimum operating conditions for the Kiwi Evaporator A plant, working with Whole Milk, are determined. The optimisation problem is two dimensional, for the TVR compressor steam pressure and the TVR evaporator section product mass flow. Various other process variables, such as the DSI temperature and the TVR product dry mass fraction also have optimum values. These are discussed in the thesis also.

There are also many operational problems with industrial falling film evaporator plants. For example the preheat sections of industrial plants can often suffer de-aeration problems, boiling in holding tubes and flash vessel flooding problems. These problems will be investigated and simple solutions determined.

In the Dairy industry evaporators have to operate under a vacuum, since the milk proteins become de-natured when heated above 70 °C. This means that a small hole in the evaporator, or preheat section, will allow non-condensable gases to leak into the process. In addition milk, itself, often contains dissolved gases that evaporate out of the milk, when it flashes in the preheat

section. It is shown, in this thesis, that the presence of non-condensable gases causes a temperature difference to occur between the top and bottom of the flash vessels. The de-aeration lines from the flash vessels must have correctly sized orifice plates, so that the gases are removed.

It is possible for milk to evaporate in the preheat section holding tubes. In is shown to cause a number of problems, such as flash vessel flooding, that are detrimental to the preheat section operation. The milk pressure must not fall below its vapour pressure. It is shown that correct sizing of the preheat section DSI pump and holding tube orifice plate is essential.

The controllability of falling film evaporators is very important. There are several reasons why the production of milk powder can be difficult to control. A linear dynamic model for the evaporator plant will be developed and used to determine why falling film evaporators are difficult to control. The purpose of this work is to understand the fundamental controllability problems with the plant. Currently, there does not appear to be any fundamental understanding of why falling film evaporators are difficult to control.

The results of the controllability analysis show that the temperature control loops of the evaporator plants at Kiwi is satisfactory. A problem was found with the DSI temperature control loop, due to the need to measure the milk temperature after the holding tubes. This caused a significant delay that meant the controller could not provide adequate disturbance rejection. However, a solution to the problem was developed, where a surface temperature probe was used directly after the DSI, with a cascade control loop.

The most serious control problem was the product dry mass fraction control loop. The evaporator is designed to overcome the film wetting criteria, while simultaneously operating with the maximum energy efficiency and minimum residence time. These design aims mean there is little mixing in the process and a large pseudo-delay that occurs in the dry mass fraction control loop. Both these problems mean the controller cannot provide adequate disturbance rejection for the product dry mass fraction control loop.

Ackowledgements

The people who deserve the most acknowledgement are my project supervisors, Clive Marsh and Huub Bakker. Without Clive's patience and committed attitude this project would never have succeeded. Particularly when the mathematical problems were becoming seriously complicated, Clive was always prepared to help. I have learnt the importance of simplicity, but it was something Clive understood all along.

A great deal of thanks must also go to Hong Chen, of Kiwi Co-op Dairies. Hong provided very important help at Kiwi with the many problems that occurred. There were many difficulties and it sometimes seemed impossible to make any progress. However, Hong was always very helpful and friendly. I am also very grateful for the bed that he loaned me, during my time at Hawera.

The work of Maria Brenmuhl and Shane Goodwin was also very important. Shane did all the important computer programming for the Evaporator A simulator. Shane had to cope with my seemingly infinite changes in the Simulink model. However, none of these rather absurd changes seemed to make him upset. Maria did all the important process optimisation work. The optimisation work was often frustrating, but Maria coped excellently with the difficulties.

The Powder 3, 4 and 5 plant operators provided a great deal of useful help. Whenever small experiments were required, or help with plant and operational procedures, the operators were always friendly and helpful. Embarrassingly, I often caused additional problems for the operators, but thankfully they never got upset about these.

Contents

Chapter 1 : Introduction

1.1) Introduction and Aims

Falling film evaporators are commonly used in the New Zealand dairy industry for the production of milk powders. Milk powder is not susceptible to bacterial damage and it is easy to transport, whereas milk itself has neither of these characteristics. As a result milk powders are an ideal export product for the New Zealand Dairy industry. However, despite their large amount of industrial use, there is a shortage of knowledge on the design, operation and control of falling film evaporators. The work discussed in this thesis was initiated with the aim of improving this situation. The aims of this work are split into three broad areas.

Develop Model

A first principles model for the Evaporator A plant at Kiwi Co-op Dairies will be developed from the Laws of Thermodynamics. The model is dynamic and includes the evaporator preheat sections. We will concentrate on developing the model for the subsequent analysis of the Evaporator A plant. Specifically, a steady state model will be developed for the optimisation/operation studies and a linear dynamic model for the controllability studies.

Optimisation Studies

Using the steady state model the operation/optimisation of the Evaporator A plant will be investigated. There are some simple aspects of the evaporator and preheat sections that will be discussed. However, an important aspect will be the evaporator operational optimisation with respect to energy costs, fouling, throughput and milk powder quality.

Controllability Studies

Using the dynamic model we will investigate the control of the evaporator plant. The dynamic model derived from first principles will be linearised to produce a linear constant coefficient dynamic model. This can be analysed using the standard traditional and some advanced control methods. Specifically we will be interested in disturbance rejection.

In this Chapter we discuss the motivation for these studies. We will firstly, in Section 1.2, describe a generic falling film evaporator and discuss the important reasons for their use in the Dairy industry. There are many reasons for using falling film evaporators but the two most important reasons are their suitability for dealing with heat sensitive foods and the high energy efficiencies of modern evaporators. We shall also discuss, in Section 1.2, the composition and some important reactions of milk solutions.

Following the discussion of the important characteristics of falling film evaporators, we will investigate the basic mass balances of the process. These mass balances explain some important characteristics of industrial falling film evaporators. The predominately linear nature of falling film evaporators and their sensitivity to feed dry matter disturbances will both be discussed.

These have important consequences for the controllability of falling film evaporators and provide a motivation for studying their controllability.

The evaporation of water is a very energy intensive process. In Section 1.3, we will discuss the energy use of falling film evaporators and explain the high energy efficiencies of modern falling film evaporator designs. The important difference in the energy efficiencies of falling film evaporators and spray dryers will be discussed. Falling film evaporators are more energy efficient than spray dryers and so their evaporation capacities must be maximised. This provides a strong motivation for the optimisation studies and also the controllability studies.

Finally, in Section 1.4, we will briefly describe the Evaporator A plant at Kiwi Dairy Co-operatives.

1.2) What is a Falling Film Evaporator and Why are They Used?

1.2.1) What is an Evaporator?

Evaporation is the process of turning a liquid into a vapour. With milk solutions, which we will be dealing with, the solute particles have very large molecular masses which cause them to have very high boiling temperatures. Consequently when evaporation is applied to milk solutions effectively only the water is evaporated. As a result evaporation is used in the dairy industry as a water removal/solute concentration process.

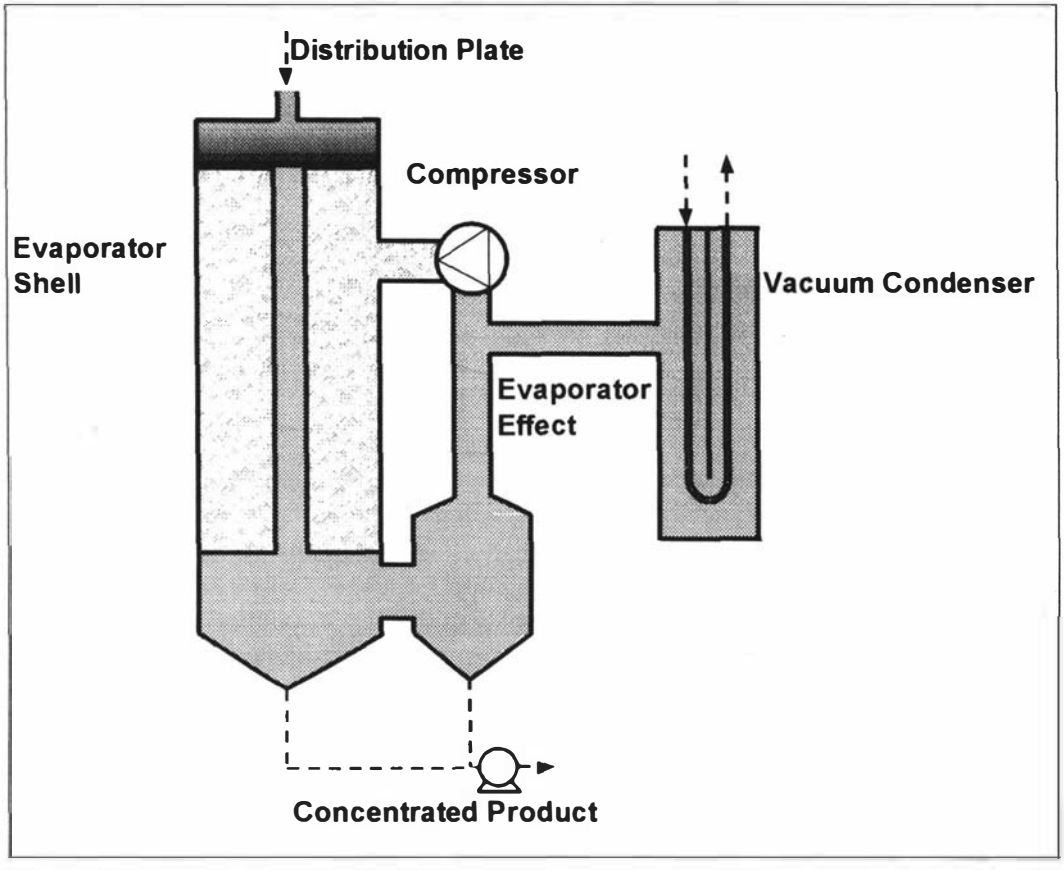

Figure 1-1 : A typical falling film evaporator.

The removal of water from milk solutions is important to the New Zealand Dairy industry. A large amount of New Zealand milk is exported and it is important that the transport costs and bacterial growth are minimised. Milk contains 90 % water and the complete removal of this significantly reduces the cost of transporting the milk. However, the complete removal of water is more important for the minimisation of bacteria growth. Bacteria do not grow in a 'moisture free' environment and so the shelf life of the milk can be considerably extended by completely removing the water.

Figure 1-1 shows a typical falling film evaporator. The milk enters at the distribution plate and is evenly distributed onto the falling film evaporator tubes. Then the milk forms a thin film on the inside of the evaporator tubes and flows downwards by gravitation. Water is evaporated from the milk due to the heat flow from the evaporator shell. This concentrates the milk before it falls from the evaporator tubes and is collected at the bottom of the evaporator. A compressor is used to compress the evaporated water vapour and give it a higher temperature/pressure. This higher temperature then provides the driving force for the evaporation heat flow, which is the basis for the whole process.

1.2.2) What is Milk?

Basic raw Whole Milk is a mixture of water and dissolved solute particles. Table 1-1 lists the components of raw Whole Milk and Skim Milk along with their typical compositions. The protein in milk exists in two forms, most of which (i.e., approximately 80 %) is casein protein whereas the remaining exists as whey protein. The fat component of milk consists of the typical fatty acids arranged into a tri-glycerol arrangement. These components and the lactose/mineral salts have been well studied and there is a large amount of literature discussing their chemical and physical properties (Kessler, 1981; Walstra and Jenness, 1984).

Table 1-1 : Approximate Whole and Skim Milk compositions.

Component	Whole Milk Composition (%)	Skim Milk Composition (%)
Water	87.5	91
Protein	3	3
Fat	4	0
Lactose	4	4
Salts	1	1

A very important characteristic of milk is the reactivity of the whey proteins at temperatures above 70 °C (Dannenberg and Kessler, 1988). In practice it is found that these whey protein reactions can cause significant fouling when evaporators are operated at temperatures above 70 °C (Kessler, 1987; Geordiadis *et al*, 1998; Schwartzberg, 1989). Consequently it is important that evaporators operate at temperatures below 70 °C. The vacuum condenser shown in Figure 1-1 is used to control the temperature of the evaporator.

Another important characteristic of milk is its viscosity. It is found that the viscosity increases dramatically as milk is concentrated (Snoeren *et al*, 1982). This is caused by the large size of the milk dry matter components. In practice the milk viscosity is approximately an exponential function of the milk dry matter. This characteristic of milk is important for the production of

milk powder, because it is found that the milk powder quality depends on the dryer feed viscosity.

1.2.3) The Industrial Production of Milk Powder

The industrial production of milk powder is a two stage process, as shown in Figure 1-2. Falling film evaporators are used to concentrate the milk solution to a critical dry matter concentration. Then a spray dryer evaporates the remaining water from the milk. There are several advantages in using this two stage production process. Firstly the falling film evaporators have considerably higher energy efficiencies than dryers and therefore the two stage process minimises the energy costs. Secondly the spray dryer milk powder product properties depend on the dryer feed viscosity. A comparatively narrow viscosity range is allowed and the two stage process allows resonable control of the viscosity. Finally the evaporator allows incorporation of various milk heat treatments, which are important for specific powder functional properties.

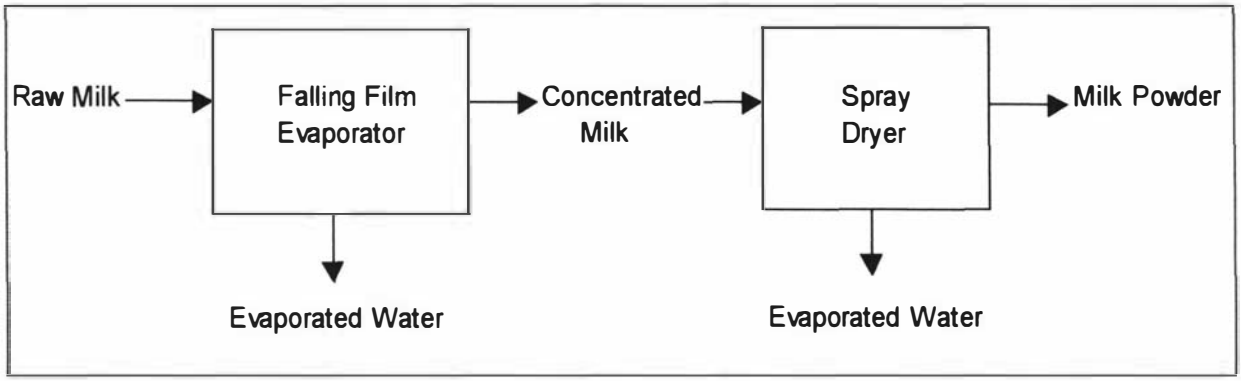

Figure 1-2 : The industrial production of milk powder.

1.2.4) Advantages of Falling Film Evaporators

Falling film evaporators are commonly used in the dairy industry because they can handle heat sensitive food solutions and their modern designs are very energy efficient. Falling film evaporators have the following important characteristics (Angeletti and Moresi, 1983).

1) Relatively short residence times.
2) Narrow range of residence times.
3) High heat transfer coefficients.
4) Minimum loss of temperature difference.

The short residence times of falling film evaporators are due to their thin falling films. These have relatively high fluid velocities and consequently the residence time of the milk in the evaporator can be quite short. However, modern falling film evaporators may not necessarily have short residence times because of the need to operate with large feed flows whilst maintaining stable falling films. This usually requires evaporator designs with multiple passes and very long evaporator tubes. Consequently the residence times can be comparatively large.

The narrow range of residence times in falling film evaporators is due to the small amount of mixing that occurs in the process. The distribution plates are designed to operate with small heights of liquid, the pipes between passes are designed for turbulent flow and the falling films

are thin with comparatively high velocities. As a result, the range of residences times is narrow. This is very important for milk solutions, which contain components that can become damaged if exposed to excessive heat.

The evaporating heat transfer coefficients of falling film evaporators are high because of the thin falling film. From heat transfer theory we know that the heat transfer coefficient depends on the thickness and the thermal conductivity heat transfer layer (i.e., $h \approx \frac{k}{\delta}$). With milk solutions the thermal conductivity depends on the dry matter concentration, temperature and composition, which are all essentially constant. However, the thickness of the heat transfer layer is relatively small for a falling film evaporator and so the heat transfer coefficients are high.

With a falling film evaporator the evaporating heat transfer temperature difference only needs to overcome the boiling point elevation, which is small for most milk solutions. Consequently falling film evaporators working with milk solutions can operate with temperature differences as small as 2 °C. We will show later that with an MVR compressor this allows the evaporator energy efficiency to be very high. This is the major advantage of modern industrial falling film evaporators.

Falling film evaporators have the disadvantage of being susceptible to fouling. This fouling is caused by the following characteristics of falling film evaporators.
1) Falling film breakdown.
2) Low falling film shear stresses

A major disadvantage of falling film evaporators is the potential instability of the falling film. At low mass flows the film will not completely cover the evaporator tubes and will instead flow in rivulets down the tubes. This phenomena is called by a variety of names (film breakdown, inadequate wetting) but the basic result is usually fouling of the tubes.

A second difficulty with the falling film evaporator is the relatively small shear forces that act on the film. These shear forces are induced by gravitation and they are comparatively small. Consequently any foulant particles can easily become attached to the evaporator tubes. Larger shear forces can be induced by using centrifugal falling film evaporators (Bouman and Waalewijn, 1994). However, the capital and operational costs of using industrial centrifugal evaporators is large.

1.2.5) Basic Evaporator Mass Balances

As mentioned above milk evaporation is a water removal process. For a continuous system this is represented by the following static equations.

$$M_p = M_f - M_{evap} \tag{1.1}$$

$$w_p = \frac{M_f . w_f}{\left[M_f - M_{evap}\right]} \tag{1.2}$$

Where, M_f	=	mass flow of liquid milk entering the evaporator.	(kg/s)
M_p	=	mass flow of liquid milk exiting the evaporator.	(kg/s)
w_f	=	dry mass fraction of milk entering the evaporator.	(kg/kg)
w_p	=	dry mass fraction of milk exiting the evaporator.	(kg/kg)
M_{evap}	=	mass flow of water evaporation in the evaporator.	(kg/s)

The first of these equations is linear but the second contains an important non-linearity. Figure 1-3 shows the resulting dry matter concentration in terms of the mass flow of evaporation. These results were determined by using a feed dry matter of 0.125 kg/kg and a feed mass flow of 15.3 kg/s. The results clearly show the non-linear nature of the evaporation process. However, it is interesting to note that the non-linearity only becomes excessive at high dry matter concentrations.

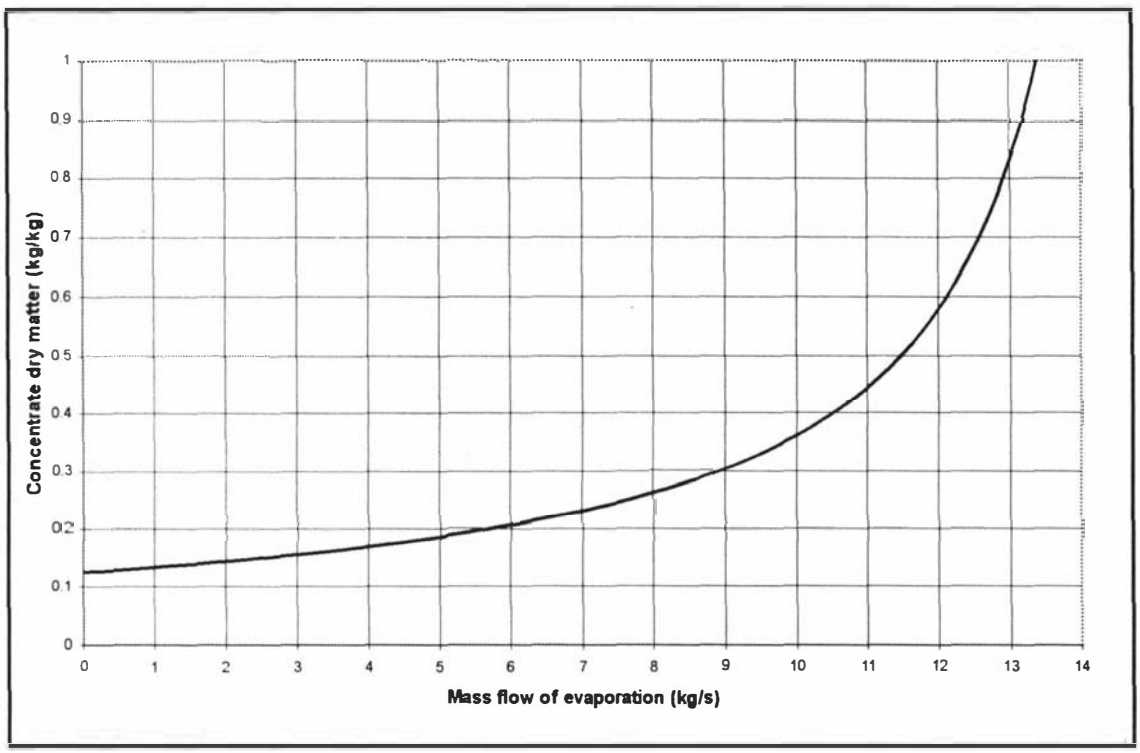

Figure 1-3 : Concentrated milk solution dry matter vs mass flow of evaporated water.

The effect of feed dry matter disturbances on the product dry matter is also very important. If we consider deviations in the feed dry matter we can produce equation (1.3) for the deviations in product dry matter. This shows that the evaporator amplifies variations in the feed dry matter and when the amount of evaporation is large then the amplification can be very significant. A typical Whole Milk falling film evaporator will have a concentration ratio of between 4 and 5. This means that a feed dry matter disturbance of 0.01 kg/kg will be amplified and cause a variation in the product dry matter of between 0.04 and 0.05 kg/kg.

$$\Delta w_p = \frac{M_f^0}{\left[M_f^0 - M_{evap}^0\right]} \Delta w_f \qquad (1.3)$$

Where, M_f^0	=	mass flow of liquid milk to the evaporator at steady state.	(kg/s)
M_{evap}^0	=	mass flow of evaporation in the evaporator at steady state.	(kg/s)
Δw_p	=	change in the evaporator product dry mass fraction.	(kg/kg)
Δw_f	=	change in evaporator feed dry matter.	(kg/kg)

The sensitivity of the evaporator process to feed dry matter disturbances suggests that process control may be required. We have already mentioned the importance of the evaporator product viscosity on the spray dryer milk powder quality. Clearly it is important that the concentrate viscosity is closely controlled, so that the milk powder quality is maintained. This is obviously achieved by controlling the dry matter of the evaporator product. When we also consider the sensitivity of the process to dry matter disturbances, then the need for control becomes much clearer.

1.3) Energy Costs of Falling Film Evaporators

1.3.1) Energy Efficiency of an Evaporator

The energy required to evaporate water is relatively large due to its high latent heat of vaporisation. The latent heat is lower at higher temperatures, so strictly the energy required to evaporate water can be reduced by operating at high temperatures. However, milk cannot be evaporated at high temperatures because of the whey protein reactions that occur at temperatures above 70 °C. Therefore the energy efficiency of the process is a major consideration. We will define the following evaporator energy efficiency.

$$Eff = \frac{q_{shell}}{W_{comp}} \qquad (1.4)$$

Where, q_{shell}	=	useful evaporation heat flow.	(W)
W_{comp}	=	'driving' heat flow, or power supplied to the evaporator.	(W)

Early evaporator designs supplied steam directly to the evaporator shell and contained only a single effect. This plant design is shown by the 'Direct Steam Single Effect Evaporator' in Figure 1-4. From energy balances it is easy to show that the energy efficiency for this configuration is approximately 1 (Perry and Green, 1984, pp 11-37; Fergusson, 1989). This is a low energy efficiency and so these plants require a large raw energy supply. However, by increasing the number of effects it is possible to increase the energy efficiency. Figure 1-4 also shows a two effect evaporator. From energy balances it is possible to show that the energy efficiency for a multiple effect plant, with equal surface areas in each effect, is approximately equal to the number of effects.

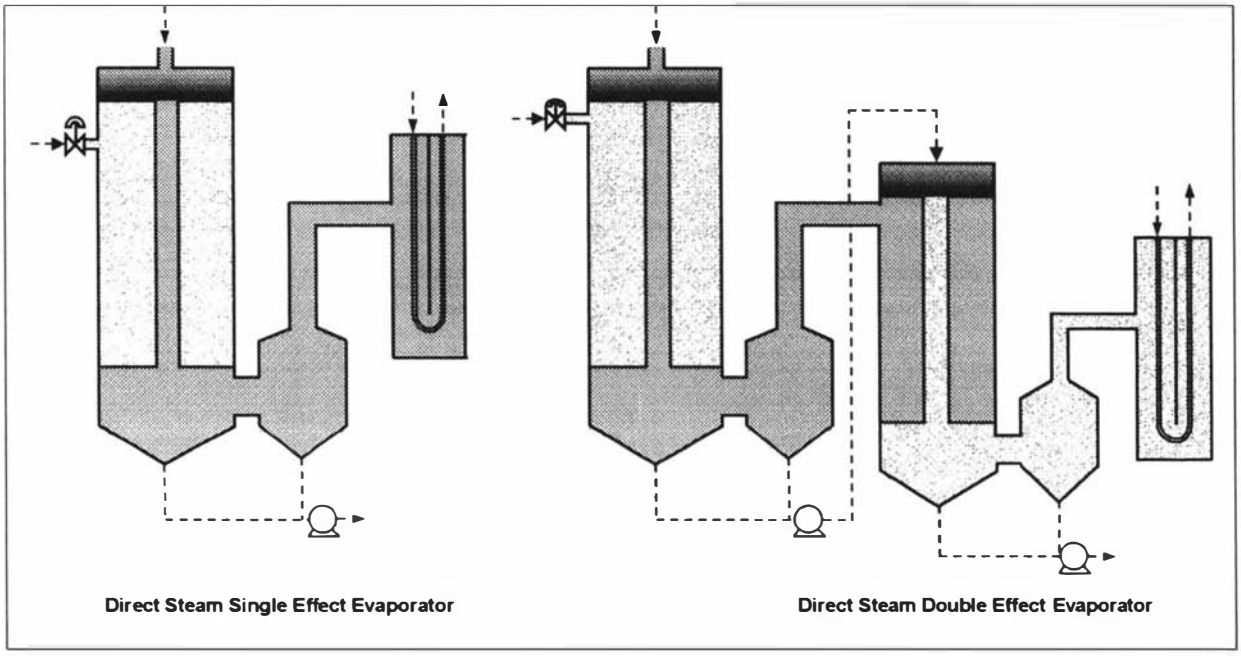

Figure 1-4 : Single and multiple effect evaporators.

The use of multiple effects reduces the evaporator operating costs but it also increases the capital costs. Consequently there is an optimum number of effects where the increase in capital cost is the same as the reduction in operating costs. It is common for the optimum to be between seven and eighteen effects. However, it is uncommon to find these large multiple effect evaporators in the Dairy industry because of the large temperature range that they must operate across. For example a large multiple effect plant will use a first effect shell temperature of 120 °C and a final effect temperature of 50 °C. This range of temperatures is not possible in the Dairy industry. The need to operate evaporators with high energy efficiencies, but across small temperature ranges, requires the use of vapour recompression.

1.3.2) Energy Efficiency with Re-Compression

The earliest vapour recompression evaporators used Thermal Vapour Re-compressors (TVR). With a TVR compressor the steam mass flow is approximately a half of the suction vapour mass flow. This means that the energy efficiency of a single effect evaporator is improved by approximately two. Although this improves the energy efficiency a significantly greater improvement can be achieved with Mechanical Vapour Re-compression (MVR). An MVR compressor uses a large turbo-compressor or fan to compress the vapour. From thermodynamics and energy balances it is possible to show that the energy efficiency of an isentropic MVR compressor is approximately given by the following (Smith and van Ness, 1987).

$$Eff \approx \frac{\lambda}{C_p.T_1\left[\left(\frac{P_2}{P_1}\right)^{\frac{R}{C_p}} - 1\right]} \qquad (1.5)$$

Where, P_1 = inlet pressure to compressor. (Pa)

P_2	=	outlet pressure from compressor.	(Pa)
T_1	=	inlet temperature to compressor.	(K)
C_p	=	heat capacity.	(J/kg.K)
R	=	universal gas constant.	(J/kg.K)
λ	=	latent heat of vapourisation.	(J/kg)

The above equation shows that the energy efficiency depends on the pressure difference the compressor acts against. This explains the popular use of the MVR evaporator design in the Dairy industry. In the Dairy industry falling film evaporators are used and these have no hydrostatic temperature loss and the boiling point elevation of many milk solutions is small. Consequently the evaporators can operate with small temperature differences and thereby require compressors to operate against small pressure differences. Using MVR evaporators it is possible to obtain energy efficiencies of over 30 (Fergusson, 1989), which is considerably greater than can be achieved with multiple effect or TVR evaporators.

1.3.3) Energy Efficiency of Spray Dryers

The spray dryers used in milk powder plants also have an energy efficiency. Ambient air is heated with high pressure steam and then used to evaporate water from the milk concentrate by mass and heat transfer. The moist air from the spray dryer cannot be re-used and so it is discharged to the atmosphere. Making an energy balance around the spray dryer we can produce the following approximation for the energy efficiency.

$$Eff \approx \frac{[T_{steam} - T_{out}]}{[T_{steam} - T_{air}]} \tag{1.7}$$

Where, T_{steam}	=	temperature of hot steam heated air.	(°C)
T_{out}	=	temperature of discharged air from spray dryer.	(°C)
T_{in}	=	temperature of ambient air entering the spray dryer.	(°C)

A typical spray dryer, working with milk, will use steam heated air of approximately 200 °C and will discharge the air at 60 °C (Nielsen *et al*, 1996). With an ambient temperature of 25 °C this produces an energy efficiency of 0.8, which is considerably lower than that of an MVR evaporator. The energy efficiency of the spray dryer can be increased by using higher steam heated air or lower discharge temperatures. However, higher steam heated temperatures can cause milk powder functional problems due to the whey protein denaturation reactions that are encouraged. Additionally lower discharge temperatures also cause operational problems due to the lack of evaporation that occurs at the bottom of the spray dryer.

From the above we can note that the energy efficiency of an MVR evaporator is considerably greater than that of a spray dryer. This means the cost of evaporation in an MVR evaporator is lower than in the spray dryer. As a result, an evaporator should be operated with the maximum possible product dry matter concentration. However, we have already discussed the detrimental impact of high evaporator product dry matters on the milk viscosity. At high concentrations the

milk viscosity increases and this reduces the product milk powder quality. As a result, there is an optimum product dry matter from the MVR evaporator plant.

1.4) The Evaporator A Plant at Kiwi Dairy Co-operatives

Figure 1-5 shows the evaporator A plant at Kiwi Co-op Dairies. Cold feed raw milk is supplied to the plate heat exchanger (HX 1750) which heats the milk from approximately 12 °C to 50 °C. The milk then passes to a shell and tube condenser (HX 1420) which is attached to the shell of the MVR evaporator. This condenser heats the milk from approximately 50 °C to 65 °C.

After exiting the MVR condenser the milk passes to the DSI preheat section of the evaporator plant. This contains two flash vessels (FV 1230 and FV 1250) and a Direct Steam Injection (DSI) unit. This preheat section heats the milk from approximately 65 °C to the DSI unit temperature (approximately 100 °C) where it is then held for a specified time in the holding tubes. The milk is then cooled to approximately 80 °C by pressure reduction flashing in the bottom of the flash vessels.

The milk flow from the second flash vessel then enters the first pass of the MVR evaporator section (HX 1300 and HX 1400). The MVR evaporator section provides most of the evaporation capacity for the plant. Its feed milk dry matter is approximately 12 %, but its product concentrate has a dry matter of approximately 40 %. This represents a considerable amount of water removal and the condensate flow from MVR evaporator is approximately 40,000 L/hr.

The product concentrate from the MVR evaporator section then passes to the TVR evaporator section (HX 1500, HX 1600 and HX 1700). This section acts as a small finisher plant for the evaporator plant. The milk is concentrated from approximately 40 % to approximately 48 % and this requires only a small amount of water removal (i.e., the condensate flow is approximately 1800 L/hr).

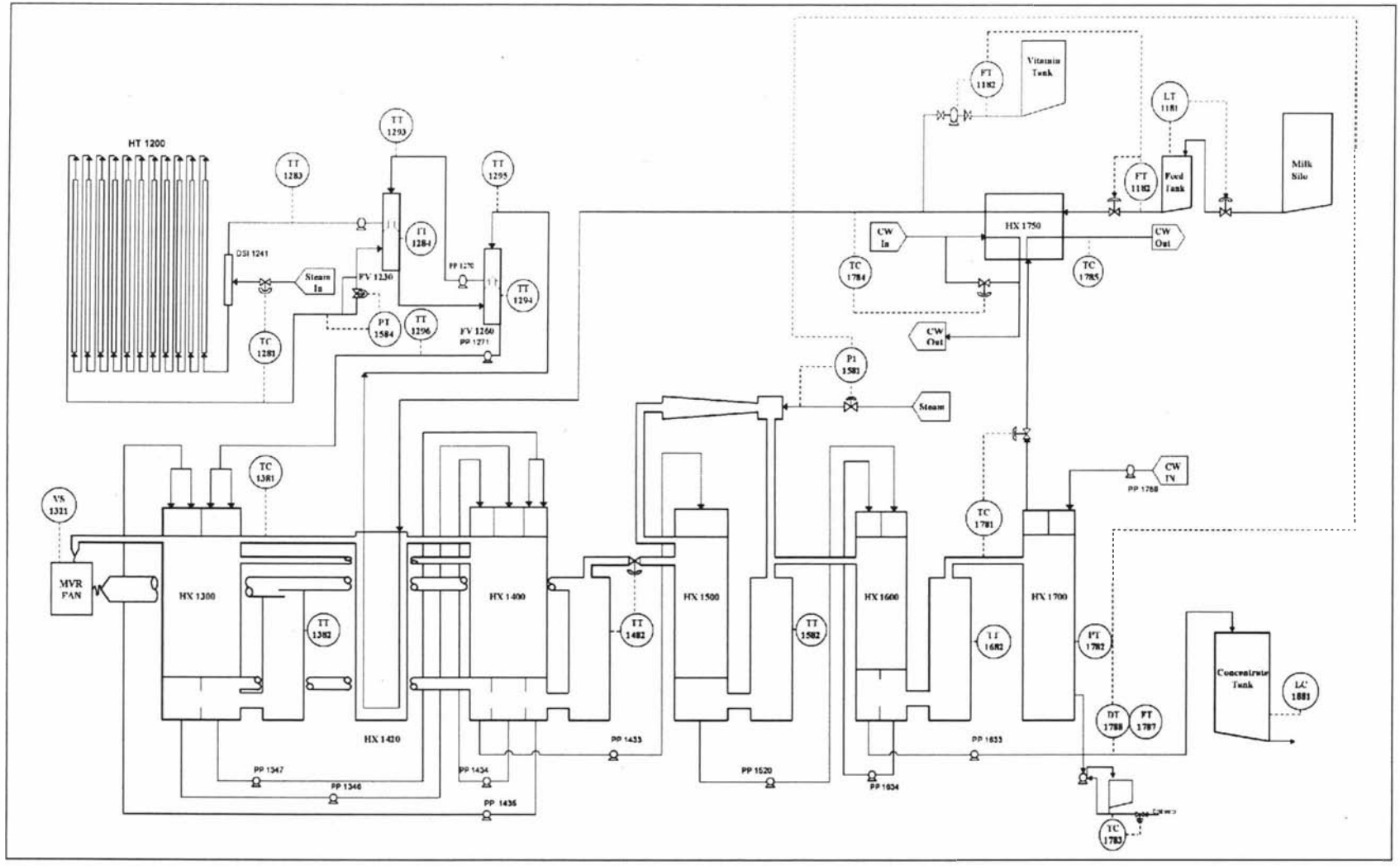

Figure 1-5 : Evaporator A plant at Kiwi Co-op Dairies.

1.5) Thesis Plan

The objectives of this Thesis were outlined at the start of this Chapter. During the remainder of this Chapter we have discussed some of the motivations for investigating the optimisation and control of falling film evaporators. The aims of the work discussed in this thesis are classified into three areas. Firstly a model will be developed for the Evaporator A plant at Kiwi Co-op Dairies. Secondly the steady state version of the model will be used to analyse the operation of the Evaporator A plant. Finally the dynamic model will be used to investigate the controllability of the Evaporator A plant.

Derive, develop and identify a model of the Evaporator A plant at Kiwi Co-operative Dairies.

The derivation of the model will be discussed in Chapters 2 and 3. Chapter 2 will be primarily concerned with deriving a model for the basic falling film evaporator. Chapter 3 will be concerned with deriving models for the additional DSI preheat section, the preheat plate heat exchanger and the shell/tube condensers that are used in the plant. Following the derivation the models will be developed in Chapter 4. Here the steady state and linear state space models for the Evaporator A plant will be developed. Finally the identification of the model will be discussed in Chapter 5.

Investigate the optimisation of the Evaporator A plant at Kiwi Dairy Co-operatives.

In this Chapter we have discussed some of the basic ideas that motivate the need for optimisation studies of milk powder plants. Firstly the energy efficiency of modern falling film evaporators is considerably greater than that of spray dryers. Consequently we want to maximise the dry matter concentration from the evaporator and thereby minimise the energy costs of the plant. Secondly there are fouling constraints on the operation of the plant. The evaporators cannot operate above 70 ^{o}C because the whey de-naturation reactions occur in this range and these cause fouling. Also the evaporator tubes must remain completely wetted, otherwise fouling will occur. In Chapter 6 we will discuss the constrained optimisation of the falling film evaporator at Kiwi Co-op Dairies.

Investigate the controllability of the Evaporator A plant at Kiwi Dairy Co-operatives.

We have discussed some of the motivating ideas for investigating the controllability of falling film evaporators. Firstly the evaporation process means that it amplifies variations in the feed dry matter. This means that the process is sensitive to disturbances in the feed dry matter. Secondly, the energy efficiency of evaporators is considerably greater than that of spray dryers. As a result, the plant operating costs are reduced if the evaporators work at maximum capacity. However, if the evaporator product dry matter cannot be well controlled then a significant safety margin is required and this requires higher levels of evaporation in the spray dryer. In Chapter 7 we will investigate the controllability of the Evaporator A control loops. The controllability of the plant product dry matter control loops will be an important part of this.

Chapter 2 : Modelling Falling Film Evaporators

2.1) Introduction

The aim of the work discussed in this thesis is to analyse the operation and control of falling film evaporators. Specifically, the Evaporator A plant at Kiwi Co-op Dairies will be considered. The analysis is model based and so a model for the evaporator plant will be developed first. The purpose of the first five Chapters of this thesis is to derive, develop and identify the model for the Evaporator A plant. We shall simplify the modelling by separating the plant into four sections. Figure 2-1 shows the complete Evaporator A plant with these four sections shown in different shadings. In this Chapter we derive models for the MVR evaporator and the TVR evaporator sections. However, these models will exclude the preheat condenser and vacuum condenser, which are considered in the next chapter.

The first part of this Chapter contains a short discussion of Thermodynamics and a literature review of evaporator modelling. This is contained in Section 2.2 and the important results are the development/discussion of the general process energy and mass balances. These are derived from the First Law of Thermodynamics and the Law of Mass of Conservation. They provide the basis for the derivation of the models for the entire Evaporator A plant.

Following the Thermodynamics discussion we shall briefly describe, in Section 2.3, the MVR evaporator and TVR evaporator sections. The distribution plates, falling films, evaporator effects and evaporator shells of the Evaporator A plant will all be discussed. There are some important differences between the MVR evaporator section and the TVR evaporator section and these will also be discussed.

After describing the MVR and TVR evaporator sections we will begin modelling the process. In Section 2.4, models will be developed for the distribution plates, evaporator effects, falling films and evaporators shells. Firstly a generic distribution plate model will be considered. The distribution plates are essentially the same throughout the plant and so only the first will be modelled. This general model can then be applied to any other distribution plate in the plant. The evaporator effect energy balances are derived after the distribution plate. We will consider the three evaporator effects, of the Evaporator A plant, individually and derive models for each. The end result will be a first order differential equation for the temperature of each evaporator effect.

Arguably the most difficult part of the evaporator model is the falling film. After considering the evaporator effect energy balances we will derive the falling film partial differential equations. These will then be simplified by transformation in the Laplace Domain. The end result will be a differential equation for the dry matter and mass flow from the falling film. Finally we shall consider the energy balances for the evaporator shells and these will be derived using the same methods as for the evaporator effect energy balances. The MVR evaporator shell and the TVR evaporator shell will be consider individually because of their different natures. The end result will be a pair of differential equations for the evaporator shell temperatures.

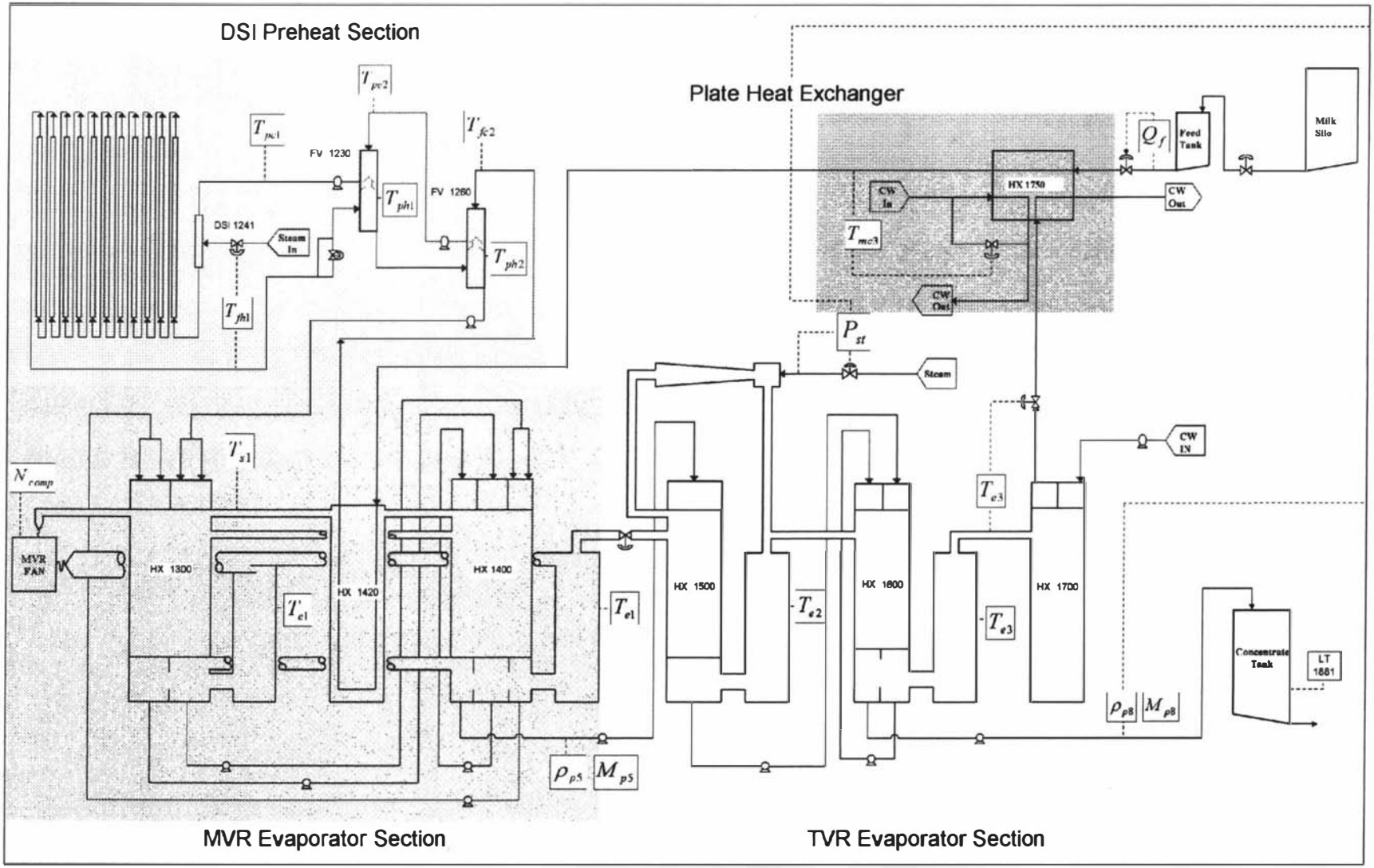

Figure 2-1 : Evaporator A plant at Kiwi Co-op Dairies.

2.2) Thermodynamics and Evaporator Modelling Literature Review

2.2.1) Thermodynamics

The process modelling done here is primarily first principles. The equations are derived from the fundamental First Law of Thermodynamics and the Law of Conservation of Mass. The Law of Conservation of Mass is given by the following (Sandler, 1989, p 30).

$$\frac{dM}{dt} = \sum_{k=1}^{K} \dot{M}_k \tag{2.1}$$

Where, M = total mass in control volume. (kg)

$\dot{M}_k$ = mass flow into control volume. (kg/s)

The First Law of Thermodynamics was originally developed experimentally by the work of Joule in the 19th century. For a control volume with constant internal properties the following equation describes the accumulation of energy with k input/output mass flows, a total net inward heat flow q, compressive work $P\frac{dV}{dt}$ and additional work W_s.

$$\frac{d}{dt}\left[M\left(U + \frac{1}{2}v^2 + \psi\right)\right] = \sum_{k=1}^{K} \dot{M}_k \left(U_k + \frac{1}{2}v_k^2 + \psi_k\right) + q + W_s - P\frac{dV_T}{dt} + \sum_{k=1}^{K} \dot{M}_k (P_k V_k) \tag{2.2}$$

Where, M = total mass of material in the control volume. (kg)

U = total internal energy of the control volume. (J/kg)

v = velocity of the control volume. (J/kg)

ψ = potential energy of the control volume. (J/kg)

$\dot{M}_k$ = mass flow of an input/output flow. (kg/s)

U_k = internal energy of an input/output flow. (J/kg)

ψ_k = potential energy of an input/output flow. (J/kg)

v_k = velocity of an input/output flow. (m/s)

q = total net heat flow into the control volume. (W)

W_s = total net work applied to the control volume. (W)

P_k = pressure of an input/output flow. (Pa)

V_k = specific volume of an input/output flow. (m^3/kg)

V_T = total volume of the energy balance control volume. (m^3)

In practice many assumptions are made to simplify this equation. Firstly the pressure work terms are removed by using the enthalpy instead of the internal energy (i.e., $H = U + PV$). Secondly kinetic and potential energy terms are neglected and the system is assumed to have a constant volume. This simplifies the equation to the following.

$$\frac{d[M.U]}{dt} = \sum_{k=1}^{K} M_k.H_k + q + W_s \tag{2.3}$$

A common modelling technique is to assume that the enthalpy and internal energies are the same. This assumption is based on the observation that the densities of liquid and solids are very large (i.e., $\rho = \frac{1}{V}$). With this assumption we produce the following version of the First Law, which is the form that we will use.

$$\frac{d[M.H]}{dt} = \sum_{k=1}^{K} M_k.H_k + q + W_s \tag{2.4}$$

From the above we know that the determination of the enthalpy is important. The differential change in enthalpy is given by the following (Sandler, 1989).

$$dH = C_p.dT + \left[V - T\left(\frac{\partial V}{\partial T}\right)_P\right]dP \tag{2.5}$$

Where, C_p	=	constant pressure heat capacity of material.	(J/kg.°C)
V	=	specific volume of material.	(m^3/kg)
T	=	temperature of the material.	(°C)
P	=	pressure of the material.	(Pa)

For liquids and solids the effect of the pressure on the enthalpy is negligible since the specific volume and compressibility are small (i.e., V and $\frac{\partial V}{\partial T}$ are both small). This means that this equation can be simplified to the following :

$$dH = C_p.dT, \qquad \Delta H = \int_{T_1}^{T_2} C_p dT \tag{2.6}$$

The heat capacity of a material always varies with temperature. However, if we are dealing with a small change in temperature, then it is possible to assume that the heat capacity is constant. Furthermore the enthalpy is arbitrarily defined as zero when the temperature is zero degrees Celsius.

$$H = C_p.T \tag{2.7}$$

With milk solutions the heat capacity depends on the dry matter and composition. In Appendix A the following linear relationship between heat capacity and dry matter is derived, using the ideal mixture assumption. The enthalpy is then given by the product of this and the temperature.

$$C_{pmilk} = C_{pwater} - C_{pTS}.w, \qquad H_{milk} = (C_{pwater} - C_{pTS}.w)T \tag{2.8}$$

Where, H_{milk} = enthalpy of the liquid milk. (J/kg)
C_{pmilk} = heat capacity of the milk solution. (J/kg.°C)
C_{pwater} = heat capacity of water. (J/kg.°C)
C_{pTS} = coefficient relating milk heat capacity and dry mass fraction. (J/kg.°C)
w = dry mass fraction of the milk. (kg/kg)

2.2.2) Evaporator literature Review

Whilst falling film evaporators are a widely used process there is a shortage of literature on their modelling. There does not appear to be any good reason for this deficiency, but it may be due to the distributed parameter nature of the falling film. This modelling deficiency can be compared to the large amount of work done with simple mixing tank evaporators (Wang and Cameron, 1994; Lee *et al*, 1989; Tonelli *et al*, 1994).

There has been a lot of work done investigating the heat transfer coefficients of falling film evaporators. A large amount of this work has been concerned with the theoretical issues of falling film waves, turbulence and the effect that these have on the heat transfer coefficients (Benjamin 1957; Dukler *et at*, 1952; Fulford, 1964). There are also many empirical studies that investigate the heat transfer coefficients (Chun and Seban, 1971; Chun and Kim, 1990; Alhusseini *et al*, 1998). However, much of this work has been done with water and other non-milk liquids. Some studies have focused exclusively on milk solutions (Bouman, 1993; Jebson and Iyer, 1991; Chen, 1992). However, the work is purely empirical and suffers from a lack of 'good' theoretical groundwork. A good theoretical basis assists in developing models that can be extrapolated outside their range of fitting.

There is a reasonable amount of static falling film evaporator models. A large paper, by Angeletti and Moresi (1983), discusses the static modelling of falling film evaporators working with food solutions. They give considerable discussion to the prediction of heat transfer coefficients. In a later paper Moresi (1985) extends this work to consider the design and optimisation of falling film evaporators.

There are very few dynamic falling film evaporator models. An early paper by Burdett (1971) develops a dynamic model for a falling film evaporator used to evaporate sea-water. However, these sea-water evaporators are quite different from the typical dairy industry evaporators. It appears that the only dynamic model that has been developed for falling film evaporators working with milk solutions is that of Quaak and Gerritsen (1990). This model is important because it does not neglect the distributed parameter falling film. In order to deal with the falling film equations they make the assumption of constant falling film velocity and constant evaporating heat transfer coefficients. With these assumptions the falling film partial differential equations can be transformed into differential equations with delays.

Later the Quaak dynamic model was used to develop a control system for a four effect falling film evaporator (Quaak *et al*, 1994; van Wijck *et al*, 1994). Quaak *et al* also developed an additional empirical model. Both models were then used to develop a multi-variable control

system for the evaporator. This was shown to provide 'good' control of the evaporator. Finally there is a model of a falling film evaporator with a MVR compressor, that was developed from the work discussed in this thesis (Winchester and Marsh, 1999)

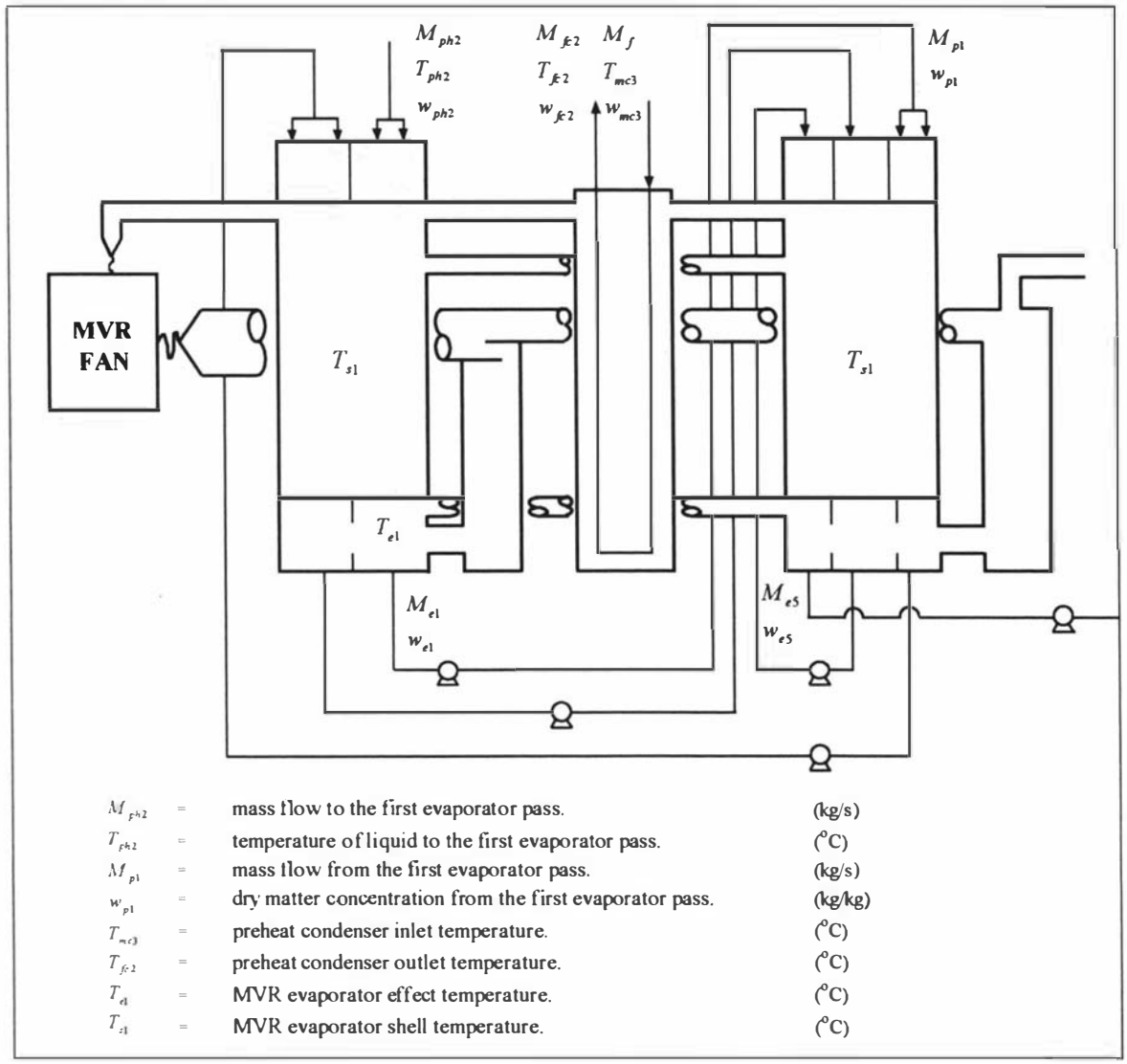

Figure 2-2 : The MVR evaporator section, of the Evaporator A plant.

2.3) The MVR and TVR Evaporator Sections

2.3.1) The MVR evaporator section

The Kiwi Co-op Dairies Evaporator A plant is relatively large and complex. It contains three effects, with mechanical and thermal vapour compressors and multiple passes are used in each effect. Figure 2-2 shows the mechanical vapour re-compression (MVR) section of the plant. This is a single effect two-calandria evaporator with five passes and a MVR compressor. The milk enters the first distribution plate with a mass flow, temperature and dry matter (i.e., M_{ph2}, T_{ph2}

and w_{ph2}). This distribution plate evenly distributes the milk onto the evaporator falling film tubes. The milk then flows down the tubes by gravitational acceleration and heat is supplied to it by conduction/convection from the evaporator shell. This heat causes water evaporation and thereby concentrates the milk dry matter. At the bottom of the evaporator tubes the milk has a mass flow and dry matter (i.e., M_{e1} and w_{e1}). It is collected and pumped to the next distribution plate where it enters with a mass flow and dry matter (i.e., M_{p1} and w_{p1}). After passing through the second pass the milk goes through the third, fourth and fifth evaporator passes before being pumped out to the TVR evaporator section.

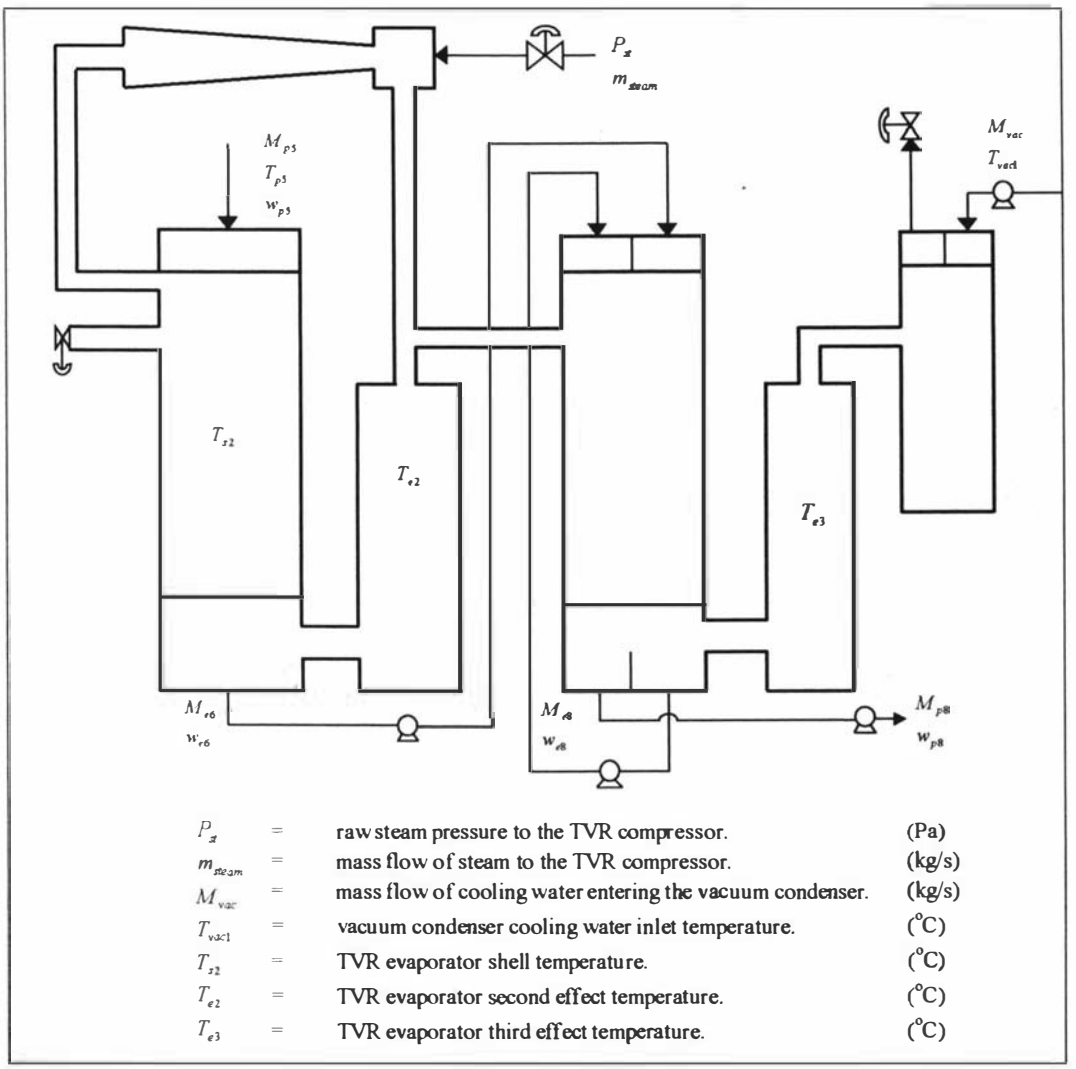

P_s	=	raw steam pressure to the TVR compressor.	(Pa)
m_{steam}	=	mass flow of steam to the TVR compressor.	(kg/s)
M_{vac}	=	mass flow of cooling water entering the vacuum condenser.	(kg/s)
T_{vac1}	=	vacuum condenser cooling water inlet temperature.	(°C)
T_{s2}	=	TVR evaporator shell temperature.	(°C)
T_{e2}	=	TVR evaporator second effect temperature.	(°C)
T_{e3}	=	TVR evaporator third effect temperature.	(°C)

Figure 2-3 : The TVR evaporator section, of the Evaporator A plant.

The preheat condenser provides the vacuum that allows the milk to be evaporated at temperatures below 70 °C. It is important that the evaporator is operated under vacuum because of the whey protein de-naturation reactions that occur at temperatures above 70 °C (Dannenberg and Kessler, 1988). Feed milk is used in the condenser tubes and it enters with a mass flow, temperature and dry matter (i.e, M_f, T_{mc3} and w_{mc3}). The inlet milk temperature is lower than

the MVR evaporator and this causes a net flow of heat from the evaporator. At the condenser outlet, the milk will be at a temperature similar to the MVR evaporator effect.

The MVR compressor provides the evaporation driving force for the evaporator. Electric power is supplied to the compressor and it compresses the evaporated water vapour from the evaporator effect. The compressed evaporated water vapour condenses at a higher temperature in the evaporator shell because of its higher pressure. The temperature difference between the evaporator shell and effect then provides the heat transfer driving force, which causes the evaporation.

2.3.2) The TVR evaporator section

Figure 2-3 shows the TVR evaporator section of the Evaporator A plant. This is a two effect system with thermal vapour re-compression (TVR) and two passes in the final effect. As with the MVR evaporator, milk enters the first distribution plate with a mass flow, temperature and dry matter (i.e., M_{p5}, T_{p5} and w_{p5}). It then flows down the evaporator tubes and is pumped to the final effect. After passing through the seventh and eighth passes the milk leaves the evaporator with a concentrate mass flow, temperature and dry matter (i.e., M_{p8}, T_{p8} and w_{p8}).

The TVR compressor uses raw steam to drive the evaporator (i.e., P_{st} and m_{steam}). As with the MVR compressor this allows the evaporated water to be compressed. The compressed water vapour then condenses in the evaporator shell and this provides the driving force for the evaporation. The TVR evaporator section also contains a condenser and this provides the vacuum for the evaporator. Cooling water is used in the condenser tubes, with a mass flow (M_{vac}) and temperature (T_{vacl}).

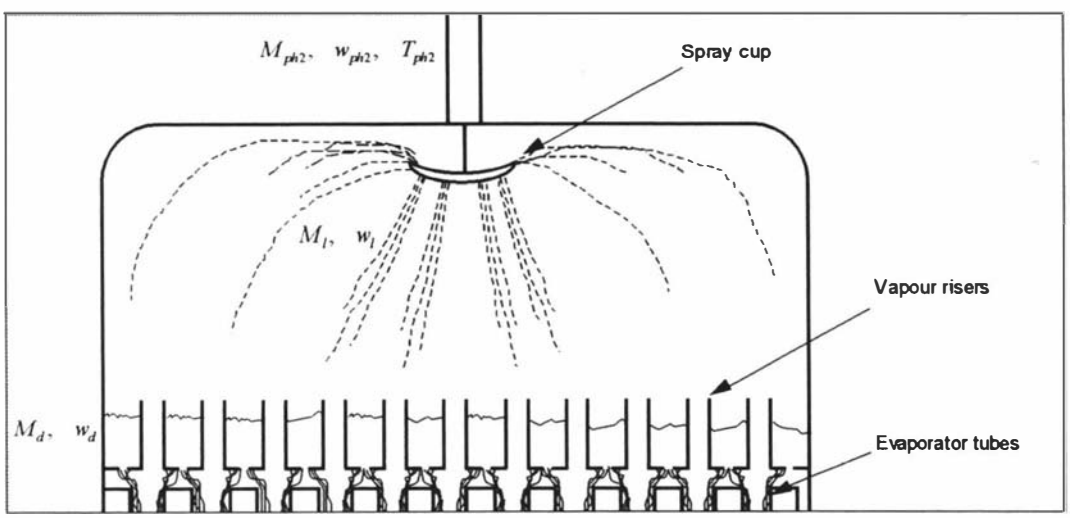

Figure 2-4 : An evaporator distribution plate.

2.4) Model Derivation

2.4.1) Distribution plate

Figure 2-4 shows a typical distribution plate, which is used to evenly distribute the milk onto the evaporator tubes. Here we want to derive differential equations for the milk flow and dry matter through the distribution plate. We will consider the first distribution plate of the MVR evaporator section, but the same model may be used for any distribution plate in the Evaporator A plant. The milk enters from the top and it will usually be at a temperature above the evaporator effect. This causes some water to vaporise (i.e., 'flash') and the milk mass flow becomes slightly reduced. The milk is then sprayed onto the distribution plate by the spray cup.

Making total and dry matter mass balances we produce the following equations. Here we have taken the milk mass flow (M_l) and dry matter (w_l) after 'flashing' as the feed properties. Later we will show how the mass flow of flashed vapour can be calculated. We have assumed a homogenous mixture above the distribution plate and we have also assumed that the distribution plate temperature is the same as the evaporator effect.

$$A_d \frac{d[\rho_d h_d]}{dt} = M_l - M_d \tag{2.9}$$

$$A_d \frac{d[\rho_d h_d w_d]}{dt} = M_l . w_l - M_d . w_d \tag{2.10}$$

Where, M_d = mass flow of liquid passing through a distribution plate. (kg/s)
w_d = dry mass fraction of liquid passing through a distribution plate. (kg/kg)
M_l = mass flow of liquid to the distribution plate, after flashing. (kg/s)
w_l = liquid dry mass fraction to the distribution plate, after flashing. (kg/kg)
A_d = cross sectional area of a distribution plate. (m^2)
h_d = height of liquid above a distribution plate. (m)
ρ = density of the liquid. (kg/m^3)

We can expand the differential in equation (2.10) and substitute equation (2.9) to produce the following.

$$\frac{dw_d}{dt} = \frac{M_l}{\rho_d . A_d . h_d}[w_l - w_d] \tag{2.11}$$

In Appendix A the functional dependence of the milk density is determined (i.e., $\rho = \frac{\rho_{water}}{[1 - a_{TS} . w]}$).

Using this we can expand the differential in equation (2.9) to produce the following differential equation for the height of liquid.

$$A_d \frac{dh_d}{dt} = Q_l - Q_d \tag{2.12}$$

Where, Q_l = volumetric flow of liquid after flashing. (m^3/s)

Q_d = volumetric flow of liquid passing through a distribution plate. (m^3/s)

If the milk enters the distribution plate system at a temperature higher than the evaporator then some of the milk will flash. The mass flow of flashed water vapour can be determined by making static mass and enthalpy balances. If we assume constant latent heat and heat capacity, with respect to temperature, then the following equation gives the mass flow of flashing.

$$m_{flash} = \frac{M_{ph2}\left(C_{pwater} - C_{pTS}.w_{ph2}\right)}{\lambda}\left[T_{ph2} - T_{el}\right], \quad M_l = M_{ph2}\left[1 - \frac{\left(C_{pwater} - C_{pTS}.w_{ph2}\right)}{\lambda}\left(T_{ph2} - T_{el}\right)\right] \tag{2.13}$$

$$w_l = \frac{w_{ph2}}{\left[1 - \frac{\left(C_{pwater} - C_{pTS}.w_{ph2}\right)}{\lambda}\left(T_{ph2} - T_{el}\right)\right]} \tag{2.14}$$

Where, m_{flash} = mass flow of flashed water vapour. (kg/s)

M_{ph2} = mass flow of liquid before flashing. (kg/s)

w_{ph2} = dry mass fraction of the milk before flashing. (kg/kg)

T_{ph2} = temperature of liquid entering the distribution plate system. (°C)

T_{el} = temperature of the distribution plate system, also MVR effect. (°C)

C_{pwater} = heat capacity of water. (J/kg.°C)

C_{pTS} = coefficient relating the milk heat capacity and dry mass fraction. (J/kg.°C)

λ = latent heat of vaporisation. (J/kg)

These equations can be substituted into the differential equations for the height of liquid and dry matter above the distribution plate. The resulting differential equations are shown by equations (2.15) and (2.16). These show the impact of the flashing on the height of liquid and dry matter above the plate. The flashing reduces the milk flow and this causes the height of liquid to decrease and the dry matter to increase.

$$\frac{dh_d}{dt} = \frac{Q_{ph2}}{A_d} - \frac{M_{ph2}\left(C_{pwater} - C_{pTS}.w_{ph2}\right)\left(T_{ph2} - T_{el}\right)}{\rho_{water}.\lambda} - \frac{Q_d}{A_d} \tag{2.15}$$

$$\frac{dw_d}{dt} = \frac{M_{ph2}}{\rho_d A_d . h_d}\left[w_{ph2} - w_d\left(1 - \frac{\left(C_{pwater} - C_{pTS}.w_{ph2}\right)}{\lambda}\left(T_{ph2} - T_{el}\right)\right)\right] \tag{2.16}$$

The flow of liquid through the distribution plate is given by a simplification of the standard orifice equation (de Nevers, 1991, pp 157-159).

$$Q_d = \frac{C_d . A_h}{\left[1-\beta^2\right]}\sqrt{\frac{2.\Delta P}{\rho_d}}, \qquad \Delta P = \rho_d . g . h_d \tag{2.17}$$

Where, Q_d = volumetric flow of liquid passing through the distribution plate. (m^3/s)

A_h = surface area of holes in the distribution plate. (m^2)

ΔP = pressure difference across the distribution plate. (Pa)

β = ratio of areas, between a distribution plate hole and calandria. (-)

C_d = discharge coefficient for the distribution plate holes. (-)

h_d = height of liquid above the distribution plate. (m)

ρ_d = density of liquid above the distribution plate. (kg/m^3)

g = acceleration due to gravity. (m/s^2)

The ratio of the distribution plate hole area to that of the calandria is very close to zero. Therefore we can assume the parameter β is zero. With this assumption the orifice plate equation simplifies to the following.

$$Q_d = C_d . A_h \sqrt{2.g.h_d} \tag{2.18}$$

The discharge coefficient (C_d) accounts for the additional energy losses that occur during the contraction and expansion through the distribution plate. For a conventional orifice plate, operating in turbulent flow, this can be determined (i.e., $C_d = \frac{\pi}{\pi+2}$, de Nevers, 1991). However, it is possible that surface tension forces become important at the small diameters that are used for distribution plates (Trinh *et al*, 1996). These additional forces are neglected in the traditional orifice plate calculations. As a result, the discharge coefficient may be different from the expected value, but the results contained in Trinh *et al* (1996) suggest that deviations are small.

If we assume constant milk density and no flashing, then the above differential equations are simplified to the following.

$$A_d \frac{dh_d}{dt} = Q_{ph2} - Q_d, \qquad Q_d = C_d . A_h \sqrt{2.g.h_d}, \qquad A_d \frac{dw_d}{dt} = \frac{Q_{ph2}}{h_d}\left[w_{ph2} - w_d\right] \tag{2.19}$$

2.4.2) Evaporator effect

MVR evaporator effect

The First Law of Thermodynamics was discussed earlier in this chapter and used to produce equation (2.4). Here we use this balance equation to produce a differential equation for the temperature of the evaporator effect. The balance is made around the distribution plate, the falling film, the pipework from the effect and the metal/vapour contained in the effect. Enthalpy

is supplied to the effect by the feed milk, while the concentrated milk and evaporated vapour remove it. Heat is supplied from the evaporator shell and also removed by losses from the evaporator surfaces. We also make the additional assumption of a negligible mass of milk and vapour, in the effect. This assumption is based on the large amount of metal in the evaporator, which dominates the evaporator's thermal inertia. With this assumption and the above energy/mass flows we produce the following equations.

$$\frac{d\left[M_{met}.C_{pmet}.T_{e1}\right]}{dt} = M_{ph2}\left(C_{pwater} - C_{pTS}.w_{ph2}\right)T_{ph2} + q_{shell1} - M_{compl}\left(C_{pwater}.T_{e1} + \lambda\right) - q_{eloss1} - M_{p5}\left(C_{pwater} - C_{pTS}.w_{p5}\right)T_{p5} \quad (2.20)$$

$$M_{ph2} = M_{p5} + M_{compl}, \qquad M_{ph2}.w_{ph2} = M_{p5}.w_{p5} \quad (2.21)$$

Where, T_{e1} = temperature of the MVR evaporator effect. (kg/s)
M_{met} = mass of metal in the evaporator effect. (kg)
C_{pmet} = heat capacity of metal. (J/kg.°C)
M_{ph2} = mass flow of liquid entering the MVR evaporator section. (kg/s)
M_{p5} = mass flow of liquid exiting the MVR evaporator section. (kg/s)
M_{compl} = mass flow of vapour compressed by the MVR compressor. (kg/s)
C_{pwater} = heat capacity of water. (J/kg.°C)
q_{shell1} = total heat flow passing through the MVR evaporator tubes. (W)

We can substitute (2.21) into (2.20) and produce the following differential equation.

$$I_{effect1}\frac{dT_{e1}}{dt} = M_{ph2}\left(C_{pwater} - C_{pTS}.w_{ph2}\right)\left(T_{ph2} - T_{e1}\right) + q_{shell1} - M_{compl}.\lambda - q_{eloss1}, \quad I_{effect1} = M_{met}.C_{pmet} \quad (2.22)$$

Where, $I_{effect1}$ = thermal inertia of evaporator effect. (J/°C)

The surface heat losses are assumed to be due to convection and thereby given by equation (2.23).

$$q_{eloss1} = U_l.A_{el1}\left(T_{e1} - T_a\right) \quad (2.23)$$

Where, q_{eloss1} = surface energy loss heat flow for the MVR evaporator effect. (W)
U_l = overal heat transfer coefficient for the surface energy losses. (W/m^2.°C)
A_{el1} = surface area of the MVR evaporator effect, for heat losses. (m^2)
T_a = ambient temperature of surroundings. (°C)

If we use the following notation we produce equation (2.25).

$$q_{feed1} = M_{ph2}\left(C_{pwater} - C_{pTS}.w_{ph2}\right)\left(T_{ph2} - T_{e1}\right), \qquad q_{comp1} = M_{comp1}.\lambda \tag{2.24}$$

$$I_{effect1}\frac{dT_{e1}}{dt} = q_{feed1} + q_{shell1} - q_{eloss1} - q_{comp1} \tag{2.25}$$

Where, q_{feed1} = Net enthalpy from the feed. (W)

q_{shell1} = Heat flow through the MVR evaporator tubes. (W)

q_{comp1} = Latent enthalpy of the compressor vapour suction flow. (W)

q_{eloss1} = Losses heat flow from the effect surfaces. (W)

TVR second evaporator effect

Here we want to produce a differential equation for the temperature of the second effect. As with the first effect, we make an energy balance around the metal, milk and vapour in the evaporator effect. The MVR evaporator product concentrate provides enthalpy, while the sixth pass product milk and evaporated vapour remove it. There is also a mass flow of condensate from the third effect evaporator shell and this removes enthalpy. Heat is supplied from the evaporator shell, removed by the third effect and the surface losses. We shall also make the additional assumption of a negligible mass of milk and vapour in the effect. With these mass and energy flows we produce the following differential equation for the second effect temperature.

$$\begin{aligned}\frac{d\left[M_{met2}.C_{pmet}.T_{e2}\right]}{dt} &= M_{p5}\left(C_{pwater} - C_{pTS}.w_{p5}\right)T_{e1} + q_{shell6} - M_{comp2}\left(C_{pwater}.T_{e2} + \lambda\right) \\ &\quad - M_{cond2}.C_{pwater}.T_{e2} - q_{shell7} - q_{shell8} - q_{eloss2} - M_{p6}\left(C_{pwater} - C_{pTS}.w_{p6}\right)T_{e2}\end{aligned} \tag{2.26}$$

$$M_{p6} = M_{p5} - M_{comp2} - M_{cond2}, \qquad M_{p6}.w_{p6} = M_{p5}.w_{p5} \tag{2.27}$$

Where, M_{met2} = mass of metal in the second evaporator effect. (kg)

M_{milk2} = mass of milk in the second evaporator effect. (kg)

M_{cond2} = mass flow of condensate from the third effect evaporator shell. (kg/s)

We can substitute equation (2.27) into (2.26) and produce the following.

$$I_{effect2}\frac{dT_{e2}}{dt} = M_{p5}\left(C_{pwater} - C_{pTS}.w_{p5}\right)\left(T_{e1} - T_{e2}\right) + q_{shell6} - q_{eloss3} - \lambda M_{comp2} - q_{shell7} - q_{shell8} \tag{2.28}$$

By defining the following terms we then produce equation (2.30).

$$q_{feed6} = M_{p5}\left(C_{pwater} - C_{pTS}.w_{p5}\right)\left(T_{e1} - T_{e2}\right), \qquad q_{comp2} = \lambda M_{comp2} \tag{2.29}$$

$$I_{effect2}\frac{dT_{e2}}{dt}=q_{feed6}+q_{shell6}-q_{eloss2}-q_{comp2}-q_{shell7}-q_{shell8} \tag{2.30}$$

Where, q_{feed6} = net enthalpy in the feed to the second effect. (W)
q_{eloss2} = surface energy loss heat flow for the second effect. (W)
q_{shell7} = heat flow through the seventh pass evaporator tubes.(W)
q_{shell8} = heat flow through the eighth pass evaporator tubes. (W)

TVR third evaporator effect

Here we want to produce a differential equation for the temperature of the third effect. The feed milk supplies enthalpy, whereas the concentrated milk and condensing steam remove it. Heat is supplied from the second effect and removed by the vacuum condenser and surface losses. These mass and energy flows can be used to produce the following :

$$\begin{aligned}\frac{d\left[M_{met}.C_{p.met}.T_{e3}\right]}{dt}=M_{p6}\left(C_{pwater}-C_{pTS}.w_{p6}\right)T_{e2}+q_{shell7}+q_{shell8}-M_{cond3}.C_{pwater}.T_{e3}\\ -q_{vac}-q_{eloss3}-M_{p8}\left(C_{pwater}-C_{pTS}.w_{p8}\right)T_{e2}\end{aligned} \tag{2.31}$$

$$M_{p6}=M_{p8}+M_{cond3}, \qquad M_{p6}.w_{p6}=M_{p8}.w_{p8} \tag{2.32}$$

We can substitute equation (2.32) into (2.31) to produce the following.

$$I_{effect3}\frac{dT_{e3}}{dt}=M_{p6}\left(C_{pwater}-C_{pTS}.w_{p6}\right)\left(T_{e2}-T_{e3}\right)+q_{shell7}+q_{shell8}-q_{vac}-q_{eloss3} \tag{2.33}$$

Defining the following term for the net enthalpy into the third effect we can produce equation (2.35).

$$q_{feed7}=M_{p6}\left(C_{pwater}-C_{pTS}.w_{p6}\right)\left(T_{e2}-T_{e3}\right) \tag{2.34}$$

$$I_{effect3}\frac{dT_{e3}}{dt}=q_{feed7}+q_{shell7}+q_{shell8}-q_{eloss3}-q_{vac} \tag{2.35}$$

Where, q_{feed7} = net enhalpy in the feed to the third effect. (W)
q_{eloss3} = surface energy loss heat flow for the third effect. (W)
q_{vac} = heat flow through the vacuum condenser. (W)

2.4.3) Falling film

The evaporator falling film is a distributed parameter system since the film velocity, dry matter and temperature vary with distance as well as time. We will simplify the analysis by assuming a constant and flat falling film velocity and concentration profile. Then the falling film is described

by making mass, dry matter and energy balances across an infinitesimal cross section, as shown in Figure 2-5. The liquid mass flow rate and dry mass fraction ($M(x,t)$ and $w(x,t)$) vary both with distance (x) down the tube and time (t).

If we make a mass and dry matter balance around the infinitesimal cross section we can produce equations (2.36) and (2.37). There is an accumulation of mass and dry matter (i.e., $dx\frac{\partial[\rho(x,t)A(x,t)]}{\partial t}$ and $dx\frac{\partial[\rho(x,t)A(x,t)w(x,t)]}{\partial t}$) and a net mass and dry matter flow (i.e., $M(x,t)-M(x+dx,t)$ and $M(x,t)w(x,t)-M(x+dx,t)w(x+dx,t)$) into the infinitesimal section.

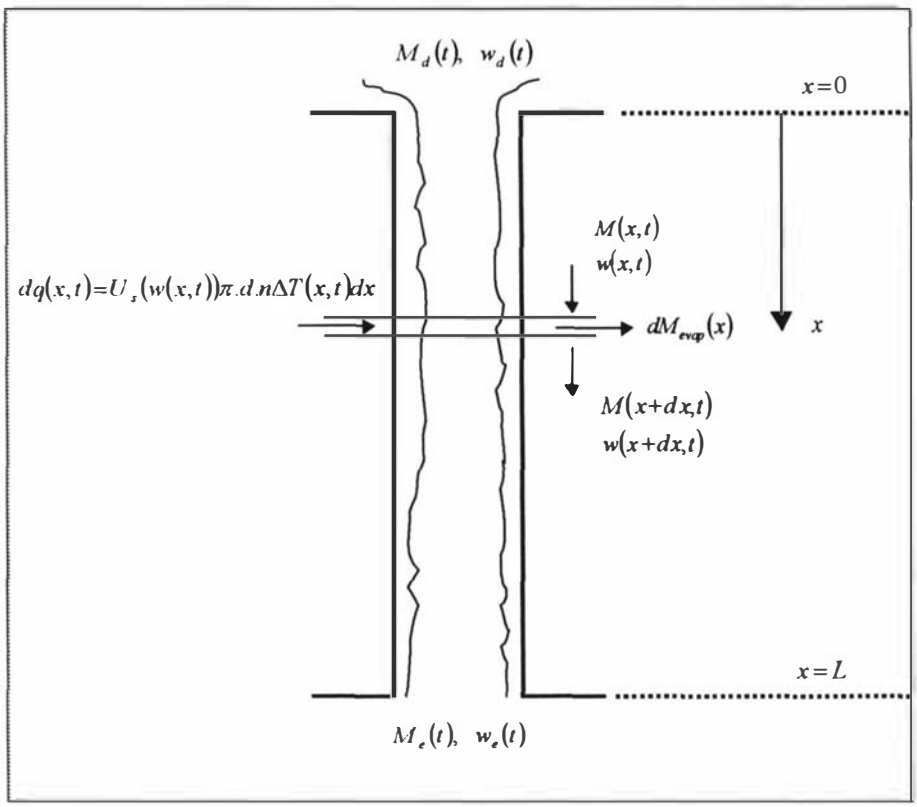

Figure 2-5 : Falling film partial differential equation derivation.

$$dx\frac{\partial[\rho(x,t)A(x,t)]}{\partial t}=M(x,t)-M(x+dx)-dM_{evap}(x,t) \tag{2.36}$$

$$dx\frac{\partial[\rho(x,t)A(x,t)w(x,t)]}{\partial t}=M(x,t)w(x,t)-M(x+dx)w(x+dx,t) \tag{2.37}$$

Where, $M(x,t)$	=	mass flow of the falling film.	(kg/s)
$w(x,t)$	=	dry matter concentration of the falling film.	(kg/kg)
v_e	=	velocity of the falling film liquid.	(m/s)
$A(x,t)$	=	cross sectional fluid flow area of the falling film.	(m^2)

With the assumption of a constant falling film velocity the mass flow is given in terms of the fluid density and the film cross sectional area (i.e., $M(x,t)=\rho(x,t)A(x,t)v_e$). The mass and dry matter balances can therefore be simplified to the following.

$$\frac{1}{v_e}\frac{\partial M(x,t)}{\partial t}+\frac{\partial M(x,t)}{\partial x}=\frac{\partial M_{evap}(x,t)}{\partial x}, \qquad \frac{1}{v_e}\frac{\partial [M(x,t)w(x,t)]}{\partial t}+\frac{\partial [M(x,t)w(x,t)]}{\partial x}=0 \qquad (2.38)$$

The mass flow of evaporation from the infinitesimal element ($\frac{\partial M_{evap}(x,t)}{\partial x}$) can be determined by making an energy balance around the element. There is an accumulation of enthalpy in the section ($dx\frac{\partial[\rho(x,t)A(x,t)C_p(w(x,t))T_{film}(x,t)]}{\partial t}$), a flow of heat from the evaporator shell ($dq(x,t)$), a net flow of enthalpy (i.e., $M(x,t)C_p(w(x,t))T_{film}(x,t)$-$M(x+dx,t)C_p(w(x+dx,t))T_{film}(x+dx,t)$) due to the mass flows to and from the section and a flow of latent enthalpy due to the evaporation of water ($(\lambda+C_{pwater})dM_{evap}(x,t)$). Here we have taken the heat capacity as a function of the milk dry matter concentration (i.e., $C_{pmilk}=C_{pwater}-C_{pTS}.w$). An important part of the equation is the difference in the heat capacity between the milk and the evaporating vapour.

$$dx\frac{\partial[\rho(x,t)A(x,t)C_p(w(x,t))T_{film}(x,t)]}{\partial t}=dq(x,t)+M(x,t)C_p(w(x,t))T_{film}(x,t) \qquad (2.39)$$
$$-M(x+dx,t)C_p(w(x+dx,t))T_{film}(x+dx,t)-(\lambda+C_{pwater}T_{film}(x,t))dM_{evap}(x,t)$$

Where, $C_p(w(x,t))$	=	heat capacity of the milk solution.	(J/kg.°C)
C_{pwater}	=	heat capacity of water.	(J/kg.°C)
$T_{film}(x,t)$	=	temperature of the falling film.	(°C)
λ	=	latent heat of vaporisation.	(J/kg)

The temperature of the falling film is not the same as that of the evaporator effect, because of the milk boiling point elevation. The milk dry matter content causes it to have a lower free energy and so it boils at a slightly higher temperature. We can determine the falling film temperature from the addition of the evaporator effect temperature and the boiling point elevation (i.e., $T_{film}=T_e+\Delta T_{bpe}$). The functional form of the boiling point elevation is investigated in Appendix A (i.e., $\Delta T_{bpe}=\frac{R.T_e^2}{\lambda}\frac{b_{TS}.w_{TS}}{[1+(b_{TS}-1)w_{TS}]}$).

Equation (2.39) can be rearranged to the following, which gives the mass flow of evaporation derivative required in equation (2.38). Here we have taken the evaporating overall heat transfer coefficient as a function of the milk dry matter concentration.

$$\frac{1}{v_e}\frac{\partial[M(x,t)C_p(w(x,t))T_{film}(x,t)]}{\partial t}+\frac{\partial[M(x,t)C_p(w(x,t))T_{film}(x,t)]}{\partial x}= \\ U_s(w(x,t))\pi.d.n.\Delta T(x,t)-(\lambda+C_{pwater}.T_{film}(x,t))\frac{\partial M_{evap}(x,t)}{\partial x} \quad (2.40)$$

Where, $U_s(w(x,t))$ = evaporating overall heat transfer coefficient. ($W/m^2.°C$)
d = diameter of the evaporator tubes. (m)
n = number of evaporator tubes. (-)

The differential in (2.40) can be expanded and (2.38) substituted to produce the following. We have used the linear relationship between the milk heat capacity and dry matter concentration.

$$M(x,t)(C_{pwater}-C_{pTS}.w(x,t))\left[\frac{1}{v_e}\frac{\partial T_{film}(x,t)}{\partial t}+\frac{\partial T_{film}(x,t)}{\partial x}\right]=U_s(w(x,t))\pi.d.n.\Delta T(x,t)-\lambda\frac{\partial M_{evap}(x,t)}{\partial x} \quad (2.41)$$

We will now assume that the left hand side of this equation is zero. This assumption is equivalent to the assumption of negligible thermal inertia in the falling film. When heat flows into the falling film, it causes no increase in the film temperature, but rather an instantaneous increase in the latent evaporation. This assumption then produces equation (2.42), which is substituted into equation (2.38), to produce equation (2.43).

$$\lambda\frac{\partial M_{evap}(x,t)}{\partial x}=U_s(w(x,t))\pi.d.n[T_s(t)-T_e(t)] \quad (2.42)$$

$$\frac{1}{v_e}\frac{\partial M(x,t)}{\partial t}+\frac{\partial M(x,t)}{\partial x}=\frac{U_s(w(x,t))\pi.d.n[T_s(t)-T_e(t)]}{\lambda} \quad (2.43)$$

The total evaporator tube heat flow is determined by the integral of the infinitesimal heat flows ($dq(x,t)$) over the length of the evaporator tube. When the boiling point elevation is neglected this is given by equation (2.44).

$$q_{shell}=\int_0^L U_s(w(x,t))\pi.d.n[T_s(t)-T_e(t)]dx \quad (2.44)$$

Where, L = length of the falling film tubes. (m)

The evaporating overall heat transfer coefficient depends on the milk dry matter concentration. This means that the infinitesimal heat transfer ($dq(x,t)$) changes along the length of the falling film. The functional relationship between the heat transfer coefficient and the dry matter is investigated in Appendix BII. However, the effect on the partial differential equations will not be investigated here. The dynamic falling film evaporator model is required for controllability

studies and a sophisticated model is of little advantage. As a result, we will simplify the partial differential equations by assuming a uniform heat flow along the length of the falling film. This allows us to combine equation (2.42) and (2.44) to produce the following (i.e., $\frac{\partial M_{evap}(x,t)}{\partial x} = \frac{U_s(w(x,t)).\pi.d.n.\Delta T(t)}{\lambda} = \frac{q_{shell}(t)}{\lambda.L}$).

$$\frac{1}{v_e}\frac{\partial M(x,t)}{\partial t}+\frac{\partial M(x,t)}{\partial x}+\frac{1}{\lambda.L}q_{shell}(t)=0 \qquad (2.45)$$

This can be transformed into the Laplace Domain to produce equation (2.46).

$$\frac{dM(x,s)}{dx}+\frac{s}{v_e}M(x,s)+\frac{1}{\lambda.L}q_{shell}(s)=0 \qquad (2.46)$$

Equation (2.46) can be integrated with the boundary conditions (i.e., $M(x,s)=M_e(s),@\,x=L$ and $M(x,s)=M_d(s),@\,x=0$) to produce equation (2.47). This is where the assumption of a uniform heat flow is important. Since the heat flow is uniform it is independent of the distance x and it is a simple matter to integrate equation (2.46).

$$M_e(s)=M_d(s)e^{-\tau_e.s}-\frac{\left[1-e^{-\tau_e.s}\right]}{\lambda.\tau_e.s}q_{shell}(s) \qquad (2.47)$$

Where, τ_e = residence time of the falling film. (s)

This transfer function is equivalent to a differential equation with delayed variables. By transformation into the time domain we produce equation (2.48).

$$M_e(t)=M_d(t-\tau_e)-M_{tubes}(t), \qquad \tau_e\frac{dM_{tubes}(t)}{dt}=\frac{1}{\lambda}[q_{shell}(t)-q_{shell}(t-\tau_e)] \qquad (2.48)$$

A similar method can be used with the dry matter partial differential equation to produce equation (2.49).

$$M_e(t).w_e(t)=M_d(t-\tau_e).w_d(t-\tau_e) \qquad (2.49)$$

Where, M_e = mass flow of milk from the bottom of the falling film. (kg/s)

w_e = dry matter of milk from the bottom of the falling film. (kg/kg)

These equations are the same as those of Quaak and Gerritsen (1990). It is important to recognise that the assumption of uniform heat flow does not require a constant heat transfer coefficient. This can be made a function of the dry matter by some appropriate functional form (i.e., the average of the dry matters at the falling film top and bottom). However, there is no 'theoretical' basis for choosing this dry matter. A better solution would be to relax the assumption of uniform heat flow and then integrate the partial differential equations.

If we now make the assumption of constant evaporating overall heat transfer coefficient, then equation (2.48) can be simplified to equation (2.50).

$$M_e(t)=M_d(t-\tau_e)-M_{tubes}(t), \qquad \frac{dM_{tubes}(t)}{dt}=\frac{U_s.A_s}{\tau_e.\lambda}\left[T_s(t)-T_s(t-\tau_e)-T_e(t)+T_e(t-\tau_e)\right] \qquad (2.50)$$

The milk from the falling film passes along a length of pipe, before entering the next evaporator pass. Depending on the length of the pipe and the fluid flow, this can cause an important delay. Dynamically this is represented by a pure delay (i.e., $w_p(t)=w_e(t-\tau_p)$), where the delay time depends on the pipe length and the fluid velocity (i.e., $\tau_p=\frac{L_p}{v_p}$). At steady state the properties are constant along the length of the pipe (i.e., $M_e^0=M_p^0$ and $w_e^0=w_p^0$). Also, the energy balance for the evaporator effect was derived with the assumption of uniform temperature throughout the effect and pipework. This means that the temperature throughout the pipework is the same as that of the effect.

The assumption of constant evaporating overall heat transfer coefficient is convenient for the simplification of the falling film partial differential equations. However, the static response of these equations is unlikely to be an accurate representation of the falling film. For the optimisation studies we are primarily concerned with the static equations and these must be very accurate. In Appendix BII the static falling film equations are solved with non-constant evaporating overall heat transfer coefficients and three falling film models produced. Later in Chapter 5 we will investigate the accuracy of these three models. The second model will be found to be the most accurate it is shown here by equation (2.51).

$$M_p=M_d-M_{tubes}, \qquad w_p=\frac{M_d.w_d}{\left[M_d-M_{tubes}\right]}, \qquad M_{tubes}=\frac{\left[U_{so}-U_{sw}.w_d\right]A_s}{\lambda}\left[T_s-T_e\right] \qquad (2.51)$$

Where, M_{tubes}	=	mass flow of evaporation in the falling film.	(kg/s)
M_d	=	mass flow of milk from the distribution plate.	(kg/s)
M_p	=	mass flow of milk from the bottom of the falling film.	(kg/s)
U_{so}	=	coefficient used in the simple film heat transfer model.	(W/m^2.°C)
U_{sl}	=	coefficient used in the simple film heat transfer model.	(W/m^2.°C)

2.4.4) Evaporator shell

MVR evaporator section

As with the evaporator effect, we use the First Law of Thermodynamics to produce a differential equation for the evaporator shell temperature. We will make a balance around the evaporator shell metal, condensed water, vapour and the MVR compressor. The compressor supplies vapour enthalpy while the condensate removes it. Heat is removed from the shell through the evaporator tubes, the evaporator shell surfaces and the preheat condenser. We shall assume that the temperature is uniform throughout the evaporator shell. With these energy and mass flows the following balance equations are produced.

$$\frac{d\left[M_{metl}.C_{pmet}.T_{sl}\right]}{dt}+\frac{d\left[M_{waterl}.C_{pwater}.T_{sl}\right]}{dt}=M_{compl}\left[C_{pwater}.T_{el}+\lambda\right]+W_{compl}-M_{scondl}.C_{pwater}.T_{sl} - q_{slossl}-q_{shellt}-q_{pcond} \quad (2.52)$$

$$\frac{dM_{waterl}}{dt}=M_{compl}-M_{scondl} \quad (2.53)$$

Where, M_{scondl} = mass flow of condensate from the evaporator shell. (kg/s)

M_{compl} = mass flow of vapour from the MVR compressor. (kg/s)

M_{waterl} = mass of water in the evaporator shell. (kg)

M_{metl} = mass of metal in the evaporator shell. (kg)

Expanding the differential in (2.52), substituting (2.53), assuming constant heat capacity and constant mass of water allows us to produce the following.

$$I_{shelll}\frac{dT_{sl}}{dt}=M_{compl}\left[C_{pwater}\left(T_{el}-T_{sl}\right)+\lambda\right]+W_{compl}-q_{slossl}-q_{shellt}-q_{pcond} \quad (2.54)$$

$$I_{shelll}=\left[M_{metl}.C_{met}+M_{waterl}.C_{pwater}\right] \quad (2.55)$$

Where, I_{shelll} = thermal inertia of the first evaporator shell. (J/K)

The surface losses heat flow is given by the standard convection heat transfer equation.

$$q_{slossl}=U_l.A_{sll}\left(T_{sl}-T_a\right) \quad (2.56)$$

If we now use the following notation we can simplify the energy balance to produce equation (2.58).

$$q_{compl}=M_{compl}.\lambda,\quad q_{condensatel}=M_{compl}.C_{pwater}\left(T_{sl}-T_{el}\right) \quad (2.57)$$

$$I_{shell1}\frac{dT_{s1}}{dt} = q_{comp1} + W_{comp1} - q_{sloss1} - q_{shellt} - q_{pcond} - q_{condensate1} \tag{2.58}$$

Where, W_{comp1} = power supplied by the compressor. (W)

q_{sloss1} = surface energy loss heat flow for the MVR evaporator shell. (W)

q_{pcond} = heat flow through the preheat condenser. (W)

$q_{condensate1}$ = net enthalpy exiting with the condensed shell water. (W)

TVR evaporator shell

Here we want to derive a differential equation for the TVR evaporator shell temperature. The TVR compressor supplies steam enthalpy, as does the compressed vapour and enthalpy is removed in the condensate flow from the shell. Heat is removed by surface losses and also through the evaporator effect tubes. With these energy and mass flows we can produce equations (2.59) and (2.60).

$$\frac{d\left[M_{met2}.C_{pmet}.T_{s2}\right]}{dt} + \frac{d\left[M_{water2}.C_{pwater}.T_{s2}\right]}{dt} = M_{comp2}\left[C_{pwater}.T_{e2} + \lambda\right] + m_{steam}.h_{steam} - M_{scond2}.C_{pwater}.T_{s2} - q_{sloss2} - q_{shell6} \tag{2.59}$$

$$\frac{d\left[M_{water2}\right]}{dt} = M_{comp2} + m_{steam} - M_{scond2} \tag{2.60}$$

Where, m_{steam} = mass flow of steam to the TVR compressor. (kg/s)

h_{steam} = enthalpy of steam supplied to the TVR compressor. (J/kg)

M_{scond2} = mass flow of condensed steam from the shell. (kg/s)

We can expand the differential in equation (2.59) and substitute equation (2.60) to produce equation (2.61). Once again we have assumed that the mass of water in the evaporator shell is constant.

$$I_{shell2}\frac{dT_{s2}}{dt} = M_{comp2}.C_{pwater}\left(T_{e2} - T_{s2}\right) + M_{comp2}.\lambda + W_{comp2} - q_{sloss2} - q_{shell6} \tag{2.61}$$

If we define the following we can simplify this equation to (2.63).

$$q_{condensate2} = M_{comp2}.C_{pwater}\left(T_{s2} - T_{e2}\right), \qquad W_{comp2} = \left[h_{steam} - C_{pwater}.T_{s2}\right]m_{steam} \tag{2.62}$$

$$I_{shell2}\frac{dT_{s2}}{dt} = q_{comp2} + W_{comp2} - q_{sloss2} - q_{shell6} - q_{condensate2} \tag{2.63}$$

Where, q_{comp2} = latent energy of vapour to compressor. (W)

W_{comp2} = net steam enthalpy to the compressor. (W)

2.4.5) Compressors

The MVR compressor map describes the relationship between the compressor speed, shell pressure and effect pressure, the work done by the compressor and the flow of compressed vapour. We have taken the compressor speed N_{comp} to be a manipulated variable, though in practice one must manipulate the power supplied to the motor driving the compressor fan and use a feedback control loop to track desired fan speeds. We are assuming that this loop has a high bandwidth and that we can effectively manipulate N_{comp}. The compressor map is described implicitly by the following pair of non-linear algebraic equations. The parameters a_{comp} through f_{comp} are coefficients, which are used to fit the MVR compressor map.

$$\frac{[P_s - P_e]}{\rho_{ve}} = a_{comp}.N_{comp}^{\ 2} + b_{comp}.N_{comp}.Q_{comp} + c_{comp}.Q_{comp}^{\ 2} \tag{2.64}$$

$$\frac{W_{comp}}{\rho_{ve}} = d_{comp}.N_{comp}^{\ 2}.Q_{comp} + e_{comp}.N_{comp}.Q_{comp}^{\ 2} + e_{comp}.Q_{comp}^{\ 3} \tag{2.65}$$

Where, Q_{comp} = volumetric flow of compressed vapour. (m^3/s)
N_{comp} = MVR compressor speed. (rpm)
W_{comp} = electric power supplied to the MVR compressor. (W)
P_s = pressure at the outlet of the MVR compressor. (Pa)
P_e = pressure at the inlet of the MVR compressor. (Pa)
ρ_{ve} = density of the inlet vapour to the MVR compressor. (kg/m^3)

These compressor equations are empirical, although their form can be derived. The nature of the MVR compressor is essentially the same as a centrifugal pump. Various equations have been derived for these pumps but the following is the most general (Fox, 1977). This is derived for an incompressible fluid and so it is not completely applicable for an MVR compressor. However, if we define the pressure head by the conventional method (i.e., $H = \frac{\Delta P}{\rho.g}$), then it produces equation (2.66).

$$H = A.N^2 - B.N.Q - C.Q^2 \tag{2.66}$$

Where, H = the heat imposed on the fluid. (m)
N = pump speed. (rpm)
Q = volumetric flow pumped. (m^3/s)

The compressor power supply is given by equation (2.67) (Smith and van Ness, 1987). This is derived by making an isentropic enthalpy balance around the compressor.

$$W_{comp} = \frac{C_p.P_1}{R.\rho_1}\left[1-\left(\frac{P_2}{P_1}\right)^{\frac{R}{C_p}}\right]M_{comp} \qquad (2.67)$$

Where, W_{comp} = power required to compress the fluid. (W)

C_p = heat capacity of the fluid. (J/kg.K)

P_1 = inlet pressure to the compressor. (Pa)

P_2 = outlet pressure from the compressor. (Pa)

However, for small pressure differences, equation (2.67) can be simplified to equation (2.68). Using equation (2.68) and equation (2.64) we can determine equation (2.69) for the compressor power supply.

$$W_{comp} = \Delta P.Q_{comp} \qquad (2.68)$$

$$\frac{W_{comp}}{\rho_{ve}} = \frac{\Delta P}{\rho_{ve}}Q_{comp} = a_{comp}.N_{comp}^2.Q_{comp} + b_{comp}.N_{comp}.Q_{comp}^2 + c_{comp}.Q_{comp}^2 \qquad (2.69)$$

Where, ΔP = pressure difference between the compressor inlet and outlet. (Pa)

In reality the compressor is not an isentropic process. It contains inefficiencies and this means that equation (2.69) is not an accurate equation for the compressor power supply. However, its general form can be used to describe a compressor. The parameters a_{comp}, b_{comp} and c_{comp} are replaced by the parameters d_{comp}, e_{comp} and f_{comp}.

The above arguments are not meant to provide proof of the compressor equations. They provide some basis for the equations (2.64) and (2.65), but it is difficult to derive an accurate model for a compressor from first principles. As a result, we have taken the general equations (2.64) and (2.65), then fitted them to the compressor characteristic curves. These curves were supplied by the manufacturers. The equations provide a good fit and the resulting compressor parameters are then determined (i.e., $a_{comp} = 0.00168$ m^2/s^2.rpm^2, $b_{comp} = 0.415$ m^{-1}.s^{-1}.rpm^{-1}, $c_{comp} = -13.67$ m^{-4}, $d_{comp} = 0.00684$ m^2/s^2.rpm^2, $e_{comp} = -0.021$ m^{-1}.s^{-1}.rpm^{-1} and $f_{comp} = -3.09$ m^{-4}). We have assumed that the vapour/liquid mixtures in the evaporator effect and shell are saturated. The vapour pressure and densities are then calculated from Antoine equations, which are discussed and developed in Appendix A.

$$\ln(P_e) = A_{water} - \frac{B_{water}}{[T_e - C_{water}]}, \qquad \ln(\rho_{ve}) = A_{vap} - \frac{B_{vap}}{[T_e - C_{vap}]} \qquad (2.70)$$

The TVR compressor model is developed and discussed in Appendix D. We are concerned with predicting the mass flow of raw steam supplied and vapour compressed by the compressor. The mass flow of raw steam is dependent on the steam supply pressure :

$$M_{steam} = A_{TVR}.P_{st}, \qquad W_{comp} = \left[h_{steam} - C_{pwater}.T_{s2}\right]A_{TVR}.P_{st} \tag{2.71}$$

Where, M_{steam} = mass flow of raw steam to the TVR compressor. (kg/s)
h_{steam} = enthalpy of saturated raw steam supplied to the TVR. (J/kg)
A_{TVR} = TVR compressor parameter. (m.s)

The mass flow of compressed evaporated steam is given by the following :

$$M_{comp} = \frac{A_{TVR}.B_{TVR}.P_{e,2}.P_{st}}{P_{st}^{C_{TVR}}}, \qquad q_{comp} = \frac{\lambda.A_{TVR}.B_{TVR}.P_{e,2}.P_{st}}{P_{st}^{C_{TVR}}} \tag{2.72}$$

Where, M_{comp} = mass flow of evaporated vapour. (kg/s)
B_{TVR} = TVR compressor parameter. ($m^{0.03}.s^{0.06}/kg^{0.03}$)
C_{TVR} = TVR compressor parameter. (-)

2.5) Conclusions

At the start of this Chapter we separated the Evaporator A plant into four sections. These were the MVR evaporator, the TVR evaporator, the DSI preheat and the preheat plate heat exchanger sections. The primary purpose of this Chapter was to derive models for the MVR evaporator and TVR evaporator sections. In the following Chapter we will derive models for the DSI unit preheat, preheat plate heat exchanger and the shell/tube condenser. The combination of the models for each of these four sections will then provide the complete model for the Evaporator A plant.

In Section 2.3 the MVR and TVR evaporator sections were described and the position of the distribution plates, evaporator effect, shell, condenser and compressors discussed. The MVR and TVR evaporator sections contain several parts that are essentially the same. For example the distribution plates and falling films are essentially the same through the plant. General models for the distribution plate and falling films have been developed in this Chapter. However, the evaporator effect and evaporator shells contain some subtle differences, which meant it was better to model these individually.

In Section 2.4 models for the component parts of the MVR and TVR evaporator sections were derived. We considered first the general distribution plate model. Following this the evaporator effect, falling film and evaporator shell models were each derived. Considerable attention was focused on the difficult falling film model. In the final part of Section 2.4 we developed models for the MVR and TVR compressors.

Chapter 3 : Modelling Evaporator Preheat and Heat Exchangers

3.1) Introduction

At the start of Chapter 2 we separated the Kiwi Co-op Dairies Evaporator A plant into four sections (i.e., MVR evaporator, TVR evaporator, DSI unit preheat section and preheat plate heat exchanger). The primary aim of Chapter 2 was to derive models for the MVR evaporator and TVR evaporator sections. In this Chapter we aim to derive models for the DSI preheat section, the preheat plate heat exchanger and the shell/tubes condensers. With the completion of these models we will have a complete model of the Evaporator A plant.

Firstly, we will consider the DSI preheat section. In Section 3.2, we derive the equations for the preheat section temperatures and mass flows. We shall also show how to incorporate the effect of air in the flash vessel temperature differential equations. However, we will be mostly concerned with deriving two models for the complete DSI preheat section. The 'Simple' model will be derived by neglecting the presence of air and assuming constant mass flows around the flash vessels. This 'Simple' model will be used to develop the linear dynamic model in Chapter 4. A second ' Advanced' model will also neglect the presence of air, but it will include the changes in mass flow around the flash vessels. This model will be used to develop the steady state model for the entire Evaporator A plant in Chapter 4.

The plate heat exchanger and condenser models will be derived in Section 3.3. The condenser model is simpler than the plate heat exchanger, so it will be considered first. A generic dynamic condenser model will be developed, but the condenser distributed parameter nature will present some difficulties. We will solve this problem by transforming the condenser partial differential equations into simple finite order ordinary differential equations with delays.

Finally the plate heat exchanger model will be derived. A dynamic heat exchanger model will be derived by the transformation of the heat exchanger partial differential equations. The result will be a set of transfer functions describing the heat exchanger outlet temperatures. However, these transfer functions do not represent finite order linear constant coefficient ordinary differential equations. This presents a major difficulty because most standard dynamic analysis is based on these differential equations. As a result, it is difficult to analyse the dynamic heat exchanger model or combine it with the rest of the Evaporator A plant dynamic models. We will overcome this problem by using numerical analysis methods. The static heat exchanger equations will also be derived.

3.2) DSI Preheat Section

3.2.1) Introduction

It is common practice, in the NZ dairy industry, for evaporator plants to contain a preheat section. These are used to provide controlled heat treatment for bacterial destruction and whey protein de-naturation (Fergusson, 1989). Figure 3-1 shows the Preheat system of the Kiwi Evaporator A plant. The direction steam injection (DSI) unit and flash vessels provide fast, direct contact milk heating, which rapidly brings the milk to the required DSI soak temperature. The required heat treatment is then regulated by the holding tube length and milk flowrate. Upon exiting the holding tubes the milk passes into a flash vessel where it is flashed by pressure reduction. The flashed vapour then condenses by direct contact with the cold feed milk in the top of the flash vessel. This direct passage of latent heat from the hot treated milk provides an energy recycle, which reduces the amount of steam required in the DSI unit. It is common to use multiple flash vessels in series to improve the energy recycle, as shown in Figure 3-1.

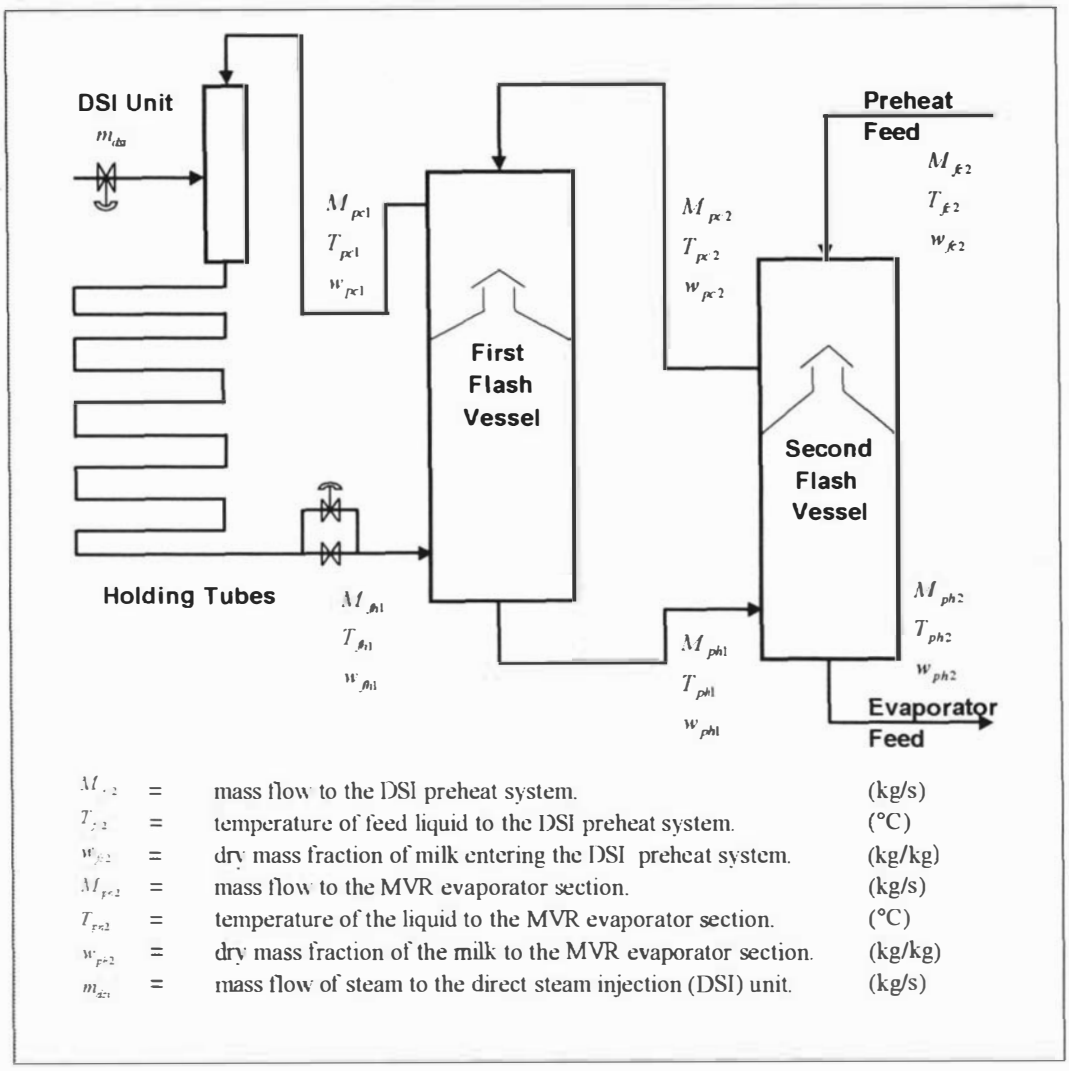

Figure 3-1 : DSI preheat section of Evaporator A plant.

Figure 3-1 shows a preheat system that consists of two flash vessels. There is a milk feed flow (M_{fc2}) to the system with a temperature (T_{fc2}). The DSI temperature (T_{DSI}) is a controlled variable and the mass flow of steam (m_{dsi}) is a manipulated variable. Commonly the mass flow of steam is regulated by manipulation of a control valve. The preheat system has an output flow of milk (M_{ph2}) with temperature (T_{ph2}) that can act as a disturbance to the evaporator.

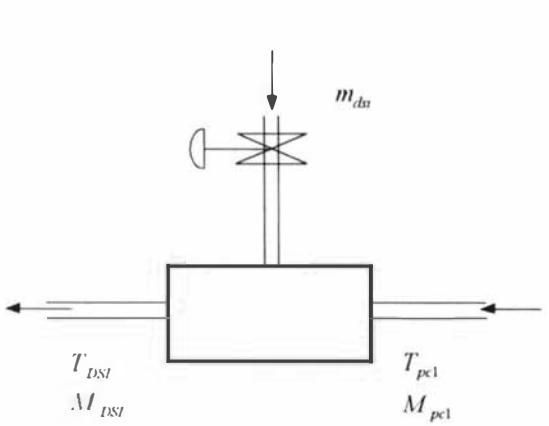

Figure 3-2 : A typical Direct Steam Injection (DSI) unit.

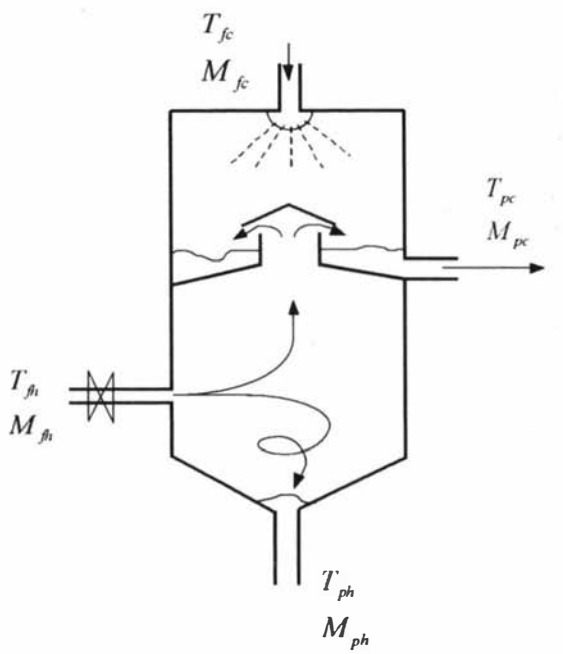

Figure 3-3 : A typical flash/infusion vessel.

3.2.2) DSI / holding tubes

The DSI unit is an instantaneous liquid/steam direct contact vessel and it is shown in Figure 3-2. If we make the assumption of a homogenous DSI unit with no heat losses, we can produce the following equations for the mass of milk, the dry matter and the temperature of the DSI unit. As in Chapter 2, we have used a linear model between the milk heat capacity and dry matter concentration (i.e., $C_p = C_{pwater} - C_{pTS}.w$).

$$\frac{d\left[M_{met}.C_{pmet}.T_{DSI} + M_{milk}\left(C_{pwater} - C_{pTS}.w_{DSI}\right)T_{DSI}\right]}{dt} = M_{pc1}\left(C_{pwater} - C_{pTS}.w_{pc1}\right)T_{pc1} - M_{DSI}\left(C_{pwater} - C_{pTS}.w_{DSI}\right)T_{DSI} + h_{steam}.m_{dsi} \quad (3.1)$$

$$\frac{dM_{milk}}{dt} = M_{pc1} - M_{DSI} + m_{dsi} \quad (3.2)$$

$$\frac{d\left[M_{milk}.w_{DSI}\right]}{dt} = M_{pc1}.w_{pc1} - M_{DSI}.w_{DSI} \quad (3.3)$$

Where, M_{met} = mass of metal in the DSI unit. (kg)

M_{milk} = mass of milk in the DSI unit. (kg)

h_{steam} = enthalpy of raw steam supply. (J/kg)

m_{dsi} = mass flow of raw steam to the DSI. (kg/s)

M_{DSI} = mass flow of liquid leaving the DSI unit. (kg/s)

M_{pc1} = mass flow of liquid entering the DSI from the first flash vessel. (kg/s)

Expanding the differential in (3.1) and substituting (3.2) and (3.3), we produce the following differential equation for the DSI unit temperature.

$$I_{DSI}\frac{dT_{DSI}}{dt} = M_{pc1}\left(C_{pwater} - C_{pTS}.w_{pc1}\right)\left(T_{pc1} - T_{DSI}\right) + \left(h_{steam} - C_{pwater}.T_{dsi}\right)m_{dsi} \tag{3.4}$$

$$I_{DSI} = \left[M_{met}.C_{pmet} + M_{milk}\left(C_{pwater} - C_{pTS}.w_{DSI}\right)\right] \tag{3.5}$$

Where, I_{DSI} = thermal inertia of the DSI unit. (J/°C)

We can similarly expand the differential in (3.3) and substitute (3.2) to produce the following differential equation for the DSI unit dry matter.

$$M_{milk}\frac{dw_{DSI}}{dt} = M_{pc1}\left(w_{pc1} - w_{DSI}\right) - m_{dsi}.w_{DSI} \tag{3.6}$$

If we now assume that the mass of milk in the DSI unit is constant and negligible and that the heat capacity of milk is constant and equal to that of water, then the following equations are produced.

$$I_{DSI}\frac{dT_{DSI}}{dt} = M_{pc1}.C_{pwater}\left(T_{pc1} - T_{DSI}\right) + \left(h_{steam} - C_{pwater}.T_{dsi}\right)m_{dsi}, \qquad I_{DSI} = M_{met}.C_{pmet} \tag{3.7}$$

$$M_{DSI} = M_{pc1} + m_{dsi}, \qquad M_{DSI}.w_{DSI} = M_{pc1}.w_{pc1} \tag{3.8}$$

The holding tubes can be modelled by assuming plug flow and no heat losses to produce a simple delay equation.

$$T_{fh1} = T_{DSI}\left(t - \tau_h\right) \tag{3.9}$$

Where, τ_h = holding tube time delay. (s)

3.2.3) Flash / infusion vessels

Figure 3-3 shows a generic flash vessel. The system consists of five phases that must each be modelled separately. These are the liquid in the top, the liquid in the bottom, the vapour in the top, the vapour in the bottom and the metal of the flash vessel. A complete set of mass and energy balances for these phases produces a set of nine coupled differential equations. We shall assume that the temperature is uniform throughout the metal and liquid phases and that there are no heat losses. However, the possibility of variations in the temperature between the top and bottom of the flash vessel will be included. Then by making mass, dry matter and energy balances around the flash vessel, we can produce the following equations.

$$\frac{d\left[M_{metb}.C_{pmet}.T_{ph}+M_{milkb}.H_{ph}\right]}{dt}+\frac{d\left[M_{mett}.C_{pmet}.T_{pc}+M_{milkt}.H_{pc}\right]}{dt} = M_{fh}.H_{fh}-M_{ph}.H_{ph}+M_{fc}.H_{fc}-M_{pc}.H_{pc} \tag{3.10}$$

$$H_{ph}=\left(C_{pwater}-C_{pTS}.w_{ph}\right)T_{ph}, \qquad H_{pc}=\left(C_{pwater}-C_{pTS}.w_{pc}\right)T_{pc} \tag{3.11}$$

$$\frac{dM_{milkb}}{dt}=M_{fh}-M_{ph}-m_{evap}, \qquad \frac{dM_{milkt}}{dt}=M_{fc}-M_{pc}+m_{evap} \tag{3.12}$$

$$\frac{d\left[M_{milkb}.w_{ph}\right]}{dt}=M_{fh}.w_{fh}-M_{ph}.w_{ph}, \qquad \frac{d\left[M_{milkt}.w_{pc}\right]}{dt}=M_{fc}.w_{fc}-M_{pc}.w_{pc} \tag{3.13}$$

Where, M_{metb}	=	mass of metal in the bottom section of the flash vessel.	(kg)
M_{mett}	=	mass of metal in the top section of the flash vessel.	(kg)
M_{milkt}	=	mass of liquid milk in the top section of the flash vessel.	(kg)
M_{milkb}	=	mass of liquid milk in the bottom section of the flash vessel.	(kg)
M_{pc}	=	flow of liquid exiting from the top of the flash vessel.	(kg/s)
M_{fc}	=	flow of liquid entering at the top of the flash vessel.	(kg/s)
M_{ph}	=	flow of liquid exiting from the bottom of the flash vessel.	(kg/s)
M_{fh}	=	flow of liquid entering at the bottom of the flash vessel.	(kg/s)
m_{evap}	=	mass flow of vapour that is flashed in the bottom of the vessel.	(kg/s)
H_{ph}	=	enthalpy of the hot product from the bottom of the flash vessel.	(J/kg)
H_{pc}	=	enthalpy of the cold product from the top of the flash vessel.	(J/kg)

The mass flow of flashing (m_{evap}) is determined by making mass, dry matter and energy balances around the orifice plate preceding the flash vessel. We have assumed that the flashing is instantaneous, so that it can be modelled using static equations.

$$M_{fh}=M_{l}-m_{evap}, \qquad M_{fh}.w_{fh}=M_{l}.w_{l} \tag{3.14}$$

$$M_{fh}\left(C_{pwater}-C_{pTS}.w_{fh}\right)T_{fh}=M_{l}\left(C_{pwater}-C_{pTS}.w_{l}\right)T_{ph}+m_{evap}\left(C_{pwater}.T_{ph}+\lambda\right) \tag{3.15}$$

Where, M_l = mass flow of the milk, after flashing has occurred. (kg/s)
w_l = dry matter of the milk, after flashing has occurred. (kg/kg)
λ = latent heat of vapourisation. (J/kg)

We can solve these equations to produce the following for the mass flow of flashing.

$$m_{evap}=\frac{M_{fh}\left(C_{pwater}-C_{pTS}.w_{fh}\right)}{\lambda}\left(T_{fh}-T_{ph}\right) \tag{3.16}$$

Expanding the differential in (3.10) and substituting (3.12) and (3.13), we can produce the following for the temperatures of the flash vessel.

$$\begin{aligned} I_{flb}\frac{dT_{ph}}{dt}+I_{flt}\frac{dT_{pc}}{dt}=&M_{fh}\left(C_{pwater}-C_{pTS}.w_{fh}\right)\left(T_{fh}-T_{ph}\right)\\ &+M_{fc}\left(C_{pwater}-C_{pTS}.w_{fc}\right)\left(T_{fc}-T_{pc}\right)+m_{evap}.C_{pwater}\left(T_{ph}-T_{pc}\right)\end{aligned} \tag{3.17}$$

$$I_{flb}=\left[M_{methb}.C_{pmet}.T_{ph}+M_{milkb}\left(C_{pwater}-C_{pTS}.w_{ph}\right)\right] \tag{3.18}$$

$$I_{flt}=\left[M_{methb}.C_{pmet}+M_{milkt}\left(C_{pwater}-C_{pTS}.w_{pc}\right)\right] \tag{3.19}$$

Where, I_{flt} = thermal inertia of the top of the flash vessel. (J/K)
I_{flb} = thermal inertia of the bottom of the flash vessel. (J/K)

The above flash vessel equations provide an almost complete description of the flash vessel. The final requirement is the thermal equilibrium model between the liquid and the vapour phases (i.e., how does T_{ph} relate to T_{pc}). Here we will assume the system reaches thermal equilibrium, but we will include the impact of air. There is expected to be a reasonable amount of air in the flash vessel because the feed milk will contain dissolved air. The air in the flash vessel can be modelled by assuming that it accumulates entirely at the top of the vessel and that the steam/air mixture is ideal.

There are two forces acting on the air in the flash vessel. These are the buoyancy force and the condensation induced pressure force. The buoyancy force acts downwards because air has a greater density than steam. However, this force is small because the bulk densities of steam and air are small. As a result, the pressure difference force, due to the condensation induced removal of steam, can easily overcome the buoyancy force. Consequently the air collects at the top of the vessel, where the steam is condensing.

With the assumption of an ideal gas mixture we can produce the following equations for the partial pressures at the top and bottom of the flash vessel.

$$P_{ph}=P_{pc}+P_{air}, \quad \text{with} \quad P_{air}=P_{ph}.y_{air}, \quad \text{implies} \quad P_{pc}=P_{ph}(1-y_{air}) \tag{3.20}$$

Where, P_{ph} = pressure of steam in the bottom of the flash vessel. (Pa)
P_{pc} = partial pressure of steam in the top of the flash vessel. (Pa)
P_{air} = partial pressure of air in the top of the flash vessel. (Pa)
y_{air} = molar concentration of air in the top of the flash vessel. (mol/mol)

We will now assume a linear relationship between the saturation pressure and temperature of steam. Strictly, the Antoine equations of Chapter 2 should be used, but for small perturbations a linear relationship is accurate. Substituting this linear relationship into equation (3.20) we produce the following linear relationship between the air molar concentration and the flash vessel temperature difference.

$$P=k_1.T+k_2, \quad P_{ph}-P_{pc}=P_{ph}.y_{air}, \quad \Delta T \overset{\Delta}{=} T_{ph}-T_{pc}=\frac{P_{ph}}{k_1}y_{air} \tag{3.21}$$

Where, k_1 = linear coefficient between saturation steam temperature and pressure. (Pa/°C)
k_2 = coefficient in the steam saturation relationship. (Pa)

The above result shows that a correctly operating flash vessel, with no air, will have a uniform temperature. As a result, we can simplify equation (3.17) and produce the following differential equation for the temperature of a flash vessel.

$$I_{fl}\frac{dT_{ph}}{dt}=M_{fh}\left(C_{pwater}-C_{pTS}.w_{fh}\right)\left(T_{fh}-T_{ph}\right)+M_{fc}\left(C_{pwater}-C_{pTS}.w_{fc}\right)\left(T_{fc}-T_{ph}\right) \tag{3.22}$$

Where, I_{fl} = thermal inertia of the flash vessel. (J/K)

If we make the additional assumptions of a negligible mass of milk and identical heat capacities for milk and water, then these equations are simplified to the following.

$$I_{fl}\frac{dT_{ph}}{dt}=M_{fh}C_{pwater}\left[T_{fh}-T_{ph}\right]+M_{fc}C_{pwater}\left[T_{fc}-T_{ph}\right] \tag{3.23}$$

$$M_{pc}=M_{fc}+m_{evap}, \quad M_{ph}=M_{fh}-m_{evap}, \quad M_{pc}.w_{pc}=M_{fc}.w_{fc}, \quad M_{ph}.w_{ph}=M_{fh}.w_{fh} \tag{3.24}$$

By combining the results in equation (3.24) and (3.16) we can produce the following equations for the static mass flows from the flash vessel. The constant a is expected to be small, because of the relative sizes of the heat capacity and latent heat of vaporisation. As a result, the product

mass flows are not expected to be very different from the feed mass flows. This observation is the basis of an important simplification to the flash vessel equations, which we now discuss.

$$M_{pc}=M_{fc}+M_{fh}.a, \qquad M_{ph}=M_{fh}[1-a], \qquad a=\frac{m_{evap}}{M_{fh}}=\frac{\left(C_{pwater}-C_{pTS}.w_{fh}\right)}{\lambda}\left(T_{fh}-T_{ph}\right) \qquad (3.25)$$

Where, a = ratio of m_{evap} to M_{fh}. (-)

3.2.4) 'Simple' and 'Advanced' models

We can further simplify the above DSI unit and flash vessel models by assuming that no air is present, the heat capacity of milk is equal to that of water and that the ratio of vapour to liquids flows is small (i.e., $m_{evap} << M_{fc2}$). This assumption of small vapour flows was discussed earlier and is based on the results in equation (3.25). With these assumptions we can produce the following differential equations for the temperature of a flash vessel and the DSI unit. We will call these equations the 'Simple' model for a preheat section, whereas the model which includes the variation in the mass flows around the flash vessels will be called the 'Advanced' model.

$$I_{fl}\frac{dT_{ph}}{dt}=M_{fc2}.C_{pwater}\left(T_{fc}+T_{fh}-2.T_{ph}\right), \qquad M_{fc}=M_{pc}=M_{fh}=M_{ph}, \qquad T_{pc}=T_{ph} \qquad (3.26)$$

$$I_{DSI}\frac{dT_{DSI}}{dt}=M_{fc2}.C_{pwater}\left(T_{pc1}-T_{DSI}\right)+\left[h_{steam}-C_{pwater}.T_{DSI}\right]m_{dsi} \qquad (3.27)$$

Using this equation we can produce the following generic static equation for the temperature of a flash vessel in a preheat system containing n flash vessels. For example Figure 3-1 shows a preheat system with two flash vessels (i.e., n = 2) and the exogenous variables T_{fc2} and T_{DSI}. The subscript i represents the position of the flash vessel in the preheat system. For example i = 1 represents the flash vessel by the DSI whereas $i = n$ represents the flash vessel that supplies the feed to the evaporator.

$$T_{ph,i}=T_{pc,i}=\left[\frac{n-i+1}{n+1}\right]T_{DSI}+\left[\frac{i}{n+1}\right]T_{fcn} \qquad (3.28)$$

Where, T_{DSI} = temperature of the DSI unit. (°C)

T_{fcn} = temperature of the feed milk to the DSI unit preheat system. (°C)

We can use (3.25) to determine the temperatures of the first and last flash vessels in a preheat system.

$$T_{ph1}=T_{pc1}=\left[\frac{n}{n+1}\right]T_{DSI}+\left[\frac{1}{n+1}\right]T_{fcn}, \qquad T_{phn}=T_{pcn}=\left[\frac{1}{n+1}\right]T_{DSI}+\left[\frac{n}{n+1}\right]T_{fcn} \qquad (3.29)$$

The configuration shown in Figure 3-1 provides a simple example of the application of these equations.

$$T_{ph1}=\frac{2}{3}T_{DSI}+\frac{1}{3}T_{fc2}, \qquad T_{ph2}=\frac{1}{3}T_{DSI}+\frac{2}{3}T_{fc2} \tag{3.30}$$

3.3) Heat Exchangers

3.3.1) Condenser model

The Kiwi Evaporator A plant contains two shell and tube condensers. The first is attached to the MVR evaporator shell and uses feed milk inside and condensing steam on the outside of the tubes. The second is attached to the third effect and uses cooling water inside and condensing steam on the outside of the tubes. Figure 3-4 shows a generic condenser with the process inputs and outputs. The inputs are the inlet liquid temperature (T_{cond1}), liquid flow (M_{cond}) and the condenser shell temperature (T_{sh}). The outputs are the outlet liquid temperature (T_{cond2}) and the condenser tube heat flow (q_{cond}).

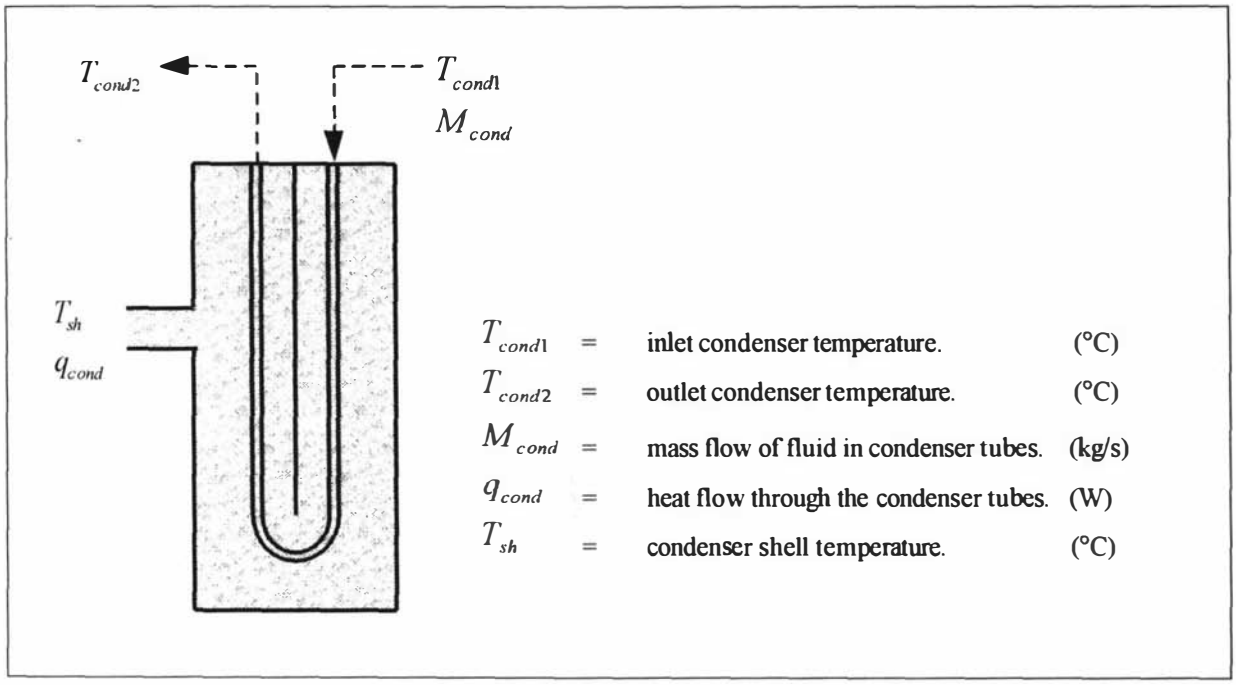

Figure 3-4 : A shell and tube condenser.

Complete model

The condenser model is developed by making energy balances around infinitesimal cross sections of the condenser tubes. The temperature of the liquid in the tubes ($T_{cond}(x,t)$) varies with distance along the condenser tubes and time. Assuming plug flow, constant liquid density/heat capacity with respect to temperature and no heat losses we can derive the following partial differential equations for the condenser liquid temperature. The condenser heat flow is given by the integral of the heat flow along the total tube length.

$$\frac{\partial T_{cond}(x,t)}{\partial t}+v_{cond}(t)\frac{\partial T_{cond}(x,t)}{\partial x}=\frac{h_i(t).A_{cond}}{\rho_{cond}.C_{pcond}.V_{cond}}[T_w(t)-T_{cond}(x,t)] \tag{3.31}$$

$$\frac{\partial T_w(x,t)}{\partial t}=\frac{h_o(t).A_{cond}}{\rho_w.C_{pw}.V_w}[T_{sh}(t)-T_w(x,t)]-\frac{h_i(t).A_{cond}}{\rho_w.C_{pw}.V_w}[T_w(t)-T_{cond}(x,t)] \tag{3.32}$$

$$q_{cond}=q_{condo}=\int_0^L h_o.\pi.D_{cond}.n_{cond}[T_{sh}(t)-T_w(x,t)]dx,\quad q_{condi}=\int_0^L h_i.\pi.D_{cond}.n_{cond}[T_w(t)-T_{cond}(x,t)]dx \tag{3.33}$$

Where, T_{sh} = temperature of the condenser shell. (°C)

T_{cond} = temperature of liquid in condenser tubes. (°C)

T_w = temperature of condenser tube wall. (°C)

q_{condo} = heat flow from the condensing steam to the condenser tubes. (W)

q_{condi} = heat flow from the condenser tubes to the condenser liquid. (W)

h_o = heat transfer coefficient from condensing steam to tubes. (W/m^2.K)

h_i = heat transfer coefficient from condenser tubes to liquid. (W/m^2.K)

v_{cond} = velocity of the water in the condenser tubes. (m/s)

The condenser steady state equations are given by solving simple first order differential equations. The superscript ^{0} has been used in the condenser equations to denote the static value for the variable. For example, T^0_{condl} refers to the static version of the inlet liquid temperature to the generic condenser.

$$T_{cond}(x)=T^0_{sh}-(T^0_{sh}-T^0_{condl})e^{\left(-\frac{x}{v_{cond}.\tau_{Tc0}}\right)},\qquad T^0_{cond2}=T^0_{sh}-(T^0_{sh}-T^0_{condl})e^{\left(-\frac{\tau_c}{\tau_{Tc0}}\right)} \tag{3.34}$$

$$T_w(x)=T_{sh}-\frac{\tau_o}{[\tau_i+\tau_o]}(T_{sh}-T_{condl})e^{\left(-\frac{x}{v_{cond}.\tau_{Tc0}}\right)},\quad q_{cond}=q_{condi}=q_{condo}=C_{pcond}M_{cond}[T_{sh}-T_{condl}]\left[1-e^{\left(-\frac{\tau_c}{\tau_{Tc0}}\right)}\right] \tag{3.35}$$

The constants $\tau_i=\frac{\rho_w.C_{pw}.V_w}{h_i.A_{cond}}$, $\tau_w=\frac{\rho_w.C_{pw}.V_w}{[h_i+h_o]A_{cond}}$, $\tau_{Tc}=\frac{\rho_{cond}.C_{pcond}.V_{cond}}{h_i.A_{cond}}$, $\tau_{Tc0}=\frac{\rho_{cond}.C_{pcond}.V_{cond}}{U_{cond}.A_{cond}}$, $\tau_o=\frac{\rho_w.C_{pw}.V_w}{h_o.A_{cond}}$ occur in the dynamic equations for the condenser. The condenser partial differential equations are non-linear. However, they can be transformed into constant coefficient equations by linearisation. This method has been used by many literature sources (Mozley, 1956; Lim, 1970; Stermole and Larson, 1964; Koppel, 1962) to produce the following constant coefficient partial differential equations. Rather than taking the fluid mass

flow, we have taken the fluid velocity as a process input. The fluid velocity is determined from the mass flow by division (i.e., $v_{cond} = \frac{M_{cond}}{\rho_{cond} \cdot A_{cr}}$).

$$\frac{\partial T_{cond}(x,t)}{\partial t} + v^0_{cond} \frac{\partial T_{cond}(x,t)}{\partial x} + \left[\frac{\partial T_{cond}(x,t)}{\partial x}\right]^0 v_{cond}(t) = \frac{h_i(t).A_{cond}}{\rho_{cond}.C_{pcond}.V_{cond}}[T_w(t) - T_{cond}(x,t)] \quad (3.36)$$

$$\frac{\partial T_w(x,t)}{\partial t} = \frac{h_o.A_{cond}}{\rho_w.C_{pw}.V_w}[T_{sh}(t) - T_w(x,t)] - \frac{h_i(t).A_{cond}}{\rho_w.C_{pw}.V_w}[T_w(t) - T_{cond}(x,t)] \quad (3.37)$$

Substituting the equations for the static temperature and the heat transfer coefficient, in terms of the fluid velocity ($h_i = h_b.v^b_{cond}$), we can produce the following equations :

$$\frac{\partial T_{cond}(x,t)}{\partial t} + v^0_{cond} \frac{\partial T_{cond}(x,t)}{\partial x} = \frac{1}{\tau_{Tc}} T_w(t) - \frac{1}{\tau_{Tc}} T_{cond}(x,t) + \frac{\left[h^0_i - 1\right]}{v^0_{cond}.\tau_{Tc0}}\left(T^0_{sh} - T^0_{cond1}\right) e^{-\frac{x}{v^0_{cond}.\tau_{Tc0}}} v_{cond}(t) \quad (3.38)$$

$$\frac{\partial T_w(x,t)}{\partial t} = \frac{1}{\tau_o} T_e(t) - \frac{1}{\tau_o} T_w(x,t) - \frac{1}{\tau_i} T_w(x,t) + \frac{1}{\tau_i} T_{cond}(x,t) - \frac{h^0_i}{v^0_{cond}\left[\tau_o + \tau_i\right]}\left(T^0_{sh} - T^0_{cond1}\right) e^{-\frac{x}{v^0_{cond}.\tau_{Tc0}}} v_{cond}(t) \quad (3.39)$$

Transformation of these equations into the Laplace Domain produces the following differential equation.

$$\frac{dT_{cond}(x,s)}{dx} + H_1(s).T_{cond}(x,s) = H_2(s).T_{sh}(s) + H_3(s).e^{-\frac{x}{v^0_{cond}.\tau_{Tc}}}.v_{cond}(s) \quad (3.40)$$

Where the transfer functions $H_1(s), H_2(s)$ and $H_3(s)$ are given by the following :

$$H_1(s) = \frac{1}{v^0_{cond}.\tau_{Tc0}}\left[\tau_{Tc0}.s + \frac{(\tau_o.s+1)}{(\tau_w.s+1)}\right], \qquad H_2(s) = \frac{1}{v^0_{cond}.\tau_{Tc0}[\tau_w.s+1]} \quad (3.41)$$

$$H_3(s) = \frac{\left[T^0_{sh} - T^0_{cond1}\right]}{\left(v^o_{cond}\right)^2 \tau_{Tc0}}\left[h^0_i - 1 - \frac{\tau_0.h^0_i}{(\tau_o + \tau_i)(\tau_w.s+1)}\right] \quad (3.42)$$

This differential equation can be solved by integration to produce the following transfer function for the outlet condenser temperature :

$$T_2(s) = \frac{H_2(s)}{H_1(s)}\left[1 - e^{-H_1(s)L}\right]T_{sh}(s) + e^{-H_1(s)L}T_1(s) + \frac{H_3(s)}{\left[H_1(s) - \frac{1}{\tau_{Tc0}.v^{\bullet}_{cond}}\right]}\left[e^{-\frac{\tau_c}{\tau_{Tc0}}} - e^{-H_1(s)L}\right]v_{cond}(s) \quad (3.43)$$

The heat flows through the condenser wall can be differentiated to produce the following differential equations.

$$\frac{dq_{condo}(t)}{dt} = h_o . A_{cond} \frac{dT_{sh}(t)}{dt} - \frac{1}{\tau_o} q_{condo}(t) + \frac{1}{\tau_0} q_{condi}(t) \tag{3.44}$$

$$\frac{dq_{condi}(t)}{dt} = \frac{1}{\tau_i} q_{condo}(t) - \left[\frac{1}{\tau_i} + \frac{1}{\tau_{Tc}}\right] q_{condi}(t) + \frac{h_i . A_{cond}}{\tau_c} [T_{cond2}(t) - T_{cond1}(t)] \tag{3.45}$$

Simple model

The above solution accommodates many mechanisms but it is also relatively complex. A considerably simpler solution can be obtained by assuming constant overall heat transfer coefficients and infinite condensation heat transfer coefficient (i.e., $T_w = T_{sh}$, or $\tau_{Tc} = \tau_{Tc0}$). This produces the following partial differential equation for the temperature of the liquid in the condenser tubes.

$$\frac{\partial T_{cond}(x,t)}{\partial t} + v_{cond}(t) \frac{\partial T_{cond}(x,t)}{\partial x} = \frac{U_{cond} . A_{cond}}{\rho_{cond} . C_{pcond} . V_{cond}} [T_{sh}(t) - T_{cond}(x,t)] \tag{3.46}$$

Where, T_{cond} = temperature of the liquid in the condenser tubes. (°C)

T_{sh} = temperature of the condenser shell. (°C)

v_{cond} = velocity of the liquid in the condenser tubes. (m/s)

A_{cond} = heat transfer surface area. (m^2)

V_{cond} = volume of liquid in the condenser tubes. (m^3)

This partial differential equation is linear but not with constant coefficients. As a result we cannot solve the equation by transformation into the Laplace Domain. However, using a first order Taylor series approximation we can produce the following constant coefficient equation.

$$\frac{\partial T_{cond}(x,t)}{\partial t} + v^0_{cond} \frac{\partial T_{cond}(x,t)}{\partial x} = \frac{1}{\tau_{Tc0}} [T_{sh}(t) - T_{cond}(x,t)] - \frac{[T^0_{sh} - T^0_{cond1}]}{\tau_{Tc0} M^0_{cond}} e^{-\frac{x}{\tau_{Tc0} . v^0_{cond}}} M_{cond}(t) \tag{3.47}$$

Where, x = distance along the condenser tube. (m)

By transforming this into the Laplace Domain we can produce the following differential equation.

$$\frac{dT_{cond}(x,s)}{dx} + \frac{1}{v^0_{cond} . \tau_{Tc0}} [\tau_{Tc0} . s + 1] T_{cond}(x,s) = \frac{1}{v^0_{cond} . \tau_{Tc0}} T_{sh}(s) - \frac{[T^0_{sh} - T^0_{cond1}]}{v^0_{cond} M^0_{cond} . \tau_{Tc0}} e^{-\frac{x}{\tau_{Tc0} . v^0_{cond}}} M_{cond}(s) \tag{3.48}$$

This can be solved to produce a transfer function for the condenser outlet temperature.

$$T_{cond2}(s)=\frac{\left[1-e^{-\frac{\tau_c}{\tau_{Tc0}}}e^{-\tau_c.s}\right]}{\left[\tau_{Tc0}.s+1\right]}T_{sh}(s)+e^{-\frac{\tau_c}{\tau_{Tc0}}}e^{-\tau_c.s}T_{cond1}(s)-\frac{\tau_c\left(T_{sh}^{0}-T_{cond1}^{0}\right)e^{-\frac{\tau_c}{\tau_{Tc0}}}}{\tau_{Tc0}.M_{cond}^{0}}\frac{\left[1-e^{-\tau_c.s}\right]}{\tau_c.s}M_{cond}(s) \quad (3.49)$$

By transforming this into the time domain we can then produce a differential equation for the condenser outlet temperature.

$$T_{cond2}(t)=T_{dum}(t)+e^{-\frac{\tau_c}{\tau_{Tc0}}}T_{cond1}(t-\tau_c)-\frac{\tau_c\left(T_{sh}^{0}-T_{cond1}^{0}\right)e^{-\frac{\tau_c}{\tau_{Tc0}}}}{\tau_{Tc0}.M_{cond}^{0}}V_{dum}(t) \quad (3.50)$$

$$\frac{dT_{dum}(t)}{dt}=-\frac{1}{\tau_{Tc0}}T_{dum}+\frac{1}{\tau_{Tc0}}T_{sh}-\frac{e^{-\frac{\tau_c}{\tau_{Tc0}}}}{\tau_{Tc0}}T_{sh}(t-\tau_c), \qquad \tau_c\frac{dV_{dum}}{dt}=M_{cond}(t)-M_{cond}(t-\tau_c) \quad (3.51)$$

Where, T_{cond2} = outlet temperature from the condenser. (°C)

V_{dum} = dummy variable used in the condenser model. (m^3)

T_{dum} = dummy variable used in the condenser model. (°C)

The condenser heat flow is given by the integral shown in equation (3.52). This can be differentiated, with respect to time, to produce the differential equation shown by equation (3.53).

$$q_{cond}(t)=\frac{1}{L}\int_0^L U_{cond}.A_{cond}\left[T_{sh}(t)-T_{cond}(x,t)\right]dx \quad (3.52)$$

$$\frac{dq_{cond}(t)}{dt}=U_{cond}.A_{cond}\frac{dT_{sh}(t)}{dt}-\frac{1}{\tau_{Tc0}}q_{cond}(t)+\frac{U_{cond}.A_{cond}}{\tau_c}\left[T_{cond1}(t)-T_{cond2}(t)\right] \quad (3.53)$$

3.3.2) Plate Heat Exchanger Model

The Evaporator A plant contains one plate heat exchanger. This heats the raw feed milk from approximately 10 °C to 50 °C using hot condensate from the MVR and TVR evaporator shells and hot water from the TVR vacuum condenser. The following figure shows the block diagram for the plate heat exchanger.

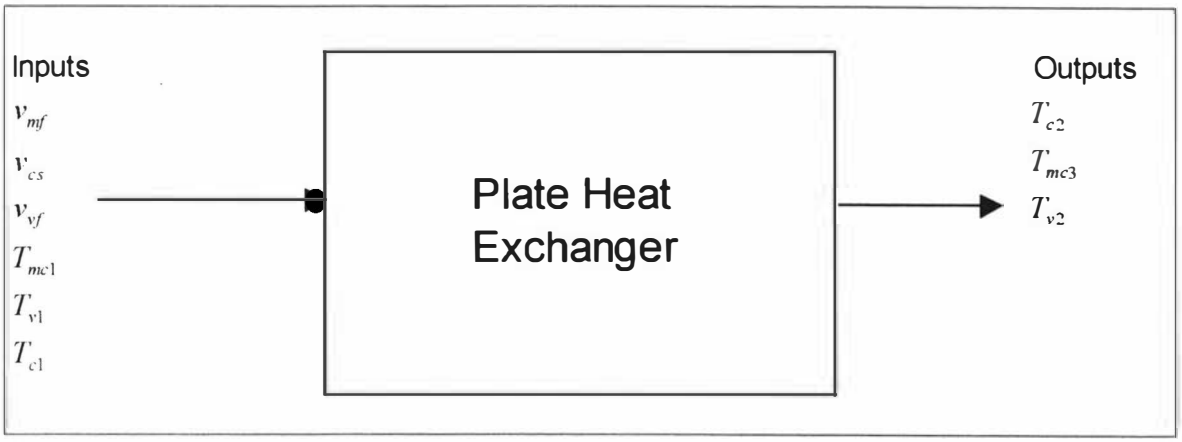

Figure 3-5 : Block diagram for the Plate Heat Exchanger.

Where, v_{mf}	=	velocity of milk through plate heat exchanger.	(m/s)
v_{cs}	=	velocity of condensate water through plate heat exchanger.	(m/s)
v_{vf}	=	velocity of hot cooling water through the plate heat exchanger.	(m/s)
T_{c1}	=	temperature of hot condensate entering the plate heat exchanger.	(°C)
T_{c2}	=	temperature of condensate exiting the plate heat exchanger.	(°C)
T_{mc1}	=	temperature of cold milk entering the plate heat exchanger.	(°C)
T_{mc3}	=	temperature of hot milk exiting the plate heat exchanger.	(°C)
T_{v1}	=	temperature of hot cooling water entering the plate heat exchanger.	(°C)
T_{v2}	=	temperature of hot cooling water exiting the plate heat exchanger.	(°C)

Figure 3-6 shows the actual plate heat exchanger configuration. Cold milk enters from the left ($T_{mc1} \approx 12°C$) and flows towards the right whilst being heated by the hot cooling water and condensate. Hot water, from the vacuum condenser, enters from the top (T_{v1}) and flows in counter-current towards the left before leaving the heat exchanger (T_{v2}). The milk is heated by conduction/convection and leaves the vacuum condenser water section at a higher temperature ($T_{mc2} \approx 30°C$). Hot condensate water enters from the right (T_{c1}) and flows in counter-current towards the left before exiting at a lower temperature (T_{c2}). The hot milk from the heat exchanger ($T_{mc3} \approx 50°C$) is controlled by manipulating the flow of hot condensate.

The fluid velocities depend on the mass flowrate, the cross sectional area of the heat exchanger and the fluid densities. For example the fluid velocities of the preheat plate exchanger are given by the following equations. As a result these fluid velocities are really the mass flows to the heat exchanger. It is, however, slightly easier to work with the fluid velocities and we will continue in this fashion for most of this analysis.

$$v_{mf} = \frac{M_f}{\rho_{mf} . A_{mf}}, \qquad v_{cs} = \frac{M_c}{\rho_{cs} . A_{cs}}, \qquad v_{vf} = \frac{M_{vac}}{\rho_{vf} . A_{vf}} \tag{3.54}$$

Where, M_f = feed mass flow to the Evaporator A plant. (kg/s)

M_c = mass flow of condensate to the plate heat exchanger. (kg/s)

M_{vac} = mass flow of cooling water to the vacuum condenser. (kg/s)

A_{mf} = cross sectional area of fluid flow on the cold side of the heat exchanger. (m^2)

A_{cs} = cross sectional area of fluid flow on the hot side of the heat exchanger. (m^2)

A_{vf} = cross sectional area of fluid flow on the hot side of the heat exchanger. (m^2)

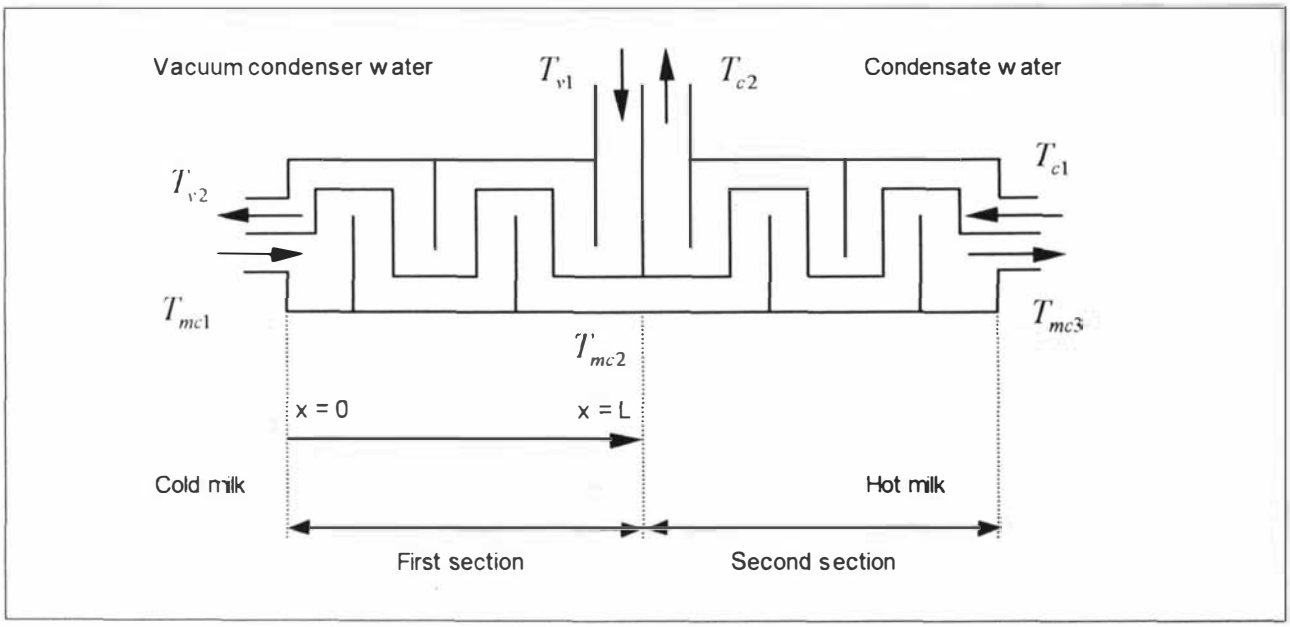

Figure 3-6 : Plate Heat Exchanger used in Evaporator Plant.

If we make energy balances around an infinitesimal cross section we can produce the following partial differential equations. As with the condenser partial differential equations, these are derived by assuming plug flow, constant density/heat capacity with respect to temperature and no heat losses. The milk, condenser and hot water temperatures vary with both length down the heat exchanger and time. For the section, using the vacuum condenser hot water, the following partial differential equations apply.

$$\tau_{mcf}\frac{\partial T_{mcf}(x,t)}{\partial t}+v_{mf}(t).\tau_{mcf}\frac{\partial T_{mcf}(x,t)}{\partial x}=T_{wf}(x,t)-T_{mcf}(x,t) \tag{3.55}$$

$$\frac{\partial T_{wf}(x,t)}{\partial t}=\frac{1}{\tau_{wvf}}\left[T_{vf}(x,t)-T_{wf}(x,t)\right]-\frac{1}{\tau_{wcf}}\left[T_{wf}(x,t)-T_{mcf}(x,t)\right] \tag{3.56}$$

$$\tau_{vvf}\frac{\partial T_{vf}(x,t)}{\partial t}+v_{vf}(t).\tau_{vvf}\frac{\partial T_{vf}(x,t)}{\partial x}=T_{vf}(x,t)-T_{wf}(x,t) \tag{3.57}$$

Where, T_{mcf} = milk temperature on the cold side of the first heat exchanger section. (°C)

T_{vf} = vacuum condenser water temperature on the hot side. (°C)
T_{wf} = temperature of the heat exchanger wall in the first section. (°C)
v_{vf} = hot water velocity in the first section of the plate heat exchanger. (m/s)
v_{mf} = milk velocity in the first section of the plate heat exchanger. (m/s)

For the hot condensate water section the following partial differential equations apply.

$$\tau_{mos}\frac{\partial T_{mcs}(x,t)}{\partial t}+v_{ms}(t).\tau_{mos}\frac{\partial T_{mcs}(x,t)}{\partial x}=T_{ws}(x,t)-T_{mcs}(x,t) \tag{3.58}$$

$$\frac{\partial T_{ws}(x,t)}{\partial t}=\frac{1}{\tau_{wis}}[T_{cs}(x,t)-T_{ws}(x,t)]-\frac{1}{\tau_{wos}}[T_{ws}(x,t)-T_{mcs}(x,t)] \tag{3.59}$$

$$\tau_{cis}\frac{\partial T_{cs}(x,t)}{\partial t}+v_{cs}(t)\tau_{cis}\frac{\partial T_{cs}(x,t)}{\partial x}=T_{cs}(x,t)-T_{ws}(x,t) \tag{3.60}$$

Where, T_{mcs} = milk temperature on the cold side in the second heat exchanger section.(°C)
T_{cs} = hot condensate water temperature in the second heat exchanger section.(°C)
T_{ws} = temperature of the heat exchanger wall in the second section. (°C)
v_{ms} = milk velocity in the second section of the heat exchanger. (m/s)
v_{cs} = condensate velocity in the second section of the heat exchanger. (m/s)

The following definitions are used.

$$\tau_{mof}=\frac{\rho_m.C_{pm}.V_{mf}}{h_{of}.A_{hf}},\quad \tau_{vif}=\frac{\rho_v.C_{pv}.V_{vf}}{h_{if}.A_{hf}},\quad \tau_{wof}=\frac{\rho_w.C_{pw}.V_{wf}}{h_{of}.A_{hf}},\quad \tau_{wif}=\frac{\rho_w.C_{pw}.V_{wf}}{h_{if}.A_{hf}} \tag{3.61}$$

$$\tau_{wf}=\frac{\rho_w.C_{pw}.V_{wf}}{[h_{of}.A_{hf}+h_{if}.A_{hf}]},\quad \tau_{Tof}=\frac{\rho_m.C_{pm}.V_{mf}}{U_{hf}.A_{hf}},\quad \tau_{Tif}=\frac{\rho_v.C_{pv}.V_{vf}}{U_{hf}.A_{hf}},\quad U_{hf}=\frac{h_{of}.h_{if}}{[h_{of}+h_{if}]} \tag{3.62}$$

$$\tau_{mos}=\frac{\rho_m.C_{pm}.V_{ms}}{h_{os}.A_{hs}},\quad \tau_{cis}=\frac{\rho_v.C_{pv}.V_{cs}}{h_{is}.A_{hs}},\quad \tau_{wos}=\frac{\rho_w.C_{pw}.V_{ws}}{h_{os}.A_{hs}},\quad \tau_{wis}=\frac{\rho_w.C_{pw}.V_{ws}}{h_{is}.A_{hs}} \tag{3.63}$$

$$\tau_{ws}=\frac{\rho_w.C_{pw}.V_{ws}}{[h_{os}.A_{hs}+h_{is}.A_{hs}]},\quad \tau_{Tos}=\frac{\rho_m.C_{pm}.V_{ms}}{U_{hs}.A_{hs}},\quad \tau_{Tis}=\frac{\rho_v.C_{pv}.V_{cs}}{U_{hs}.A_{hs}},\quad U_{hs}=\frac{h_{os}.h_{is}}{[h_{os}+h_{is}]} \tag{3.64}$$

Where, V_{mf} = volume of liquid in the first cold section of the heat exchanger. (m^3)
h_{of} = heat transfer coefficient, between the tube walls and hot liquid. ($W/m^2.°C$)
h_{if} = heat transfer coefficient, between the tubes walls and hot liquid. ($W/m^2.°C$)

A_{hf} = heat transfer surface area, first plate heat exchanger section. (m^2)

A_{hs} = heat transfer surface area, second plate heat exchanger section. (m^2)

V_{vf} = volume of liquid in the first hot section of the heat exchanger. (m^3)

V_{mf} = volume of metal in the first section of the heat exchanger. (m^3)

There are two common methods that could be used to solve the plate heat exchanger partial differential equations. Firstly finite difference approximations, to the spatial derivatives, can be used to produce a system of first order differential equations. Alternatively, the partial differential equations can be solved by linearisation and transformation in the Laplace Domain. The use of finite differences is simple but also inconvenient because an accurate representation requires a large number of finite differences. As a result a large number of differential equations will be required to represent the plate heat exchanger. This is very inconvenient and instead we will use the Laplace transformation method.

If we assume constant fluid velocities (i.e., $v_{mf}(t)$, $v_{vf}(t)$, $v_{ms}(t)$ and $v_{cs}(t)$ are constant with time) then the partial differential equations can be transferred into the Laplace Domain. The result is the following two pairs of differential equations. This shows that the first and second sections of the plate heat exchanger are de-coupled and furthermore that the equations for both sections are identical.

$$\begin{bmatrix} \frac{dT_{mcf}(x,s)}{dx} \\ \frac{dT_{vf}(x,s)}{dx} \\ \frac{dT_{mcs}(x,s)}{dx} \\ \frac{dT_{cs}(x,s)}{dx} \end{bmatrix} = \begin{bmatrix} -H_1(s) & H_2(s) & 0 & 0 \\ -H_4(s) & H_3(s) & 0 & 0 \\ 0 & 0 & -H_5(s) & H_6(s) \\ 0 & 0 & -H_7(s) & H_8(s) \end{bmatrix} \begin{bmatrix} T_{mcf}(x,s) \\ T_{vf}(x,s) \\ T_{mcs}(x,s) \\ T_{cs}(x,s) \end{bmatrix} \tag{3.65}$$

Since the equations for the first section of the heat exchanger are decoupled from those of the second, we will only consider the first section. The transfer functions $H_1(s)$, $H_2(s)$, $H_3(s)$ and $H_4(s)$ are given by the following equations. These are the same as the transfer functions $H_5(s)$, $H_6(s)$, $H_7(s)$ and $H_8(s)$, except the properties for the second section must be used.

$$H_1(s) = \frac{1}{v_{mf}^0}\left[s + \frac{1}{\tau_{Tof}} \frac{(\tau_{wif}.s+1)}{(\tau_{wf}.s+1)} \right], \quad H_2(s) = \frac{1}{\tau_{Tof}.v_{mf}^0(\tau_{wf}.s+1)} \tag{3.66}$$

$$H_3(s) = \frac{1}{v_{vf}^0}\left[s + \frac{1}{\tau_{Tif}} \frac{(\tau_{wof}.s+1)}{(\tau_{wf}.s+1)} \right], \quad H_4(s) = \frac{1}{\tau_{Tif}.v_{vf}^0(\tau_{wf}.s+1)} \tag{3.67}$$

If the thermal inertia of the heat exchanger walls is not important then (3.66) and (3.67) can be approximated by (3.68).

$$H_1(s)=\frac{1}{v_{mf}^0}\left[s+\frac{1}{\tau_{Tof}}\right],\quad H_2(s)=\frac{1}{\tau_{Tof}.v_{mf}^0},\quad H_3(s)=\frac{1}{v_{vf}^0}\left[s+\frac{1}{\tau_{Tif}}\right],\quad H_2(s)=\frac{1}{\tau_{Tif}.v_{vf}^0} \tag{3.68}$$

The above equations for the first section of the heat exchanger are a pair of linear constant coefficient differential equations. They can be solved to produce the transfer functions between the heat exchanger inlet and outlet temperatures. However, a difficulty is the assumption of constant fluid velocities, since these are manipulated, on the Evaporator A plant. The feed flow is manipulated manually and the condensate flow is manipulated to control the heat exchanger outlet temperature. Consequently we cannot make this assumption and produce an adequate representation of the heat exchanger. However, by relaxing this assumption the partial differential equations do not have an explicit solution. A solution to this problem is to linearise the partial differential equations about an operating point. This can be done using a first term Taylor series approximation to produce linear constant coefficient partial differential equations. However, in order to do this we first need the plate heat exchanger steady state equations. These are needed to determine the static temperature derivatives with respect to distance (i.e., $\frac{\partial T_{mcf}}{\partial x}^0$ and $\frac{\partial T_{vf}}{\partial x}^0$).

Steady State

The following pair of differential equations describe the plate heat exchanger steady state. Strictly there are four of these equations, but we have already shown that the equations for the first section are identical to those for the second section. Therefore we need only consider the equations for the vacuum condenser water section and these equations will then also describe the condensate water section.

$$\begin{bmatrix}\frac{dT_{mcf}}{dx}\\ \frac{dT_{vf}}{dx}\end{bmatrix}=\begin{bmatrix}-\frac{1}{\tau_{Tof}.v_{mf}} & \frac{1}{\tau_{Tof}.v_{mf}}\\ -\frac{1}{\tau_{Tif}.v_{vf}} & \frac{1}{\tau_{Tif}.v_{vf}}\end{bmatrix}\begin{bmatrix}T_{mcf}\\ T_{vf}\end{bmatrix} \tag{3.69}$$

These equations can be solved to produce explicit equations for the temperatures along the heat exchanger length. With the boundary conditions ($T_v=T_{v1}\,@\,x=L, T_{mc}=T_{mc1}\,@\,x=0$) the following equations are produced.

$$T_{mcf}(x)=\frac{\left[T_{mc1}\frac{\tau_{Tof}.v_{mf}}{\tau_{Tif}.v_{vf}}e^{\left[-\frac{\tau_{mf}}{\tau_{Tof}}+\frac{\tau_{vf}}{\tau_{Tif}}\right]}-T_{v1}\right]}{\left[\frac{\tau_{Tof}.v_{mf}}{\tau_{Tif}.v_{vf}}e^{\left[-\frac{\tau_{mf}}{\tau_{Tof}}+\frac{\tau_{vf}}{\tau_{Tif}}\right]}-1\right]}+\frac{[T_{v1}-T_{mc1}]}{\left[\frac{\tau_{Tof}.v_{mf}}{\tau_{Tif}.v_{vf}}e^{\left[-\frac{\tau_{mf}}{\tau_{Tof}}+\frac{\tau_{vf}}{\tau_{Tif}}\right]}-1\right]}e^{\left[-\left(\frac{1}{\tau_{Tof}.v_{mf}}-\frac{1}{\tau_{Tif}.v_{vf}}\right)x\right]} \tag{3.70}$$

$$T_{vf}(x)=\frac{\left[T_{mc1}\frac{\tau_{Tof}.v_{mf}}{\tau_{Tif}.v_{vf}}e^{\left[-\frac{\tau_{mf}}{\tau_{Tof}}+\frac{\tau_{vf}}{\tau_{Tif}}\right]}-T_{v1}\right]}{\left[\frac{\tau_{Tof}.v_{mf}}{\tau_{Tif}.v_{vf}}e^{\left[-\frac{\tau_{mf}}{\tau_{Tof}}+\frac{\tau_{vf}}{\tau_{Tif}}\right]}-1\right]}+\frac{[T_{v1}-T_{mc1}]\frac{\tau_{Tof}.v_{mf}}{\tau_{Tif}.v_{vf}}}{\left[\frac{\tau_{Tof}.v_{mf}}{\tau_{Tif}.v_{vf}}e^{\left[-\frac{\tau_{mf}}{\tau_{Tof}}+\frac{\tau_{vf}}{\tau_{Tif}}\right]}-1\right]}e^{\left[-\left(\frac{1}{\tau_{Tof}.v_{mf}}-\frac{1}{\tau_{Tif}.v_{vf}}\right)x\right]} \tag{3.71}$$

The outlet temperatures for the vacuum condenser water section are given by the following equations.

$$T_{mc2}=\frac{e^{\left[-\frac{\tau_{mf}}{\tau_{Tof}}+\frac{\tau_{vf}}{\tau_{Tif}}\right]}\left[\frac{\tau_{Tof}.v_{mf}}{\tau_{Tif}.v_{vf}}-1\right]}{\left[\frac{\tau_{Tof}.v_{mf}}{\tau_{Tif}.v_{vf}}e^{\left[-\frac{\tau_{mf}}{\tau_{Tof}}+\frac{\tau_{vf}}{\tau_{Tif}}\right]}-1\right]}T_{mc1}+\frac{\left[e^{\left[-\frac{\tau_{mf}}{\tau_{Tof}}+\frac{\tau_{vf}}{\tau_{qf}}\right]}-1\right]}{\left[\frac{\tau_{Tof}.v_{mf}}{\tau_{Tif}.v_{vf}}e^{\left[-\frac{\tau_{mf}}{\tau_{Tof}}+\frac{\tau_{vf}}{\tau_{Tif}}\right]}-1\right]}T_{v1} \tag{3.72}$$

$$T_{v2}=\frac{\frac{\tau_{Tof}.v_{mf}}{\tau_{Tif}.v_{vf}}\left[e^{\left[-\frac{\tau_{mf}}{\tau_{Tof}}+\frac{\tau_{vf}}{\tau_{Tif}}\right]}-1\right]}{\left[\frac{\tau_{Tof}.v_{mf}}{\tau_{Tif}.v_{vf}}e^{\left[-\frac{\tau_{mf}}{\tau_{Tof}}+\frac{\tau_{vf}}{\tau_{Tif}}\right]}-1\right]}T_{mc1}+\frac{\left[\frac{\tau_{Tof}.v_{mf}}{\tau_{Tif}.v_{vf}}-1\right]}{\left[\frac{\tau_{Tof}.v_{mf}}{\tau_{Tif}.v_{vf}}e^{\left[-\frac{\tau_{mf}}{\tau_{Tof}}+\frac{\tau_{vf}}{\tau_{Tif}}\right]}-1\right]}T_{v1} \tag{3.73}$$

We can also show that the heat exchanger is described by the standard log mean temperature difference equations. By subtracting the two temperature differential equations we can produce the following equation.

$$\frac{d(T_{mcf}-T_{vf})}{dx}=\left[\frac{1}{\tau_{Tif}.v_{vf}}-\frac{1}{\tau_{Tof}.v_{mf}}\right]\left[T_{mcf}-T_{vf}\right] \tag{3.74}$$

This is integrated to produce equation (3.75). Here we have substituted the definitions for the heat exchanger constants τ_{Tif}, τ_{Tof}, τ_{vf} and τ_{mf}. We have also assumed that the heat capacities of water and milk are the same.

$$\ln\left[\frac{T_{v1}-T_{mc2}}{T_{v2}-T_{mc1}}\right]=\left[\frac{\tau_{vf}}{\tau_{\tau_{if}}}-\frac{\tau_{mf}}{\tau_{Tof}}\right]=U_{hf}.A_{hf}\left[\frac{1}{M_{vac}.C_p}-\frac{1}{M_f.C_p}\right] \tag{3.75}$$

Where, M_{vac}	=	mass flow of vacuum condenser water.	(kg/s)
M_f	=	mass flow of milk to the plate heat exchanger.	(kg/s)
C_p	=	heat capacity.	(kg/s)
A_{hf}	=	heat transfer surface area.	(m^2)
U_{hf}	=	overall heat transfer coefficient.	($W/m^2.K$)

The static heat flow is given by the following equations and these can be substituted into the above to produce the standard log mean temperature difference equation.

$$q=M_f.C_p(T_{mc2}-T_{mc1})=M_{vac}.C_p(T_{v1}-T_{v2}), \qquad q=U_{hf}.A_{hf}\frac{[(T_{v1}-T_{mc2})-(T_{v2}-T_{mc1})]}{\ln\left[\frac{T_{v2}-T_{mc1}}{T_{v1}-T_{mc2}}\right]} \tag{3.76}$$

In order to relax the assumption of constant fluid velocities, in the partial differential equations, the temperature derivatives with respect to distance are required. These are given by equation (3.77).

$$\left(\frac{\partial T_{mcf}}{\partial x}\right)^0=v_{mf}^0.N_1e^{[-\beta_2.x]}, \qquad \left(\frac{\partial T_{vf}}{\partial x}\right)^0=v_{vf}^0.N_2.e^{[-\beta_2.x]} \tag{3.77}$$

Where N_1 and N_2 are given by the following equations.

$$v_{mf}^0.N_1=\frac{\left[T_{v1}^0-T_{mc1}^0\right]\left[\frac{1}{\tau_{Tif}.v_{vf}^0}-\frac{1}{\tau_{Tof}.v_{mf}^0}\right]}{\left[\frac{\tau_{Tof}.v_{mf}}{\tau_{Tif}.v_{vf}}e^{\left[-\frac{\tau_{mf}}{\tau_{Tof}}+\frac{\tau_{vf}}{\tau_{Tif}}\right]}-1\right]}, \qquad v_{vf}^0.N_2=\frac{\left[T_{v1}^0-T_{mc1}^0\right]\left[\frac{\tau_{Tof}.v_{mf}^0}{\tau_{Tif}.v_{vf}^0}-1\right]}{\left[\frac{\tau_{Tof}.v_{mf}}{\tau_{Tif}.v_{vf}}e^{\left[-\frac{\tau_{mf}}{\tau_{Tof}}+\frac{\tau_{vf}}{\tau_{Tif}}\right]}-1\right]} \tag{3.78}$$

Explicit Laplace Domain Representation

We return now to the plate heat exchanger partial differential equations. The partial differential equations cannot be solved by Laplace Domain transformation because they do not have constant coefficients. However, we can transform the equations into constant coefficient partial differential equations by linearisation about an operating point. This is done using first order Taylor series approximations and the resulting Laplace Domain representation is given by the following. We have considered only the first section of the plate heat exchanger.

$$\begin{bmatrix} \frac{dT_{mcf}(x,s)}{dx} \\ \frac{dT_{vf}(x,s)}{dx} \end{bmatrix} = \begin{bmatrix} -H_1(s) & H_2(s) \\ -H_4(s) & H_3(s) \end{bmatrix} \begin{bmatrix} T_{mcf}(x,s) \\ T_{vf}(x,s) \end{bmatrix} - \begin{bmatrix} N_1.e^{(-\beta_2.x)} & 0 \\ 0 & N_2.e^{(-\beta_2.x)} \end{bmatrix} \begin{bmatrix} v_{mf}(s) \\ v_{vf}(s) \end{bmatrix} \quad (3.79)$$

Where, T_{mcf} = temperature of the cold liquid in the first section of the heat exchanger. (°C)

T_{vf} = temperature of the vacuum condenser water in the first section. (°C)

v_{mf} = velocity of the cold liquid in the first section of the heat exchanger. (m/s)

v_{vf} = velocity of the vacuum condenser water in the first section. (m/s)

This is more easily represented by using matrices and the resulting system is given by equation (3.80).

$$\frac{d\mathbf{T}(x,s)}{dx} - \mathbf{A}(s).\mathbf{T}(x,s) = -\mathbf{B}(x).\mathbf{v}(s) \quad (3.80)$$

This first order system can be easily solved to produce equation (3.81).

$$e^{-\mathbf{A}(s)L}\mathbf{T}(L,s) - e^{-\mathbf{A}(s)0}\mathbf{T}(0,s) = -\mathbf{v}(s)\int_0^L e^{-\mathbf{A}(s)x}\mathbf{B}(x)dx \quad (3.81)$$

Where, the exponential function is given by Cayley-Hamilton theory.

$$e^{[-\mathbf{A}(s)L]} = \begin{bmatrix} e^{(\alpha_1(s)L)}\left[\frac{\alpha_2(s)}{\beta_1(s)}\sinh(\beta_1(s)L) + \cosh(\beta_1(s)L)\right] & -e^{(\alpha_1(s)L)}\frac{H_2(s)}{\beta_1(s)}\sinh(\beta_1(s)L) \\ \frac{H_4(s)}{\beta_1(s)}e^{(\alpha_1(s)L)}\sinh(\beta_1(s)L) & e^{(\alpha_1(s)L)}\left[\cosh(\beta_1(s)L) - \frac{\alpha_2(s)}{\beta_1(s)}\sinh(\beta_1(s)L)\right] \end{bmatrix} \quad (3.82)$$

$$\alpha_1(s) = \frac{[H_1(s) - H_3(s)]}{2}, \qquad \alpha_2(s) = \frac{[H_1(s) + H_3(s)]}{2} \quad (3.83)$$

$$\beta_1(s) = \frac{\sqrt{[(H_1(s) + H_3(s))^2 - 4.H_2(s).H_4(s)]}}{2}, \quad \beta_2 = \frac{1}{\tau_{Tof}.v_{mf}^0} - \frac{1}{\tau_{Tif}.v_{vf}^0} \quad (3.84)$$

By simple manipulation we can then produce the following transfer functions. These describe the impact of the process inputs (T_{mcl}, T_{vl}, M_f and M_{vac}) on the vacuum condenser hot water section. We have continued using the fluid velocities as inputs, rather than the fluid mass flows. The outputs are the hot milk temperature (T_{mc2}) and the hot water temperature (T_{v2}). Strictly these transfer functions can be transformed back into the time domain to produce differential equations. However, the transfer functions contain transcendental functions and it is difficult to

make this transformation. Therefore, we cannot produce finite order ordinary differential equations for the heat exchanger outlet temperatures. This is a serious problem for the development of a dynamic model because most standard dynamic analysis is based on finite order constant coefficient linear ordinary differential equations. The transcendental functions can be transformed using Pade approximations to produce the required equations. This approach is used in Chapter 4 to transform the falling film and condenser transfer functions into finite order ordinary differential equations. However, the plate heat exchanger transfer functions are considerably more difficult to transform than the falling film and condenser equations.

$$A_1(s)=\alpha_2(s)\sinh(\beta_1(s)L)+\beta_1(s)\cosh(\beta_1(s)L) \tag{3.85}$$

$$A_2(s)=[\alpha_1(s)-\beta_2]^2-\beta_1(s)^2 \tag{3.86}$$

$$A_3(s)=\beta_1(s)\sinh(\beta_1(s)L)+\alpha_2(s)\cosh(\beta_1(s)L) \tag{3.87}$$

$$\frac{T_{mc2}(s)}{T_{mc1}(s)}=\frac{\beta_1(s)e^{-\alpha_1(s)L}}{A_1(s)}\quad,\qquad \frac{T_{mc2}(s)}{T_{v1}(s)}=\frac{H_2(s)\sinh[\beta_1(s)L]}{A_1(s)} \tag{3.88}$$

$$\frac{T_{mc2}(s)}{v_m(s)}=-\frac{\beta_1(s)N_1e^{[-\beta_2 L]}}{A_2(s)}\left[\frac{(\alpha_1(s)-\beta_2)}{\beta_1(s)}-\frac{(A_3(s)+(\alpha_1(s)-\beta_2-\alpha_2(s))e^{[-(\alpha_1(s)-\beta_2)L]})}{A_1(s)}\right] \tag{3.89}$$

$$\frac{T_{mc2}(s)}{v_v(s)}=\frac{N_2.H_2(s)e^{[-\beta_2 L]}}{A_2(s)}\left[\frac{(\alpha_1(s)-\beta_2)\sinh(\beta_1(s)L)-\beta_1(s)\cosh(\beta_1(s)L)+\beta_1(s)e^{[-(\alpha_1(s)-\beta_2)L]}}{A_1(s)}\right] \tag{3.90}$$

$$\frac{T_{v2}(s)}{T_{mc1}(s)}=\frac{H_4(s)\sinh[\beta_1(s)L]}{A_1(s)}\quad,\qquad \frac{T_{v2}(s)}{T_{v1}(s)}=\frac{e^{\alpha_1(s)L}\beta_1(s)}{A_1(s)} \tag{3.91}$$

$$\frac{T_{v2}(s)}{v_v(s)}=-\frac{\beta_1(s).N_2}{A_2(s)}\left[\frac{(\alpha_1(s)-\beta_2)}{\beta_1(s)}+\frac{(A_3(s)-(\alpha_1(s)-\beta_2+\alpha_2(s))e^{[(\alpha_1(s)-\beta_2)L]})}{A_1(s)}\right] \tag{3.92}$$

$$\frac{T_{v2}(s)}{v_m(s)}=\frac{N_1.H_4(s)}{A_2(s)}\left[\frac{(\alpha_2(s)-\beta_1(s))\sinh(\beta_1(s)L)+\beta_1(s)\cosh(\beta_1(s)L)-\beta_1(s)e^{[(\alpha_1(s)-\beta_2)L]}}{A_1(s)}\right] \tag{3.93}$$

The complexity of the above transfer functions suggests the possibility of simple algebra mistakes. However, the transfer functions were verified using numerical finite difference approximations to the partial differential equations. The finite difference approximations were linearised, to produce a state space representation of the plate heat exchanger. Using some simple hypothetical numbers the state space representation Bode plots were compared to those for the above transfer functions. The comparison was exact across the frequency range.

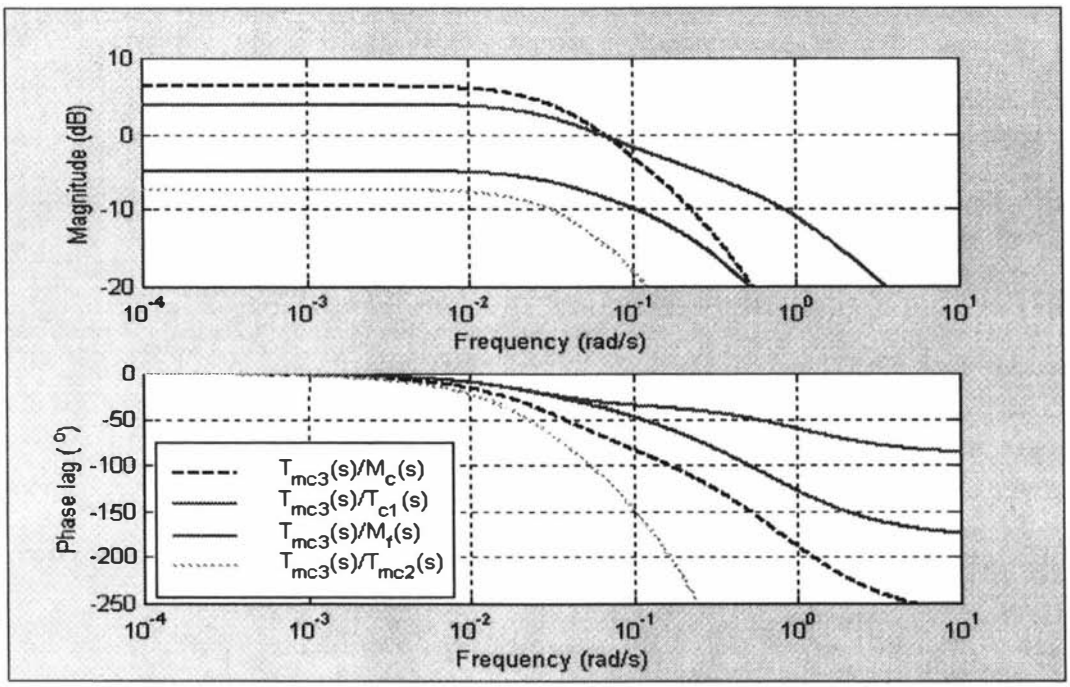

Figure 3-7 : Numerically determined Bode plots.

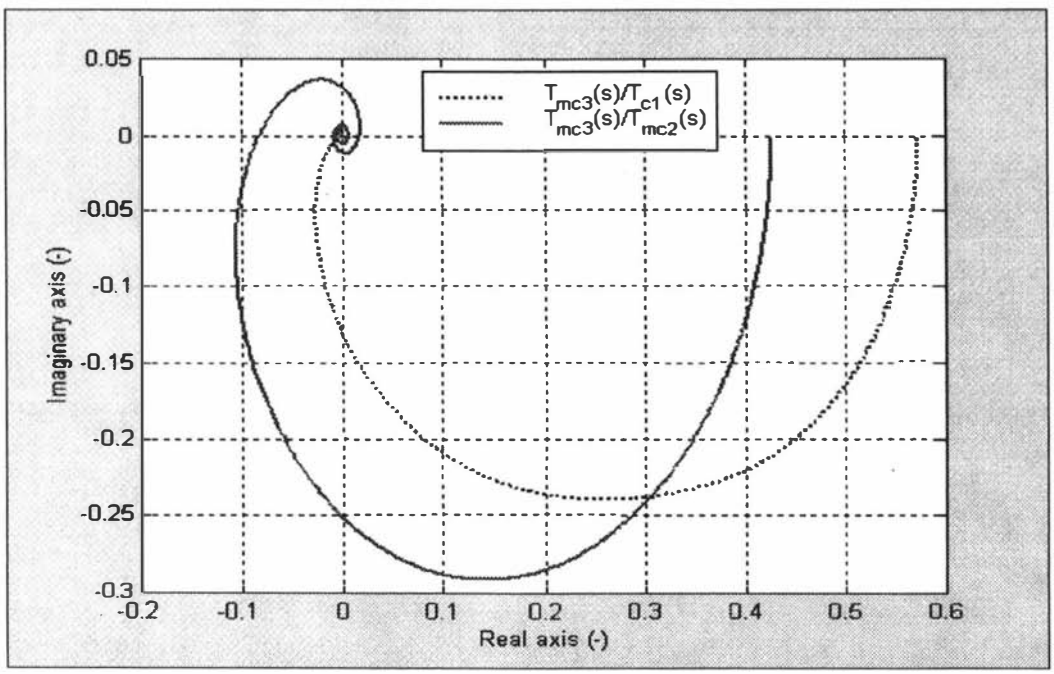

Figure 3-8 : Nyquist plots for transfer functions $\frac{T_{mc3}(s)}{T_{mc2}(s)}$ and $\frac{T_{mc3}(s)}{T_{c1}(s)}$.

Numerical Bode and Nyquist plots

The above transfer functions can be used to numerically calculate the Bode and Nyquist plots for the plate heat exchanger. The heat exchanger consists of two de-coupled sections placed in series. The first uses hot water from the vacuum condenser and the second uses hot water from the MVR evaporator shell. We will determine the Bode and Nyquist plots for the four transfer

functions, of the second section, acting on the outlet hot milk temperature. The resulting Bode plots are shown in Figure 3-7 and the Nyquist plots in Figures 3-8 and 3-9.

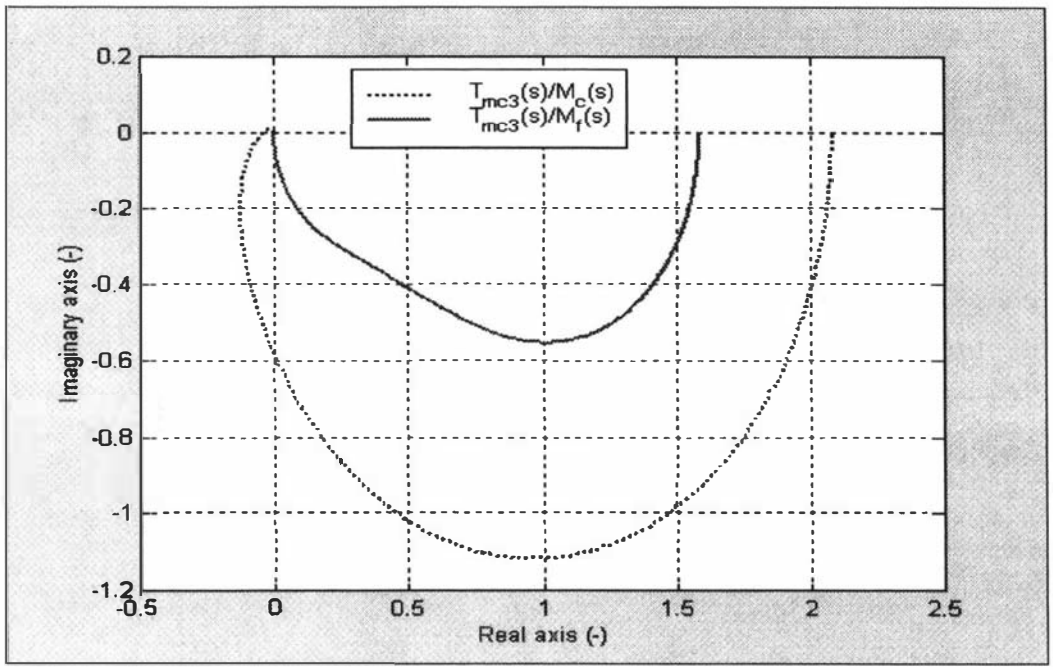

Figure 3-9 : Nyquist plots for transfer functions $\frac{T_{mc3}(s)}{M_c(s)}$ and $\frac{T_{mc3}(s)}{M_f(s)}$.

There are some clear similarities between these transfer functions and conventional polynomial transfer functions. The $\frac{T_{mc3}(s)}{T_{mc2}(s)}$ transfer function appears to contain a significant pure delay and a third order dynamic. Its magnitude appears to follow a third order dynamics whereas its phase lag continuously falls and therefore suggests a pure delay. The important $\frac{T_{mc3}(s)}{M_c(s)}$ transfer function appears to be third order. Likewise the $\frac{T_{mc3}(s)}{T_{c1}(s)}$ transfer function appears to be second order and the $\frac{T_{mc3}(s)}{M_f(s)}$ transfer function first order.

3.4) Conclusions

In Chapter 2 the entire Evaporator A plant was separated into four sections. These sections were the MVR evaporator section, the TVR evaporator section, the DSI unit preheat section and the preheat plate heat exchanger section. Chapter 2 was primarily concerned with deriving models for the MVR evaporator and TVR evaporator sections. The aim of this Chapter was to derive the models for the remaining DSI preheat section, preheat plate heat exchanger and shell/tube condensers.

In Section 4.2 the DSI preheat section was considered. We firstly gave a brief description of the process and then we derived the energy balances and mass balances for the DSI unit and the flash vessels. An important part of this was the thermal equilibrium between the liquid and vapour

phases. It was shown that the presence of air causes a temperature difference between the top and bottom of the vessel. The final result was a set of static and differential equations for the temperatures of the DSI unit and the flash vessels.

In Section 4.3 we investigated the preheat plate heat exchanger and the shell/tube condensers. The partial differential equations for these were presented and transformed in the Laplace Domain. For the shell/tube condensers we were able to produce an ordinary differential equation with time delays, whereas the result for the plate heat exchanger was a set of transcendental transfer functions.

The models derived in this and the previous Chapter potentially provide a complete description of the Evaporator A plant. However, they are still in a somewhat 'raw' state. In the next two Chapters we aim to develop and identify these models into a form that can be used for the optimisation and controllability studies. Chapter 4 will develop the steady state and linear dynamic models of the Evaporator A plant.

Chapter 4 : Model Development

4.1) Introduction

The work discussed in this thesis aims to analyse the operation and control of the Evaporator A plant at Kiwi Co-op Dairies. Optimisation and controllability studies will be made to determine the 'best' operating conditions and methods for controlling the plant. In Chapters 2 and 3, models were derived for the entire evaporator plant. These were developed for analysing the Evaporator A plant operation and control, but they must be further developed before they can be used. Specifically, we need a validated steady state model for the optimisation studies and a linear dynamic model for the controllability studies. In this Chapter, we will develop the steady state and linear dynamic models.

Firstly, the steady state model will be developed in Section 4.2. We will separate the Evaporator A plant into four sections and consider each independently before combining these to produce the complete model. These four sections are the MVR evaporator section, the TVR evaporator section, the DSI preheat section and the preheat plate heat exchanger. Typical operating points will be determined for each individual section and also the complete Evaporator A model. The plant geometries are listed in the Appendix E and the process parameters (i.e., heat transfer coefficients) are taken from the identification of Chapter 5.

In Section 4.3, we discuss the methodology for developing a linear dynamic model. Specifically, we investigate the linearisation of dynamic models using truncated Taylor series approximations and the description of pure delays using Pade approximations. This has been included to provide some background to the linearisation work, which will be done in Section 4.4.

The linear dynamic model will be developed in Section 4.4. As with the steady state model development, we separate the plant into four parts and develop each individually. The linear dynamic models are developed using the methods discussed in Section 4.3. However, in order to simplify the linearisation, we have made a number of significant assumptions. For example, distribution plate flashing, variable heat transfer coefficients and multiple evaporator passes have all been neglected. These assumptions were not made in the development of the steady state model and therefore the linear dynamic model is not a generalisation of the steady state model.

4.2) Steady State

4.2.1) Introduction

We shall develop the Evaporator A steady state model by separating it into four parts and initially considering each part independently. These parts are the preheat plate heat exchanger, the DSI preheat section, the MVR evaporator section and the TVR evaporator section. At the end of this section, we then combine the four models to produce the complete steady state model for the Evaporator A plant.

Various parameters are used in the steady state model. Many of these are listed in the Nomenclature of this thesis, but others are given in Appendix E. One of the most important parts of the steady state model is the evaporating overall heat transfer coefficients. The 'simple linear' model is used, because in Chapter 5 this is found to be the most accurate. We use the parameters for Whole Milk, which are $U_{so} = 1900.7$ W/m^2.K and $U_{sw} = 2906.1$ W/m^2.K. Another important part of the model is the relationship between heat capacity and milk dry matter. The linear model derived in Appendix A is used and the parameters for Whole Milk are $C_{pwater} = 4190$ J/kg.°C and $C_{pTS} = 1984$ J/kg.°C.

4.2.2) Plate Heat Exchanger

The steady state equations for the preheat plate heat exchanger were derived in Chapter 3. The resulting equations for the plate heat exchanger outlet temperatures were shown by (3.72) and (3.73) and the equivalent equations are shown here by (4.1), (4.2), (4.3) and (4.4). These give the heat exchanger outlet temperatures (i.e., T_{mc2}, T_{v2}, T_{mc3} and T_{c2}) in terms of the inlet temperatures, fluid velocities and milk dry matter (i.e., T_{v1}, T_{c1}, T_{mc1}, v_{mf}, v_{ms}, v_{cs}, v_{vf} and w_f).

$$T_{mc2} = \frac{e^{\left[-\frac{\tau_{mf}}{\tau_{Tof}}+\frac{\tau_{vf}}{\tau_{Tif}}\right]}\left[\frac{\tau_{Tof}.v_{mf}}{\tau_{Tif}.v_{vf}}-1\right]}{\left[\frac{\tau_{Tof}.v_{mf}}{\tau_{Tif}.v_{vf}}e^{\left[-\frac{\tau_{mf}}{\tau_{Tof}}+\frac{\tau_{vf}}{\tau_{Tif}}\right]}-1\right]}T_{mc1} + \frac{\left[e^{\left[-\frac{\tau_{mf}}{\tau_{Tof}}+\frac{\tau_{vf}}{\tau_{Tif}}\right]}-1\right]}{\left[\frac{\tau_{Tof}.v_{mf}}{\tau_{Tif}.v_{vf}}e^{\left[-\frac{\tau_{mf}}{\tau_{Tof}}+\frac{\tau_{vf}}{\tau_{Tif}}\right]}-1\right]}T_{v1} \tag{4.1}$$

$$T_{v2} = \frac{\frac{\tau_{Tof}.v_{mf}}{\tau_{Tif}.v_{vf}}\left[e^{\left[-\frac{\tau_{mf}}{\tau_{Tof}}+\frac{\tau_{vf}}{\tau_{Tif}}\right]}-1\right]}{\left[\frac{\tau_{Tof}.v_{mf}}{\tau_{Tif}.v_{vf}}e^{\left[-\frac{\tau_{mf}}{\tau_{Tof}}+\frac{\tau_{vf}}{\tau_{Tif}}\right]}-1\right]}T_{mc1} + \frac{\left[\frac{\tau_{Tof}.v_{mf}}{\tau_{Tif}.v_{vf}}-1\right]}{\left[\frac{\tau_{Tof}.v_{mf}}{\tau_{Tif}.v_{vf}}e^{\left[-\frac{\tau_{mf}}{\tau_{Tof}}+\frac{\tau_{vf}}{\tau_{Tif}}\right]}-1\right]}T_{v1} \tag{4.2}$$

$$T_{mc3}=\frac{e^{\left[-\frac{\tau_{ms}}{\tau_{Tos}}+\frac{\tau_{cs}}{\tau_{Tis}}\right]}\left[\frac{\tau_{Tos}.v_{ms}}{\tau_{Tis}.v_{cs}}-1\right]}{\left[\frac{\tau_{Tos}.v_{ms}}{\tau_{Tis}.v_{cs}}e^{\left[-\frac{\tau_{ms}}{\tau_{Tos}}+\frac{\tau_{cs}}{\tau_{Tsi}}\right]}-1\right]}T_{mc2}+\frac{\left[e^{\left[-\frac{\tau_{ms}}{\tau_{Tos}}+\frac{\tau_{cs}}{\tau_{Tis}}\right]}-1\right]}{\left[\frac{\tau_{Tos}.v_{ms}}{\tau_{Tis}.v_{cs}}e^{\left[-\frac{\tau_{ms}}{\tau_{Tos}}+\frac{\tau_{cs}}{\tau_{Tsi}}\right]}-1\right]}T_{c1} \tag{4.3}$$

$$T_{c2}=\frac{\frac{\tau_{Tos}.v_{ms}}{\tau_{Tis}.v_{cs}}\left[e^{\left[-\frac{\tau_{ms}}{\tau_{Tos}}+\frac{\tau_{cs}}{\tau_{Tis}}\right]}-1\right]}{\left[\frac{\tau_{Tos}.v_{ms}}{\tau_{Tis}.v_{cs}}e^{\left[-\frac{\tau_{ms}}{\tau_{Tos}}+\frac{\tau_{cs}}{\tau_{Tis}}\right]}-1\right]}T_{mc2}+\frac{\left[\frac{\tau_{Tos}.v_{ms}}{\tau_{Tis}.v_{cs}}-1\right]}{\left[\frac{\tau_{Tos}.v_{ms}}{\tau_{Tis}.v_{cs}}e^{\left[-\frac{\tau_{ms}}{\tau_{Tos}}+\frac{\tau_{cs}}{\tau_{Tis}}\right]}-1\right]}T_{c1} \tag{4.4}$$

The solution of these equations is trivial provided that the surface areas and heat transfer coefficients are known. The heat transfer surface areas and fluid flow cross sectional areas are given in the Nomenclature and also in Appendix E. Here we have taken the heat transfer coefficients as 2500 W/m^2.K. With a set of inputs (i.e., $w_f = 0.125$ kg/kg, $T_{mc1} = 12.0\,^{\circ}$C, $M_f = 15.3$ kg/s, $T_{v1} = 53.2\,^{\circ}$C, $M_{vac} = 3.50$ kg/s, $T_{c1} = 69.9\,^{\circ}$C and $M_c = 9.49$ kg/s) we can calculate the heat exchanger temperature profile and the outlet temperatures. The resulting temperature profile is shown in Figure 4-1 and this also gives the outlet temperatures (i.e., $T_{mc2} = 22.02\,^{\circ}$C, $T_{mc3} = 50.0\,^{\circ}$C, $T_{v2} = 12.0\,^{\circ}$C and $T_{c2} = 25.4\,^{\circ}$C).

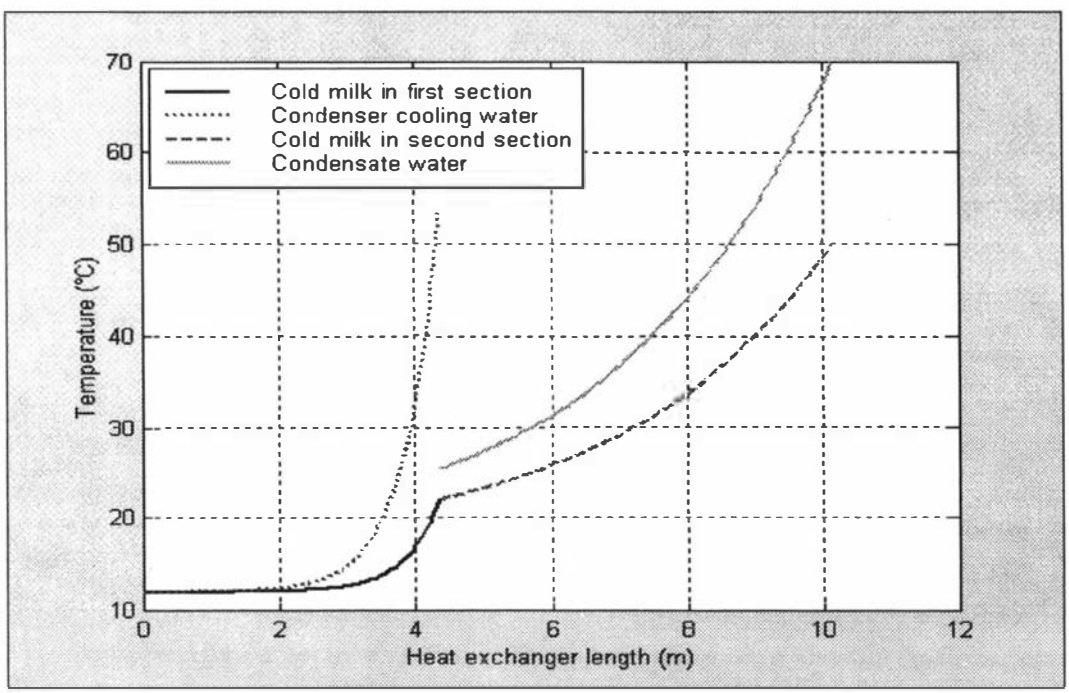

Figure 4-1 : Plate heat exchanger temperature profile.

4.2.3) Preheat Section

The steady state equations for the preheat section were derived in Chapter 3. Two models were derived, the first consisting of implicit equations (Advanced) and the second explicit equations (Simple). The second model was derived from the first by neglecting the changes in mass flows through the preheat section. However, the assumptions required to produce the 'Simple' model are expected to reduce its accuracy.

Advanced model

Using the results from Chapter 3 we can produce the following equations for the mass flows around the flash vessel.

$$M_{ph2} = M_{fc2} + m_{dsi},\quad M_{ph1} = \frac{\left[M_{fc2} + m_{dsi}\right]}{\left[1-a_2\right]},\quad M_{fh1} = \frac{\left[M_{fc2} + m_{dsi}\right]}{\left[1-a_1\right]\left[1-a_2\right]},\quad M_{pc2} = \frac{\left[M_{fc2} + a_2.m_{dsi}\right]}{\left[1-a_2\right]} \tag{4.5}$$

$$a_1 = \frac{\left(C_{pwater} - C_{pTS}.w_{fh1}\right)}{\lambda}\left(T_{fh1} - T_{ph1}\right),\qquad a_2 = \frac{\left(C_{pwater} - C_{pTS}.w_{ph1}\right)}{\lambda}\left(T_{ph1} - T_{ph2}\right) \tag{4.6}$$

The flash vessel temperatures are given by equations (4.7) and (4.8).

$$M_{fc2}\left(C_{pwater} - C_{pTS}.w_{fc2}\right)\left(T_{pc2} - T_{fc2}\right) = M_{ph1}\left(C_{pwater} - C_{pTS}.w_{ph1}\right)\left(T_{ph1} - T_{ph2}\right) \tag{4.7}$$

$$M_{pc2}\left(C_{pwater} - C_{pTS}.w_{pc2}\right)\left(T_{pc1} - T_{pc2}\right) = M_{fh1}\left(C_{pwater} - C_{pTS}.w_{fh1}\right)\left(T_{fh1} - T_{ph1}\right) \tag{4.8}$$

We can substitute equations (4.5) and (4.6), to produce the following pair of equations.

$$M_{fc2}\left(C_{pwater} - C_{pTS}.w_{fc2}\right)\left(T_{pc2} - T_{fc2}\right) = \frac{\left[M_{fc2} + m_{dsi}\right]}{\left[1-a_2\right]}\left(C_{pwater} - C_{pTS}.w_{ph1}\right)\left(T_{ph1} - T_{ph2}\right) \tag{4.9}$$

$$\frac{\left[M_{fc2} + a_2.m_{dsi}\right]}{\left[1-a_2\right]}\left(C_{pwater} - C_{pTS}.w_{pc2}\right)\left(T_{pc1} - T_{pc2}\right) = \frac{\left[M_{fc2} + m_{dsi}\right]}{\left[1-a_2\right]\left[1-a_1\right]}\left(C_{pwater} - C_{pTS}.w_{fh1}\right)\left(T_{fh1} - T_{ph1}\right) \tag{4.10}$$

The DSI unit energy balance then produces a third implicit equation.

$$\left(h_{steam} - C_{pwater}.T_{dsi}\right)m_{dsi} = M_{pc1}\left(C_{pwater} - C_{pTS}.w_{pc1}\right)\left(T_{DSI} - T_{pc1}\right) \tag{4.11}$$

Using the above implicit equations (4.9), (4.10) and (4.11), with a set of inputs (i.e., $m_{dsi} = 0.35$ kg/s, $T_{fc2} = 63.7\,^{\circ}\mathrm{C}$, and $M_f = 15.3$ kg/s), we can calculate the operating conditions (i.e., $T_{ph1} = 91.5\,^{\circ}\mathrm{C}$, $T_{ph2} = 77.9\,^{\circ}\mathrm{C}$ and $T_{DSI} = 104.4\,^{\circ}\mathrm{C}$). The variables a_1 and a_2, required in equations (4.9), (4.10) and (4.11), are calculated using equation (4.6).

Simple model

As mentioned above, the assumption of constant preheat mass flows produces a 'Simple' preheat model. The preheat flash vessel temperatures are given by equation (4.12) and the DSI unit temperature is given by equation (4.14).

$$T_{ph1} = \frac{2}{3}T_{DSI} + \frac{1}{3}T_{fc2}, \qquad T_{ph2} = \frac{1}{3}T_{DSI} + \frac{2}{3}T_{fc2} \tag{4.12}$$

$$m_{dsi}\left(h_{steam} - C_{pwater}.T_{dsi}\right) = M_{fc2}.C_{pwater}\left(T_{DSI} - T_{ph1}\right) = \frac{M_{fc2}.C_{pwater}}{3}\left(T_{DSI} - T_{fc2}\right) \tag{4.13}$$

$$T_{DSI} = \frac{\left[3.m_{dsi}.h_{steam} + M_{fc2}.C_{pwater}.T_{fc2}\right]}{\left[M_{fc2}.C_{pwater} + 3.C_{pwater}.m_{dsi}\right]} \tag{4.14}$$

These equations are a lot simpler than the 'Advanced' model. However, the predicted temperatures and DSI unit mass flow are relatively different. This can be shown by considering a preheat system with the same inputs (i.e., $m_{dsi} = 0.4\,\text{kg/s}$, $T_{fc2} = 63.7\,^{\circ}\text{C}$ and $M_f = 15.3\,\text{kg/s}$). The operating conditions are $T_{ph1} = 89.3\,^{\circ}\text{C}$, $T_{ph2} = 76.5\,^{\circ}\text{C}$ and $T_{DSI} = 102.2\,^{\circ}\text{C}$, which are a little different from those of the 'Advanced' model.

4.2.4) MVR Section

The MVR evaporator section steady state is determined by the solution of the equations for the evaporator effect, evaporator shell (combined with the preheat condenser equations), MVR compressor and the falling film mass balances. In Chapter 2, the evaporator effect and shell energy balances are derived. We will take the energy balances given by equations (2.25) and (2.58) and are shown here by equations (4.15) and (4.16).

$$q_{feed1} + q_{shellt} = q_{comp1} + q_{eloss1} \tag{4.15}$$

$$W_{comp1} + q_{comp1} = q_{shellt} + q_{pcond} + q_{sloss1} + q_{condensate1} \tag{4.16}$$

The static condenser heat flow is given by equation (4.17). This was derived in Chapter 3 and is the same as equation (3.35).

$$q_{pcond} = M_f\left(C_{pwater} - C_{pTS}.w_f\right)\left(T_{s1} - T_{mc3}\right)\left(1 - e^{-\frac{\tau_{pre}}{\tau_{Tpre}}}\right) \tag{4.17}$$

$$\tau_{pre} = \frac{M_{pre}}{\rho_{pre}.V_{pre}}, \qquad \tau_{Tpre} = \frac{\rho_{pre}.V_{pre}\left(C_{pwater} - C_{pTS}.w_f\right)}{U_{pre}.A_{pre}} \tag{4.18}$$

The compressor characteristic curves are given by equations (4.19) and (4.20). These were discussed in Chapter 2 and are the same as equations (2.64) and (2.65). The vapour densities and

pressures are given by the Antoine saturation equations, which are discussed in Chapter 2 and are shown by equation (2.70).

$$\frac{[P_{s1}-P_{e1}]}{\rho_{ve1}}=a_{comp}.N_{comp}^2+b_{comp}.N_{comp}\left(\frac{M_{compl}}{\rho_{ve}}\right)+c_{comp}\left(\frac{M_{compl}^2}{\rho_{ve}^2}\right) \tag{4.19}$$

$$\frac{W_{compl}}{\rho_{ve1}}=d_{comp}.N_{comp}^2\left(\frac{M_{compl}}{\rho_{ve}}\right)+e_{comp}.N_{comp}\left(\frac{M_{compl}^2}{\rho_{ve}^2}\right)+f_{comp}\left(\frac{M_{compl}^3}{\rho_{ve}^3}\right) \tag{4.20}$$

Equation (4.19) is a quadratic for the mass flow of compressed vapour (M_{compl}) and it can be solved to produce equation (4.21). There are two solutions to equation (4.19), but we have taken the larger solution because it represents the 'real' operating conditions. This mass flow of compressed vapour is also equal to the mass flow of evaporated water, as shown by equation (4.22).

$$M_{compl}=-\frac{\rho_{ve}.b_{comp}.N_{comp}}{2.c_{comp}}-\frac{\rho_{ve}\sqrt{(b_{comp}.N_{comp})^2-4.c_{comp}\left(a_{comp}.N_{comp}^2-\frac{(P_{s1}-P_{e1})}{\rho_{ve1}}\right)}}{2.c_{comp}} \tag{4.21}$$

$$M_{compl}=M_{flash1}+M_{tubest}=M_{ph2}-M_{p5} \tag{4.22}$$

Where, M_{compl} = mass flow of compressed vapour. (kg/s)

M_{flash1} = mass flow of flash vapour. (kg/s)

M_{tubest} = total mass flow of evaporated water in the MVR evaporator section. (kg/s)

M_{ph2} = mass flow of milk to the MVR evaporator section. (kg/s)

M_{p5} = mass flow of milk from the MVR evaporator section. (kg/s)

The mass flow of evaporation in the falling film is modelled using equation (4.23). In Chapter 5 it is shown that this is the most accurate model. The heat transfer parameters are taken for Whole Milk and they are U_{so} =1900.7 W/m^2.°C and U_{sw} = 2901.6 W/m^2.°C. The heat transfer surface areas (A_{si}) are listed in Appendix E, along with the other geometric parameters for the Evaporator A plant. Using equation (4.23) we can calculate the mass flow of evaporation and the evaporation heat flow (i.e., $q_{shell}=\lambda M_{tubes}$) for a falling film evaporator pass. It should also be remembered that there are five passes in the MVR evaporator section. As a result we have a mass flow (M_{pi}) and dry matter (w_{pi}) from the evaporator pass i and they depend on the mass flow (M_{di}) and dry matter (w_{di}) from the pass i distribution plate.

$$M_{pi}=M_{di}-M_{tubesi}, \qquad w_{pi}=\frac{M_{di}.w_{di}}{[M_{di}-M_{tubesi}]}, \qquad M_{tubesi}=[U_{so}-U_{sw}.w_{di}]\frac{A_{si}.\Delta T}{\lambda} \tag{4.23}$$

Where, U_{so}	=	simple linear heat transfer model coefficient.	($W/m^2.°C$)
U_{sw}	=	simple linear heat transfer model coefficient.	($W/m^2.°C$)
A_{si}	=	evaporating tubes heat transfer area for the i pass.	(m^2)
M_{tubesi}	=	mass flow of evaporation from the i pass.	(kg/s)
ΔT	=	temperature difference between evaporator shell and effect.	(°C)

From the above we can see that the steady state for the MVR evaporator section is given by the solution of two implicit equations. These are the energy balances for the MVR evaporator effect and shell. All of the other equations can be solved and substituted into the energy balances. With a set of inputs (i.e., $N_{comp} = 2850$ rpm, $M_{ph2} = 15.65$kg/s, $T_{ph2} = 77.9$ °C, $w_{ph2} = 0.122$kg/kg, $M_f = 15.3$ kg/s, $T_{mc3} = 50$ °C and $T_a = 30$ °C) we can solve these equations to determine the implicit variables ($T_{e1} = 66.2$ °C and $T_{s1} = 69.9$ °C) and the output variables ($T_{e1} = 66.2$ °C, $M_{p5} = 4.68$kg/s and $w_{p5} = 0.408$kg/kg).

4.2.5) TVR Section

The TVR section steady state equations are similar to those for the MVR section. In Chapter 2, the TVR evaporator effect and shell energy balances are derived. We take the energy balances given by equations (2.30), (2.35) and (2.63), which are shown here by equations (4.24), (4.25) and (4.26).

$$q_{feed6} + q_{shell6} = q_{comp2} + q_{eloss2} + q_{shell7} + q_{shell8} \tag{4.24}$$

$$W_{comp2} + q_{comp2} = q_{shell6} + q_{sloss2} + q_{condensate2} \tag{4.25}$$

$$q_{feed7} + q_{shell7} + q_{shell8} = q_{eloss3} + q_{vac} \tag{4.26}$$

The vacuum condenser heat flow (q_{vac}) heat flow is also given by equation (4.17), which was used for the preheat condenser. We again use the simple linear falling film heat transfer model, which is shown by equation (4.27).

$$M_{pi} = M_{di} - M_{tubesi}, \qquad w_{pi} = \frac{M_{di}.w_{di}}{[M_{di} - M_{tubesi}]}, \qquad M_{tubesi} = [U_{so} - U_{sw}.w_{di}]\frac{A_{si}.\Delta T}{\lambda} \tag{4.27}$$

From the above we can see that the steady state for the TVR evaporator section is given by the solution of three implicit equations. These are the energy balances for the second evaporator effect, evaporator shell and the third evaporator effect. With a set of inputs (i.e., $M_{p5} = 4.68$ kg/s, $w_{p5} = 0.408$ kg/kg, $T_{p5} = 66.2$ °C, $P_{sp} = 5.00$ bar, $M_{vac} = 3.5$ kg/s and $T_{vac} = 24.0$ °C) we can determine the implicit variables (i.e., $T_{s2} = 63.4$ °C, $T_{e2} = 57.5$ °C and

$T_{e3} = 53.2\,°C$) and the output variables (i.e., $T_{e3} = 53.2\,°C$, $M_{p8} = 4.070$ kg/s and $w_{p8} = 0.469$ kg/kg).

4.2.6) Complete Evaporator A Steady State

By combining the four steady state models we produce the complete model for the Evaporator A plant. The inputs are the feed milk flow, dry matter and temperature, the vacuum condenser cooling water flow and temperature, the condensate mass flow to the plate heat exchanger, the MVR compressor speed, the preheat DSI unit steam mass flow and the TVR compressor steam pressure (i.e., M_f, w_f, T_f, M_{vac}, T_{vac1}, M_c, N_{comp}, m_{dsi} and P_{sp}). The outputs are the product concentrate, evaporator temperatures, plate heat exchanger temperatures and preheat temperatures (M_{p5}, w_{p5}, M_{p8}, w_{p8}, T_{e1}, T_{e3}, T_{mc3}, T_{DSI}, T_{ph1} and T_{ph2}). Figure 4-2 shows the connections between the four Evaporator A plant sections. This clearly shows the important feedback loops through the DSI preheat section and plate heat exchanger.

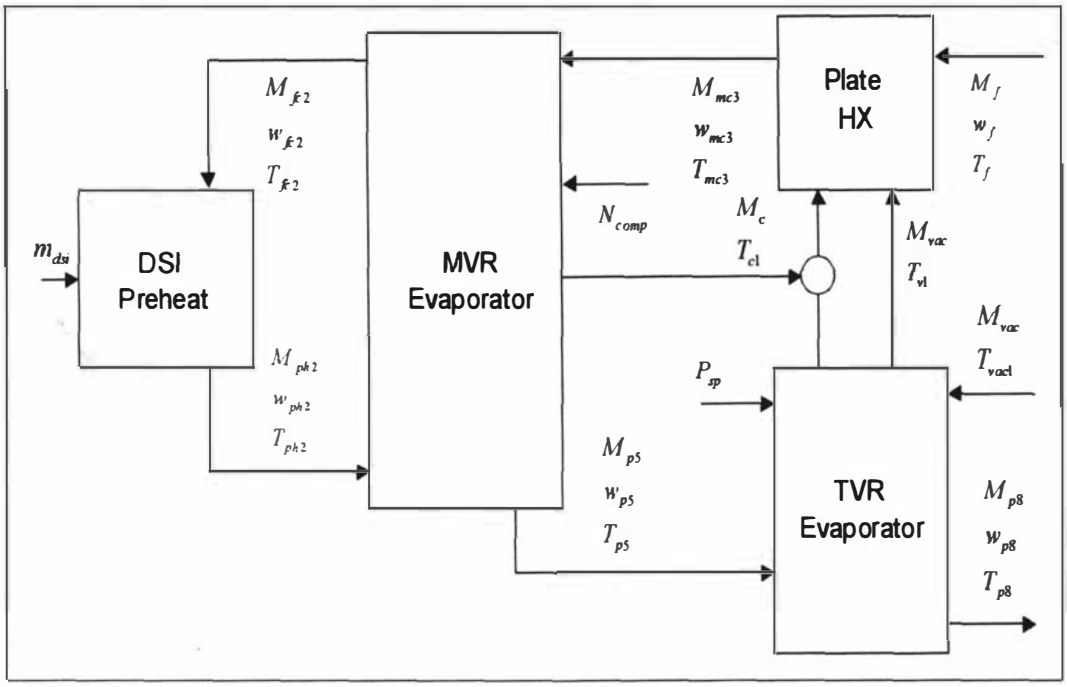

Figure 4-2 : Interconnections between systems for the complete Evaporator A plant model.

We are interested in the process gains between the model inputs and outputs. These are important, because they give an indication of the process sensitivity. Table 4-1 shows the calculated process gains about a static operating point. Many of these results can be understood by considering the 'overall' energy and mass balances for the Evaporator A plant. These are shown by equations (4.28) – (4.31), for the energy balance, and (4.32), for the mass balances.

$$q_{feedm} + q_{steam} + W_{comp1} + q_{cool} = q_{cond1} + q_{cond2} + q_{loss} \tag{4.28}$$

$$q_{feedm} = M_f\left(C_{pwater} - C_{pTS}.w_f\right)\left(T_f - T_{e3}\right), \qquad q_{steam} = \left(m_{dsi} + A_{TVR}.P_{sp}\right)\left(h_{steam} - C_{pwater}.T_{e3}\right) \tag{4.29}$$

$$q_{cool} = M_{vac}.C_{pwater}(T_{vac1} - T_{v2}), \quad q_{cond1} = M_c.C_{pwater}(T_{c2} - T_{e3}) + M_r.C_{pwater}(T_{s1} - T_{e3}), \tag{4.30}$$

$$q_{cond2} = M_{scond2}.C_{pwater}(T_{s2} - T_{e3}) + M_{cond2}C_{pwater}(T_{e2} - T_{e3}) \tag{4.31}$$

$$M_f + m_{dsi} + A_{TVR}.P_{sp} = M_{p8} + M_{scond1} + M_{scond2} + M_{cond2} + M_{cond3}, \quad M_f.w_f = M_{p8}.w_{p8} \tag{4.32}$$

Where, q_{feedm} = net enthalpy in the feed milk to the evaporator plant. (W)

q_{steam} = net enthalpy in the steam to the DSI unti and TVR compressor. (W)

q_{cool} = net enthalpy in the cooling water to the vacuum condenser. (W)

q_{cond1} = net enthalpy removed by the condensate from the MVR evaporator. (W)

q_{cond2} = net enthalpy removed by the condensate from the TVR evaporator. (W)

W_{comp1} = power supplied to the MVR compressor. (W)

q_{loss} = heat losses from the surfaces of the MVR and TVR evaporators. (W)

M_c = mass flow of condensate water passing through the heat exchanger. (kg/s)

M_r = mass flow of condensate water bypassing the heat exchanger. (kg/s)

Table 4-1 : Static process gains for Evaporator A plant, for Whole Milk.

	N_{comp} = 2850 rpm	P_{sp} = 500000 Pa (x1e^5)	M_f = 15.3 kg/s	T_f = 12 °C	w_f = 0.125 kg/kg	M_c = 9.042 kg/s	m_{dsi} = 0.35 kg/s	M_{vac} = 3.5 kg/s	T_{vac1} = 24 °C
T_{mc3} = 50.00 °C	0.0102	0.4642	-7.0553	0.9252	63.0646	5.6412	80.4789	2.3559	0.1357
T_{e1} = 66.19 °C	0.0148	0.4657	-8.1040	0.9283	66.8355	5.2575	122.4784	2.3637	0.1361
T_{s1} = 69.96 °C	0.0190	0.5262	-9.2156	1.0487	83.1947	5.9396	138.1457	2.6705	0.1538
T_{DSI} = 104.38 °C	0.0151	0.4730	-10.8913	0.9428	94.2602	5.3570	220.4121	2.4007	0.1383
T_{ph1} = 91.45 °C	0.0155	0.4835	-10.3280	0.9636	90.1516	5.4991	190.1540	2.4536	0.1413
T_{ph2} = 77.89 °C	0.0158	0.4946	-9.7036	0.9859	85.5886	5.6554	156.8154	2.5104	0.1446
T_{e2} = 57.48 °C	0.0078	2.1249	-3.9926	0.5062	81.0893	2.7282	66.8373	-1.8905	0.4564
T_{s2} = 63.36 °C	0.0262	3.1531	-10.2654	1.0919	181.6718	5.8757	142.9105	-0.9932	0.6135
T_{e3} =53.24 °C	-0.0088	1.5531	1.7387	-0.0198	2.3725	-0.3552	-1.4717	-3.8431	0.4533
w_{p5} = 0.408kg/kg	0.0007	0.0100	-0.2250	0.0200	3.4741	0.1132	2.5828	0.0508	0.0029
w_{p8} = 0.469kg/kg	0.0009	0.0185	-0.3039	0.0269	4.1057	0.1524	3.4900	0.0700	0.0038
M_{p5} = 4.68 kg/s	-0.0079	-0.1148	2.8887	-0.2288	-2.3793	-1.2984	-29.6076	-0.5827	-0.0336
M_{p8} = 4.07 kg/s	-0.0079	-0.1603	2.9032	-0.2335	-3.0213	-1.3215	-30.2383	-0.6069	-0.0328

There are several important things that can be noted from the process gains in Table 4-1. Firstly there is a great degree of coupling between the four sections of the Evaporator A plant. As a

result every input has a direct impact on the entire plant, rather than just a small part of the process. This is important, because it means the plant must be considered in its entirety.

Another important result is the strong impact of the feed dry matter on the plant. This acts on the physical properties of the milk (i.e., heat capacity and heat transfer coefficients) and also directly on the product dry matter, via the mass balance. For example, an increase in the feed dry matter causes a reduction in the milk heat capacity and this increases the net enthalpy to the plant, because the sign of q_{feedm} is negative. The result is an increase in all the evaporator plant temperatures. However, an increase in the feed dry matter also causes a direct increase in the product dry matter.

The feed mass flow acts directly on the evaporator temperatures, product mass flow and dry matters, via the mass and energy balances. An increase in the mass flow causes a reduction in the net enthalpy to the evaporator plant. Once again, this is caused by the negative sign of the q_{feedm} energy flow and the result is a reduction in the evaporator temperatures. However, the feed mass flow also acts on the mass balances, with an increase in the feed mass flow causing an increase in the product mass flows and a reduction in the product dry matters.

The mass flow of cooling water (M_{vac}) has an interesting impact on the evaporator temperatures. An increase in M_{vac} causes an increase in q_{cool}, which we expect to cause an increase in the temperatures of the plant. However, the TVR evaporator section temperatures all reduce, in contrast to those of the DSI preheat and MVR evaporator sections, which all increase. In fact the reduction in the TVR evaporator section temperatures is caused by the 'internal' energy balances for that section.

The mass flow of steam to the DSI unit (m_{dsi}) has a strong impact on the evaporator plant temperatures. The overall energy balance shows that an increase in m_{dsi} causes an increase in the steam enthalpy to the plant. Unsurprisingly, this causes the evaporator temperatures to increase.

Another very important result is the impact of the MVR evaporator section temperature on the total plant evaporation. Any impact that causes an increase in the MVR temperature can be oberved to also cause an increase in the product dry matter and a reduction in the product mass flow. Even an increase in m_{dsi}, which dilutes the feed milk, causes a substantial increase in the product dry matter, since it has a large impact on the MVR temperature. In Chapter 6 the cause of this effect is explained, with reference to the MVR compressor equations.

4.3) Linear Dynamic Model Development Methodology

4.3.1) Linearisation of Non-Linear Differential Equations

The differential equations derived in the previous two chapters are non-linear. Non-linear dynamic models are inconvenient because they often have no analytical solution. Consequently, most traditional analytical dynamic analysis has been based on systems with linear constant coefficient differential equations. This is because the analytical solutions for these systems are given by simple exponential functions. A non-linear system of first order differential equations can be converted to a linear system with constant coefficients by using first order Taylor series

approximations. For example the following differential equation can be approximated by a truncated Taylor series (Skogestad and Postlewaite, 1996, pp 8-10).

$$\frac{dx}{dt}=f(x,u), \qquad \frac{dx}{dt}=f(x,u)\approx f(x^0,u^0)+\left.\frac{\partial f}{\partial x}\right|_0 (x-x^0)+\left.\frac{\partial f}{\partial u}\right|_0 (u-u^0) \tag{4.33}$$

Where the superscript ^{0} denotes the steady state value of the variables. For example x^o denotes the steady state value of the variable x and the linearisation is made around these steady values. This notation is used throughout this Chapter. It is common to redefine the variables as deviation variables ($x=x-x^0, u=u-u^0$) so that this is simplified to the following. This differential equation is linear with constant coefficients

$$\frac{dx}{dt}=\left.\frac{\partial f}{\partial x}\right|_0 x+\left.\frac{\partial f}{\partial u}\right|_0 u \tag{4.34}$$

4.3.2) Linearisation of Pure Delays

An important part of many dynamic models is the linearisation of pure delays. The conventional approach for dealing with pure delays is to use Pade approximations. In the Laplace Domain the pure delay is given by an exponential function and this is transformed to a polynomial function using the Pade approximation. For example, an n-th order Pade approximation of the Laplace Domain pure delay is given by equation (4.35) (Skogestad and Postlewaite, 1996, p 121).

$$e^{(-\tau_h \cdot s)}\approx \frac{\left(1-\frac{\tau_h}{2.n}s\right)^n}{\left(1+\frac{\tau_h}{2.n}s\right)^n} \tag{4.35}$$

Where, τ_h = pure delay time. (s)
n = order of the Pade approximation. (-)

When transformed into the time domain this produces a finite order ordinary differential equation. For example, equation (4.36) shows the resulting differential equation for a first order Pade approximation.

$$\frac{\tau_h}{2}\frac{dy(t-\tau_h)}{dt}+y(t-\tau_h)=y-\frac{\tau_h}{2}\frac{dy}{dt} \tag{4.36}$$

4.4) Linear Dynamic Model

4.4.1) Introduction

As with the steady state model, we develop the linear dynamic model by separating the Evaporator A plant into four parts and considering each independently. Then, at the end of this section we combine these to produce the complete linear dynamic model for the Evaporator A plant. However, the dynamic model developed here contains many assumptions and it is not a

dynamic version of the steady state model. For example, we assume constant falling film overall heat transfer coefficients, whereas the steady state model does not make this assumption. Without these assumptions the linear model development would have been excessively difficult. Furthermore the impact on the system dynamics would probably have been minor. Since we are primarily concerned with the dynamics, rather than the static process gains, these assumptions are considered to be reasonable.

4.4.2) Plate Heat Exchanger

The previous chapter showed that the partial differential equations for the plate heat exchanger could be solved by linearisation and integration in the Laplace Domain. The resulting transfer functions are shown by equations (3.85) to (3.93). However, these transfer functions do not represent linear differential equations with constant coefficients. Consequently the state space representation of the plate heat exchanger could not be developed. However, the Bode plots and Nyquist plots could be determined numerically. This was done for the second section of the Evaporator A plate heat exchanger and the resulting Bode plots are shown by Figure 3-7, Figure 3-8 and Figure 3-9.

We can use the transfer functions of Chapter 3 to produce the transfer functions for both the first and second sections of the heat exchanger. These can be combined and used to numerically calculate the Bode and Nyquist plots for the Evaporator A plate heat exchanger. The Bode plots have been calculated and they are shown in Chapter 7 by Figure 7-5, Figure 7-6 and Figure 7-8.

4.4.3) DSI Preheat Section

Here we develop the linear dynamic model for the evaporator DSI preheat section. We use the simple dynamic model, which was derived in Chapter 3. The following differential equations are used to describe the preheat system. These equations are the same as equations (3.26) and (3.27).

$$I_{DSI}\frac{dT_{DSI}}{dt} = M_{fc2}.C_{pwater}\left(T_{ph1}-T_{DSI}\right)+\left[h_{steam}-C_{pwater}.T_{DSI}\right]m_{dsi},\quad \tau_{DSI}=\frac{I_{DSI}}{\left(M^{0}_{fc2}+m_{dsi}\right)C_{pwater}} \qquad (4.37)$$

$$I_{fl1}\frac{dT_{ph1}}{dt} = M_{fc2}.C_{pwater}\left(T_{fh1}-2.T_{ph1}+T_{ph2}\right),\qquad \tau_{fl1}=\frac{I_{fl1}}{M^{0}_{fc2}.C_{pwater}} \qquad (4.38)$$

$$I_{fl2}\frac{dT_{ph2}}{dt} = M_{fc2}.C_{pwater}\left(T_{ph1}-2.T_{ph2}+T_{fc2}\right),\qquad \tau_{fl2}=\frac{I_{fl2}}{M^{0}_{fc2}.C_{pwater}} \qquad (4.39)$$

Where, I_{DSI}	=	thermal inertia of the DSI.	(J/K)
I_{fl1}	=	thermal inertia of the first flash vessel.	(J/K)
I_{fl2}	=	thermal inertia of the second flash vessel.	(J/K)
T_{DSI}	=	temperature of the DSI unit.	(°C)
T_{ph1}	=	temperature of the first flash vessel.	(°C)
T_{ph2}	=	temperature of the second flash vessel.	(°C)

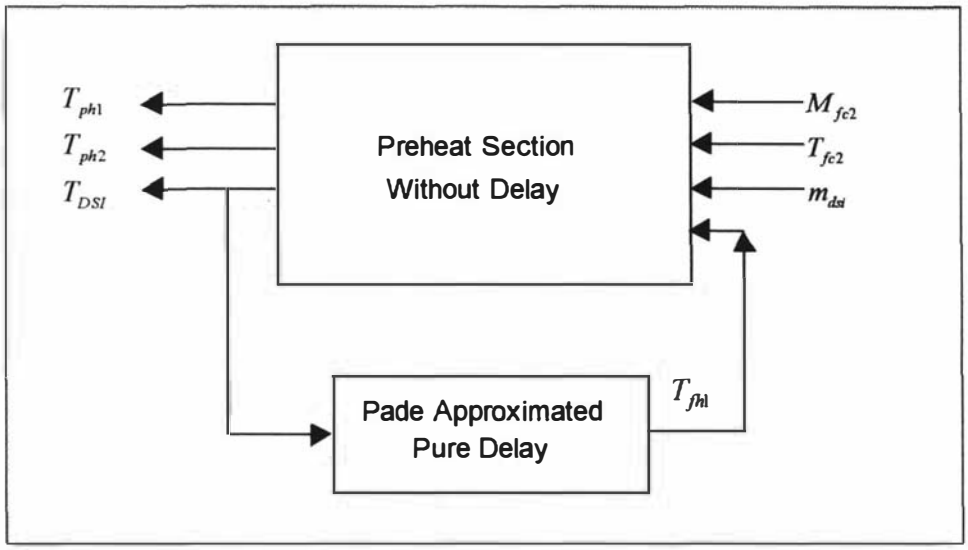

Figure 4-3 : Connection of preheat section linear models.

Equations (4.37), (4.38) and (4.39) are linearised to produce the following state space representation for the system.

$$\begin{bmatrix} \frac{dT_{DSI}}{dt} \\ \frac{dT_{ph1}}{dt} \\ \frac{dT_{ph2}}{dt} \end{bmatrix} = \begin{bmatrix} -\frac{1}{\tau_{DSI}} & \frac{1}{\tau_{DSI}} & 0 \\ 0 & -\frac{2}{\tau_{f1}} & \frac{1}{\tau_{f1}} \\ 0 & \frac{1}{\tau_{f12}} & -\frac{2}{\tau_{f12}} \end{bmatrix} \begin{bmatrix} T_{DSI} \\ T_{ph1} \\ T_{ph2} \end{bmatrix} + \begin{bmatrix} \frac{C_{pwater}\left(T^0_{ph1} - T^0_{DSI}\right)}{I_{DSI}} & 0 & 0 & \frac{\left[h_{steam} - C_{pwater}.T^0_{DSI}\right]}{I_{DSI}} \\ \frac{C_{pwater}\left(T^0_{fh1} + T^0_{ph2} - 2.T^0_{ph1}\right)}{I_{f1}} & 0 & \frac{1}{\tau_{f1}} & 0 \\ \frac{C_{pwater}\left(T^0_{ph1} + T^0_{fc2} - 2.T^0_{ph2}\right)}{I_{f12}} & \frac{1}{\tau_{f12}} & 0 & 0 \end{bmatrix} \begin{bmatrix} M_{fc2} \\ T_{fc2} \\ T_{fh1} \\ m_{dsi} \end{bmatrix} \quad (4.40)$$

The additional equation required to describe this system is the delay between the DSI unit and the end of the holding tubes. This pure delay can be represented by a Pade approximation. The complete linear dynamic model is then produced by feeding back the pure delay variable to the first flash vessel, as shown in Figure 4-3.

4.4.4) MVR Evaporator Section

Here we develop the linear dynamic model for the MVR evaporator section. As the basis we will take the differential equations developed in Chapters 2 and 3. However, to simplify the equations the assumptions listed below are made. The assumptions are not expected to impact on the process dynamics, which are important for the controllability analysis. This reasoning is based on the nature of the process dynamics. The process delays (i.e., falling film, condenser, preheat holding tubes, etc) have the most important impact on the dynamics and these are not significantly changed by these assumptions.

1) Constant heat transfer coefficients.
2) Negligible boiling point elevation.
3) Multiple evaporation passes represented as a single pass.
4) No flashing in distribution plates.
5) Constant milk heat capacity and density, equal to water.
6) Pumping delays are neglected.

Distribution plate

The differential equations for the distribution plate are given by the following. The MVR evaporator effect contains five evaporator passes, but we are assuming that these can be represented by a single evaporator pass. Consequently, only one distribution plate in the MVR evaporator section is modelled. The resulting differential equations were derived in Chapter 2 and shown by equation (2.19), while they are shown here by the following.

$$A_{d1}\frac{dh_{d1}}{dt}=\frac{M_{ph2}}{\rho_d}-Q_{d1},\qquad Q_{d1}=C_d.A_{h1}\sqrt{2.g.h_{d1}} \tag{4.41}$$

$$A_{d1}\frac{dw_{d1}}{dt}=\frac{M_{ph2}}{\rho_d.h_{d1}}\left[w_{ph2}-w_{d1}\right] \tag{4.42}$$

The distribution plate equations can be linearised to product equation (4.43) and (4.44), with the linear constant $d_1=\frac{1}{\rho_d.A_{d1}}$ and time constants $\tau_{w1}=\frac{\rho_d.A_{d1}.h_{d1}}{M_{ph2}}$ and $\tau_{h1}=\frac{A_{d1}.Q_{d1}^0}{g(C_d.A_{h1})^2}$.

$$\frac{dh_{d1}}{dt}=d_1.M_{ph2}-\left[\frac{1}{\tau_{h1}}\right]h_{d1} \tag{4.43}$$

$$\frac{dw_{d1}}{dt}=\left[\frac{1}{\tau_{w1}}\right]w_{ph2}-\left[\frac{1}{\tau_{w1}}\right]w_{d1} \tag{4.44}$$

MVR Compressor

The compressor characteristic curve is given by the following. This equation was developed in Chapter 2 and is shown there by equation (2.64).

$$\frac{(P_{s1}-P_{e1})}{\rho_{vel}}=a_{comp}.N_{comp}^2+b_{comp}.N_{comp}.Q_{comp1}+c_{comp}.Q_{comp1}^2,\qquad Q_{comp1}=\frac{q_{comp1}}{\rho_{ve1}.\lambda} \tag{4.45}$$

This can be linearised, in terms of T_{e1}, T_{s1} and N_{comp} to the following equations.

$$Q_{compl}=\left.\frac{\partial Q_{compl}}{\partial T_{el}}\right|_0 T_{el}+\left.\frac{\partial Q_{compl}}{\partial T_{sl}}\right|_0 T_{sl}+\left.\frac{\partial Q_{compl}}{\partial N_{comp}}\right|_0 N_{comp},\quad \left.\frac{\partial Q_{compl}}{\partial T_{el}}\right|_0=-\frac{\left[\dfrac{P_{el}^0.B_{water}}{\rho_{vel}^0\left(T_{el}^0-C_{water}\right)^2}+\dfrac{\left(P_{sl}^0-P_{el}^0\right)B_{vap}}{\rho_{vel}^0\left(T_{el}^0-C_{vap}\right)^2}\right]}{\left[b_{comp}.N_{comp}^0+2.c_{comp}.Q_{compl}^0\right]} \quad (4.46)$$

$$\left.\frac{\partial Q_{compl}}{\partial T_{sl}}\right|_0=\frac{P_{sl}^0.B_{water}}{\rho_{vel}^0\left(T_{sl}^0-C_{water}\right)^2\left[b_{comp}.N_{comp}^0+2.c_{comp}.Q_{compl}^0\right]},\quad \left.\frac{\partial Q_{compl}}{\partial N_{comp}}\right|_0=-\frac{\left(2.a_{comp}.N_{comp}^0+b_{comp}.Q_{compl}^0\right)}{\left(b_{comp}.N_{comp}^0+2.c_{comp}.Q_{compl}^0\right)} \quad (4.47)$$

These can be used to determine the following linear equation for the compressor heat flow.

$$q_{compl}=\alpha_{compl}.T_{el}+\alpha_{comp2}.T_{sl}+\alpha_{comp3}.N_{comp} \quad (4.48)$$

$$\alpha_{compl}=\rho_{vel}^0.\lambda\left.\frac{\partial Q_{compl}}{\partial T_{el}}\right|_0+\frac{\lambda.Q_{compl}^0.\rho_{vel}^0.B_{vap}}{\left(T_{el}^0-C_{vap}\right)^2},\quad \alpha_{comp2}=\rho_{vel}^0.\lambda\left.\frac{\partial Q_{compl}}{\partial T_{sl}}\right|_0,\quad \alpha_{comp3}=\rho_{vel}^0.\lambda\left.\frac{\partial Q_{compl}}{\partial N_{comp}}\right|_0 \quad (4.49)$$

The compressor power supply is given by the following equation. This equation was developed in Chapter 2 and was shown there by equation (2.65).

$$\frac{W_{compl}}{\rho_{vel}}=d_{comp}.N_{comp}^2.Q_{compl}+e_{comp}.N_{comp}.Q_{compl}^2+f_{comp}.Q_{compl}^3 \quad (4.50)$$

This can be linearised to the following.

$$W_{compl}=\beta_{compl}.T_{el}+\beta_{comp2}.T_{sl}+\beta_{comp3}.N_{comp} \quad (4.51)$$

$$\begin{aligned}\beta_{compl}=\frac{\partial W_{compl}}{\partial T_{el}}=\rho_{vel}^0\left(d_{comp}.N_{comp}^2+2.e_{comp}.N_{comp}.Q_{compl}+3.f_{comp}.Q_{compl}^2\right)\left.\frac{\partial Q_{compl}}{\partial T_{el}}\right|_0\\ +\left(d_{comp}.N_{comp}^2.Q_{compl}+e_{comp}.N_{comp}.Q_{compl}^2+f_{comp}.Q_{compl}^3\right)\frac{\rho_{vel}.B_{vap}}{\left(T_{el}^0-C_{vap}\right)^2}\end{aligned} \quad (4.52)$$

$$\beta_{comp2}=\frac{\partial W_{compl}}{\partial T_{sl}}=\left[\rho_{vel}^0\left(d_{comp}.N_{comp}^2+2.e_{comp}.N_{comp}.Q_{compl}+3.f_{comp}.Q_{compl}^2\right)\right]\left.\frac{\partial Q_{compl}}{\partial T_{sl}}\right|_0 \quad (4.53)$$

$$\begin{aligned}\beta_{comp3}=\frac{\partial W_{compl}}{\partial N_{comp}}=\rho_{vel}^0\left(2.d_{comp}.N_{comp}.Q_{compl}+e_{comp}.Q_{compl}^2\right)\\ +\rho_{vel}^0\left(d_{comp}.N_{comp}^2+2.e_{comp}.N_{comp}.Q_{compl}+3.f_{comp}.Q_{compl}^2\right)\left.\frac{\partial Q_{compl}}{\partial N_{comp}}\right|_0\end{aligned} \quad (4.54)$$

Preheat Condenser

We are using the simple condenser model, which was derived in Chapter 3. The condenser is described by equations (4.55)-(4.58) and these are the same as equations (3.50), (3.51) and (3.53) from Chapter 3.

$$T_{fc2}(t)=T_{pcond}(t)+e^{-\frac{\tau_{pre}}{\tau_{Tpre}}}T_{mc3}(t-\tau_{pre})-\frac{\tau_{pre}\left(T_{s1}^{0}-T_{mc3}^{0}\right)e^{-\frac{\tau_{pre}}{\tau_{Tpre}}}}{M_{f}^{0}.\tau_{Tpre}}V_{cond}(t) \tag{4.55}$$

$$\frac{dT_{pcond}(t)}{dt}=-\frac{1}{\tau_{Tpre}}T_{pcond}(t)+\frac{1}{\tau_{Tpre}}T_{s1}(t)-\frac{e^{-\frac{\tau_{pre}}{\tau_{Tpre}}}}{\tau_{Tpre}}T_{s1}(t-\tau_{pre}) \tag{4.56}$$

$$\tau_{pre}\frac{dV_{cond}(t)}{dt}=\frac{1}{\tau_{pre}}M_{f}(t)-\frac{1}{\tau_{pre}}M_{f}(t-\tau_{pre}) \tag{4.57}$$

$$\frac{dq_{pcond}}{dt}=U_{pre}.A_{pre}\frac{dT_{s1}}{dt}-\frac{1}{\tau_{Tpre}}q_{pcond}+\frac{U_{pre}.A_{pre}}{\tau_{pre}}\left[T_{fc2}-T_{mc3}\right] \tag{4.58}$$

These equations, except for (4.58), are already linear differential equations with constant coefficients. We can linearise equation (4.58) and produce a set of linear constant coefficient equations for the condenser. However, the resulting equations can be more easily represented by the following Laplace Domain transfer functions.

$$T_{fc2}(s)=\frac{\left[1-e^{-\frac{\tau_{pre}}{\tau_{Tpre}}}e^{-\tau_{pre}.s}\right]}{\left[\tau_{Tpre}.s+1\right]}T_{s1}(s)+e^{-\frac{\tau_{pre}}{\tau_{Tpre}}}e^{-\tau_{pre}.s}.T_{mc3}(s)-\frac{\tau_{pre}\left(T_{s1}^{0}-T_{mc3}^{0}\right)e^{-\frac{\tau_{pre}}{\tau_{Tpre}}}}{\tau_{Tpre}.M_{f}^{0}}\frac{\left[1-e^{-\tau_{pre}.s}\right]}{\tau_{pre}.s}M_{f}(s) \tag{4.59}$$

$$q_{pcond}(s)=\frac{\rho_{c}.C_{pc}.V_{pre}.s}{\left[\tau_{Tpre}.s+1\right]}T_{s1}(s)+\frac{C_{pc}.M_{f}^{0}}{\left[\tau_{Tpre}.s+1\right]}T_{fc2}(s)-\frac{C_{pc}.M_{f}^{0}}{\left[\tau_{Tpre}.s+1\right]}T_{mc3}(s)+\frac{C_{p}\left(T_{fc2}^{0}-T_{mc3}^{0}\right)}{\left[\tau_{Tpre}.s+1\right]}M_{f}(s) \tag{4.60}$$

An additional problem is the pure delay in the condenser outlet temperature equation. We need to determine a suitable order for the Pade approximation. It appears that a simple first order approximation is acceptable, because of the exponential term preceding the delayed variables. When the pure delay is large this exponential term becomes small and the importance of the delayed variable is reduced.

Evaporator Effect

The MVR evaporator effect temperature is given by the following differential equation. This was derived in Chapter 2 and was shown there by equation (2.25).

$$I_{effect1}\frac{dT_{e1}}{dt}=q_{feed1}+q_{shell1}-q_{comp1}-q_{loss1} \tag{4.61}$$

This can be linearised to the following with the linear constants $a_1=\frac{\left[U_s.A_{st}-\alpha_{comp2}\right]}{I_{effect1}}$, $a_2=\frac{\left[C_{pwater}\left(T^0_{ph2}-T^0_{e1}\right)\right]}{I_{effect1}}$, $a_3=\frac{C_{pwater}M^0_{ph2}}{I_{effect1}}$, $a_4=\frac{\alpha_{comp3}}{I_{effect1}}$, $a_5=\frac{U_l.A_{el1}}{I_{effect1}}$ and the time constant $\tau_{Te1}=\frac{I_{effect1}}{\left[M^0_{ph2}.C_{pwater}+U_s.A_{st}+\alpha_{comp1}+U_l.A_{el1}\right]}$.

$$\frac{dT_{e1}}{dt}=-\frac{1}{\tau_{Te1}}T_{e1}+a_1.T_{s1}+a_2.M_{ph2}+a_3.T_{ph2}-a_4.N_{comp}+a_5.T_a \tag{4.62}$$

Falling Film

The falling film is described by the following delayed equations. These were derived in Chapter 2 and are shown there by equations (2.49) and (2.50). We have represented all five passes of the MVR evaporator with a single falling film evaporator pass. Consequently, these three equations actually describe all five passes of the evaporator.

$$M_{e5}(t)=M_{d1}(t-\tau_{et})-M_{tubest}(t) \tag{4.63}$$

$$w_{e5}(t)=\frac{M_{d1}(t-\tau_{et}).w_{d1}(t-\tau_{et})}{\left[M_{d1}(t-\tau_{et})-M_{tubes1}(t)\right]} \tag{4.64}$$

$$\frac{\tau_{et}.\lambda}{U_s.A_{st}}\frac{dM_{tubest}(t)}{dt}=\left[T_{s1}(t)-T_{e1}(t)-T_{s1}(t-\tau_{et})+T_{e1}(t-\tau_{et})\right] \tag{4.65}$$

Where, $M_{tubest}(t)$	=	mass of evaporation during the MVR evaporator five passes.	(kg/s)
$M_{d1}(t)$	=	mass flow through the first distribution plate.	(kg/s)
$w_{d1}(t)$	=	dry mass fraction of milk through the first distribution plate.	(kg/kg)
τ_{et}	=	total residence time of all five passes of the MVR evaporator.	(s)
$M_{e5}(t)$	=	mass flow from the bottom of the fifth falling film.	(kg/s)
$w_{e5}(t)$	=	dry mass fraction of milk from the bottom of the fifth falling film.	(kg/kg)

The first of these equations is linear in terms of $M_{d1}(t-\tau_{et})$ and $M_{tubest}(t)$. However, the second is non-linear in terms of these same variables, so it must be linearised. Using the Taylor series approximation we can produce the following linear approximation.

$$w_{e5}(t)=\beta_w.w_{d1}(t-\tau_{et})-\beta_Q.M_{d1}(t-\tau_{et})+\beta_M.M_{tubest}(t) \tag{4.66}$$

Where the coefficients are $\beta_{\dot{M}} = \frac{M_{d1}^0}{\left[M_{d1}^0 - M_{tubest}^0\right]}$, $\beta_Q = \frac{M_{tubest}^0 . w_{d1}^0}{\left[M_{d1}^0 - M_{tubest}^0\right]^2}$ and $\beta_M = \frac{M_{d1}^0 . w_{d1}^0}{\left[M_{d1}^0 - M_{tubest}^0\right]^2}$.

The differential equation for $M_{tubest}(t)$ is also linear in terms of $T_{s1}(t)$, $T_{e1}(t)$, $T_{s1}(t-\tau_{et})$ and $T_{e1}(t-\tau_{et})$. However, the equation contains delayed versions of the evaporator effect and shell temperatures and delayed variables are also used in equations (4.63) and (4.64). It is common for industrial falling film evaporators to have long tubes and hence large delays. Consequently, the accurate representation of these delayed variables is very important. We will use Pade approximations to produce finite order ordinary differential equations for the delayed variables. However, we would like to determine an appropriate order for the Pade approximations.

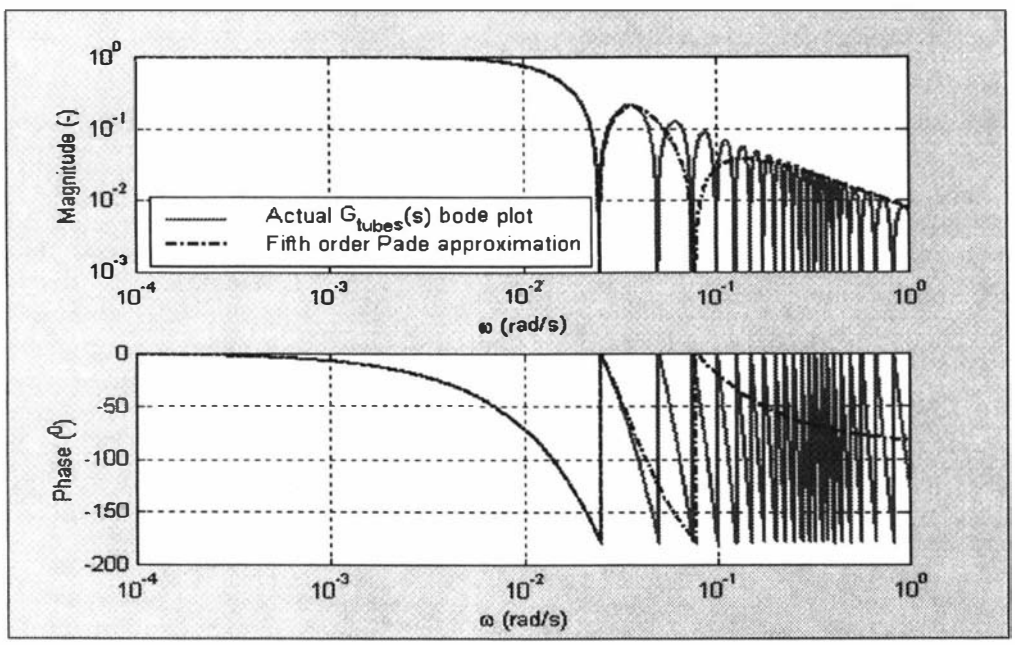

Figure 4-4 : $G_{tubes}(s)$ bode plot and fifth order Pade approximation.

Transforming the $M_{tubest}(t)$ differential equation into the Laplace domain we produce the following transfer function.

$$\frac{M_{tubest}(s)}{\left[T_{s1}(s) - T_{e1}(s)\right]} = \frac{U_s . A_{st}}{\lambda} G_{tubes}(s) \quad \text{with} \quad G_{tubes}(s) = \frac{\left[1 - e^{-\tau_{et} . s}\right]}{\tau_{et} . s} \tag{4.67}$$

Explicit equations can be determined for the $G_{tubes}(s)$ Bode magnitude and phase lag. This is done by substituting the complex term $j.w$ for the laplace variable and determining the magnitude and phase of the resulting complex equation.

$$G_{tubes}(j.w) = \frac{\left[1 - e^{-j.\tau_{et}.w}\right]}{j.\tau_{et}.w} = \frac{\sin(\tau_{et}.w)}{\tau_{et}.w} - j\frac{\left[1 - \cos(\tau_{et}.w)\right]}{\tau_{et}.w} \tag{4.68}$$

$$|G_{tubes}(j.\omega)| = \sqrt{\frac{[1-\cos(\tau_{et}.w)]^2}{\tau_{et}^2.w^2} + \frac{\sin^2(\tau_{et}.w)}{\tau_{et}^2.w^2}} = \frac{2}{\tau_{et}.\omega}\sin\left(\frac{\tau_{et}.\omega}{2}\right) \quad (4.69)$$

$$\angle G_{tubes}(j.\omega) = \arctan\left[-\frac{1-\cos(\tau_{et}.w)}{\sin(\tau_{et}.w)}\right] = \arctan\left[-\frac{2.\sin^2\left(\tau_{et}.w/2\right)}{2.\sin\left(\tau_{et}.w/2\right).\cos\left(\tau_{et}.w/2\right)}\right] = -\frac{\tau_{et}.w}{2} \quad (4.70)$$

Where, ω = frequency. (rad/s)

These explicit functions can be compared to the Pade approximations. Figure 4-4 shows the Bode plots for the actual $G_{tubes}(s)$ transfer function and the fifth order Pade approximation. There is an interesting resonance effect in the falling film equations and this is clearly shown by the results in Figure 4-4. It can be shown that at least a third order Pade approximation is required to produce the resonance effect. However, a fifth order approximation is required to produce an accurate representation of the first resonance frequency.

Evaporator Shell

The MVR evaporator shell temperature is given by the following differential equation. This was derived in Chapter 2 and is shown there by equation (2.58).

$$I_{shell1}\frac{dT_{s1}}{dt} = q_{comp1} + W_{comp1} - q_{shell1} - q_{sloss1} - q_{pcond} - q_{condensate1} \quad (4.71)$$

This can be linearised, with the constants $b_1 = \frac{[U_s.A_{st} + \alpha_{comp1}(1-b_5) + M^0_{comp1}.C_{pwater} + \beta_{comp1}]}{I_{shell1}}$, $b_2 = \frac{[\alpha_{comp3}(1-b_5) + \beta_{comp3}]}{I_{shell1}}$, $b_3 = \frac{U_l.A_{sl1}}{I_{shell1}}$, $b_4 = \frac{1}{I_{shell1}}$, $b_5 = \frac{C_{pwater}}{\lambda}\left(T^0_{s1} - T^0_{e1}\right)$ and the time constant $\tau_{Ts1} = \frac{I_{shell1}}{[U_s.A_{st} - \alpha_{comp2}(1-b_5) + M^0_{comp1}.C_{pwater} - \beta_{comp2} + U_l.A_{sl1}]}$ to produce the following linear constant coefficient differential equation.

$$\frac{dT_{s1}}{dt} = -\frac{1}{\tau_{Ts1}}T_{s1} + b_1.T_{e1} + b_2.N_{comp} + b_3.T_a - b_4.q_{pcond} \quad (4.72)$$

Complete MVR section linear dynamic representation

Using the combined distribution plate, evaporator effect, falling film, evaporator shell and condenser equations we can produce the complete MVR evaporator linear model. However, we first determine the state space models for the evaporator neglecting the condenser and falling film. The state space model for this system is given by the following :

$$\begin{bmatrix} \frac{dh_{d1}}{dt} \\ \frac{dw_{d1}}{dt} \\ \frac{dT_{e1}}{dt} \\ \frac{dT_{s1}}{dt} \end{bmatrix} = \begin{bmatrix} -\frac{1}{\tau_{h1}} & 0 & 0 & 0 \\ 0 & -\frac{1}{\tau_{w1}} & 0 & 0 \\ 0 & 0 & -\frac{1}{\tau_{Te1}} & a_1 \\ 0 & 0 & b_1 & -\frac{1}{\tau_{Ts1}} \end{bmatrix} \begin{bmatrix} h_{d1} \\ w_{d1} \\ T_{e1} \\ T_{s1} \end{bmatrix} + \begin{bmatrix} d_1 & 0 & 0 & 0 & 0 & 0 \\ 0 & \frac{1}{\tau_{w1}} & 0 & 0 & 0 & 0 \\ a_2 & 0 & a_3 & -a_4 & 0 & a_5 \\ 0 & 0 & 0 & b_2 & -b_4 & b_3 \end{bmatrix} \begin{bmatrix} M_{ph2} \\ w_{ph2} \\ T_{ph2} \\ N_{comp} \\ q_{pcond} \\ T_a \end{bmatrix} \quad (4.73)$$

The complete MVR system is produced by combining the above state space representation with the falling film and the preheat condenser equations. Figure 4-5 shows the interconnections between these three systems. The MVR Evaporator Effect is described by equation (4.73), the Preheat Condenser is described by equations (4.59) and (4.60) and the falling film is described by equations (4.63), (4.66) and (4.67).

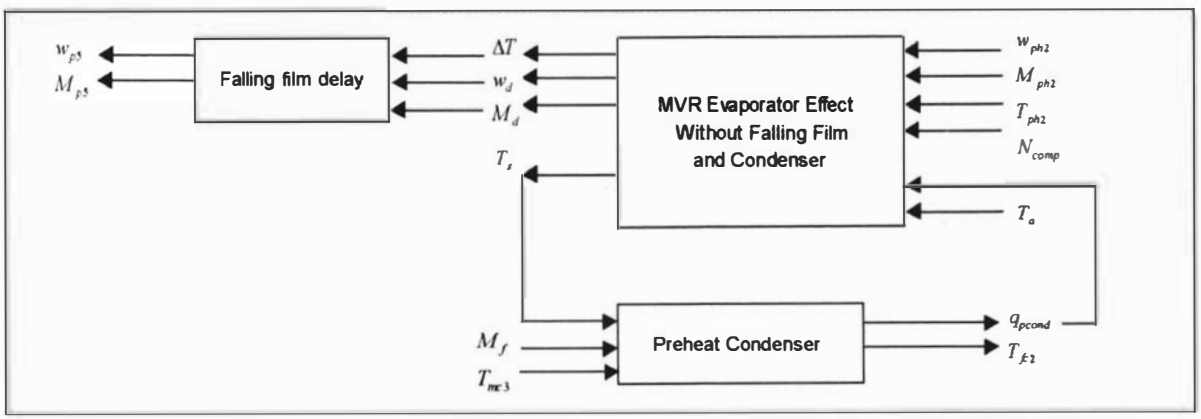

Figure 4-5 : MVR Evaporator Section Linear Model Connections.

4.4.5) TVR Evaporator Section

Much of the TVR evaporator section model is a replication of that for the MVR. However, there are two important differences, firstly the TVR compressor equations are different and secondly the evaporator contains two effects. As with the MVR evaporator equations, we simplify the system by making the following assumptions :

1) Constant heat transfer coefficients.
2) Negligible boiling point elevation.
3) Multiple evaporation passes represented as a single pass.
4) No flashing in distribution plates.
5) Constant heat capacity and density.
6) Pumping delays are neglected.

TVR Compressor

The equations for the TVR compressor are given by equations (4.74) and (4.75). These were derived in Chapter 2 and are given there by equations (2.71) and (2.72).

$$W_{comp2} = \left[h_{steam} - C_{pwater}.T_{s2}\right]A_{TVR}.P_{sp} \tag{4.74}$$

$$q_{comp2} = \frac{\lambda.A_{TVR}.B_{TVR}.P_{e2}.P_{sp}}{P_{sp}^{C_{TVR}}} \tag{4.75}$$

These equations can be linearised to produce the following.

$$W_{comp2} = \beta_{comp2}.T_{s2} + \beta_{comp3}.P_{sp},\ \beta_{comp2} = -C_{pwater}.A_{TVR}.P_{sp}^{0},\ \beta_{comp3} = \left[h_{steam} - C_{pwater}.T_{s2}\right]A_{TVR} \tag{4.76}$$

$$q_{comp} = \alpha_{comp1}.T_{e2} + \alpha_{comp3}.P_{sp},\ \alpha_{comp1} = \frac{\lambda.A_{TVR}.B_{TVR}.P_{e2}^{0}.B_{water}.P_{sp}^{0}}{\left(T_{e2}^{0} + C_{water}\right)^{2} P_{sp}^{C_{TVR}}},\ \alpha_{comp3} = \frac{(1-C_{TVR})\lambda.A_{TVR}.B_{TVR}.P_{e2}^{0}}{P_{sp}^{C_{TVR}}} \tag{4.77}$$

Distribution plate

The same linear distribution plate equations, used for the MVR section, apply for the TVR section. However, with the TVR section we are modelling a two effect system and so two distribution plates must be modelled. We will simply reapply the linear equations (4.43) - (4.44) to produce equations (4.78)-(4.79), with the linear constants $td_1 = \frac{1}{\rho_d.A_{d6}}$ and $tdd_1 = \frac{1}{\rho_d.A_{d7}}$ and the time constants $\tau_{w6} = \frac{\rho_d.A_{d6}.h_{d6}}{M_{p5}}$, $\tau_{w7} = \frac{\rho_d.A_{d7}.h_{d7}}{M_{p6}}$, $\tau_{h6} = \frac{A_{d6}.Q_{d6}^{0}}{g(C_d.A_{h6})^2}$ and $\tau_{h7} = \frac{A_{d7}.Q_{d7}^{0}}{g(C_d.A_{h7})^2}$.

$$\frac{dh_{d6}}{dt} = td_1 M_{p5} - \left[\frac{1}{\tau_{h6}}\right]h_{d6},\qquad \frac{dw_{d6}}{dt} = \left[\frac{1}{\tau_{w6}}\right]w_{p5} - \left[\frac{1}{\tau_{w6}}\right]w_{d6} \tag{4.78}$$

$$\frac{dh_{d7}}{dt} = tdd_1 M_{p6} - \left[\frac{1}{\tau_{hd6}}\right]h_{d6},\qquad \frac{dw_{d7}}{dt} = \left[\frac{1}{\tau_{w7}}\right]w_{p6} - \left[\frac{1}{\tau_{w7}}\right].w_{d7} \tag{4.79}$$

Second evaporator effect

The second effect temperature is given by the following differential equation. This equation was derived in Chapter 2 and was shown there by equation (2.30).

$$I_{effect2}\frac{dT_{e2}}{dt} = q_{feed6} + q_{shell6} - q_{comp2} - q_{eloss2} - q_{shell7} - q_{shell8} \tag{4.80}$$

This can be linearised to the following, with the linear constants $ta_1 = \frac{[U_{s6}.A_{s6}]}{I_{effect2}}$, $ta_2 = \frac{[C_p(T^0_{p5} - T^0_{e2})]}{I_{effect2}}$, $ta_3 = \frac{C_p M^0_{p5}}{I_{effect2}}$, $ta_4 = \frac{[U_{s7}.A_{s7} + U_{s8}.A_{s8}]}{I_{e2}}$, $ta_5 = \frac{\alpha_{comp3}}{I_{effect2}}$, $ta_6 = \frac{U_l.A_{el2}}{I_{effect2}}$ and the time constant $\tau_{Te2} = \frac{I_{effect2}}{[M^0_{p5}.C_p + U_{s6}.A_{s6} + U_{s7}.A_{s7} + U_{s8}.A_{s8} + \alpha_{compl} + U_l.A_{el2}]}$.

$$\frac{dT_{e2}}{dt} = -\frac{1}{\tau_{Te2}} T_{e2} + ta_1.T_{s2} + ta_2.M_{p6} + ta_3.T_{p5} + ta_4.T_{e3} - ta_5.P_{sp} + ta_6.T_a \tag{4.81}$$

Second evaporator shell

The second effect shell temperature is given by the following differential equation. As with the evaporator effect, we have assumed constant evaporating heat transfer coefficient, constant milk solution heat capacity, and negligible boiling point elevation. This differential equation was derived in Chapter 2 and is shown there by equation (2.63).

$$I_{shell2} \frac{dT_{s2}}{dt} = q_{comp2} + W_{comp2} - q_{shell6} - q_{sloss2} - q_{condensate2} \tag{4.82}$$

This can be linearised to the following, with the constants $tb_1 = \frac{[U_{s6}.A_{s6} + \alpha_{compl}(1 - tb_4) + M^0_{comp2}.C_{pwater}]}{I_{shell2}}$, $tb_2 = \frac{[\alpha_{comp3}(1 - tb_4) + \beta_{comp3}]}{I_{shell2}}$, $tb_3 = \frac{U_l.A_{sl2}}{I_{shell2}}$, $tb_4 = \frac{C_{pwater}}{\lambda}(T^0_{s2} - T^0_{e2})$ and the time constant $\tau_{Ts} = \frac{I_{shell2}}{[U_s.A_{s6} + M^0_{comp2}.C_{pwater} + U_l.A_{sl2} - \beta_{comp2}]}$.

$$\frac{dT_{s2}}{dt} = -\frac{1}{\tau_{Ts2}} T_{s2} + tb_1.T_{e2} + tb_2.P_{sp} + tb_3.T_a \tag{4.83}$$

Third evaporator effect

The third effect temperature is given by the following differential equation. Once again, we have assumed constant heat transfer coefficient, heat capacity and negligible boiling point elevation. This equation was derived in Chapter 2 and is shown there by equation (2.35).

$$I_{effect3} \frac{dT_{e3}}{dt} = q_{feed7} + q_{shell7} + q_{shell8} - q_{vac} - q_{eloss3} \tag{4.84}$$

This can be linearised to the following, with the constants $tc_1 = \frac{\left[U_{s7}.A_{s7} + U_{s8}.A_{s8} + M^0_{p6}.C_{pwater}\right]}{I_{effect3}}$, $tc_2 = \frac{\left[C_{pwater}\left(T^0_{e2} - T^0_{e3}\right)\right]}{I_{effect3}}$, $tc_3 = \frac{1}{I_{effect3}}$, $tc_4 = \frac{U_l.A_{el3}}{I_{effect3}}$ and the time constant $\tau_{Te3} = \frac{I_{effect3}}{\left[M^0_{p6}.C_{pwater} + U_{s7}.A_{s7} + U_{s8}.A_{s8} + U_l.A_{el3}\right]}$.

$$\frac{dT_{e3}}{dt} = -\frac{1}{\tau_{Te3}}T_{e3} + tc_1.T_{e2} + tc_2.M_{p6} - tc_3.q_{vac} + tc_4.T_a \qquad (4.85)$$

Vacuum Condenser

The same condenser equations, used for the MVR evaporator preheat condenser, also apply for the TVR vacuum condenser. The transfer functions for the condenser outlet temperature and heat flow are given by the following :

$$T_{vac2}(s) = \frac{\left[1 - e^{-\frac{\tau_{vac}}{\tau_{Tvac}}}e^{-\tau_{vac}.s}\right]}{\left[\tau_{Tvac}.s+1\right]}T_{e3}(s) + e^{-\frac{\tau_{vac}}{\tau_{Tvac}}}e^{-\tau_{vac}.s}.T_{vacl}(s) - \frac{\tau_{vac}\left(T^0_{e3} - T^0_{vacl}\right)e^{-\frac{\tau_{vac}}{\tau_{Tvac}}}}{\tau_{Tvac}M^0_{vac}}\frac{\left[1 - e^{-\tau_{vac}.s}\right]}{\tau_{vac}.s}M_{vac}(s) \qquad (4.86)$$

$$\frac{1}{C_{pwater}}q_{vac}(s) = \frac{\rho_{water}.V_{vac}.s}{\left[\tau_{Tvac}.s+1\right]}T_{e3}(s) + \frac{M^0_{vac}}{\left[\tau_{Tvac}.s+1\right]}T_{vac2}(s) - \frac{M^0_{vac}}{\left[\tau_{Tvac}.s+1\right]}T_{vacl}(s) + \frac{\left(T^0_{vac2} - T^0_{vacl}\right)}{\left[\tau_{Tvac}.s+1\right]}M_{vac}(s) \qquad (4.87)$$

Complete TVR evaporator section linear model

The complete TVR section linear model will be developed by first determining the linear models for the second effect and third effect separately. These will then be combined with the falling film and vacuum condenser models, to produce the complete TVR evaporator section model. The second effect state space model is given by the following.

$$\begin{bmatrix} \frac{dh_{d6}}{dt} \\ \frac{dw_{d6}}{dt} \\ \frac{dT_{e2}}{dt} \\ \frac{dT_{s2}}{dt} \end{bmatrix} = \begin{bmatrix} -\frac{1}{\tau_{hd6}} & 0 & 0 & 0 \\ 0 & -\frac{1}{\tau_{wd6}} & 0 & 0 \\ 0 & 0 & -\frac{1}{\tau_{Te2}} & ta_1 \\ 0 & 0 & tb_1 & -\frac{1}{\tau_{Ts2}} \end{bmatrix} \begin{bmatrix} h_{d6} \\ w_{d6} \\ T_{e2} \\ T_{s2} \end{bmatrix} + \begin{bmatrix} 0 & td_1 & 0 & 0 & 0 & 0 \\ \frac{1}{\tau_{w6}} & 0 & 0 & 0 & 0 & 0 \\ 0 & ta_2 & ta_3 & -ta_5 & ta_6 & ta_4 \\ 0 & 0 & 0 & tb_2 & tb_3 & 0 \end{bmatrix} \begin{bmatrix} w_{p5} \\ M_{p5} \\ T_{p5} \\ P_{st} \\ T_a \\ T_{e3} \end{bmatrix} \qquad (4.88)$$

The third effect state space model is given by the following.

$$\begin{bmatrix} \frac{dh_{d7}}{dt} \\ \frac{dw_{d7}}{dt} \\ \frac{dT_{e3}}{dt} \end{bmatrix} = \begin{bmatrix} -\frac{1}{\tau_{hd7}} & 0 & 0 \\ 0 & -\frac{1}{\tau_{wd7}} & 0 \\ 0 & 0 & -\frac{1}{\tau_{Te3}} \end{bmatrix} \begin{bmatrix} h_{d7} \\ w_{d7} \\ T_{e3} \end{bmatrix} + \begin{bmatrix} 0 & tdd_1 & 0 & 0 & 0 \\ \frac{1}{\tau_{w7}} & 0 & 0 & 0 & 0 \\ 0 & tc_2 & tc_1 & tc_4 & -tc_3 \end{bmatrix} \begin{bmatrix} w_{p6} \\ M_{p6} \\ T_{e2} \\ T_a \\ q_{vac} \end{bmatrix} \quad (4.89)$$

These linear models are combined with the linear falling film delay model to produce the complete TVR section model. The connections between the models are shown by the block diagram in Figure 4-6. The TVR Second Evaporator Effect is described by equation (4.88) and the Third Evaporator Effect is described by equation (4.89). The Vacuum Condenser is described by equations (4.86) and (4.87). The equations for the falling films are the same as those used for the MVR evaporator section.

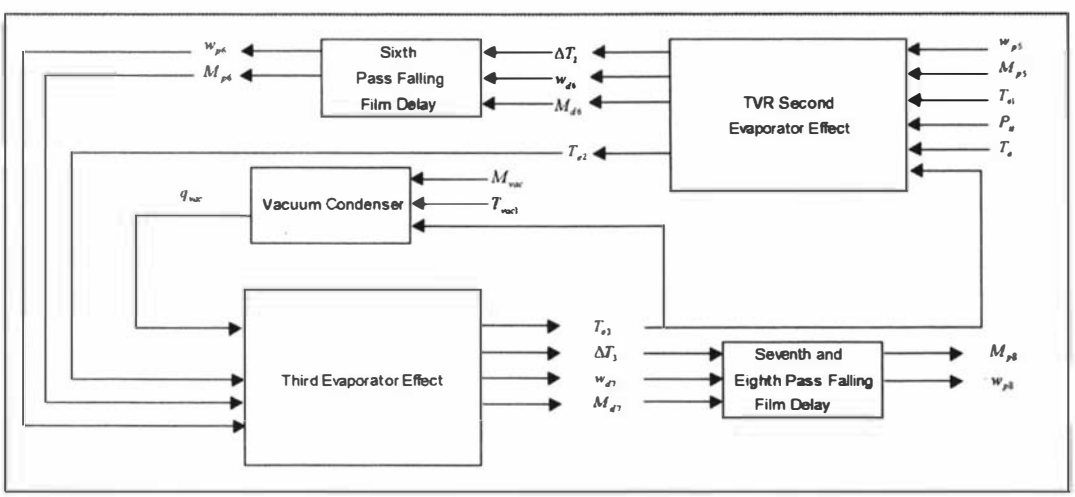

Figure 4-6 : Connections for TVR section Linear Models.

4.4.6) Complete Evaporator A Model

We now develop the complete Evaporator A plant linear dynamic model. The linear models for the MVR evaporator, the TVR evaporator and the DSI unit preheat will be combined. The preheat plate heat exchanger provides a difficulty because it is not modelled by finite order constant coefficient differential equations. This makes it difficult to combine with the other sections of the Evaporator A plant. The preheat plate heat exchanger can be combined with the other sections using numerical methods. This is required for the multi-variable analysis of Chapter 7. However, the remainder of the controllability analysis will not require a complete Evaporator A plant dynamic model.

In Chapter 7 it is shown that the disturbance rejection capabilities of the plate heat exchanger are good. This means that a control loop on the outlet hot milk temperature will break the feedback loops through the heat exchanger from the MVR and TVR evaporator sections. As a result the remaining controllability analysis of Chapter 7 does not require a complete dynamic model of the Evaporator A plant. Therefore we will develop two dynamic models for the complete Evaporator A plant. The first numerically calculates the transfer function for the Evaporator A plant. This is

used for the multi-variable analysis of Chapter 7. The second model neglects the preheat plate heat exchanger and only considers the DSI preheat section, the MVR evaporator section and the TVR evaporator section. Figure 4-7 shows the connections between the four sections to produce the second dynamic model for the complete Evaporator A plant.

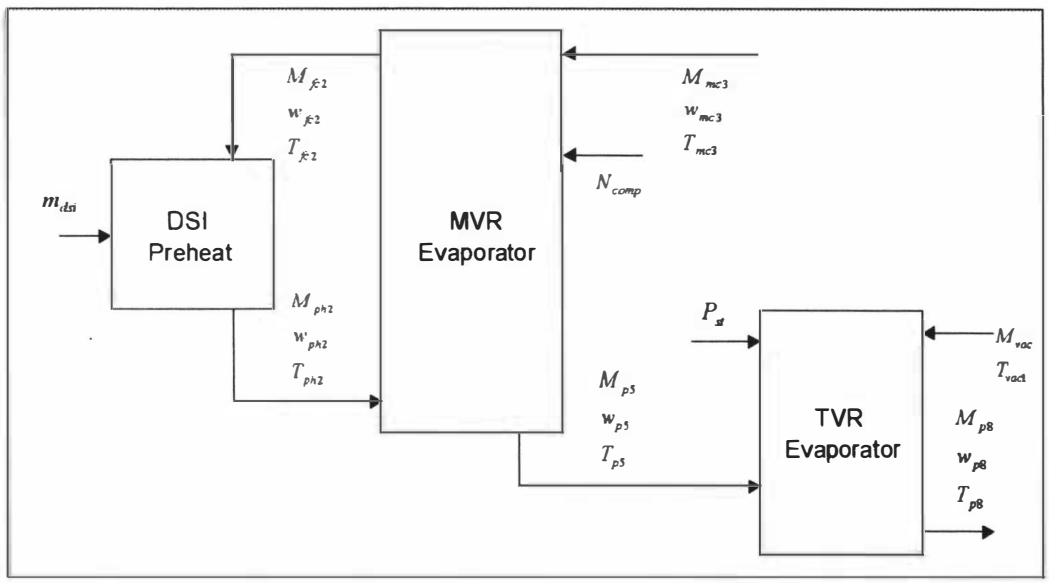

Figure 4-7 : Interconnections between systems for the complete Evaporator A plant model.

4.5) Conclusions

The purpose of this Chapter was to develop the steady state and linear dynamic models of the Evaporator A plant. The steady state model was developed in Section 4.2. We separated the Evaporator A plant into four sections and modelled each independently. Then these models were combined to produce the steady state model for the entire Evaporator A plant. The resulting steady state model was used to determine a static operating point. Then process gains between the inputs and outputs were calculated and the results are shown in Table 4-1.

The linear dynamic model was developed in Section 4.4. We used the same technique of separating the plant into four sections and considering each independently. At the end of Section 4.4 we combined these to produce the model for the entire Evaporator A plant, by simplifying the dynamic model and making many assumptions about the process. For example the falling film evaporating heat transfer coefficients were assumed to be constant. Another important assumption is the neglect of any feedback through the preheat plate heat exchanger. Many of these assumptions were not made in the development of the steady state model and so the resulting linear dynamic model is not a generalisation of the steady state model.

The models developed in this Chapter must now be identified. In their current state they cannot be used, because we are uncertain about their accuracy. The purpose of the next Chapter is to identify the values of various process parameters that optimise the model accuracy. This will be predominantly done for the steady state model, because quantitative accuracy is very important for the optimisation studies. However, we also consider the dynamic falling film delays.

Chapter 5 : Model Identification

5.1) Introduction

A first principles model will usually contain unknown parameters. For example physical properties or heat transfer coefficients may not be known. Often it is possible to determine these parameters from literature correlations. However, another method is to identify appropriate parameter values from process historical data. This process of determining the parameters that give a 'best fit' model is called parameter identification. In this chapter we will be looking at the identification of process parameters for the Evaporator A model developed in the previous chapters. Table 5-1 shows a list of some of the process parameters, which are used in the model. In this Chapter we seek to identify as many of these parameters as possible.

Table 5-1 : Evaporator A model process parameters.

	Description	Units
U_{pre}	Preheat condenser overall heat transfer coefficient.	($W/m^2.°C$)
U_l	Surface energy losses overall heat transfer coefficient.	($W/m^2.°C$)
c_{comp}	Parameter accommodating MVR compressor duct pressure drop.	(m^{-4})
U_{water}	Falling film overall heat transfer coefficient for water.	($W/m^2.°C$)
U_{lo}, U_w	Parameter to describe the effect of dry matter on heat transfer.	($W/m^2.°C$)
U_{eo}, U_{ew}	Parameter to describe the effect of dry matter on heat transfer.	($W/m^2.°C$)
U_{so}, U_{sw}	Parameter to describe the effect of dry matter on heat transfer.	($W/m^2.°C$)
τ_e	Evaporator falling film residence times.	(s)
B_{TVR}	TVR compressor parameter.	($m^{0.03}.s^{0.06}/kg^{0.03}$)

We will identify the process parameters by using optimisation methods. The process parameters are determined by minimising the model deviation from historical data. We use the standard technique of calculating the sum of squared errors in the model deviations and minimising this by varying the process parameters. After identifying the process parameters, we investigate the model validity. This will be done by making straight comparisons with the historical data, but also by investigating the model residuals. A 'good' identified model will give a uniform plot of residuals vs the operating conditions. In addition we will check the resulting parameters for consistency against the traditional correlations. For example heat transfer coefficients can be checked against literature correlations.

A difficulty, with the identification of this model, is the large number of process parameters. A complete steady state identification involves a dozen or more parameters. To simplify the process, we separate the model into parts and make an independent identification on each part.

For example the preheat condenser energy balance can used to identify the condenser overall heat transfer coefficient. We can identify this heat transfer coefficient, by using this balance, rather than considering the entire Evaporator A plant model.

The Evaporator A plant online computers can be used to record a large number of process variables. These variables are tabulated in Appendix E along with the geometries of the evaporator plant. However, despite the large number of process variables measured some important ones are missing. The feed density is not measured and it is difficult to know the dry matter of the evaporator feed milk. The mass flow of steam to the DSI is not measured and this causes a slight dilution of the feed milk solution and is quite important. However, the most prominent omissions are the second effect shell temperature and vacuum condenser cooling water conditions. We have to calculate these variables using parts of the model. This has the disadvantage of reducing the number of balance equations in the model and therefore our ability to identify the process parameters.

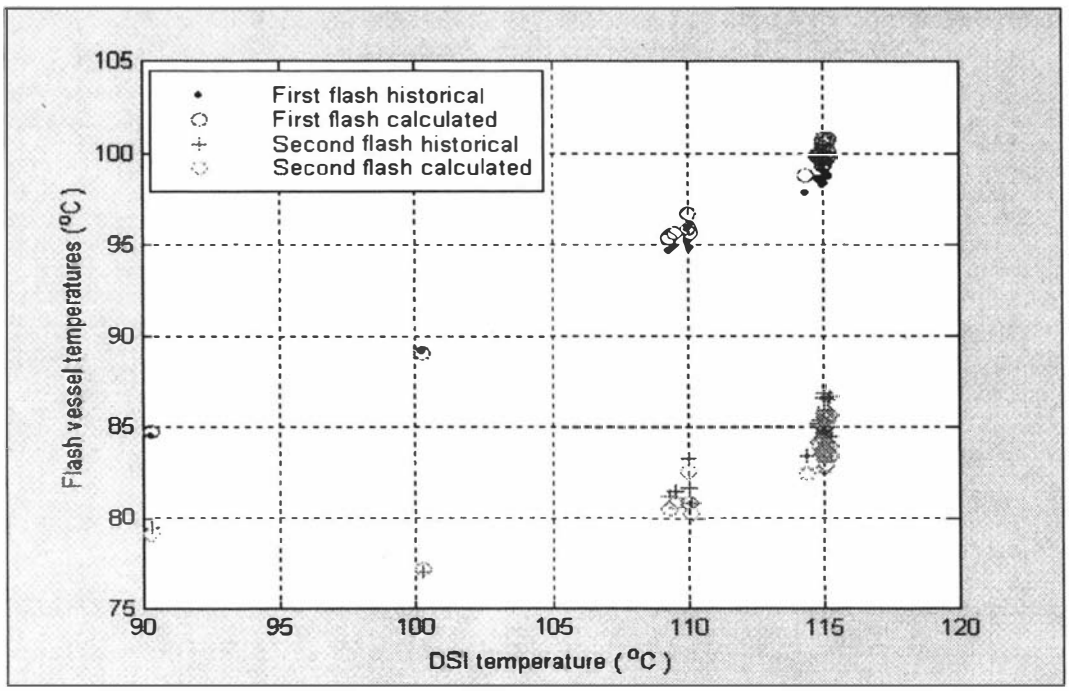

Figure 5-1 : Historical and advanced model flash vessel temperatures vs T_{DSI} temperature.

5.2) DSI Preheat Section

5.2.1) Introduction

The preheat steady state model contains no unknown parameters and so we will only be concerned with validating the model. Specifically we investigate the flash vessel temperatures and determine the accuracy of the 'Advanced' steady state model. We will not consider the preheat dynamics.

5.2.2) Preheat Steady State Temperatures

In the previous chapter two steady state models for the preheat temperatures and mass flows were developed. We are examining the accuracy of the 'Advanced' model by comparing the flash vessel temperature predictions with historical data from the Evaporator A plant. The model has been rearranged so the outputs are the flash vessel temperatures (T_{ph1} and T_{ph2}) and the DSI steam mass flow (m_{dsi}). The inputs are the evaporator feed flow (M_{ph2}), the preheat outlet condenser temperature (T_{fc2}) and the DSI unit temperature (T_{DSI}). A set of water historical data was collected and the resulting flash vessel temperatures are shown in Figure 5-1. Also shown in Figure 5-1 are the calculated flash vessel temperatures using the 'Advanced' model.

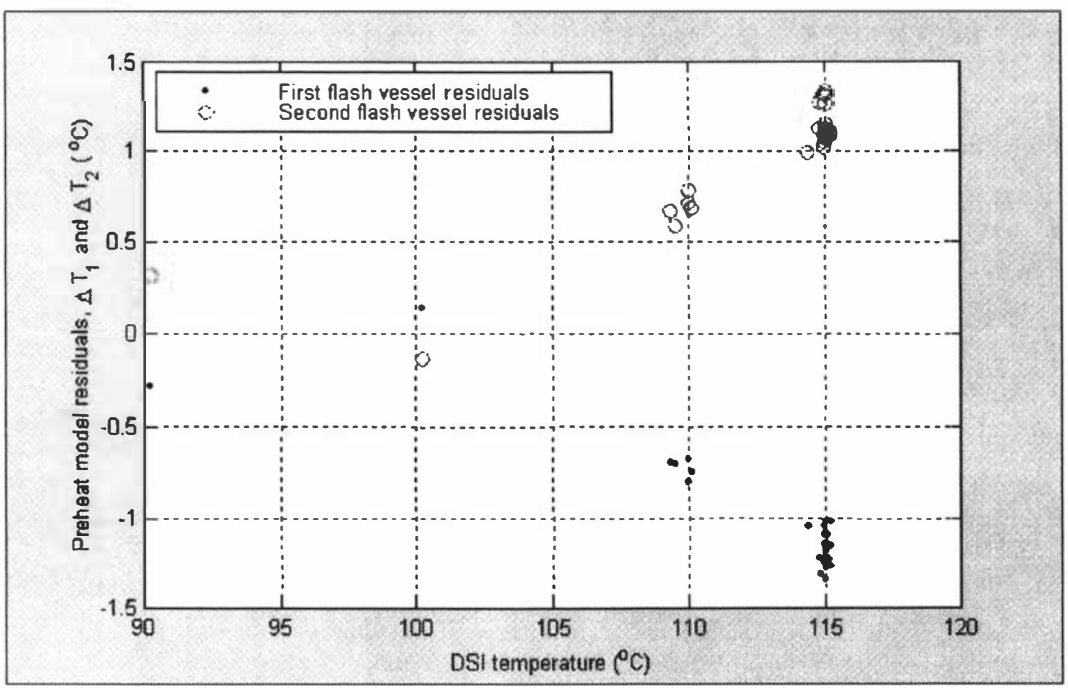

Figure 5-2 : Preheat model residuals vs DSI temperature.

Figure 5-1 shows that the preheat model is relatively accurate. However, we would like to investigate the model residuals and determine if they are uniform across the plant operating range. We will define the following model residuals.

$$\Delta T_1 = T_{ph1} - T_{ph1h}, \qquad \Delta T_2 = T_{ph2} - T_{ph2h} \tag{5.1}$$

Where, T_{ph1} = predicted first flash vessel temperature. (°C)

T_{ph1h} = experimental first flash vessel temperature. (°C)

T_{ph2} = predicted second flash vessel temperature. (°C)..

T_{ph2h} = experimental second flash vessel temperature. (°C)

With the historical data used in Figure 5-1 we can calculate the model residuals and these are shown in Figure 5-2. Interestingly the absolute value of the residuals increases with the DSI unit temperature. However, the model accuracy is quite good, with Figure 5-2 showing a maximum deviation of only 1.5 °C.

5.3) MVR Section

5.3.1) Introduction

Here we investigate the identification of process parameters for the MVR evaporator section. We will separate the identification into the following parts.

1) Preheat condenser overall heat transfer coefficient (U_{pre}).
2) Surface losses overall heat transfer coefficient (U_l).
3) MVR compressor vapour ductwork pressure drop (c_{comp}).
4) Water falling film evaporating overall heat transfer coefficient (U_{water}).
5) Falling film evaporating heat transfer coefficients (U_{eo}, U_{ew}, U_{lo}, U_{lw}, U_{so} and U_{sw}).

The first four parameters can be identified using a single parameter optimisation. This is considerably easier than a multiple-variable optimisation and it is the reason for separating the identification into parts. However, the milk heat transfer coefficient parameters cannot be identified using a single parameter optimisation method. Special attention will therefore be focused on the identification of the two parameter milk heat transfer coefficient models.

5.3.2) Preheat Condenser Overall Heat Transfer Coefficient

The explicit equation for the preheat condenser outlet temperature is given by the following. This equation was derived in Chapter 3 and is shown there by equation (3.34).

$$T_{fc2} = T_{s1} - (T_{s1} - T_{mc3})e^{\left(\frac{U_{pre} \cdot A_{pre}}{M_f \cdot C_p}\right)} \tag{5.2}$$

Where, T_{fc2}	=	preheat condenser outlet temperature.	(°C)
T_{s1}	=	evaporator shell temperature.	(°C)
T_{mc3}	=	preheat condenser inlet temperature.	(°C)
M_f	=	evaporator feed mass flow.	(kg/s)
U_{pre}	=	preheat condenser overall heat transfer coefficient.	(W/m^2.°C)
A_{pre}	=	heat transfer surface area for the preheat condenser.	(m^2)

All the variables in the above equation are known except for the overall heat transfer coefficient. The temperatures of the condenser and evaporator shell are measured and we can determine the water/milk physical properties from the equations of Appendix A. Therefore this equation provides a balance equation that can be used to identify the condenser overall heat transfer coefficient. A set of historical data for water and Sophie-Lo milk solution was collected and used

to identify the coefficient. The optimum overall heat transfer coefficient was then determined to be 2260 W/m^2.K.

We are now interested in determining if the overall heat transfer coefficient is constant or varies with operating conditions. This can be tested by plotting the balance equation residuals vs the plant operating conditions. However, we will not use this method to investigate the heat transfer coefficient. Instead, we consider this problem by rearranging equation (5.2) into the following explicit form for the overall heat transfer coefficient.

$$U_{pre} = \frac{M_f.C_p}{A_{pre}} \ln\left[\frac{T_{s1} - T_{mc3}}{T_{s1} - T_{fc2}}\right] \tag{5.3}$$

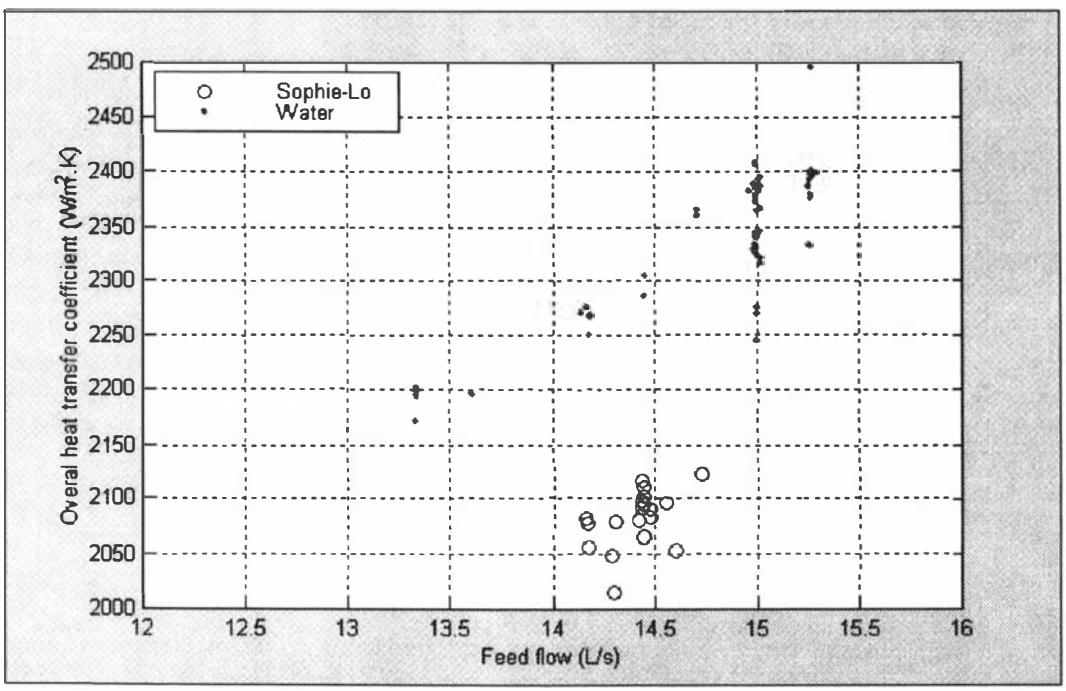

Figure 5-3 : Experimental preheat overall heat transfer coefficient vs evaporator feed flow.

Using the historical data we can calculate the overall heat transfer coefficient and the results are shown in Figure 5-3. This shows a clear trend between the heat transfer coefficient and the evaporator feed flow. In addition the overall heat transfer coefficients are lower for Sophie-Lo than for water. This is presumably because of the different physical properties of water and Sophie-Lo. The milk solution has a higher viscosity and density, but a lower thermal conductivity and heat capacity.

The preheat condenser heat transfer coefficients can also be calculated from the correlations discussed in Appendix BII. Using the Dittus and Boelter correlation we can determine the forced convection coefficient and using the Chun and Kim correlation we can determine the condensation coefficient. The resulting overall heat transfer coefficients are shown in Figure 5-4. The Chun and Kim correlation tends to under-predict the condensing heat transfer coefficient and this explains the under-prediction shown here.

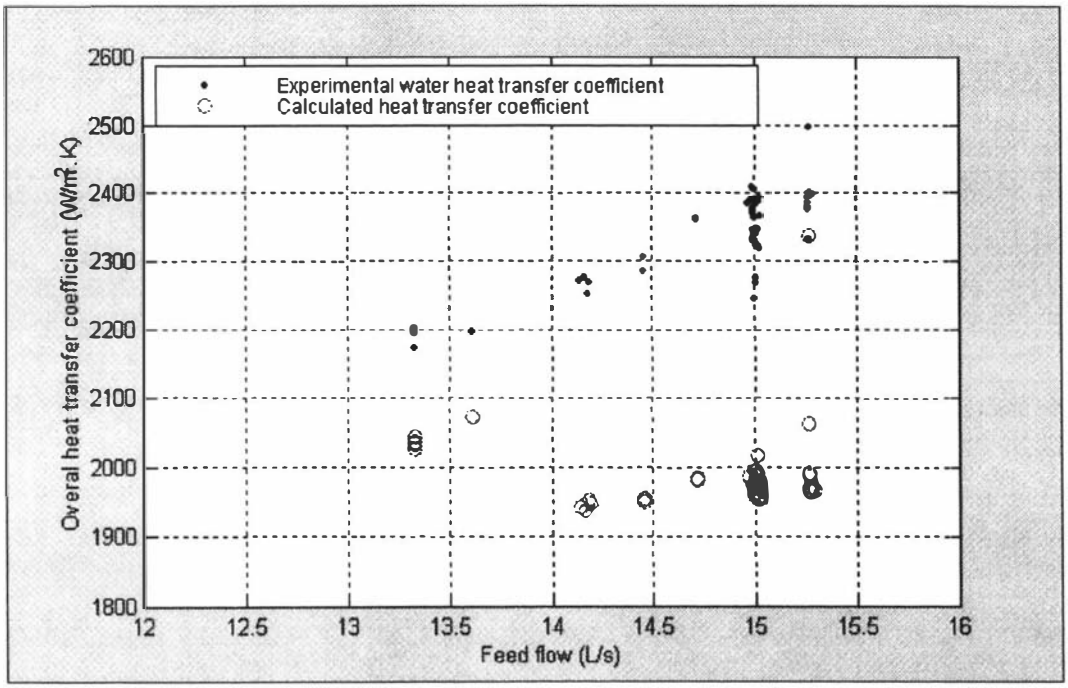

Figure 5-4 : Experimental water heat transfer coefficients and calculated correlation results.

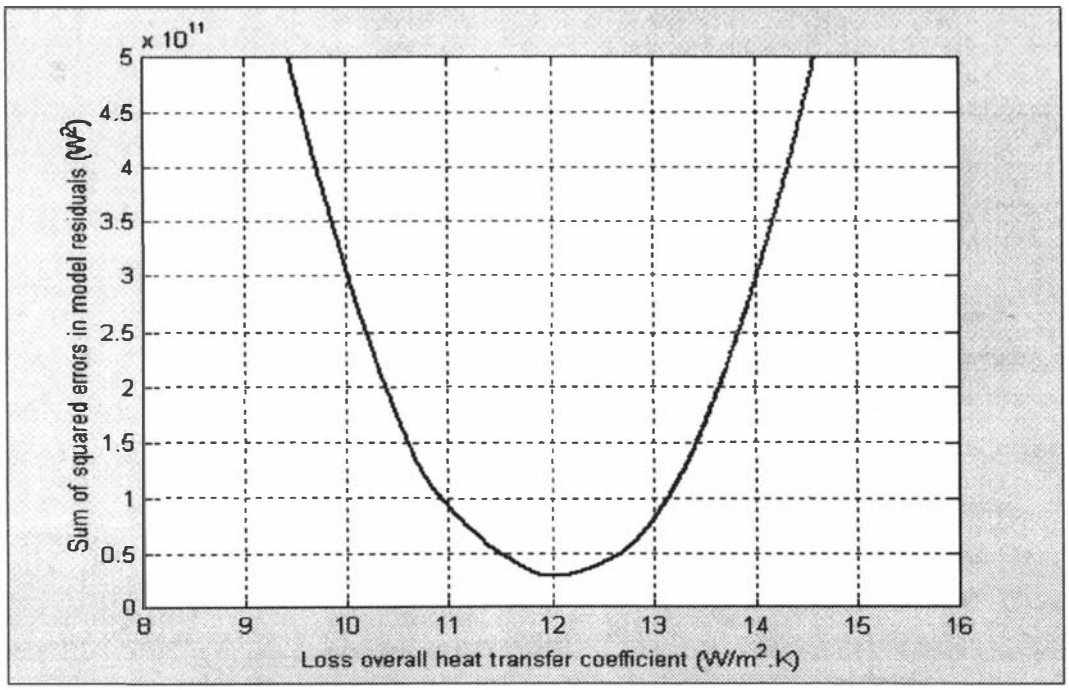

Figure 5-5 : Overall energy balance sum of squared errors.

5.3.3) Evaporator Surface Energy Losses Overall Heat Transfer Coefficient

At this stage we are interested in identifying the surface losses overall heat transfer coefficient (U_l). Heat losses from the MVR evaporator surfaces occur by convection and radiation heat

transfer. The overall energy balance for the MVR evaporator section is given by equation (5.4). This equation is developed by the addition of the MVR evaporator effect and evaporator shell energy balances. These energy balances were derived in Chapter 2 and are given there by equations (2.25) and (2.58).

$$q_{feed1} + W_{comp1} = q_{pcond} + q_{eloss1} + q_{sloss1} + q_{condensate1} \tag{5.4}$$

The q_{feed1}, q_{pcond}, W_{comp1} and $q_{condensate1}$ terms can be determined from historical data and the physical property equations in Appendix A. The power supplied to the compressor (W_{comp1}) depends on the compressor pressure difference ($P_{s1} - P_{e1}$), the evaporated vapour density (ρ_{ve1}) and the mass flow of compressed vapour (M_{comp1}). The pressure difference and vapour density can be determined from the Antoine saturation equations (2.70). In addition the volumetric flow of evaporated vapour can be determined from the amount of evaporation in the MVR evaporator section. Equation (5.4) therefore provides a balance equation that can be used to identify the loss overall heat transfer coefficient. A set of historical data from the Evaporator A plant on Water and Sophie-Lo was collected and used to identify the overall heat transfer coefficient. Figure 5-5 shows the resulting model sum of squared errors vs the loss overall heat transfer coefficient and clearly the optimum is 12 W/m^2.°C.

The heat transfer due to natural convection can be estimated from literature correlations. These correlations are discussed in Appendix BII and they predict an overall heat transfer coefficient of 3.9 W/m^2.°C. However, this will be lower than the actual heat transfer coefficient, because of the additional radiation heat transfer.

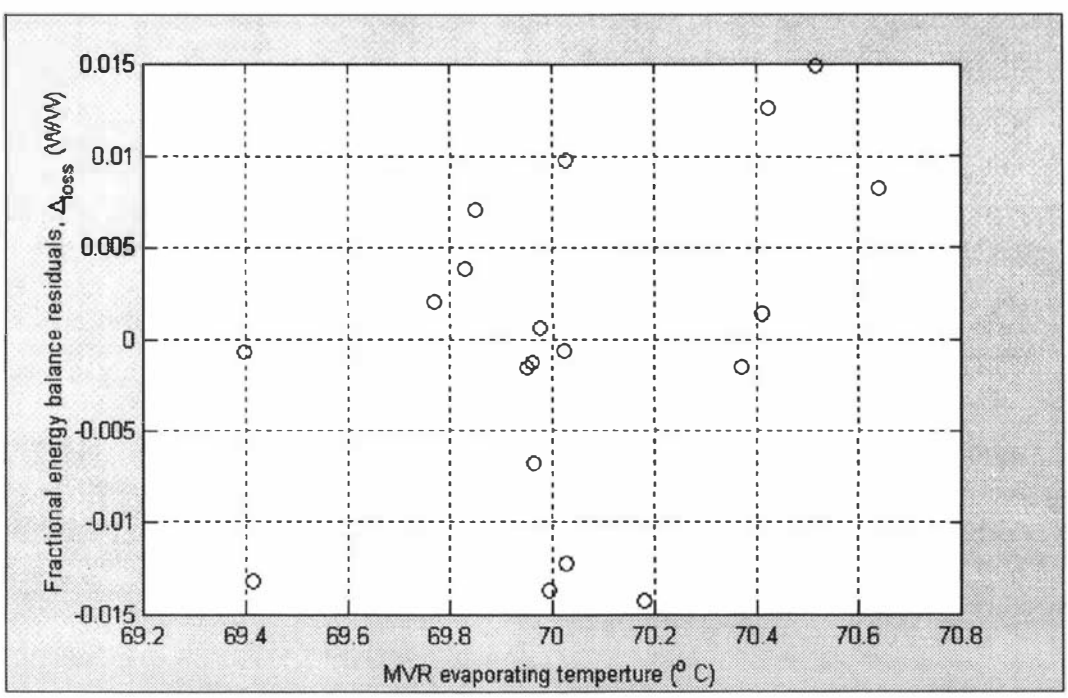

Figure 5-6 : Overall energy balance residuals vs MVR evaporating temperature.

Now we are interested in determining if the loss overall heat transfer coefficient is non-constant. Strictly because of the importance of radiation, we expect the losses heat transfer coefficient to be non-constant. We test this by investigating the energy balance residuals, which we define by the following equation.

$$\Delta_{loss} = \frac{\left[q_{feed1} + W_{comp1} - q_{pcond} - q_{eloss1} - q_{sloss1} - q_{condensate1}\right]}{\left[q_{feed1} + W_{comp1}\right]} \tag{5.5}$$

Where, Δ_{loss} = fractional energy balance residual. (W/W)

Figure 5-6 shows the residuals vs the MVR evaporating temperature. The residuals appear to be relatively well ranged, but there may be a weak trend with the evaporating temperature. This is consistent with the non-linear nature of radiation heat transfer, where the apparent heat transfer coefficient increases at higher temperatures. However, because the fractional residuals are all less than 2 % we will not consider this effect.

5.3.4) MVR Compressor Vapour Duct Losses

Here we are interested in the MVR compressor model and the impact of additional pressure losses through the vapour ductwork. The compressor model is given by the following quadratic equation, which can be solved for the mass flow of compressed vapour (M_{comp1}). This equation is presented in Chapter 2 and is shown there by equation (2.64). The parameters a_{comp}, b_{comp} and c_{comp} were determined from the manufacturer compressor curves.

$$\frac{\left[P_{s1} - P_{e1}\right]}{\rho_{ve1}} = a_{comp}.N_{comp}^2 + b_{comp}.N_{comp}\left(\frac{M_{comp1}}{\rho_{ve1}}\right) + c_{comp}\left(\frac{M_{comp1}^2}{\rho_{ve1}^2}\right) \tag{5.6}$$

$$M_{comp1} = -\frac{\rho_{ve} b_{comp}.N_{comp}}{2.c_{comp}} - \frac{\rho_{ve1}\sqrt{\left(b_{comp}.N_{comp}\right)^2 - 4.c_{comp}\left(a_{comp}.N_{comp}^2 - \frac{P_{s1} - P_{e1}}{\rho_{ve1}}\right)}}{2.c_{comp}}, \quad M_{comp1} = M_{ph2} - M_{p5} \tag{5.7}$$

At steady state the mass flow of compressed vapour is equal to the mass flow of evaporated water, as shown in equation (5.7). All the information in this equation can be determined from historical data. The compressor pressure difference is determined by the evaporator effect/shell temperatures, the vapour density from the effect temperature and the compressor speed is recorded online. In addition the mass of evaporation is determined from the evaporator feed flow and the MVR product mass flow. Consequently we can make predictions for the mass flow of evaporation and compare these with historical data. This provides a test of the compressor model and Figure 5-7 shows a set of predicted and historical results for the evaporator when operating on water. The calculated results follow the same trend as the historical data, but there is also a clear deviation.

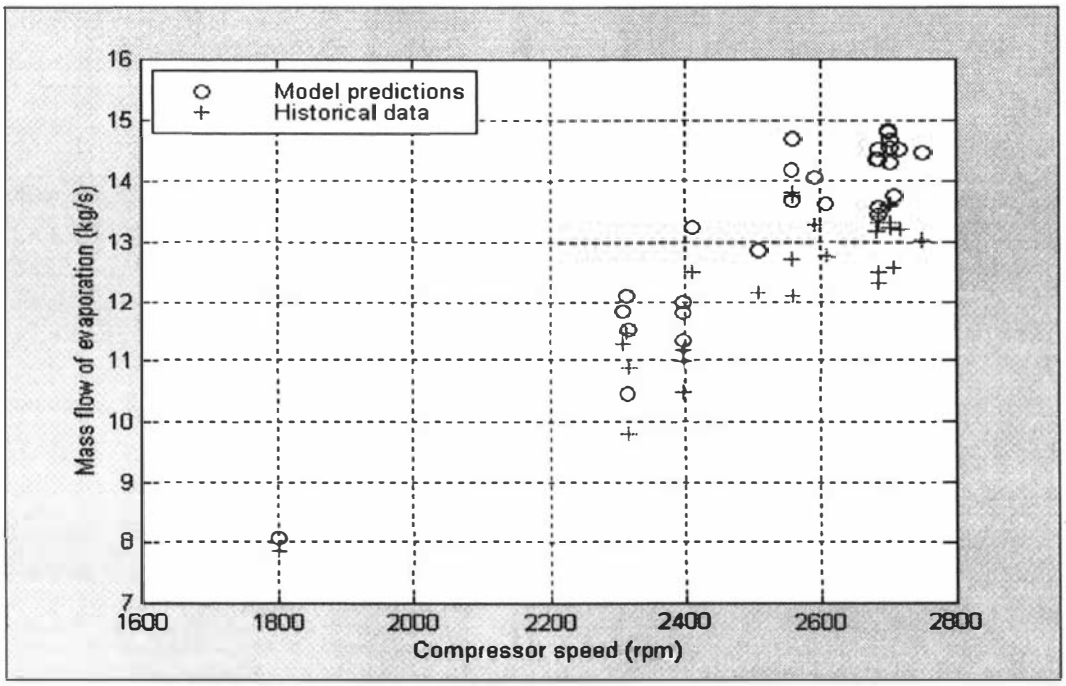

Figure 5-7 : Comparisons of historical mass flow of evaporation and compressor curve calculations.

A probable explanation, for the deviation shown in Figure 5-7, is an additional pressure drop through the compressor vapour ductwork. This ductwork is quite long and the vapour passes through it at a relatively high velocity. Consequently there will be a frictional pressure drop (ΔP_{drop}) and this will cause the actual compressor pressure difference to be larger than expected (i.e., $P_{sl} - P_{el} + \Delta P_{drop}$). We expect the additional frictional pressure drop to be proportional to the square of the volumetric flow of vapour. Then a simple manipulation of equation (5.6) shows that the additional frictional pressure drop can be incorporated by identifying the compressor parameter c_{comp}.

$$\frac{\Delta P}{\rho_{ve}} = \frac{P_{sl} - P_{el} + \Delta P_{drop}}{\rho_{ve}} = \frac{P_{sl} - P_{el} + f.\rho_{ve}.Q_{comp}^2}{\rho_{ve}} = a_{comp}.N_{comp}^2 + b_{comp}.N_{comp}.Q_{comp} + c_{comp}.Q_{comp}^2 \quad (5.8)$$

Where, f = parameter representing the frictional pressure drop. (m^{-4})

With the historical data from Figure 5-7 we can calculate the model sum squared errors vs the c_{comp} parameter. Figure 5-8 shows the results and clearly the optimum c_{comp} value is –14.83 m^{-4}.

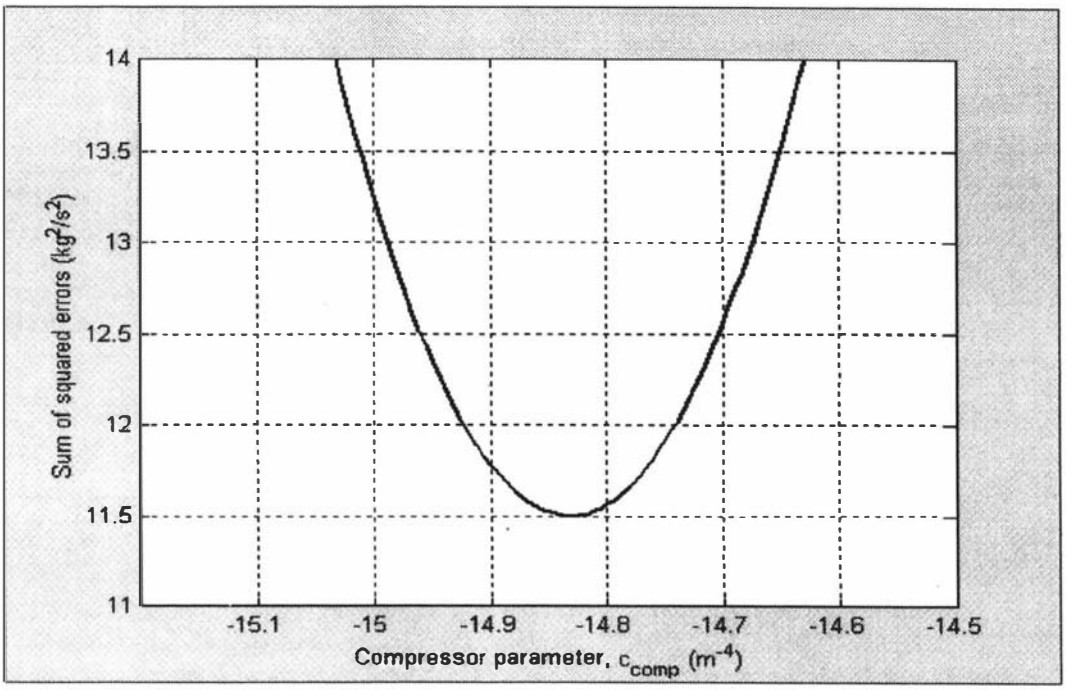

Figure 5-8 : Optimisation plot for the determination of the compressor parameter c_{comp}.

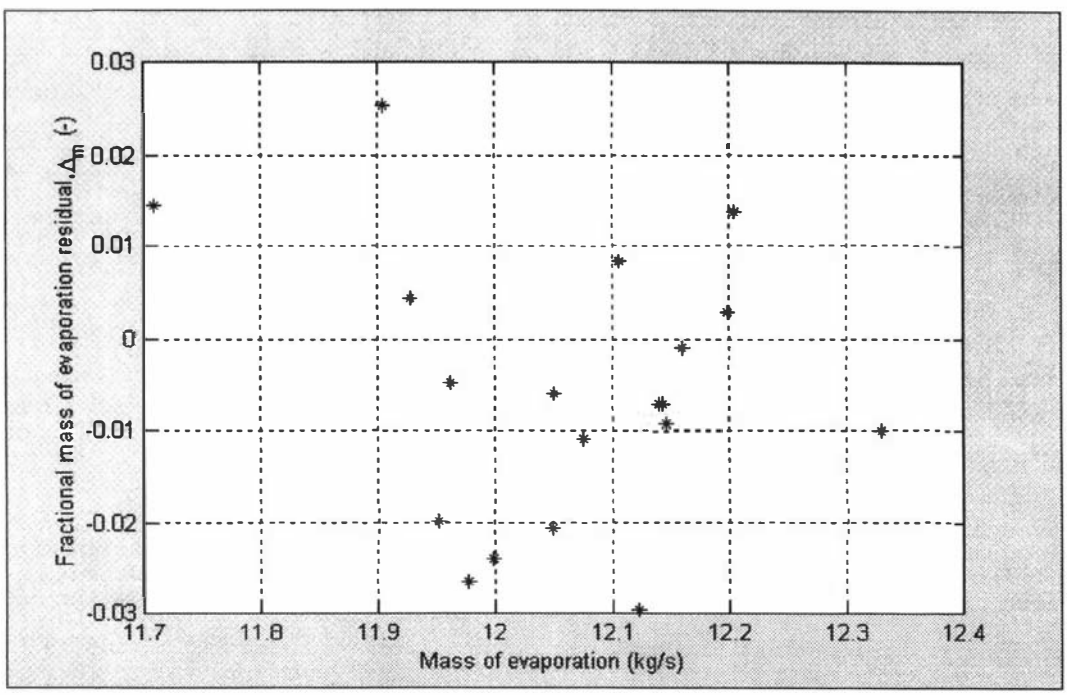

Figure 5-9 : Fractional mass of evaporation residuals vs mass of evaporation.

As with the previous identifications, we are interested in testing the results by investigating the balance equation residuals. We define the following fractional residual, where M_{comp1} is calculated using the identified compressor model. Figure 5-9 shows the residuals vs the mass flow of evaporated water. The residuals appear to be well ranged across the operating range and furthermore they are all less than 3 %, so the identification appears to be accurate.

$$\Delta_m = \frac{\left[M_{ph2} - M_{p5} - M_{comp1}\right]}{M_{comp1}} \tag{5.9}$$

Where, Δ_m	=	fractional mass of evaporation residual.	(-)
M_{ph2}	=	MVR evaporator feed mass flow.	(kg/s)
M_{p5}	=	MVR evaporator product mass flow.	(kg/s)

We have already discussed the need for identifying c_{comp}. The change in c_{comp}, between the original compressor curve and the identified result, is probably due to the pressure drop through the vapour ductwork. It has been stated (Ferguson, 1989) that a well designed compressor has a vapour duct pressure drop that is equivalent to a 0.5 °C saturation temperature drop. We can calculate how the change in c_{comp} relates to a pressure drop and hence temperature drop. This is valuable, because it provides a simple consistency check on the compressor model identification. The compressor curve was given by equation (5.6), which can be rearranged to produce an equation for the additional pressure drop through the compressor.

$$\Delta P_{drop} = \rho_{ve} . \Delta c_{comp} . Q_{comp}^2 \tag{5.10}$$

Where, ΔP_{drop}	=	additional pressure drop through MVR compressor.	(Pa)
ρ_{ve}	=	vapour density.	(kg/m^3)
Δc_{comp}	=	change in c_{comp} between compressor curve and identified.	(m^{-4})
Q_{comp}	=	volumetric flow of vapour through the compressor.	(m^3/s)

If we use this equation, in combination with the Antoine saturation equations, we can calculate that the equivalent temperature drop is 0.6 °C. This temperature drop is the reduction in the saturation temperature due to the pressure drop in the compressor vapour ductwork. It is very similar to the expected literature result and so we are quite confident that the identified result is representative.

5.3.5) Water Evaporating Overall Heat Transfer Coefficient

Here we are interested in the evaporating overall heat transfer coefficient for water. If we make a total mass balance between the MVR evaporator feed and the product we can produce equation (5.11). This equation is the static version of equation (2.21) from Chapter 2.

$$M_{evap} = M_{ph2} - M_{p5} = M_{flash1} + M_{tubest} = \frac{M_{ph2} . C_{pwater}}{\lambda}\left(T_{ph2} - T_{e1}\right) + U_s . A_{st}\left(T_{s1} - T_{e1}\right) \tag{5.11}$$

Where, M_{flash1}	=	mass flow of flashed vapour in the MVR evaporator.	(kg/s)
M_{evap}	=	mass of evaporated water in the MVR evaporator.	(kg/s)
M_{ph2}	=	mass flow to the MVR evaporator first pass.	(kg/s)

M_{p5} = mass flow from the MVR evaporator section. (kg/s)

U_s = falling film evaporating overall heat transfer coefficient. ($W/m^2.°C$)

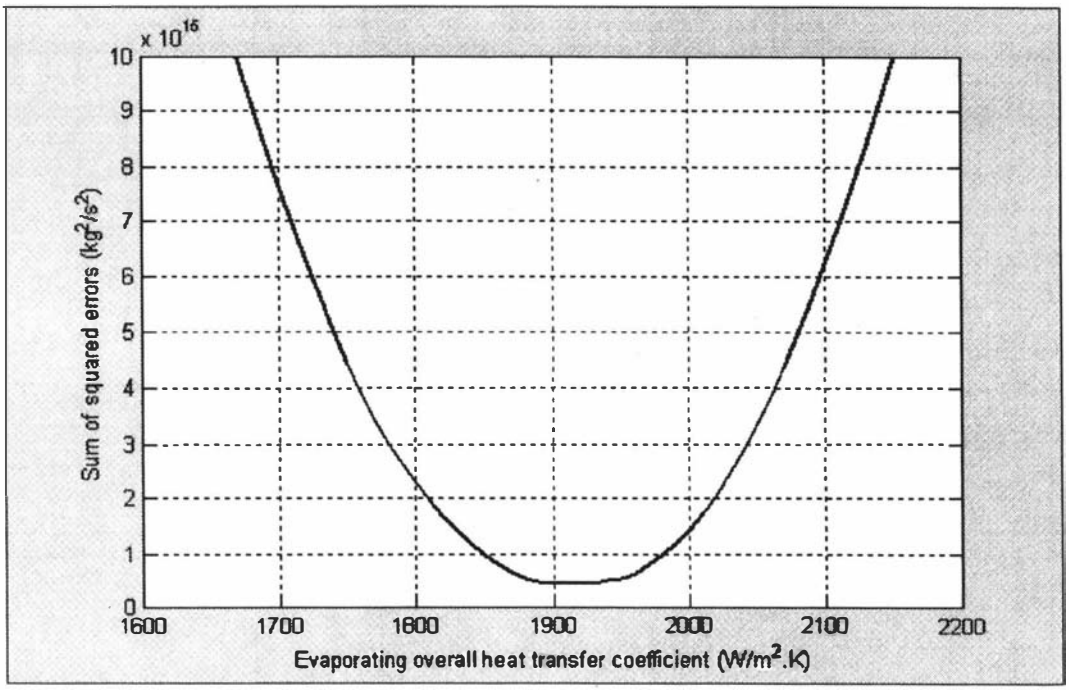

Figure 5-10 : Sum of squared errors vs evaporating overall heat transfer coefficient.

We can determine all the variables in equation (5.11), except for the evaporating overall heat transfer coefficient, from the Evaporator A plant historical data. Consequently this equation can be used to identify the evaporating heat transfer coefficient. Figure 5-10 shows the sum of squared errors in the balance equation and clearly the optimum overall heat transfer coefficient is approximately 1900 $W/m^2.°C$.

As with the earlier identification work we are interested in determining if the overall heat transfer coefficient is non-constant. In particular we are interested in determining if the evaporator temperature has an impact. We expect the overall heat transfer coefficient to vary with temperature, because of changes in the water viscosity and thermal conductivity. Here we test this by plotting the balance equation residuals vs the evaporator temperature. We will define the following fractional residual, which uses the identified overall heat transfer coefficient (U_s) and the plate historical data (M_{ph2}, M_{p5}, T_{e1} and T_{s1}).

$$\Delta_u = \frac{\left[M_{flash1} + U_s A_{st}(T_{s1} - T_{e1}) - M_{ph2} + M_{p5}\right]}{M_{tubes1}} \qquad (5.12)$$

Where, Δ_u = fractional residual in evaporating mass balance. (-)

Figure 5-11 shows the fractional residuals vs the evaporator temperature and there is a clear trend between these variables. In addition the fractional residuals are relatively large, which suggests that we need to incorporate the effect of temperature on the water overall heat transfer coefficient.

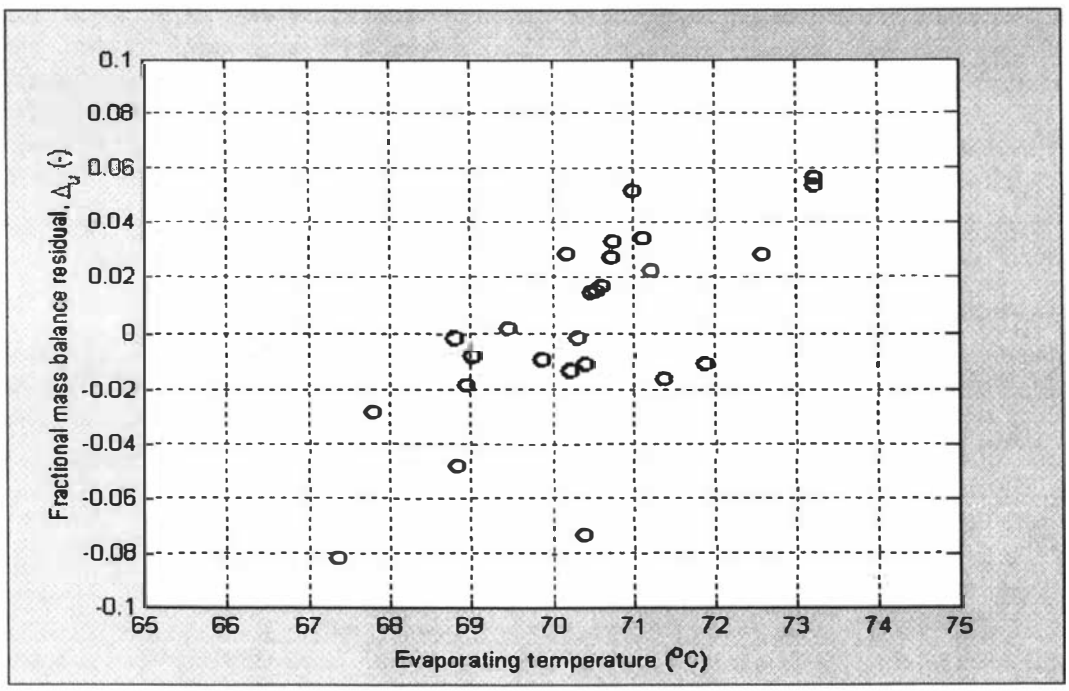

Figure 5-11 : Fractional residuals Δ_u vs the evaporating temperature.

We are also interested in comparing the identified water heat transfer coefficient with those determined from heat transfer correlations. The water evaporating balance equation can be rearranged into equation (5.13) for the evaporating overall heat transfer coefficient.

$$U_s = \frac{\left[M_{evap} - \frac{M_{ph2} C_{pwater}}{\lambda}\left(T_{ph2} - T_{el}\right)\right]}{\left[\left(A_{s1} + A_{s2} + A_{s3} + A_{s4} + A_{s5}\right)\left(T_{s1} - T_{el}\right)\right]} \qquad (5.13)$$

Figure 5-12 shows overall heat transfer coefficients as calculated from equation (5.13). These can be compared to the heat transfer coefficients calculated from correlations. For example, the Chun and Kim (1990) correlation is given by equation (5.14) and this applies for both the evaporating and condensing coefficients. However, the correlation of Alhusseini (1998) is developed using a larger amount of experimental results and is expected to be more accurate. The Alhusseini correlation is discussed in Appendix BI along with that of Chun and Kim.

$$Nu = 1.33Re^{-\frac{1}{3}} + 9.56x10^{-6} Re^{0.89} Pr^{0.94} + 0.0082, \qquad \frac{1}{U} = \frac{1}{h_{evap}} + \frac{\Delta x}{k_{wall}} + \frac{1}{h_{cond}} \qquad (5.14)$$

Where, h_{evap} = evaporating heat transfer coefficient. ($W/m^2.°C$)

h_{cond}	=	condensing heat transfer coefficient.	(W/m^2.°C)
k_{wall}	=	thermal conductivity of evaporator tubes.	(W/m.°C)
Δx	=	thickness of the evaporator tubes.	(m)
U	=	overall heat transfer coefficient.	(W/m^2.°C)
$Nu\left(=\frac{h}{k}\left(\frac{\mu^2}{\rho^2.g}\right)^{\frac{1}{3}}\right)$	=	Nusselt dimensionless number.	(-)
$Re\left(=\frac{4.\Gamma}{\mu}\right)$	=	Reynolds dimensionless number.	(-)
$Pr\left(=\frac{C_p.\mu}{k}\right)$	=	Prandtl dimensionless number.	(-)

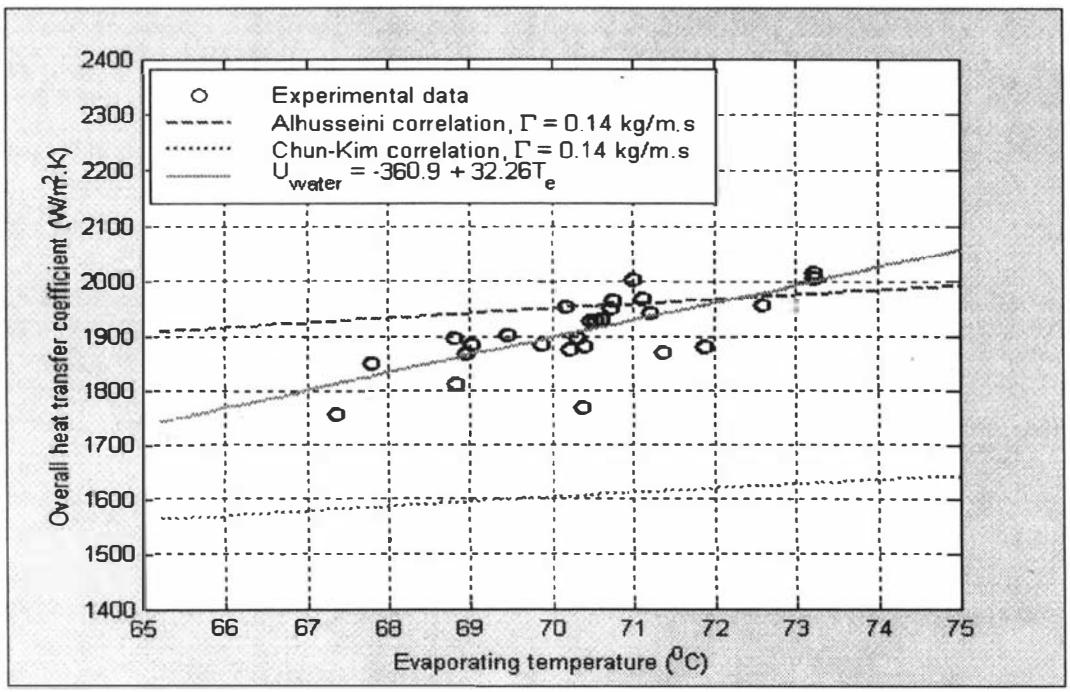

Figure 5-12 : Experimental and correlation overall heat transfer coefficients.

The condensing and evaporating Reynolds numbers depend on the film liquid loadings. However, we shall assume that the film liquid loadings are constant at 0.14 kg/m.s. The heat transfer coefficients also depend on the temperature, since this impacts on the physical properties of water. These physical properties can be determined using the equations discussed in Appendix A. The resulting comparison between the experimental and correlation results are shown in Figure 5-12. These show that the Chun and Kim correlation under predicts the heat transfer coefficients whereas the Alhusseini correlation is quite accurate.

We can determine a linear model for the overall heat transfer coefficient, in terms of the evaporating temperature, using standard regression analysis (Montgomery, 1991, pp 500-501). Since the model is linear in parameters this presents no difficulty and the resulting equation is

shown in Figure 5-12. The mass balance fractional residuals, with the linear overall heat transfer coefficient model, are shown in Figure 5-13.

It is interesting to note that the correlations results in Figure 5-12 predict less temperature dependence than the historical data. The cause of this discrepancy is unknown, but it is possibly caused by the assumption of a constant liquid loading. In Chapter 6 it is shown that the mass flow of evaporation in the MVR evaporator section varies with temperature. This makes it likely that the liquid loadings will also increase with temperature, since more evaporation will occur at higher temperatures. As a result, there is probably more temperature dependence in the identified linear equation that occurs in reality.

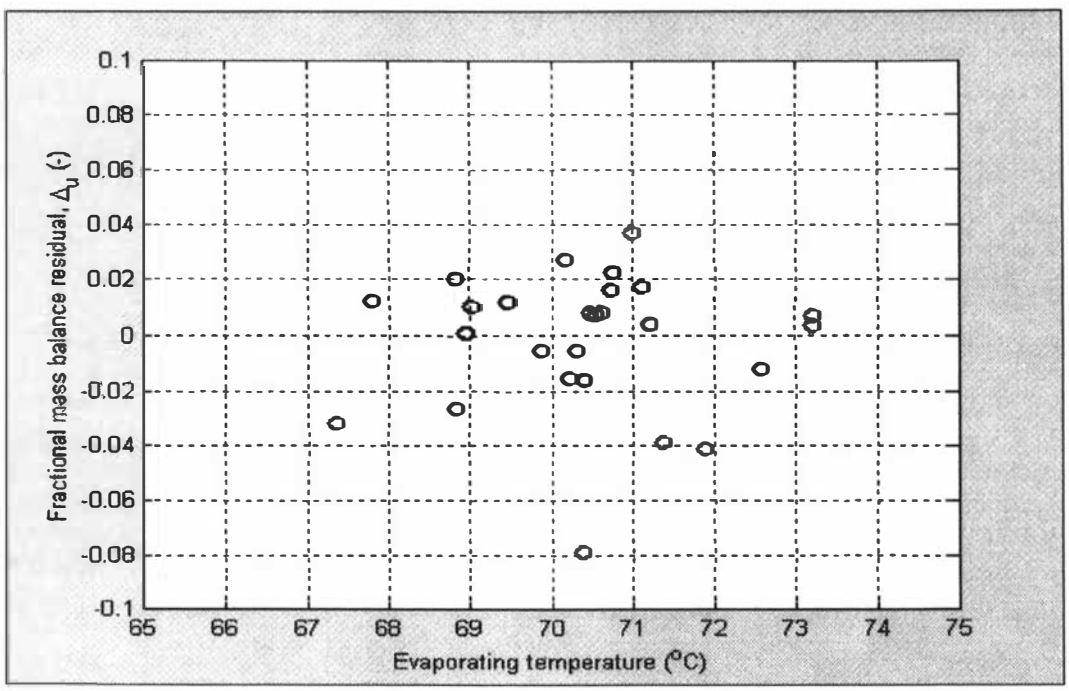

Figure 5-13 : Fractional residuals Δ_u vs evaporating temperature.

5.3.6) Milk Evaporating Overall Heat Transfer Coefficient

Introduction

Here we consider the evaporating heat transfer coefficients for milk solutions, which are found to reduce with increases in dry matter concentration. This is because the dry matter concentration has a substantial impact on the milk solution physical properties and thereby the heat transfer coefficients. For example the viscosity and density is found increase and the thermal conductivity and heat capacity reduce, when the milk dry matter increases. These physical property changes cause a reduction in the heat transfer coefficient. Here we wish to identify models for the relationship between the evaporating overall heat transfer coefficient and the milk solution dry matter.

In Appendix BII three steady state models for accommodating the impact of dry matter on the evaporating heat transfer coefficients are discussed. A 'linear integrated' model (i.e.,

$U = U_{lo} - U_{lw}.w$) produces the following for the mass flow of evaporation in an evaporator pass. This model is shown in Appendix BII by equation (BII.11).

$$\frac{U_{lo}.A_s.\Delta T}{\lambda} = M_{tubes} - \frac{U_{lw}.M_d.w_d}{U_{lo}} \ln\left[1 - \frac{M_{tubes}.U_{lo}}{M_d(U_{lo} - U_{lw}.w_d)}\right] \tag{5.15}$$

Where, M_{tubes}	=	mass flow of evaporation in the evaporator pass.	(kg/s)
M_d	=	mass flow of milk from the distribution plate.	(kg/s)
w_d	=	milk dry matter from the distribution plate.	(kg/kg)
ΔT	=	evaporator temperature difference.	(°C)
A_s	=	evaporator heat transfer surface area.	(m^2)
U_{lo}	=	heat transfer model parameter.	($W/m^2.°C$)
U_{lw}	=	heat transfer model parameter.	($W/m^2.°C$)

The linear integrated heat transfer coefficient model can be expanded using a Maclaurin series approximation. If we restrict this expansion to its first term, then we can produce a 'simple linear' heat transfer model, which is shown in Appendix BII by equation (BII.12) and here by equation (5.16). However, because it is only an approximation of equation (5.15) we have defined new names for the heat transfer parameters (i.e., $U_{so} \neq U_{lo}$ and $U_{sw} \neq U_{lw}$).

$$M_{tubes} = [U_{so} - U_{sw}.w_d]\frac{A_s.\Delta T}{\lambda} \tag{5.16}$$

An 'exponential integrated' model (i.e., $U = \frac{U_{eo}}{[1 + U_{ew}e^{\beta.w}]}$) produces the following for the mass flow of evaporation in an evaporator pass. As with the linear model, this is presented in Appendix BII and is shown there by equation (BII.17).

$$M_{tubes} + U_{ew}.\left[M_d e^{\beta w_d} - M_p e^{\beta w_p}\right] + U_{ew}.\beta M_d.w_d\left[Ei(\beta.w_p) - Ei(\beta.w_d)\right] = \frac{U_{e0}.A_s.\Delta T}{\lambda} \tag{5.17}$$

$$M_p = M_d - M_{tubes}, \qquad w_p = \frac{M_d.w_d}{[M_d - M_{tubes}]} \tag{5.18}$$

Where, M_p	=	milk mass flow from the evaporator pass.	(kg/s)
w_p	=	milk dry matter from the evaporator pass.	(kg/kg)

The above heat transfer models all contain more than one parameter. The 'integrated linear' model contains two parameters, the 'simple linear' model contains two and the 'integrated exponential' model contains three parameters. This means we cannot identify the models using the simple one-parameter optimisation method that we used for the other MVR evaporator

section parameters. The multi-parameter nature of the heat transfer identification means that we must consider the problem carefully. We will approach the problem from three directions.

1) Firstly we consider some heat transfer correlations.
In general heat transfer correlations cannot be expected to produce accurate predictions. However, they do provide a valuable consistency test for the heat transfer models that are identified from process data.

2) Secondly we use dry matter samples to identify the model parameters.
Measurements of the dry matters from each Evaporator A pass allow the determination of the mass flow of evaporation across a range of dry matter concentrations. With this data we can then identify the heat transfer models.

3) Thirdly we use 'online' flow/density measurements to identify the models.
The Evaporator A online flow/density measurements can be collected and used to determine the total evaporation in the MVR and TVR evaporator sections.

In the remainder of this section, we shall consider each of these methods and try to identify suitable models for the milk solution heat transfer coefficients. Firstly, the heat transfer correlation of Alhusseini will be used, with the physical property equations of Appendix A, to calculate the heat transfer coefficients for Whole and Skim Milk. Secondly, we shall consider the identification of the heat transfer parameters using dry matter samples. These were collected for Whole and Butter Milk throughout the Evaporator A plant. The dry matter samples will allow the complete identification of all three models. Finally we will consider the on-line flow and density data. These were collected for Whole Milk and Sophie-Lo, but only a limited range of operating conditions were available. In order to use this on-line data a simplification will need to be made to the heat transfer models. By assuming that the heat transfer coefficients at zero dry matter are equal to those for water, we can reduce the number of model parameters.

Three other important points should be noted about the heat transfer coefficients for milk.
1) The milk solution physical properties depend on milk composition.
2) The heat transfer coefficients can be reduced by fouling on the evaporator tubes.
3) The heat transfer is likely to be a combination of convection and nucleate boiling.

The different milk solution components are found to have different impacts on the physical properties and thereby heat transfer coefficients. For example the protein content has a large impact on the milk viscosity and an important impact on the thermal conductivity. However, the fat content has considerably less impact on the viscosity, but it has a large impact on the thermal conductivity. As a result, different milk solutions have different functional relationships between the dry matter concentration and heat transfer coefficient.

Another important effect is fouling of the evaporator tubes. During operation it is common to find milk dry matter components become attached to the evaporator tube surfaces. This causes an additional resistance to heat transfer and consequently the overall heat transfer coefficient is reduced. However, a well designed and operated evaporator should not suffer from serious fouling problems. As a result, we will not model the impact of fouling on the evaporating heat

transfer coefficients. To avoid fouling the experimental data should be taken from the start of an evaporator run.

The importance of nucleate boiling in the evaporation of milk solutions is not well understood. It has been suggested that nucleate boiling starts at temperature differences of 0.5 °C for milk and 5 °C for water (Bouman *et al*, 1993). The lower temperature difference required for milk solutions is due to its lower surface tension. However, it is unknown why the reported milk nucleate boiling occurs at such significantly lower temperature differences. Despite this, it is clear that milk solutions will evaporate by a combination of convection and nucleate boiling. Therefore we expect the heat transfer coefficients to depend on temperature difference, as well as dry matter concentration (Holman, 1989). However, we shall neglect the impact of nucleate boiling and assume that the heat transfer coefficients are independent of the driving temperature difference. This assumption is based on the relatively constant temperature differences that modern evaporator plants operate with. For example the MVR evaporator section of the Evaporator A plant normally operates with temperature differences of between 3-4 °C.

Heat transfer correlations

Here we consider the prediction of the heat transfer coefficients from correlations. Using the physical property equations of Appendix A and the correlations of Appendix BI, we can calculate the overall heat transfer coefficients of milk in a falling film evaporator. The results for Whole Milk and Skim Milk, as calculated from the Alhusseini correlation, are shown in Figure 5-14. To calculate these results we have used a liquid loading of 0.14 kg/m.s for the determination of the falling film Reynolds number.

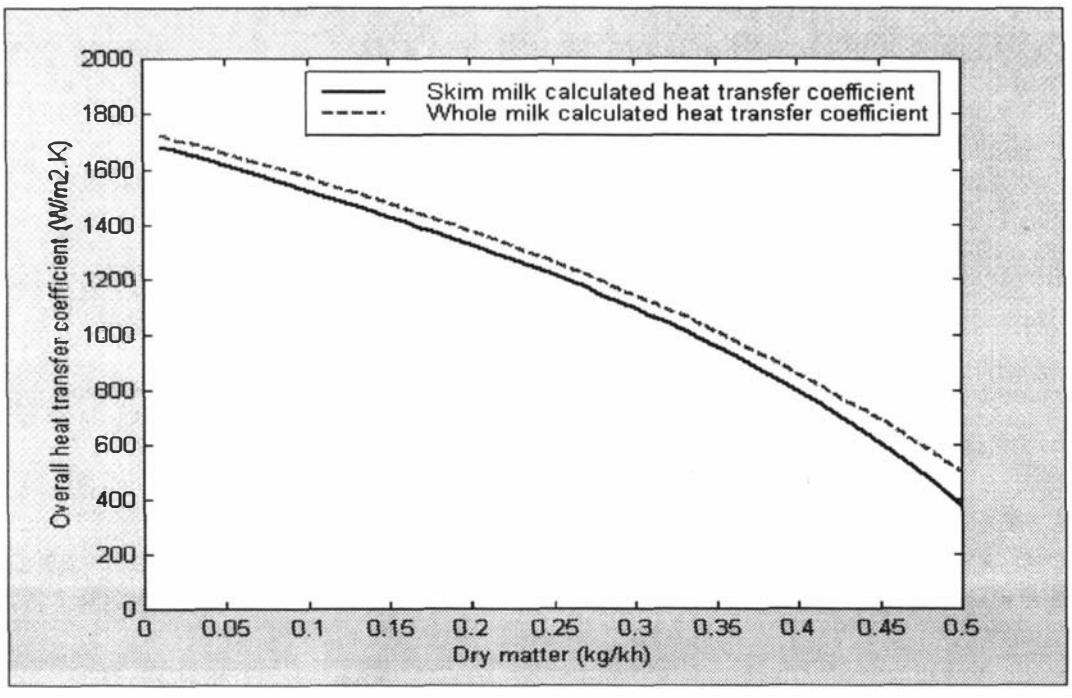

Figure 5-14 : Correlation Skim Milk and Whole Milk overall heat transfer coefficients.

There are, however, a number of problems with calculating the heat transfer coefficients from these correlations. Firstly, we are not completely confident about the accuracy of the physical

property models. It is unknown how accurate these are across a range of milk solution compositions. Secondly, the falling film heat transfer correlations were developed empirically from experimental heat transfer data. Many of these experimental fluids are likely to be substantially different from milk solutions and consequently the correlations are unlikely to be applicable for milk. Thirdly the heat transfer correlations do not include the impact of nucleate boiling. These problems are shown by the results in Figure 5-14. It is known that the heat transfer coefficients for Skim Milk are larger than those of Whole Milk (Trinh *et al*, 1996), but the Alhusseini correlation has produced nearly identical results for both. However, despite these problems the correlations do provide a definite indication of the magnitude of the heat transfer coefficients. We can therefore use these results as a consistency 'test' for the other heat transfer models that we develop.

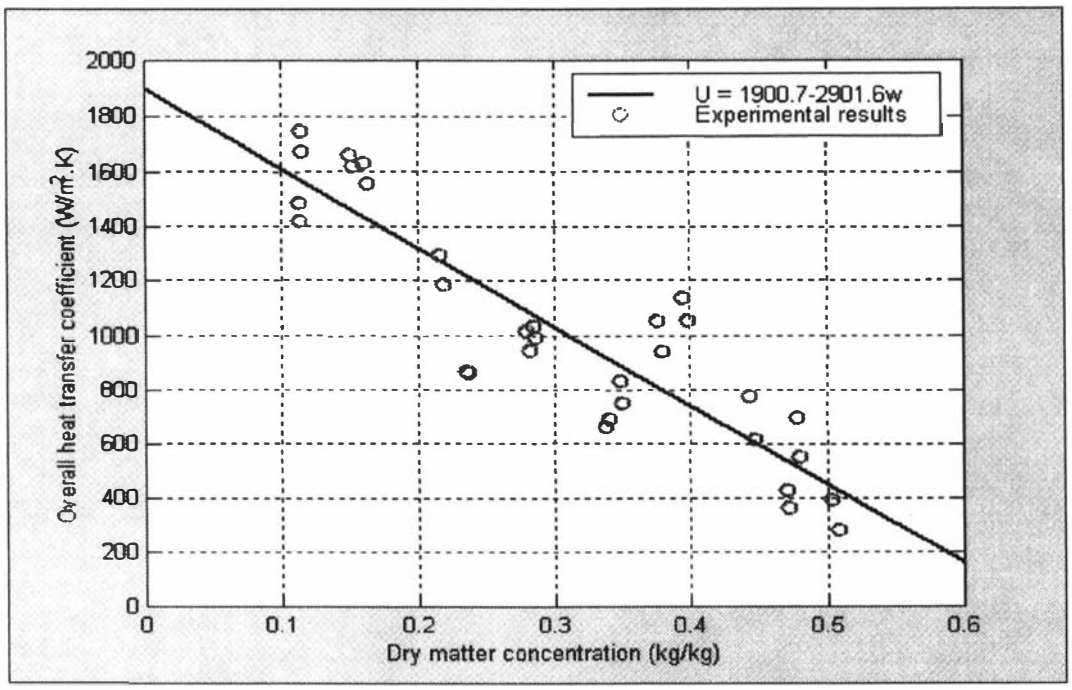

Figure 5-15 : Experimental Whole Milk overall heat transfer coefficients.

Heat transfer identification, dry matter samples

Here we consider the identification of heat transfer models from experimental dry matter samples. Dry matter samples were taken through the Evaporator A plant for Whole Milk and Butter Milk. Given the evaporator feed and product flows, these allow the mass flow of evaporation to be determined for all the evaporator passes.

Firstly we shall consider the 'simple linear' model, as shown by equation (5.16). Using the calculated mass flows of evaporation we can calculate the overall heat transfer coefficients. The linear relationship between the dry matter and overall heat transfer coefficient is then determined using simple regression analysis. Figure 5-15 shows the calculated Whole Milk overall heat transfer coefficients vs dry matter and the resulting identified linear heat transfer model. Figure 5-16 also shows the calculated overall heat transfer coefficients for Butter Milk, along with the identified linear heat transfer relationship.

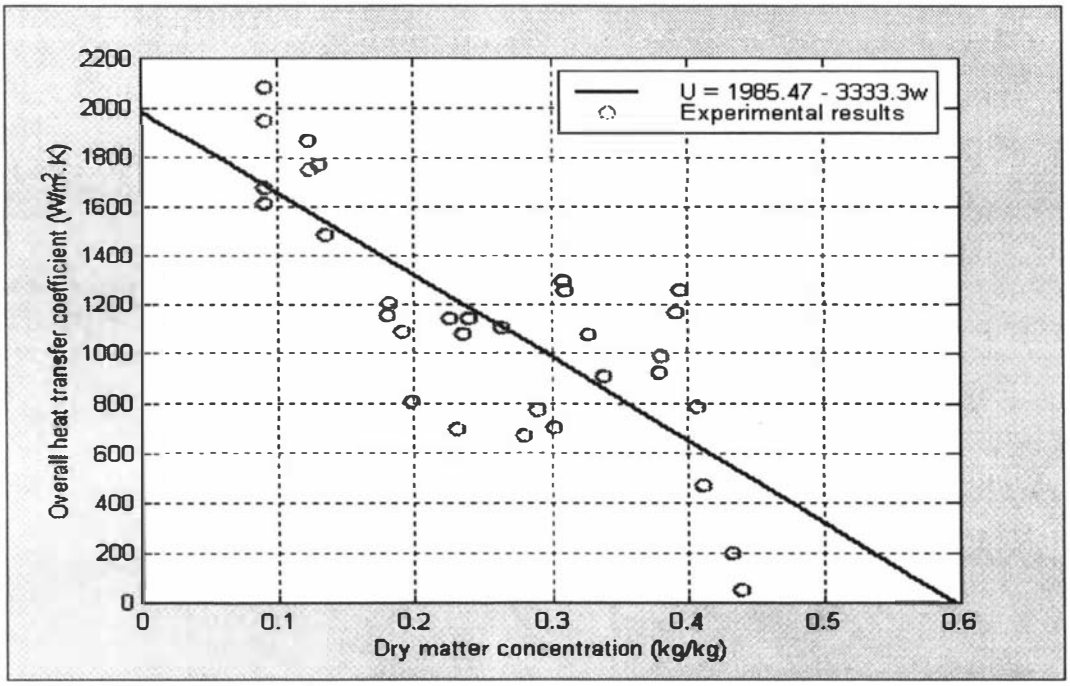

Figure 5-16 : Experimental Butter Milk overall heat transfer coefficients.

We should, at this stage, take a closer look at the results shown in Figure 5-15 and Figure 5-17. In particular the heat transfer coefficients above 0.3 kg/kg are larger than the identified equation. It is possible that these discrepancies are caused by additional nucleate boiling occurring in the TVR evaporator section. Typically the TVR section, when working with milk, operates with temperatures differences between 3 and 7 °C, which is larger than that of the MVR evaporator. In this range of temperature differences it is likely that nucleate boiling is occurring and this may explain the larger heat transfer coefficients.

We now consider the heat transfer models given by equation (5.15) and (5.17). Using the dry matter samples we can identify the parameters which minimise the balance equation sum of squared errors. The linear model contains two parameters and the exponential model three. We can, however, reduce the exponential model parameters by using the derivation of Appendix BII. It is shown that the β parameter can be estimated from a viscosity model (i.e, $\mu = \mu_{water} e^{\beta_1 w}$ and $\beta = \frac{\beta_1}{3}$). The viscosity parameter β_1 will vary for different milk solutions, but it is normally approximately 10-20 (Middleton, 1996). Consequently we can calculate that β should be between 3 and 7. We will use a value of 4.5 for this parameter and thereby reduce the exponential model parameters to two.

With the dry matter samples we have calculated the balance equation sum of squared errors and identified the model parameters. Figure 5-17 shows the identified Whole Milk model predictions for the heat transfer coefficients vs dry matter concentration. Also shown are some literature results for the heat transfer coefficients of Whole Milk (Trinh *et al*, 1996). The literature data suggests that the heat transfer coefficients depend on dry matter concentration, evaporating temperature and also evaporator temperature difference. The effect of dry matter and temperature are clearly due to the impact of the milk solution physical properties. However, there is no

adequate explanation for the impact of temperature difference. Possibly the milk is evaporating by nucleate boiling, which is known to depend on the temperature difference, but this is not clear.

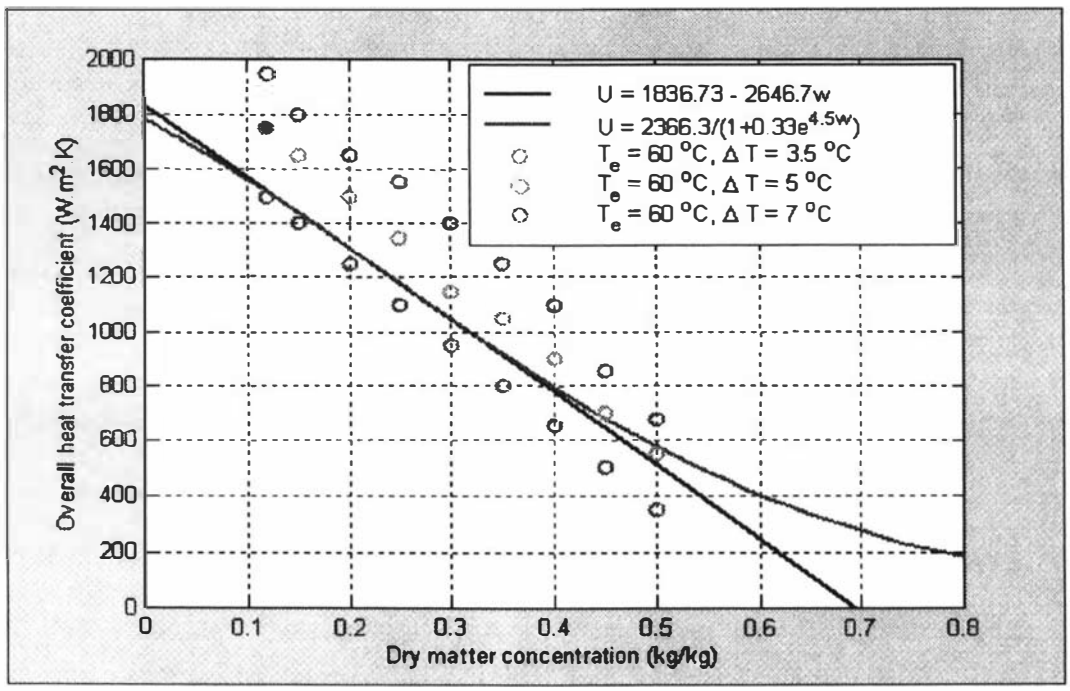

Figure 5-17 : Whole Milk overall heat transfer coefficients vs dry matter concentration.

Heat transfer identification, on-line data

Here we shall consider the identification of the heat transfer models using online flow and density measurements. The Evaporator A plant contains a volumetric feed flow and two mass flow/density meters, after the MVR and TVR evaporator sections (i.e., Q_f, M_{p5}, M_{p8}, ρ_{p5} and ρ_{p8}). With these measurements we can determine the total mass flow of evaporation in the MVR and TVR evaporation sections. However, a difficulty with the online data is the small range of plant operating conditions. Typically the plant works with very similar feed dry matters and product mass flow/dry matters. This makes it impossible to identify the two-parameter heat transfer models, because these require data across a range of dry matter concentrations. Therefore, before considering the identification of heat transfer models with on-line data we will consider a simple method for simplifying the heat transfer models.

Figure 5-17 shows that the extrapolated zero dry matter overall heat transfer coefficient is very similar to the water coefficient. There is also a clear consistency between the results in Figure 5-17 and those in Figure 5-15 and Figure 5-16. All these models have an extrapolated zero dry matter overall heat transfer coefficient that is similar to water. If we substitute the water overall heat transfer coefficient into equations (5.15) and (5.17), then we produce the following. This simplification of the heat transfer coefficient models is very important. We have already identified the overall heat transfer coefficient for water, so we only need to identify the parameters U_{ew} and U_{lw}. This can be achieved considerably more easily with the on-line data.

$$U = U_{water} - U_{lw}.w, \qquad U = \frac{U_{water}\left[1+U_{ew}\right]}{\left[1+U_{ew}e^{\beta.w}\right]} \tag{5.19}$$

Where, U_{water} = falling film evaporator overall heat transfer coefficient. ($W/m^2.°C$)

It is possible to add the mass balances for the evaporator passes to produce the following mass balances for the entire MVR evaporator section. A similar mass balance equation can be produced for the TVR evaporator section. These provide the balance equations that we need to identify the overall heat transfer coefficient parameters U_{ew} and U_{lw}, when working with the on-line data.

$$M_{d1} - M_{p5} = \frac{U_{water}A_{st}\Delta T}{\lambda} + \frac{U_{lw}.M_{d1}.w_{d1}}{U_{water}}\log\left[1 - \frac{\left(M_{d1} - M_{p5}\right)U_{water}}{M_{d1}\left(U_{water} - U_{lw}.w_{d1}\right)}\right] \tag{5.20}$$

$$M_{d1} - M_{p5} = \frac{U_{water}\left(1+U_{ew}\right)A_{st}\Delta T}{\lambda} - U_{ew}\left[M_{d1}e^{\beta.w_{d1}} - M_{p5}e^{\beta.w_{p5}}\right] - U_{ew}.\beta.M_{d1}.w_{d1}\left[Ei\left(\beta.w_{p5}\right) - Ei\left(\beta.w_{d1}\right)\right] \tag{5.21}$$

Where, A_{st} = total surface area of the MVR evaporator section. (m^2)

M_{d1} = mass flow of milk from the first MVR evaporator distribution plate. (kg/s)

w_{d1} = dry matter of milk from the first MVR evaporator distribution plate. (kg/kg)

M_{p5} = mass flow of the milk from the fifth evaporator pass. (kg/s)

w_{p5} = dry matter of the milk from the fifth evaporator pass. (kg/kg)

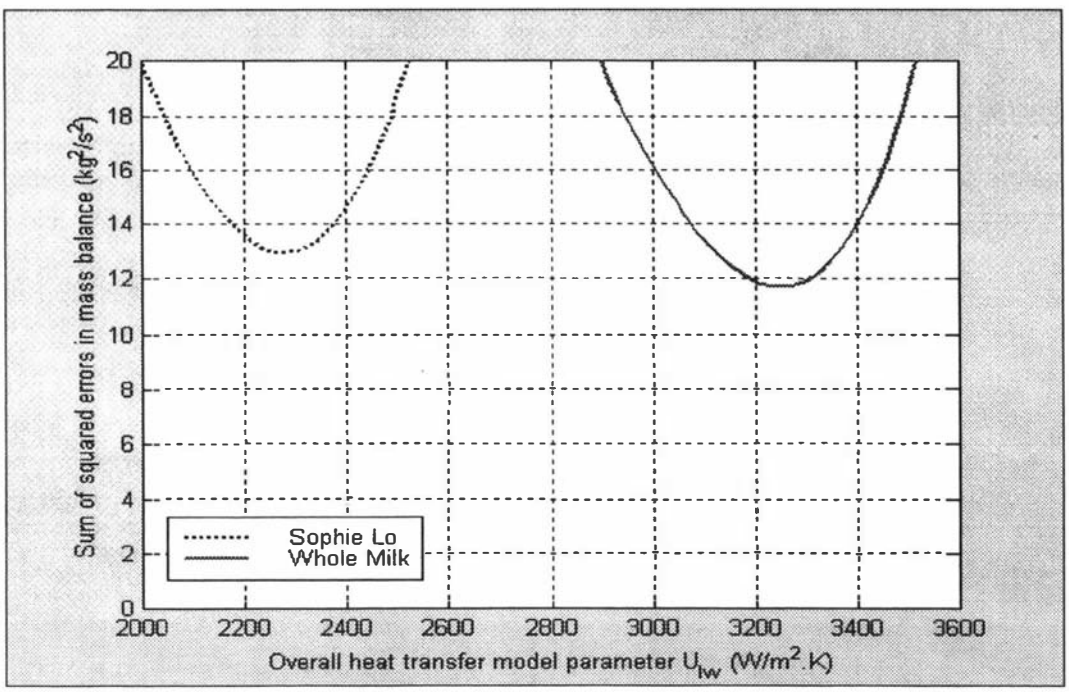

Figure 5-18 : Identification for the linear heat transfer coefficient model.

Historical online data was collected from the plant when working with Whole and Sophie-Lo milk solutions. This data was used with the balance equations (5.20) - (5.21). Figure 5-18 and Figure 5-19 show the resulting sum of squared errors vs the heat transfer coefficient parameters. The optimum U_{lw} parameter for Whole Milk is 3250.2 W/m^2.°C and for Sophie-Lo it is 2276.3 W/m^2.°C. Whereas the optimum U_{ew} parameter for Whole Milk parameter is 0.6159 and for Sophie-Lo it is 0.2652.

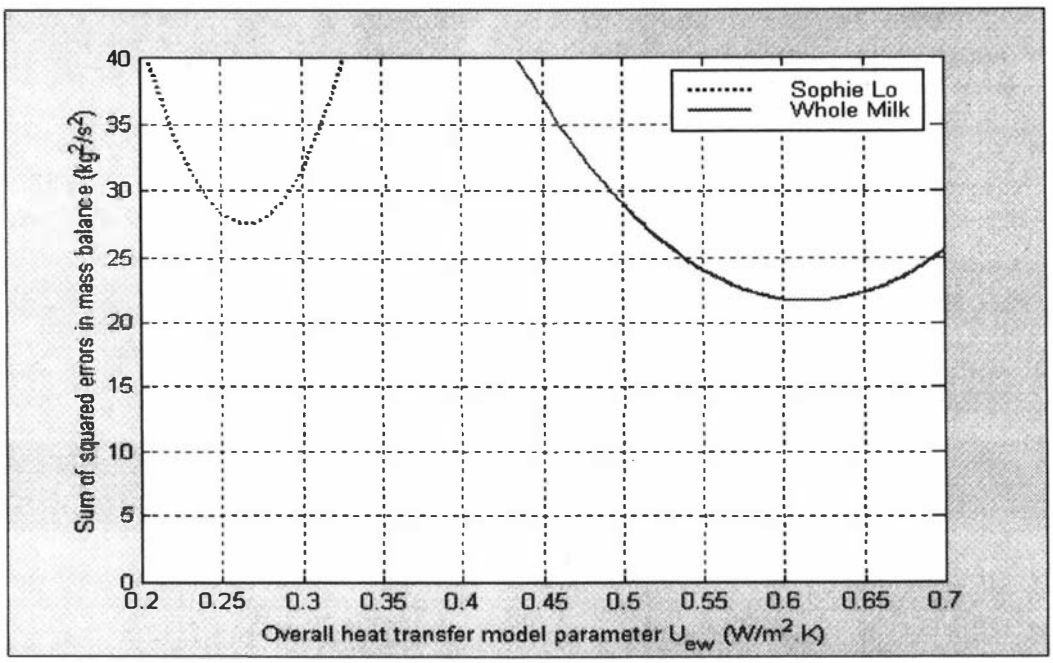

Figure 5-19 : Exponential model sum of squared errors vs heat transfer parameter.

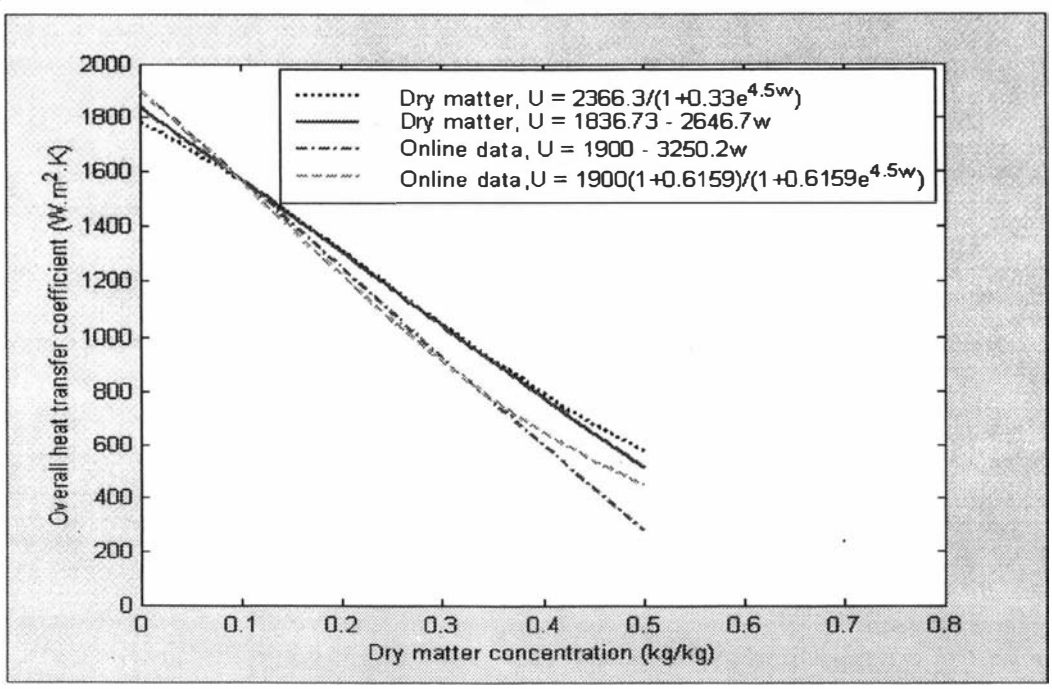

Figure 5-20 : Whole Milk identified heat transfer coefficient models.

Comparison of identified heat transfer models

The heat transfer coefficients determined from the literature correlaions, dry matter samples and on-line data can be compared. Strictly the same heat transfer model should result from all three methods. This, therefore, provides an important consistency test for the identified models. Figure 5-20 shows the Whole Milk heat transfer models that were identified from the dry matter and the on-line computer data. There is a good comparison between these results and those determined from the heat transfer correlations. However, the models determined from the on-line data produce lower heat transfer coefficients than the dry matter samples. This could be due to fouling of the evaporator. The dry matter samples were taken at the start of the evaporator run, when no fouling would exist. However, the on-line data was taken during a variety of times, when the plant had often been in operation for several hours.

Figure 5-21 shows the Whole Milk model that was identified from the dry matter samples and the Sophie-Lo model. The Sophie-Lo model heat transfer coefficients are higher than those for Whole Milk and this is probably due to the different compositions of the two milk solutions. Sophie-Lo contains less protein and fat than Whole Milk, but more lactose. The protein and fat both appear to have a strong impact on the heat transfer coefficients, because of their large impact on the thermal conductivity and viscosity. However, the lactose does not have as much impact on these physical properties and so the heat transfer coefficients for Sophie-Lo are higher.

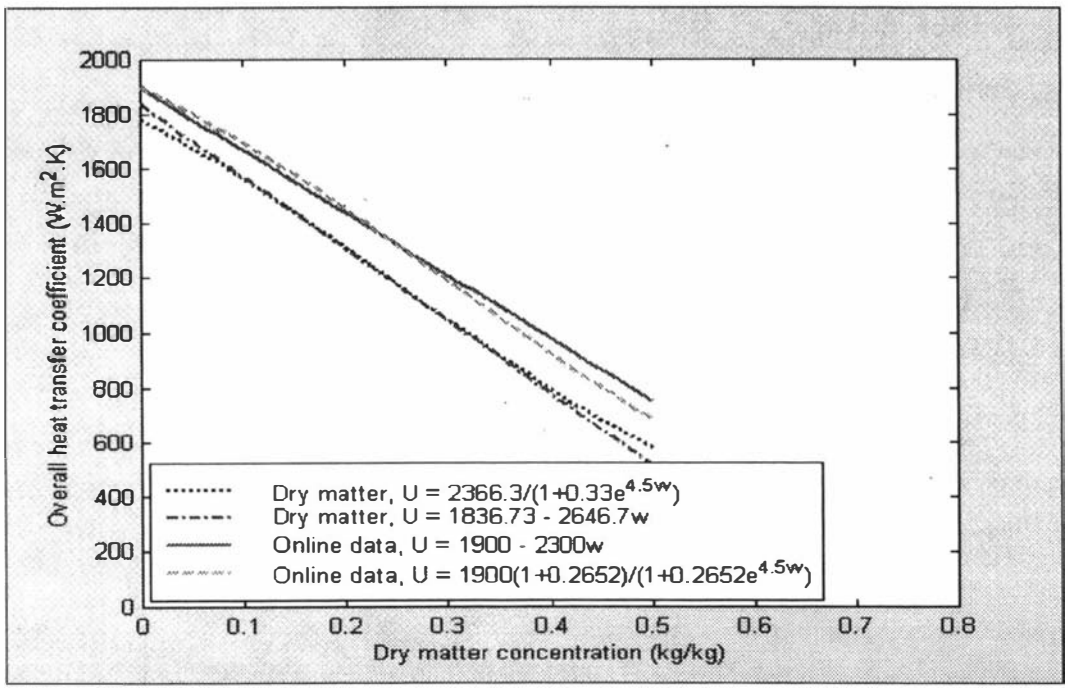

Figure 5-21 : Sophie-Lo and Whole Milk identified heat transfer coefficient models.

In the above analysis we have used three different heat transfer coefficient models. These are the integrated (5.15) and simple linear (5.16) heat transfer models and the integrated exponential model (5.17). We are interested in determining which model is the most accurate. Here we investigate the sum of squared errors in the mass balances, as determined from the dry matter samples. The model with the lowest sum of squared errors obviously fits the experimental data best and can be considered the most accurate model. Figure 5-22 shows the mass balance sum of squared errors for the three models. Also, we have considered the constant heat transfer

coefficient case. A constant heat transfer coefficient, that minimised the mass balances, was determined. This constant heat transfer coefficient was 1400 W/m^2.°C and the corresponding sum of squared errors is also shown in Figure 5-22. It is clear that the simple linear model is the most accurate. This is surprising, because this model neglects the increase in dry matter down the falling film. Presumably this is not important or the integrated models have incorrectly incorporated this effect.

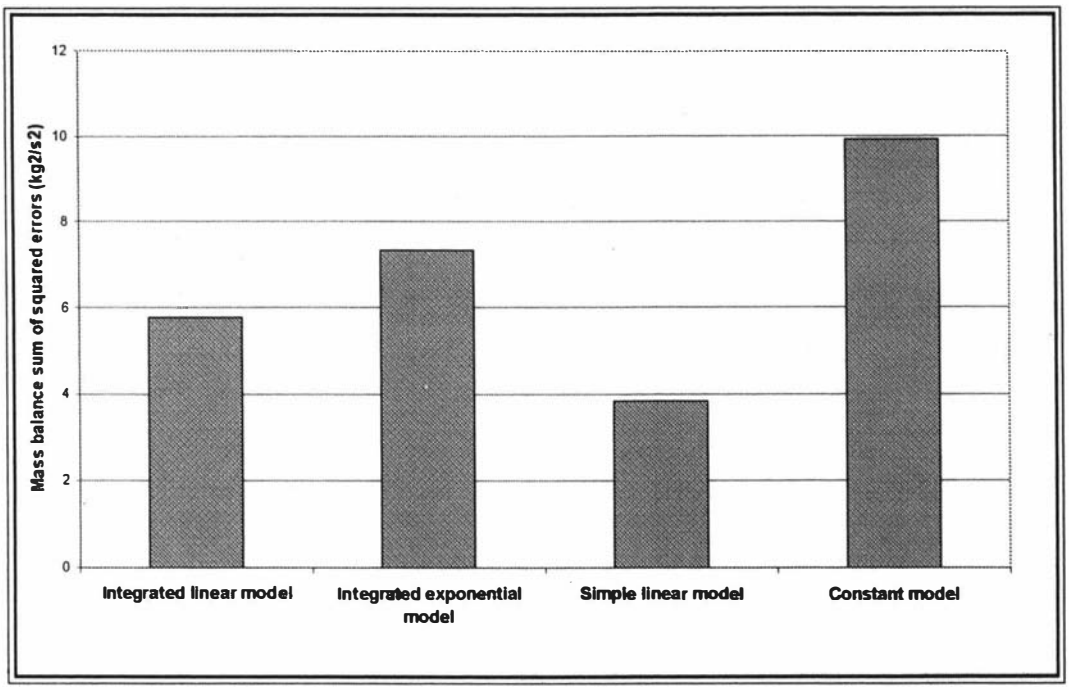

Figure 5-22 : Comparison of Whole Milk heat transfer coefficient models.

5.4) TVR Section

5.4.1) Introduction

The parameter identification for the TVR evaporator section will be separated into two parts. Firstly the determination of steady state parameters from water data and secondly the determination of the falling film residence times from milk historical data. We are primarily concerned with the steady state determination of the TVR compressor parameter B_{TVR} . However, unlike the MVR evaporator section, we cannot separate the static identification into parts and consider each individually. Consequently we must identify the TVR compressor parameter along with the overall heat transfer coefficient in a two parameter identification process. Following this we will investigate the dynamic TVR evaporator section residence times.

5.4.2) TVR Compressor Parameter and Overall Evaporating Heat Transfer Coefficients

The energy balances for the TVR second effect, shell and third effect are given by the following. These equations were derived in Chapter 2 and they are shown there by equations (2.30), (2.63) and (2.35).

$$q_{feed6} + q_{shell6} = q_{comp2} + q_{shell7} + q_{shell8} + q_{eloss2}\,,\; W_{comp2} + q_{comp2} = q_{shell6} + q_{condensate2} + q_{sloss2} \quad (5.22)$$

$$q_{feed7} + q_{shell7} + q_{shell8} = q_{vac} + q_{eloss3} \tag{5.23}$$

The addition of the energy balances for the second effect and shell gives the following overall energy balance for the second effect.

$$q_{feed6} + W_{comp2} = q_{shell7} + q_{shell8} + q_{eloss2} + q_{sloss2} + q_{condensate2} \tag{5.24}$$

These balance equations contain many parameters, which are known or have been identified in the MVR evaporator section. The losses overall heat transfer coefficient is known and the physical properties of water can be determined from the equations of Appendix A. However, we are unsure about the TVR compressor parameters, or the evaporating water heat transfer coefficient. In Appendix D the TVR compressor parameters are determined from the manufacturer specifications, but we would like to determine the accuracy of the parameters. In particular we are concerned about the parameter B_{TVR}. This parameter is directly proportional to the mass flow of suction vapour, which represents a large amount of the evaporator capacity. Also the water evaporating heat transfer coefficients are likely to be different from the MVR evaporator section, because of the lower temperatures, shorter TVR evaporator tubes and larger temperature differences. Therefore the TVR water identification is a two parameter process.

A difficulty with the Evaporator A TVR evaporator section is the lack of measurements. The second effect shell temperature and the vacuum condenser cooling water temperatures and flow are not measured. We can use the second effect shell energy balance to calculate the shell temperature and the third effect energy balance to calculate the condenser heat flow. However, this leaves only a single energy balance to identify the process parameters. Fortunately there is also the mass balance for the TVR section, which is given by the following. We will use the TVR second effect overall energy balance and the total TVR mass balance to identify the required process parameters.

$$M_{p5} = M_{p8} + M_{flash6} + M_{tubes6} + M_{flash7} + M_{tubes7} + M_{tubes8} \tag{5.25}$$

Historical data was collected from the Evaporator A plant when operating with water. We can identify the process parameters by minimising the second effect overall energy and TVR section mass balance deviation sum of squared errors. By doing this, we can determine that $B_{TVR} = 45$ $m^{0.03}.s^{0.06}/kg^{0.03}$ and $U_0 = 1400$ $W/m^2.°C$. These parameters can be compared with our expectations. The B_{TVR} parameter is determined as 58 $m^{0.03}.s^{0.06}/kg^{0.03}$ in Appendix D and the overall heat transfer coefficient is given as 1490 $W/m^2.°C$ from the results of the MVR evaporator section. There is a difference between these and the identified results, but it is a not a significant discrepancy. However, we wish to test the identified parameters by investigating the balance equation residuals. We will define the following fractional residual.

$$\Delta_{T1} = \frac{\left| q_{feed6} + W_{comp2} - q_{shell3} - q_{eloss2} - q_{sloss2} - q_{condensate2} \right|}{q_{feed6} + W_{comp}} \tag{5.26}$$

Where, Δ_{T1} = fractional energy balance residual. (-)

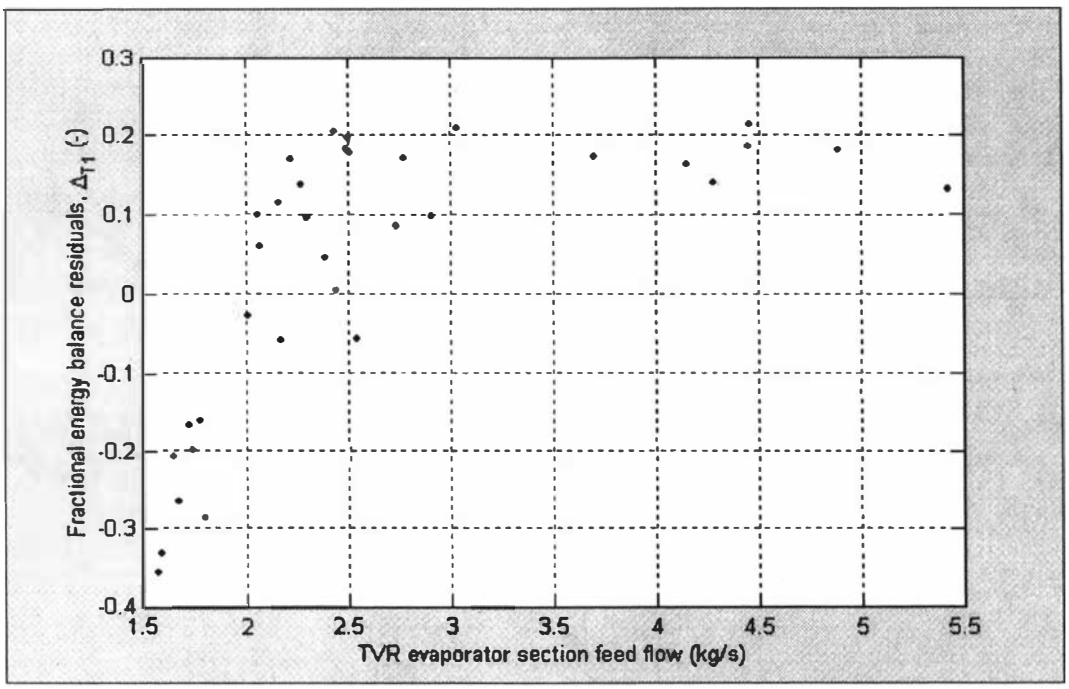

Figure 5-23 : Energy balance equation residuals vs TVR mass feed flow.

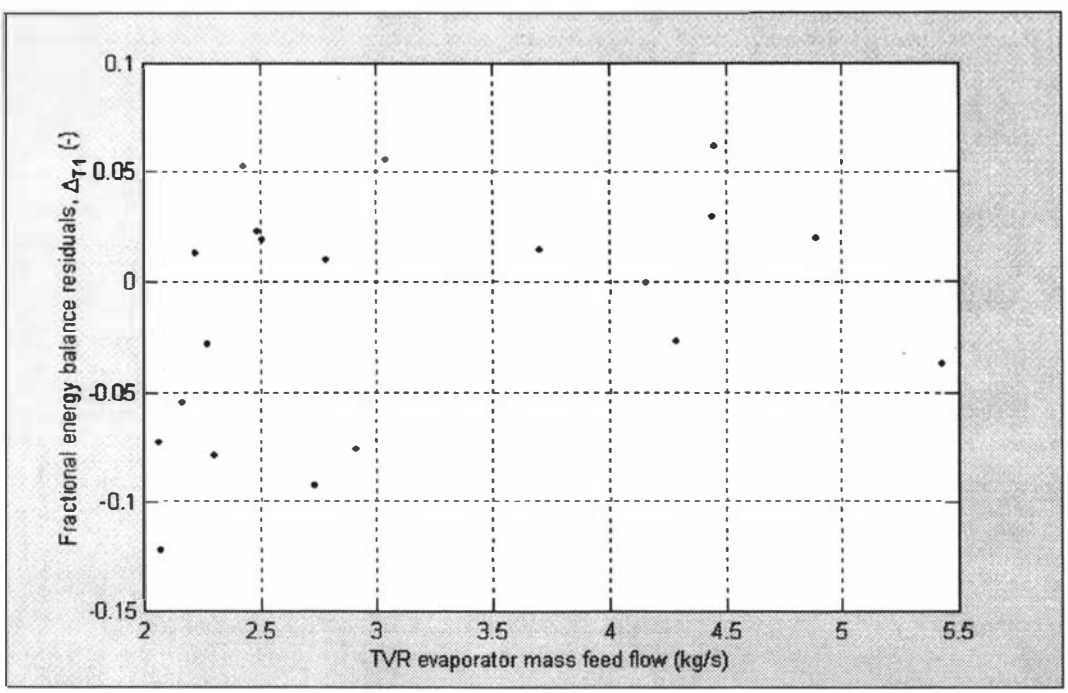

Figure 5-24 : Energy balance residuals vs TVR feed flow, with film break-up points neglected.

Figure 5-23 shows the overall energy balance residuals (Δ_{T1}) vs the TVR evaporator mass feed flow rate. Many of the residuals are within 20 % but there are some points with large residuals at

low flow rates. In Appendix C the water historical data is used to calculate the mass flows from the falling films. The results suggest that the large residuals in Figure 5-23 are caused by break-up of the falling film at low flowrates. This causes the effective heat transfer coefficients to be lower and thereby causes the large residuals shown in Figure 5-23.

We are not interested in the heat transfer coefficients during film break-up. As a result, the data points corresponding to film break-up will be neglected and the parameter identification repeated. By doing this we can identify new values for the process parameters of B_{TVR} =47 $m^{0.03}.s^{0.06}/kg^{0.03}$ and U_0 =1690 $W/m^2.°C$. These results can again be tested by considering the energy balance residuals and these are plotted in Figure 5-24. This shows that the residuals are evenly spread across the range of feed flows and we can be confident about the identification.

5.4.3) Dynamic TVR Section Residence Times

In Appendix BI a model is discussed that can be used to predict the residence time of a falling film. We will determine if this model is consistent with experimental results from the Evaporator A plant. The residence times of the TVR evaporator section can be determined from the product milk densities during start-up and shut-down. For example Figure 5-25 shows the product milk densities from the MVR and TVR evaporator sections during the Evaporator A start up. This clearly shows the delay between the MVR and the TVR product densities. The Laplace Domain transfer function, between the MVR and TVR density signals, is given by the following.

$$\frac{w_{p8}(s)}{w_{p5}(s)} = \frac{M^0_{p5}}{M^0_{p8}} \frac{e^{\left[-\left(\tau_{p5}+\tau_{e6}+\tau_{p6}+\tau_{e7}+\tau_{e8}\right)\right]}}{\left[\tau_{hd6}.s+1\right]\left[\tau_{hd7}.s+1\right]\left[\tau_{hd8}.s+1\right]} \tag{5.27}$$

If we neglect the distribution plate dynamics, then this can be simplified.

$$\frac{w_{p8}(s)}{w_{p5}(s)} = \frac{M^0_{p5}}{M^0_{p8}} e^{\left[-\left(\tau_{p5}+\tau_{e6}+\tau_{p6}+\tau_{e7}+\tau_{e8}\right)s\right]}, \quad w_{p8}(t) = \frac{M^0_{p5}}{M^0_{p8}} w_{p5}\left(t-\tau_{p5}-\tau_{e6}-\tau_{p6}-\tau_{e7}-\tau_{p7}-\tau_{e8}\right) \tag{5.28}$$

Where, τ_{p5} = pumping delay, MVR density meter and TVR first distribution plate. (s)

τ_{e6} = falling film residence time for the sixth evaporator pass. (s)

τ_{p7} = pumping delay from the TVR seventh pass to the eighth pass. (s)

τ_{p6} = pumping delay from the TVR sixth pass to the seventh pass. (s)

τ_{e7} = falling film residence time for the seventh pass. (s)

τ_{e8} = falling film residence time for the eighth pass. (s)

τ_{hd6} = sixth pass distribution plate time constant. (s)

τ_{hd7} = seventh pass distribution plate time constant. (s)

M^0_{p5} = mass flow from the fifth evaporator pass, at steady state. (kg/s)

M^0_{p8} = mass flow from the eighth evaporator pass, at steady state. (kg/s)

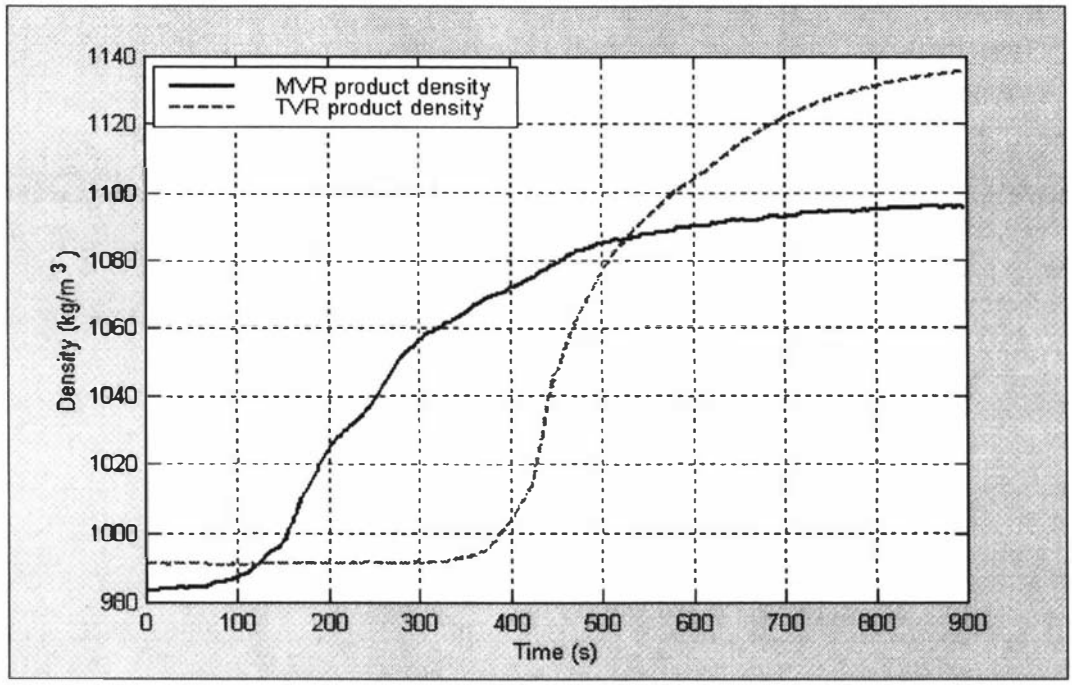

Figure 5-25 : MVR and TVR product densities during start up, Sophie-Lo milk solution.

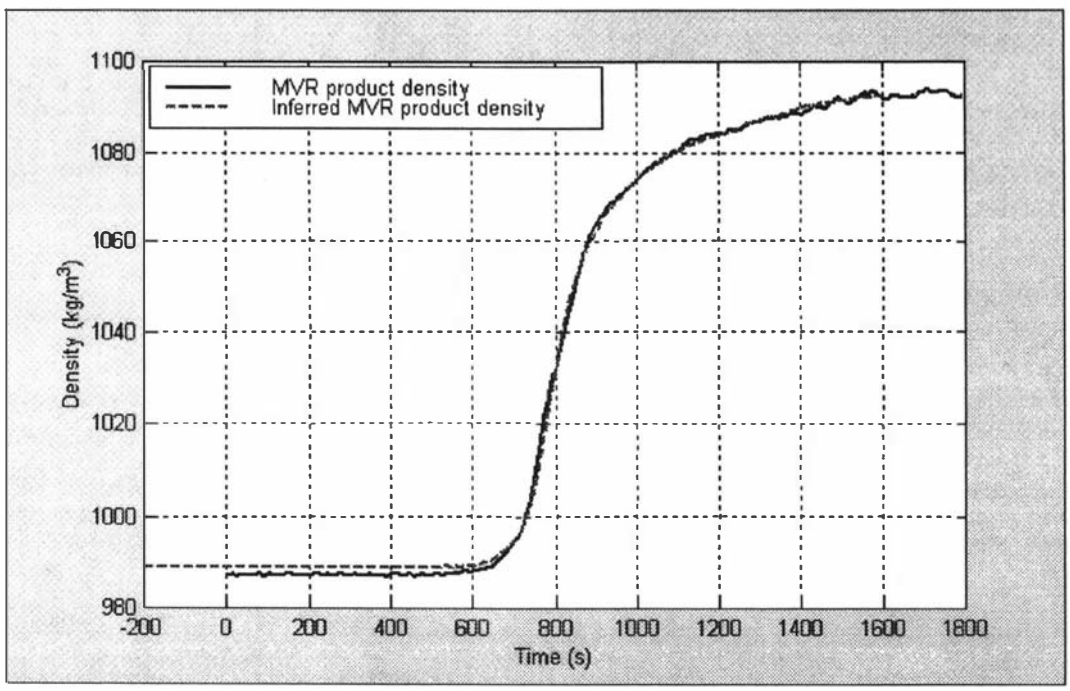

Figure 5-26 : MVR and TVR densities, superimposed on each other.

The validity of neglecting the distribution plate dynamics can be investigated by looking at the MVR and TVR evaporator section product densities during start up. We can take the TVR density and infer the MVR product density using equation (5.28). This inferred MVR density can be compared with the actual MVR density and the result is shown in Figure 5-26. A gain of 1.45 and a residence time of 230 s were used to infer the MVR product density. The two densities are

very similar and this suggests that neglecting the distribution plate dynamics is a reasonable assumption.

Using equation (5.28), with a set of historical data, we can determine the TVR evaporator section total residence time. Historical data was collected for the start-up and shut-down of the Evaporator A plant when working with Sophie-Lo milk solution. Figure 5-27 shows the Sophie-Lo model sum of squared errors vs the TVR evaporator residence time. The optimal start-up residence time is 225 seconds and the shut-down time is 190 seconds. It is unknown what causes the difference in the residence times for the start-up and shut-down.

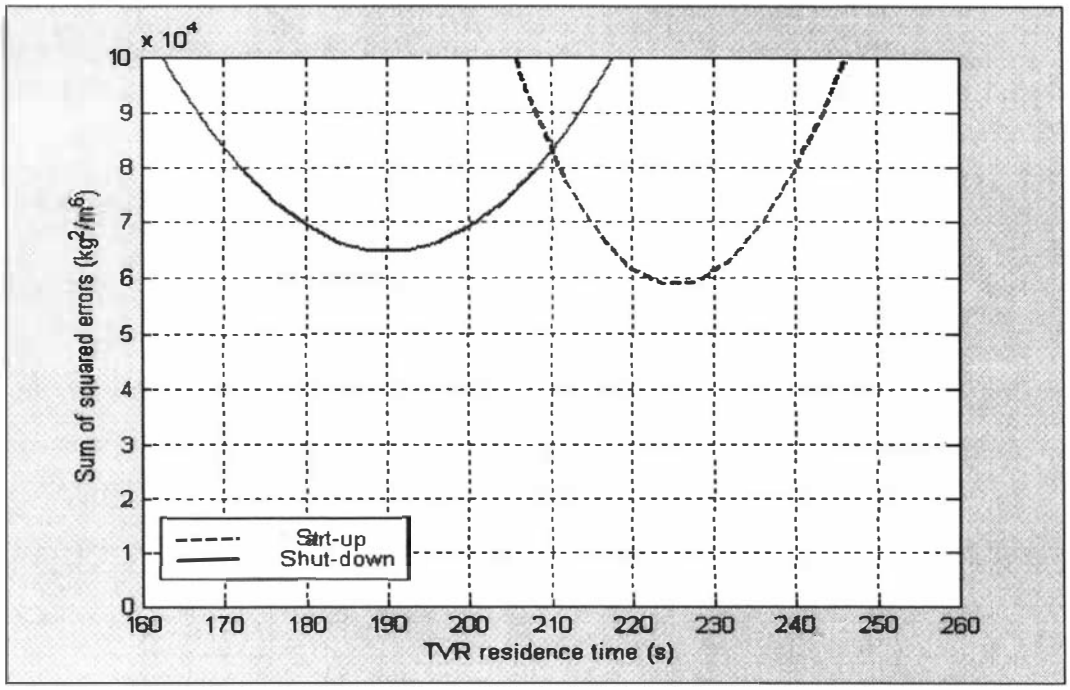

Figure 5-27 : Sophie-Lo, start-up and shut-down TVR evaporator residence time identification.

We are now interested in determining the falling film residence times. The falling film residence times and the pumping delays can be determined from the following. This assumes that the falling film velocities are constant.

$$\tau_e = \frac{L_e}{v_e}, \qquad \tau_p = \frac{L_p}{v_p} \tag{5.29}$$

Where, τ_p	=	pumping delay.	(s)
τ_e	=	falling film residence time.	(s)
v_p	=	pumping velocity.	(m/s)
L_p	=	pumping pipe-work length.	(m)
L_e	=	falling film evaporator tube length.	(m)
v_e	=	falling film velocity.	(m/s)

The falling film evaporator tubes are 10 metres and the product concentrate pipes are 20 metres long, in the TVR evaporator section. The pipes are 3 inch diameter and using the steady state model we can calculate the pumping delays for the TVR evaporator section. For example the fifth pass typically has a mass flow of 4.5 kg/s and a density of 1090 kg/m^3. With the 20 metre pipes this gives a residence time of $\tau_p = 22s$.

The results in Figure 5-27 show that the total residence time of the TVR evaporator section is between 190 and 225 s. There are three pumping delays, which each have residence times of approximately 20 s. As a result, we can determine that the falling films have a residence time of between 130 and 165 s. If the falling film velocities are constant then each falling film has a residence time of between 43 and 55 s. With 10 metre tubes the falling film velocities are then between 0.23 and 0.18 m/s. These results are consistent with those found in Appendix BI. The falling film velocities of Whole and Skim milk solutions were found to reduce from approximately 0.5 m/s to 0.15 m/s, during the milk concentration process. Sophie-Lo contains less protein than Skim or Whole milk and so its falling film velocities are likely to be slightly higher.

The results determined here are not meant to provide an accurate identification of the falling film residence times. We are primarily concerned with giving a simple verification of the falling film model discussed in Appendix BI. It appears that the model is, in fact, consistent with the results from the Evaporator A plant. Most importantly it appears that the typical falling film residence time is approximately 50 s for each pass and each pumping delay is approximately 20 s.

In the MVR evaporator section the falling film and pumping delay residence times may be different from those of the TVR evaporator section. However, given the falling film model from Appendix BI and the steady state model we can determine the residence times for the MVR evaporator section. The evaporator tubes are longer, at 16 metres and the concentrate pipes are longer, at 23 metres. Appendix BI gives falling film velocities of between 0.5 and 0.25 m/s and the falling film residence times are between 32 and 64 s.

5.5) Conclusions

In this Chapter we have identified many of the unknown parameters that are used in the Evaporator A plant model. A complete identification of the parameters has not been made and in particular many of the dynamic parameters are unknown. The important falling film residence times have been investigated, but the results are not completely conclusive and more work is required in this area. It will be shown in Chapter 7 that the falling film residence times are, from a controllability perspective, the most important dynamic parameters in the model. However, the thermal inertias will be found to be less important in the controllability analysis. Consequently the emphasis on the falling film residence times is justified.

In Section 5.2 we considered the DSI preheat section steady state model. This did not contain any model parameters, so we considered the model accuracy by making comparisons with historical data from the Evaporator A plant. The 'Advanced' model from Chapter 4 was used and the model produced good predictions. However, the model still appears to contain deficiencies, since its residuals showed a correlation with the DSI unit temperature.

In Section 5.3 we considered the identification of model parameters for the MVR evaporator section. The identification was separated into parts, because of the difficulty of considering all the parameters simultaneously. Fortunately the online historical data, of the Evaporator A plant, is quite good for the MVR evaporator section and so it was possible to consider the equations independently. The preheat condenser overall heat transfer coefficient, the evaporator surface energy losses overall heat transfer coefficient, the MVR compressor vapour duct pressure losses and the water evaporating overall heat transfer coefficient were all identified successfully.

As part of the MVR evaporator section identification, we considered the heat transfer coefficients for milk solutions. It was shown that the evaporating heat transfer coefficients reduce with increases in the milk dry matter concentration. Three different methods were considered for the development of models for the effect of dry matter on heat transfer. Firstly, heat transfer correlations were investigated. Secondly dry matter samples were taken from each of the Evaporator A plant passes and used to identify models. Thirdly online flow and density measurements were used to identify models.

The heat transfer coefficient correlations were considered first. A good comparison was produced for the water heat transfer coefficients. However, the results for milk did not seem to be as reliable. For example the correlation predictions for Skim Milk and Whole Milk were very similar, which contradicts the literature results with higher Skim Milk coefficients. This problem is possibly caused by physical property equations, which are not completely reliable, or possibly nucleate boiling, which is neglected in the convection equations.

The dry matter samples and online flow/density measurements were used to identify heat transfer models for Whole Milk, Butter Milk and Sophie-Lo. Three models were derived in Appendix BII and then the model parameters identified in Section 5.3. Comparisons between the dry matter and online data models were quite good, which provides an important clarification of the resulting models. Ultimately we would like general models for the heat transfer coefficients in terms of the milk components. However, the range of milk solutions considered was not enough to do this. Of the three heat transfer models, developed in Appendix B11, the 'simple linear' model was found to provide the best fitting.

In Section 5.4 the identification of parameters for the TVR evaporator section were considered. The important B_{TVR} parameter was identified first. A two parameter identification was required, because of the coupling between the TVR evaporator section mass and energy balances. These could not be separated like those for the MVR evaporator section. A major difficulty with the identification was the occurrence of film beak-down at low mass flows. This causes the 'effective' heat transfer coefficients to significantly reduce. In Appendix C it is shown that a large number of the TVR evaporator section data could not be used for identification, because of the film break-down.

Chapter 6 : Optimum Operating Regime

6.1) Introduction

In this Chapter we investigate the optimum operating regime of the Evaporator A plant. The process optimisation is essentially a method for determining the process controller set-points, or alternatively the manipulated variables. We will be considering the evaporation costs and we aim to determine the process set-points which minimise this. The Evaporator A plant has six important process control set-points, with process and manipulated variables.

Table 6-1 : Process and manipulated variables for the Evaporator A plant.

	Process Variable	Manipulated Variable
1	Evaporator product mass flow (M_{p8})	Evaporator feed flow (M_f)
2	MVR evaporator temperature (T_{e1})	Heat exchanger condensate flow (M_c)
3	TVR final effect temperature (T_{e3})	Vacuum condenser water flow (M_{vac})
4	TVR product dry matter (w_{p8})	TVR steam pressure set-point (P_{sp})
5	MVR product dry matter (w_{p5})	MVR compressor speed (N_{comp})
6	DSI unit temperature (T_{DSI})	DSI unit steam mass flow (m_{dsi})

Some of the optimum conditions for these set-points can be determined relatively easily. Specifically the DSI unit temperature, the MVR evaporator temperature and the TVR evaporator temperature. The determination of these optimum conditions is discussed in Section 6.5.

The optimum conditions for M_f, N_{comp} and P_{sp} are determined by the energy optimisation. The Kiwi Co-op Dairies Powder 3 plant uses three evaporation sections. These are the MVR evaporator section, the TVR evaporator section and the spray dryer. Each evaporating section has a different energy efficiency and different energy source. In Chapter 1 the energy efficiencies of the MVR, TVR evaporators and spray dryers were shown to be significantly different. In Section 6.3 we investigate the impact of these energy efficiencies on the total plant evaporation cost. Then in Section 6.5 we use this to investigate the optimisation of the plant evaporation costs.

There are constraints on the optimisations considered in this Chapter. In Section 6.4 we investigate the following four important process constraints. These will then be incorporated into the optimisation problems considered in Section 6.5.

1) Evaporation capacity constraints.
2) Film breakdown constraints.
3) Evaporator temperature constraints.
4) Concentrate dry matter constraints.

In Section 6.2, of this Chapter, we also consider some operational and design aspects of the DSI preheat section. Specifically we investigate the impact of air in the flash vessels, flooding of the first flash vessel and milk evaporation in the holding tubes.

6.2) DSI Preheat Operation

6.2.1) Introduction

We now investigate some common operational issues that occur with evaporator preheat sections. Specifically we will consider the problems of non-condensable gases, vapour formation in the holding tubes and flash vessel flooding.

The bottom of the first flash vessel is the first point where evaporation occurs and this causes non-condensable gases (i.e., air) to be released from the milk. De-aeration lines must be attached to the flash vessels in order to remove these gases. For the Evaporator A plant these de-aeration lines are attached to the first evaporator effect. In Chapter 3 it was shown that an excessive temperature difference between the flash vessel top and bottom can be an indication of air.

The milk pressure in the preheat holding tubes must not fall below its vapour pressure. Otherwise it will start evaporating and vapour bubbles will form in the milk solution. These vapour bubbles will collect at the top of the holding tubes and act as restrictions on the milk flow. To overcome this problem, the pressure in the holding tubes should be controlled using a back-pressure controller. This uses an orifice plate and a manipulated by-pass control valve, at the end of the holding tubes.

A major problem with the flash vessels is the possibility of milk bypassing the holding tubes. This occurs when the milk 'floods' the top of the vessel and flows directly into the bottom. The flash vessel contains a weir and this is supposed to restrict contact between the top and bottom of the vessel. However, if the milk level rises above the weir, then it is possible for it to bypass the holding tubes. This is a very serious problem, because the purpose of the preheat section is to provide a controlled heat treatment.

6.2.2) Impact of Air on Preheat Operation

We showed in Section 3.2 of Chapter 3 that the presence of air causes a temperature difference between the top and bottom of a flash vessel. Using the 'simple' steady flash vessel model, developed in Chapter 3, we can produce steady state equations for the impact of air on a flash vessel. With the results from the linear saturation relationship (i.e. $T_{pc}=T_{ph}(1-y_{air})-\frac{k_2}{k_1}y_{air}$) we can produce equation (6.1) for the temperatures of a single flash vessel.

$$T_{ph}=\frac{1}{[2-y_{air}]}T_{fc}+\frac{1}{[2-y_{air}]}T_{fh}+\frac{k_2.y_{air}}{k_1[2-y_{air}]}, \qquad T_{pc}=\frac{[1-y_{air}]}{[2-y_{air}]}T_{fc}+\frac{[1-y_{air}]}{[2-y_{air}]}T_{fh}-\frac{k_2 y_{air}}{k_1[2-y_{air}]} \quad (6.1)$$

We can also extend this result to the two flash vessel system of the Evaporator A plant. The first flash vessel should contain most of the air because the milk evaporates first in this vessel and it operates at a higher temperature than the second. Using the 'simple' flash vessel model in

combination with equation (6.1) we can produce equations (6.2) - (6.3) for the flash vessel temperatures.

$$T_{pc1} = \frac{[1 - y_{air}]}{[3 - 2.y_{air}]} T_{fc2} + \frac{2[1 - y_{air}]}{[3 - 2.y_{air}]} T_{DSI} - \frac{k_2 y_{air}}{k_1 [3 - 2.y_{air}]} \tag{6.2}$$

$$T_{ph1} = \frac{1}{[3 - 2.y_{air}]} T_{fc2} + \frac{2}{[3 - 2.y_{air}]} T_{DSI} + \frac{2.k_2.y_{air}}{k_1 [3 - 2.y_{air}]} \tag{6.3}$$

$$T_{pc2} = T_{ph2} = \frac{[2 - y_{air}]}{[3 - 2.y_{air}]} T_{fc2} + \frac{1}{[3 - 2.y_{air}]} T_{DSI} + \frac{k_2.y_{air}}{k_1 [3 - 2.y_{air}]} \tag{6.4}$$

The mass flow of steam to the DSI unit can be determined by making an energy balance around the DSI.

$$m_{steam} = \frac{M_{fc2}.C_{pwater}[T_{DSI} - T_{pc1}]}{[h_{steam} - C_{pwater}.T_{DSI}]} = \frac{M_{fc2}.C_{pwater}}{[h_{steam} - C_{pwater}.T_{DSI}]} \frac{\left[T_{DSI} - (1 - y_{air})T_{fc2} + \frac{k_2}{k_1} y_{air}\right]}{[3 - 2y_{air}]} \tag{6.5}$$

These equations show that air has two important impacts on a preheat system. Firstly the mass flow of steam required by the DSI unit increases, as shown by equation (6.5). Secondly it causes the temperature of the second flash vessel to increase, as shown by equation (6.4). Both of these effects are actually caused by the temperature difference between the top and bottom of the first flash vessel. The temperature at the top of the first flash vessel reduces and therefore more steam is required to heat the DSI unit to the same temperature. However, the increased temperature at the bottom of the first vessel causes an increase in enthalpy to the second vessel and so its temperature rises.

The increase in the steam mass flow to the DSI unit means that the energy efficiency of the unit is reduced. The Evaporator A plant has a temperature control loop placed around the DSI unit and this compensates for variations in the feed milk temperature. As a result, of the air in the flash vessel, the DSI temperature control loop increases the mass flow of steam. However, since the DSI unit temperature is the same, the energy efficiency of the DSI unit is lower. Obviously we should remove this possibility by providing adequate de-aeration of the flash vessels.

Variations of air concentration in the flash vessel cause milk temperature variations to the MVR evaporator section. Later in this Chapter it will be shown that the temperature of the MVR evaporator has an impact on its mass flow of evaporation. Therefore it would be preferable if temperature disturbances to the MVR evaporator could be minimised. Once again this requires adequate de-aeration of the flash vessels.

Industrial evaporator plants have de-aeration lines that should remove any air that accumulates in the preheat system. The de-aeration lines are small pipes, containing an orifice plate, attached to the flash vessels and another lower pressure vessel. It is important that the de-aeration orifice

plates are correctly sized. If the plate is too small then air will accumulate in the flash vessels and the above problems will occur. However, if the plate is too large then large amounts of steam will escape from the system and this will cause other problems. We have shown that a probable indication of air problems is the temperature difference between the top and bottom of the flash vessel. Ideally a flash vessel should operate without any temperature difference and this provides a simple test of the de-aeration lines.

6.2.3) Holding Tube Pressures

Earlier we discussed the importance of maintaining an adequate pressure in the preheat holding tubes. If the milk is not to vaporise in the holding tubes then the pressure at the top of the tubes must be larger than the vapour pressure of the milk. Figure 6-1 shows the configuration that should be used to remove the possibility of milk vaporising in the holding tubes. The pressure after the holding tubes is measured and a combined orifice plate and control valve is used to regulate the pressure.

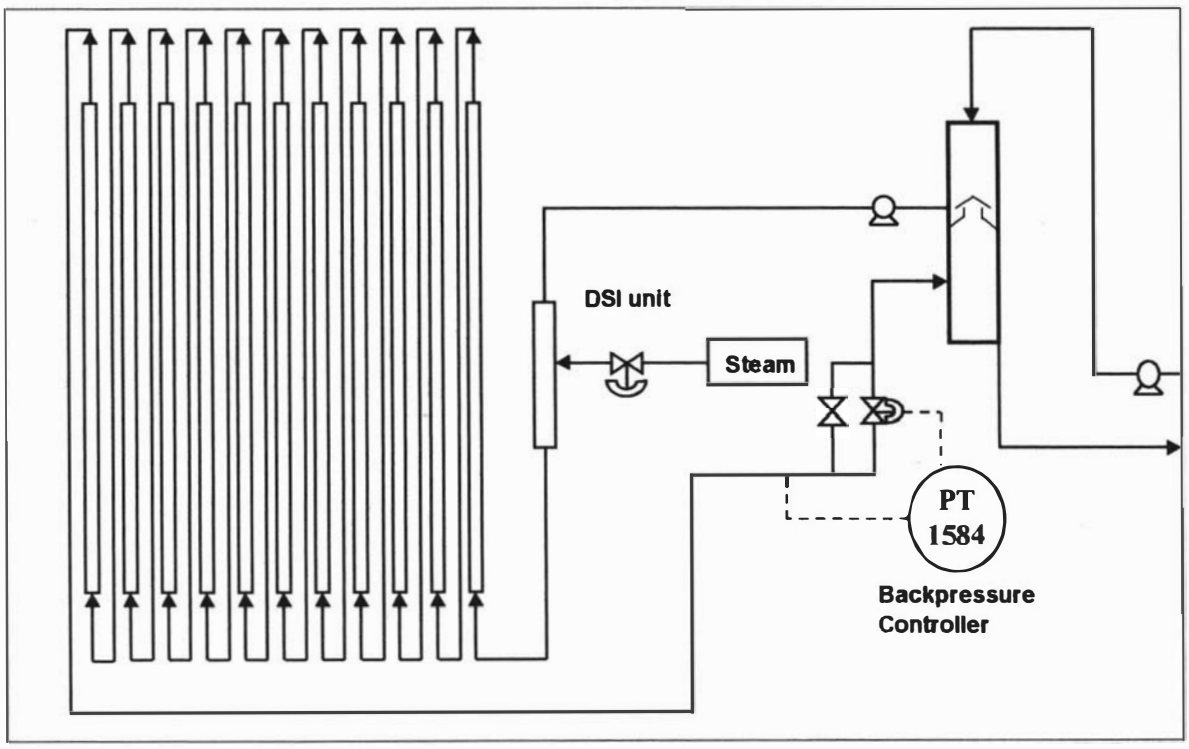

Figure 6-1 : DSI preheat section back-pressure control loop.

The requirement for an adequate holding tube pressure is given by equation (6.6). However, it should also be remembered that this neglects any additional pressure drop due to the back-pressure control valve. A control valve should be sized so it is operating in the middle of its range and this can be accommodated by including a safety margin into equation (6.6).

$$P_h = \Delta P_{orif} + P_{phl} - \Delta P_{head} > P_{vap} \qquad (6.6)$$

Where, P_h = pressure at the top of the holding tubes. (Pa)

ΔP_{head} = pressure drop due to the height of the holding tubes. (Pa)

ΔP_{orif}	=	pressure drop due to the back-pressure orifice plate.	(Pa)
P_{phl}	=	pressure of the flash vessel.	(Pa)
P_{vap}	=	vapour pressure of milk.	(Pa)

The orifice plate pressure drop is given by the standard orifice plate equation and the holding tube pressure drop is given by the hydrostatic head.

$$\Delta P_{orif} = \frac{\rho}{2}\left[\frac{Q_{DSI}}{C_d . A_{orif}\left(1-\beta^2\right)}\right]^2, \quad \Delta P_{head} = \rho . g . h_t \tag{6.7}$$

Where, C_d	=	orifice plate discharge coefficient.	(-)
A_{orif}	=	cross sectional area of orifice plate hole.	(m^2)
Q_{DSI}	=	volumetric flow of liquid through the holding tubes.	(m^3/s)
β	=	ratio of orifice plate diameter to pipe diameter.	(-)
ρ	=	density of liquid in holding tubes.	(kg/m^3)
h_t	=	height of holding tubes.	(m)

These equations show that the pressure at the top of the holding tubes depends on the orifice plate size. Smaller orifice plates give greater pressure drops and consequently higher pressures at the top of the holding tubes. The choice of the orifice plate size thereby determines whether the milk will vaporise at the top of the holding tubes.

The pressure in the flash vessel and the required milk vapour pressure can be determined from the simple preheat model and the Antoine saturation equations. If the DSI temperature varies across a wide range then the flash vessel temperatures will also vary. Consequently the pressure in the flash vessels will change and also the pressure at the top of the holding tubes. This means that the orifice plate needs to be sized for the maximum DSI temperature, when the milk vapour pressure is at its highest. If we neglect the milk boiling point elevation then the flash vessel pressure is given by the following, where T_{phl} is given by equation (3.30).

$$P_{phl} = e^{\left[A_{water} - \frac{B_{water}}{T_{phl} - C_{water}}\right]}, \quad P_{vap} = e^{\left[A_{water} - \frac{B_{water}}{T_{DSI} - C_{water}}\right]}, \quad T_{phl} = \frac{2}{3}T_{DSI} + \frac{1}{3}T_{fc2} \tag{6.8}$$

We can substitute these into equation (6.6) and thereby produce an explicit equation for the required back-pressure orifice plate size. Clearly the required orifice plate size depends on the DSI temperature and the height of the holding tubes. Larger DSI unit temperatures and longer holding tubes require smaller back-pressure orifice plates.

$$\frac{\rho}{2}\left[\frac{Q_{DSI}}{C_d . A_{orif}\left(1-\beta^2\right)}\right]^2 > e^{\left[A_{water} - \frac{B_{water}}{T_{DSI} - C_{water}}\right]} - e^{\left[A_{water} - \frac{B_{water}}{T_{phl} - C_{water}}\right]} + \rho . g . h_t \tag{6.9}$$

6.2.4) Preheat Flash Vessel Level

An additional important aspect is the height of liquid above the DSI pump. The flow balance through the DSI and holding tubes produces the following equation.

$$\Delta P_{flood} + \Delta P_{pump} - \Delta P_{loss} - \Delta P_{orif} = 0 \qquad (6.10)$$

Where, ΔP_{flood}	=	hydrostatic pressure due to liquid height above DSI pump.	(Pa)
ΔP_{pump}	=	pressure gain from DSI pump.	(Pa)
ΔP_{loss}	=	pressure drop due to frictional losses in holding tubes.	(Pa)
ΔP_{orif}	=	pressure drop due to back-pressure orifice plate.	(Pa)

This shows that the pressure gain, from the DSI pump, is then lost through the holding tubes and back-pressure orifice plate. An important aspect of this is that the pump must supply enough pressure to adequately overcome the orifice plate pressure drop. Otherwise the height of liquid, above the DSI pump, will rise above the flash vessel weir and flood the vessel. It is therefore important that the orifice plate and DSI pump are correctly sized for the range of DSI temperatures. Under-sizing the orifice plate will cause flash vessel flooding, but over-sizing will cause vaporisation in the holding tubes.

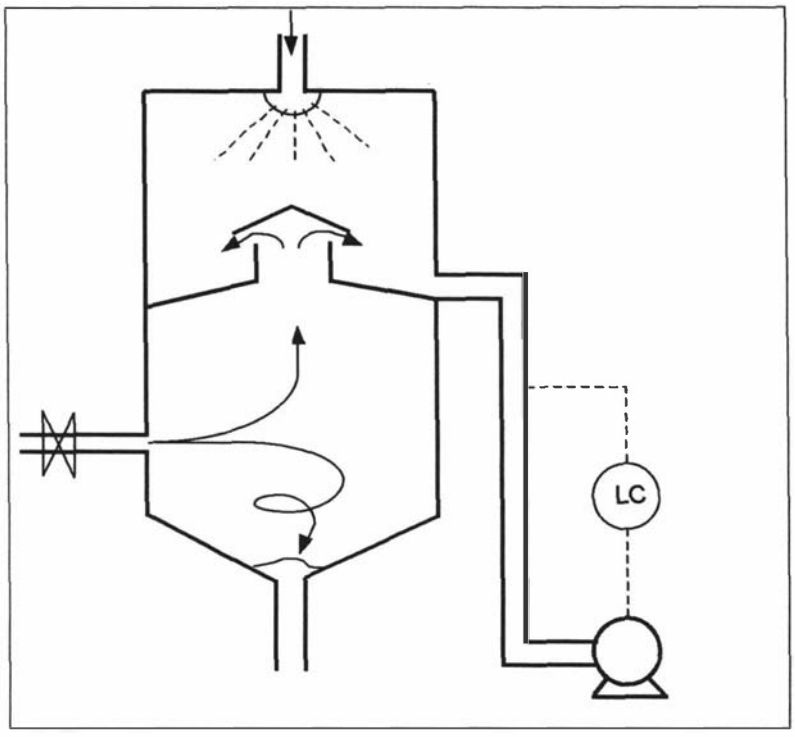

Figure 6-2 : Preheat flash vessel level control.

The level of liquid milk above the DSI feed pump must not rise above the flash vessel weir because this will cause 'flooding'. This flooding occurs when the milk level rises and flows into the bottom of the flash vessel. The result is that milk can bypass the DSI/holding tubes. In order to overcome this a level control loop can be placed around the DSI feed pump. A level sensor

measures the height of liquid above the feed pump and manipulates the pump speed. The configuration for this control loop is shown in Figure 6-2.

6.3) Energy Costs in a Powder Plant

6.3.1) Energy Costs

The evaporation of water requires energy to overcome the latent heat of vaporisation. For a large powder plant the energy required to evaporate water can be a large part of the operating costs. The cost of evaporation is given by equation (6.11). The cost of evaporation, per unit of evaporated water, (C_{unit}) is determined by dividing this by M_{tubes}.

$$C_{evap} = C_{en} W_{comp} = \frac{C_{en} W_{comp} q_{shell}}{q_{shell}} = \frac{C_{en} q_{shell}}{Eff}, \qquad Eff = \frac{q_{shell}}{W_{comp}} \tag{6.11}$$

Where, C_{evap} = total cost of evaporating water in the process. ($/s)

C_{en} = cost of energy, used to evaporate water. ($/J)

Eff = energy efficiency of the evaporation process. (-)

W_{comp} = 'driving' heat flow, or power supplied to the evaporation process. (W)

Table 6-2 : Energy Costs at Kiwi Coop Dairies, for the Evaporator A plant.

	C_{en}	C_{en} ($/MJ)	Eff (MJ/MJ)	C_{unit} ($/kg)	C_{unit} ($/Tonne)	
MVR	0.0892 ($/kWhr)	0.02303	58.65	0.00092	0.919	
TVR	15.91 ($/T)	0.00679	4.61	0.00345	3.444	
Spray Dryer	15.91 ($/T)	0.00679	0.60	0.02649	26.49	
	Feed flow (kg/hr)	Product flow (kg/hr)	Feed dry matter (kg/kg)	Product dry matter (kg/kg)	Mass flow of evaporation (kg/s)	Cost of evaporation ($/hr)
MVR	55,080	16,861	0.125	0.408	10.616	35.12
TVR	16,861	14,659	0.408	0.469	0.611	7.58
Spray Dryer	14,659	7,062	0.469	0.975	2.110	201.22

The factor Eff represents the energy efficiency of the evaporation process. For an MVR evaporator this factor is usually between 40 ~ 80, for a TVR evaporator 4 ~ 8 and for a spray dryer 0.4 ~ 0.8. However, equation (6.11) shows that the evaporation cost also depends on the energy source. For example the Evaporator A plant uses electricity to drive the MVR evaporator whereas the TVR evaporator uses steam and the spray dryer uses natural gas. At Kiwi Co-op Dairies the cost of electricity is around three times the cost of steam and this reduces the difference in the cost of evaporation, between the MVR and TVR sections.

It is unusual for a milk powder plant to use natural gas as the energy source for the spray dryer. For example the Kiwi Co-op Powder 4 and Powder 5 plants use steam as the energy source for the spray dryer, whereas the Powder 3 plant uses natural gas. As a result, we shall conduct the economic analysis with steam as the energy source for the spray dryer. Table 6-2 shows the specific costs at Kiwi (C_{unit}).

The total cost of evaporation is given by equation (6.12). The evaporation cost in each section is calculated in Table 6-2 for the static plant operating condition of Section 4.2 (i.e., $C_{mvr} = 0.92$\$/Tonne, $C_{tvr} = 3.45$\$/Tonne and $C_{dry} = 26.49$\$/Tonne). An important result shown in Table 6-2 is the high total cost of evaporation in the spray dryer. The spray dryer evaporation cost represents approximately 80 % of the total evaporation cost. This suggests that significant reductions in the total evaporation cost can be achieved by reducing the evaporation in the spray dryer.

$$TC = C_{mvr} M_{mvr} + C_{tvr} M_{tvr} + C_{dry} M_{dry} \tag{6.12}$$

Where, TC	=	total cost of evaporating water.	(\$/s)
C_{mvr}	=	cost per unit of water evaporation in MVR evaporator section.	(\$/kg)
C_{tvr}	=	cost per unit of water evaporation in TVR evaporator section.	(\$/kg)
C_{dry}	=	cost per unit of water evaporation in the spray dryer.	(\$/kg)
M_{mvr}	=	mass flow of evaporation in the MVR evaporator section.	(kg/s)
M_{tvr}	=	mass flow of evaporation in the TVR evaporator section.	(kg/s)
M_{dry}	=	mass flow of evaporation in the spray dryer.	(kg/s)

6.3.2) Simple Energy Cost Analysis

The amount of evaporation in each section affects the dry matter from that section. The following equations give the mass flow of evaporation in terms of the product dry matters. Notice that the DSI steam mass flow affects the evaporation that must occur in the MVR section.

$$w_{p5} = \frac{M_f . w_f}{\left[M_f + M_{DSI} - M_{mvr}\right]}, \qquad M_{mvr} = M_f . w_f \left[\frac{1}{w_f} - \frac{1}{w_{p5}}\right] + m_{dsi} \tag{6.13}$$

$$w_{p8} = \frac{M_f . w_f}{\left[M_f + M_{DSI} - M_{mvr} - M_{tvr}\right]}, \qquad M_{tvr} = M_f . w_f \left[\frac{1}{w_{p5}} - \frac{1}{w_{p8}}\right] \tag{6.14}$$

$$w_{dry} = \frac{M_f . w_f}{\left[M_f + m_{dsi} - M_{mvr} - M_{tvr} - M_{dry}\right]}, \qquad M_{dry} = M_f . w_f \left[\frac{1}{w_{p8}} - \frac{1}{w_{dry}}\right] \tag{6.15}$$

Where, m_{dsi} = mass flow of steam to the DSI unit. (kg/s)

w_{dry} = dry matter from the spray dryer. (kg/kg)

The above equations can be substituted into equation (6.12) to produce equation (6.16) for the total evaporation cost in terms of the concentrate dry matters. Since $C_{mvr} < C_{tvr}$ and $C_{tvr} < C_{dry}$ we know that the evaporation total cost is minimised when the dry matters w_{p5} and w_{p8} are maximised.

$$\frac{TC}{M_f.w_f} = \frac{C_{mvr}}{w_f} - \frac{C_{dry}}{w_{dry}} + \frac{C_{mvr}.m_{dst}}{M_f.w_f} + \frac{1}{w_{p5}}[C_{tvr} - C_{mvr}] + \frac{1}{w_{p8}}[C_{dry} - C_{tvr}] \qquad (6.16)$$

We are interested in how the total evaporation cost changes with respect to the concentrate dry matters w_{p5} and w_{p8}. This can be determined by differentiating equation (6.16) with respect to the dry matters to produce the following.

$$\left(\frac{\partial TC}{\partial w_{p5}}\right) = -M_f.w_f\left[\frac{C_{tvr} - C_{mvr}}{\left(w_{p5}^0\right)^2}\right], \qquad \left(\frac{\partial TC}{\partial w_{p8}}\right) = -M_f.w_f\left[\frac{C_{dry} - C_{tvr}}{\left(w_{p8}^0\right)^2}\right] \qquad (6.17)$$

Table 6-3 shows the incremental cost reductions due to a 0.01 kg/kg increase in the MVR and TVR product dry matters. These results are calculated from the earlier results listed in Table 6-1. Based on a 20-hour daily operation and 200 days operation per year, Table 6-3 shows that $ 33,032 will be saved if the TVR and MVR product dry matters are both increased by 0.01 kg/kg. If the TVR dry matter concentration could be increased by 0.05 kg/kg, then the savings would be larger. However, we will show later that this is a very difficult task.

Table 6-3 : Incremental cost savings.

Increased dry matter	Incremental Cost Reduction ($/hr)
w_{p5}	1.044
w_{p8}	7.214

6.4) Operating Constraints

6.4.1) Introduction

For the Evaporator A plant there are four important operational constraints. These are the evaporation capacities, the falling film breakdown, the evaporator temperature and the concentrate dry matter constraints. In this section we discuss these constraints and the methods which can be used to predict them.

6.4.2) Plant Capacity Constraints

Each section of the Kiwi powder plant has a maximum evaporation capacity. This constraint depends on the capacity of the driving process. For example the MVR compressor has a

maximum power constraint, the TVR compressor has a maximum steam pressure supply and the spray dryer has a maximum air flow, inlet temperature and minimum outlet air temperature.

MVR Compressor

The MVR evaporator section capacity depends on the compressor power supply (W_{compl}), the evaporating temperature (T_{el}) and the product of evaporating overall heat transfer coefficient and surface area ($U_s.A_{st}$). There are constraints on the power supply, the evaporating temperature and the available heat transfer surface area. The heat transfer coefficients and surface area are set by the milk physical properties and the plant design. These are environmental variables and they cannot be adjusted. Here we shall consider the constraint caused by the compressor power supply. Later, in Section 6.4.4, we also consider the constraint imposed by the temperature.

The maximum power supply to the MVR compressor of the Evaporator A plant is assumed to be 500 kW. This value has been determined from the operating procedures of the Evaporator A plant, since the manufacturer specifications do not give the power supply constraint. We now show how this constrains the MVR evaporator section evaporation capacity. The MVR compressor characteristic curve is given by equation (6.18). This is a quadratic that can be solved for the compressor speed (N_{comp}) in terms of the mass flow of vapour (M_{compl}), to produce equation (6.19).

$$\frac{[P_{sl}-P_{el}]}{\rho_{vel}}=a_{comp}.N_{comp}^2+b_{comp}.N_{comp}\left(\frac{M_{compl}}{\rho_{vel}}\right)+c_{comp}\left(\frac{M_{compl}^2}{\rho_{vel}^2}\right) \tag{6.18}$$

$$N_{comp}=\frac{M_{compl}}{\rho_{vel}.2.a_{comp}}\left[\sqrt{\left[b_{comp}{}^2-4.a_{comp}\left(c_{comp}-\frac{\rho_{vel}(P_{sl}-P_{el})}{M_{compl}^2}\right)\right]}-b_{comp}\right] \tag{6.19}$$

The compressor power supply is given by equation (6.20).

$$\frac{W_{compl}}{\rho_{vel}}=d_{comp}.N_{comp}^2\left(\frac{M_{compl}}{\rho_{vel}}\right)+e_{comp}.N_{comp}\left(\frac{M_{compl}^2}{\rho_{vel}^2}\right)+f_{comp}\left(\frac{M_{compl}^3}{\rho_{vel}^3}\right) \tag{6.20}$$

Substituting the compressor speed we produce equation (6.21) for the MVR compressor power supply and energy efficiency (Eff). This energy efficiency is approximately equal to the ratio of the MVR compressor power supply and the latent energy of the evaporated water vapour (i.e., $Eff=\frac{q_{shellt}}{W_{compl}}\approx\frac{q_{compl}}{W_{compl}}$). Since the mass of evaporated water is the same as the compressed mass flow (i.e., $M_{compl}=M_{flashl}+M_{tubest}$) we can use equation (6.21) to determine the evaporator capacity constraint.

$$W_{compl} = [A_1 + A_2]\frac{M_{compl}^3}{\rho_{vel}^2}, \quad Eff \approx \frac{\lambda.\rho_{vel}^2}{[A_1 + A_2]M_{compl}^2}, \quad A_1 = \left[b_{comp}.A_3 - \frac{d_{comp}.c_{comp}}{a_{comp}} + f_{comp}\right] \tag{6.21}$$

$$A_2 = \left[\frac{d_{comp}.\rho_{vel}(P_{sl} - P_{el})}{a_{comp}M_{compl}^2} - A_3\sqrt{\left[b_{comp}^2 - 4.a_{comp}\left(c_{comp} - \frac{\rho_{vel}(P_{sl} - P_{el})}{M_{compl}^2}\right)\right]}\right] \tag{6.22}$$

$$A_3 = \frac{1}{2.a_{comp}}\left(\frac{d_{comp}.b_{comp}}{a_{comp}} - e_{comp}\right) \tag{6.23}$$

Two important results can be observed from equation (6.21). Firstly the energy efficiency increases with the evaporated vapour density, which is a strong function of temperature. Therefore the efficiency and hence evaporation capacity increases at higher temperature. Secondly the energy efficiency reduces as the mass flow of compressed vapour increases. This second point has important consequences for the evaporation cost, which depends on the power supply used by the compressor.

Using the steady state model developed in Chapter 4, we can determine the MVR evaporator section capacity, in terms of its temperature. Figure 6-3 shows the MVR evaporation capacity vs the evaporator temperature, as calculated from the steady state model. The steady state model was rearranged so that the compressor power supply (W_{compl}) was an input and we have set this to 500 kW. Normally the MVR compressor speed (N_{compl}) is taken as the compressor input, but by rearranging the model we can consider the power capacity constraint more easily. The other model inputs, except for the plate heat exchanger condensate flow, were the same as those used in Chapter 4 (i.e., $P_{sp} = 5\,\text{bar}$, $M_f = 15.3\,\text{kg/s}$, $w_f = 0.125\,\text{kg/kg}$, $T_f = 12\,°\text{C}$, $m_{dsi} = 0.4\,\text{kg/s}$, $M_{vac} = 5\,\text{kg/s}$ and $T_{vacl} = 24\,°\text{C}$). The model was rearranged so that the MVR evaporator temperature (T_{el}) was an input, rather than the mass flow of condensate to the plate heat exchanger. Figure 6-3 clearly shows the increase in the MVR evaporator capacity with temperature.

TVR Compressor

The TVR evaporator section capacity depends on the TVR steam pressure set-point (P_{sp}). This pressure affects the mass flow of raw steam (m_{steam}), which affects the total mass of evaporation. However, the maximum raw steam pressure is 10 bar and this provides a constraint on the evaporation capacity. Figure 6-4 shows some historical data from the Evaporator A plant. The mass flow of evaporation in the TVR evaporator section is plotted vs the TVR compressor steam pressure. This clearly shows the relationship between these variables and furthermore that the maximum evaporation capacity is approximately 0.8 kg/s.

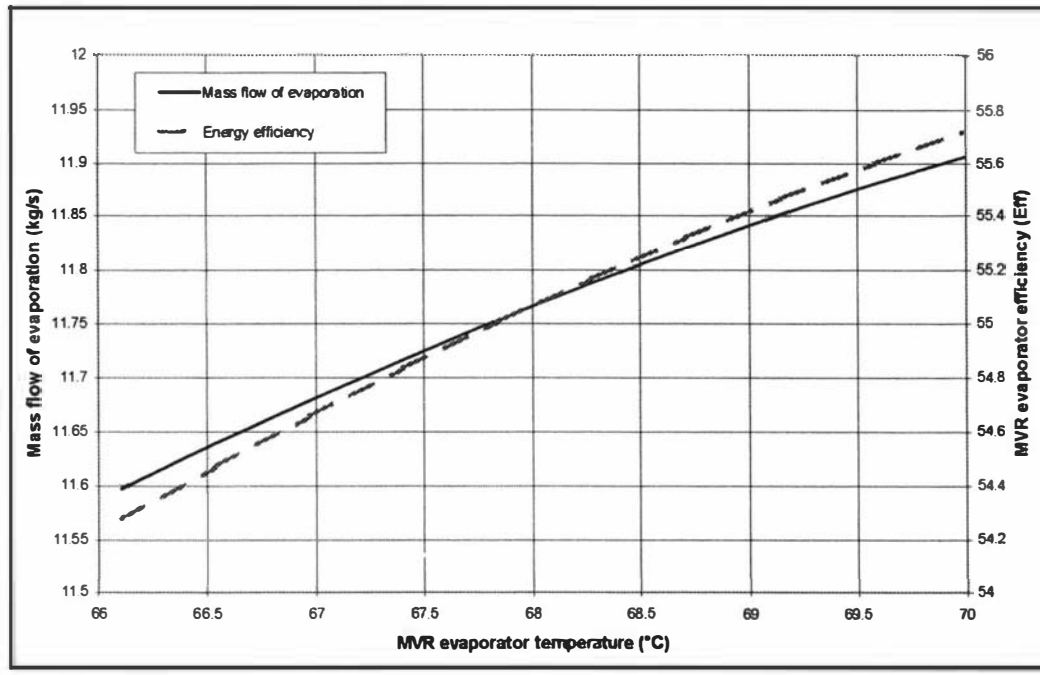

Figure 6-3 : Mass of compressed vapour vs MVR compressor evaporating temperature.

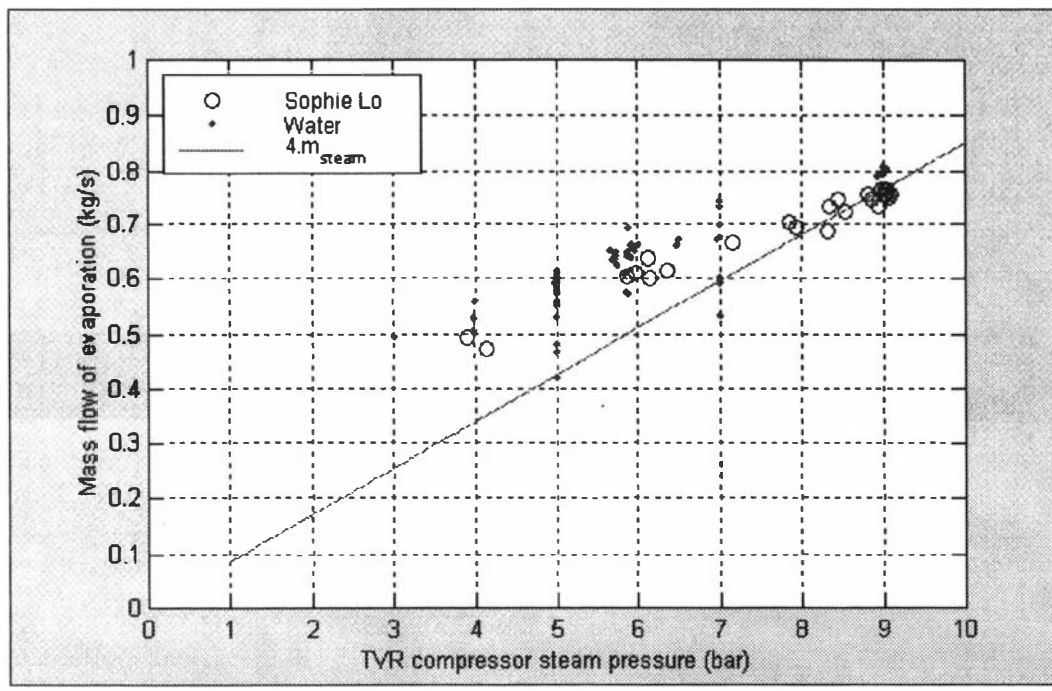

Figure 6-4 : Historical mass flow of evaporation vs TVR steam pressure.

It is common practice for a TVR compressor to be designed with a mass flow of compressed vapour (m_{comp2}) that is approximately twice the flow of raw steam ($m_{comp2} \approx 2.m_{steam}$). The mass flow of evaporation in the second effect is approximately equal to the mass flow of raw steam and compressed vapour (i.e., $M_{tubes6} \approx m_{stream} + m_{comp2}$). Also the TVR evaporator section contains an additional effect, where the total evaporation in both passes is approximately the

same as the TVR compressor steam flow (i.e., $M_{tubes7}+M_{tubes8}\approx m_{steam}$). Consequently every unit mass flow of steam causes approximately four units of evaporation (i.e., $M_{tubes6}+M_{tubes7}+M_{tubes8}\approx 4.m_{steam}=4.A_{TVR}.P_{sp}$). Figure 6-4 also shows that the mass flow of evaporation, as given by this simple rule, is consistent with the historical data from the Evaporator A plant. However, it should be remembered that this simplification is only an indication of the TVR evaporator section capacity and the complete model should be used for accurate calculations.

Spray Dryer Evaporation Capacity

The mass flow of evaporation in the spray dryer is given by equation (6.24). This is derived by making an energy balance around the spray dryer with the assumptions of constant latent heat, heat capacity and no energy losses.

$$M_{evap}=\frac{M_{air}.C_{p.air}}{\lambda}[T_{in}-T_{out}] \qquad (6.24)$$

Where, M_{air}	=	mass flow of air to the spray dryer.	(kg/s)
$C_{p.air}$	=	heat capacity of air in spray dryer.	(J/kg.K)
λ	=	latent energy of water vaporisation.	(J/kg)
T_{in}	=	air inlet temperature to the spray dryer.	(°C)
T_{out}	=	air outlet temperature from the spray dyer.	(°C)

There are some constraints on the operation of the spray dryer. The air flow to the spray dryer is restricted by the fan capacity. Also the inlet and outlet air temperatures have important restrictions. With industrial spray dryers the inlet air is heated using steam condensers or gas burners. At Kiwi Co-op Dairies the Powder 3 plant, which uses the Evaporator A plant to produce milk concentrate, uses natural gas to heat the inlet air. The air heater has a maximum capacity, which acts as a constraint on the inlet air temperature. However, it is also found that high air inlet temperatures cause solubility problems with the resulting milk powder (Nielsen *et al*, 1996; Fergusson, 1989). This is due to the burning of the milk concentrate while it is in the spray dryer.

The spray dryer therefore has a maximum evaporation capacity. For the Powder 3 plant at Kiwi the mass flow of air is approximately 41.36 kg/s, the hot inlet air temperature is 200 °C and the outlet temperature 60 °C. These produce an evaporation capacity of 2.475 kg/s, when the heat capacity is 1 kJ/kg.°C and the latent heat is 2,340 kJ/kg.

The constraint on the spray dryer evaporation capacity in turn causes a constraint on the TVR product mass flow. Commercial standards require the moisture content of milk powders to be below a minimum of approximately 3 %. Later we show that the TVR product dry matter (w_p) is also constrained. The combination of the milk powder moisture, the TVR product dry matter and spry dryer evaporation constraints then causes a constraint on the TVR product mass flow

(M_{p8}). If we make a mass balance around the spray dryer we produce equation (6.25), which describes this constraint.

$$M_{p8} \leq \frac{\overline{M}_{spray}}{\left[1-\frac{\overline{w}_{p8}}{w_d}\right]}, \qquad M_d \leq \frac{\overline{M}_{spray}}{\left[\frac{w_d}{\overline{w}_{p8}}-1\right]} \tag{6.25}$$

Where, $\overline{M}_{spray}$	=	maximum spray dryer evaporation capacity.	(kg/s)
M_{p8}	=	mass flow from the TVR evaporator section.	(kg/s)
$\overline{w}_{p8}$	=	maximum TVR product concentrate dry matter.	(kg/kg)
w_d	=	minimum dry matter content of milk powder.	(kg/kg)
M_d	=	mass flow of powder produced.	(kg/s)

Later we shall show that the TVR product dry matter constraint for Whole Milk is 0.48 kg/kg. With the powder moisture constraint of 3 % and spray dryer evaporation capacity of 2.475 kg/s, this produces a maximum TVR product mass flow of 4.9 kg/s, or 17,888 kg/hr.

A final important result is the energy efficiency for the spray dryer. This can be determined by using equation (6.24) and the definition for the energy efficiency to produce equation (6.26). Using the typical operating temperatures from above we can determine that the energy efficiency is approximately 0.78. This is considerably lower than that for the evaporators and this explains the high cost of evaporation in the spray dryer.

$$Eff = \frac{\left[T_{in} - T_{out}\right]}{\left[T_{in} - T_{amb}\right]} \tag{6.26}$$

Where, Eff	=	energy efficiency of the spray dryer.	(-)
T_{in}	=	hot air inlet temperature, to the spray dryer.	(°C)
T_{out}	=	hot air outlet temperature, from the spray dryer.	(°C)
T_{amb}	=	ambient air temperature, before entering the spray dryer.	(°C)

6.4.3) Film Breakdown Constraint

Film breakdown occurs when a falling film no longer completely covers the surface it flows on. When this happens the liquid flows as rivulets, rather than completely covering the surface. With industrial falling film evaporators it is commonly found that film breakdown causes fouling. This seems to be because regions of low velocity milk become over-concentrated and burn onto the surface. The presence of burnt dry matter then makes the surface more difficult to wet and so more film breakdown occurs. Consequently, it is important that no film breakdown occurs, otherwise a very serious fouling problem can result. Therefore this acts as an operating constraint on the evaporator.

For cylindrical tubes, falling film breakdown occurs when the tube diameter is large, or the liquid mass flow is small. The requirement for both of these parameters is given by the falling film liquid loading (Γ), which is the ratio of the falling film mass flow to the wetted surface perimeter. For cylindrical tubes, this is given by $\Gamma = \frac{M}{\pi . d}$, where d is the tube diameter and M is the falling film mass flow. The liquid loading required for adequate wetting of an isothermal surface can be determined from the following model of Hartley and Murgatroyd (1964). This equation is derived and discussed in Appendix C along with some simple extensions to it.

$$\Gamma_{min} = \frac{1}{3}(15)^{\frac{3}{5}}\left[\frac{\rho.\mu}{g}\right]^{\frac{1}{5}}[\sigma(1-\cos(\theta))]^{\frac{3}{5}} \qquad (6.27)$$

Where, Γ_{min}	=	minimum liquid loading required for a stable falling film.	(kg/m.s)
μ	=	Newtonian viscosity.	(kg/m.s)
ρ	=	density.	(kg/m^3)
σ	=	surface tension.	(kg/m^3)
θ	=	contact angle of liquid with surface.	(rad)

The properties of the milk solution (e.g., μ, ρ, σ etc) depend on the dry matter concentration. This means that the minimum liquid loading also depends on the milk dry matter. In Appendix A models for the milk density and viscosity are discussed. In addition the milk surface tension and contact angles also depend on the milk dry matter. Some important work has been done determining these for milk solutions (Paramalingam, *et al*, 1999). These physical property equations, along with the contact angles and surface tensions of Appendix C, allow the minimum liquid loading to be calculated. However, the calculations are relatively complex and we instead use a simple polynomial function for the minimum liquid loading in terms of the milk dry matters. In Appendix C the following polynomial function is determined from literature data for the minimum liquid loading of a Skim Milk solution.

$$\Gamma_{min} = 0.04356 + 0.0344w + 0.4520w^2 \qquad (6.28)$$

Where, Γ_{min} (kg/m.s)	=	minimum falling film liquid loading for complete tube wetting.	
w	=	milk dry matter concentration.	(kg/kg)

6.4.4) Evaporator Temperature Constraint

The MVR evaporator capacity increases at higher temperatures. This was explained earlier with reference to the MVR compressor curves. However, there are also many evaporator operational problems at higher temperatures. Milk solutions tend to foul at higher temperatures and whey protein denaturation is also more likely to occur. Kessler (1987) has investigated the impact of temperature on evaporator fouling. Working with whey solutions, which are likely to have high fouling rates, the amount of fouling deposit was shown to increase with temperature. Both the deposits of protein and mineral salts were found to increase with temperature, although the milk

pH also had a significant impact on the relative amount of fouling by each type. Figure 6-5 shows the specific fouling rates determined from their work.

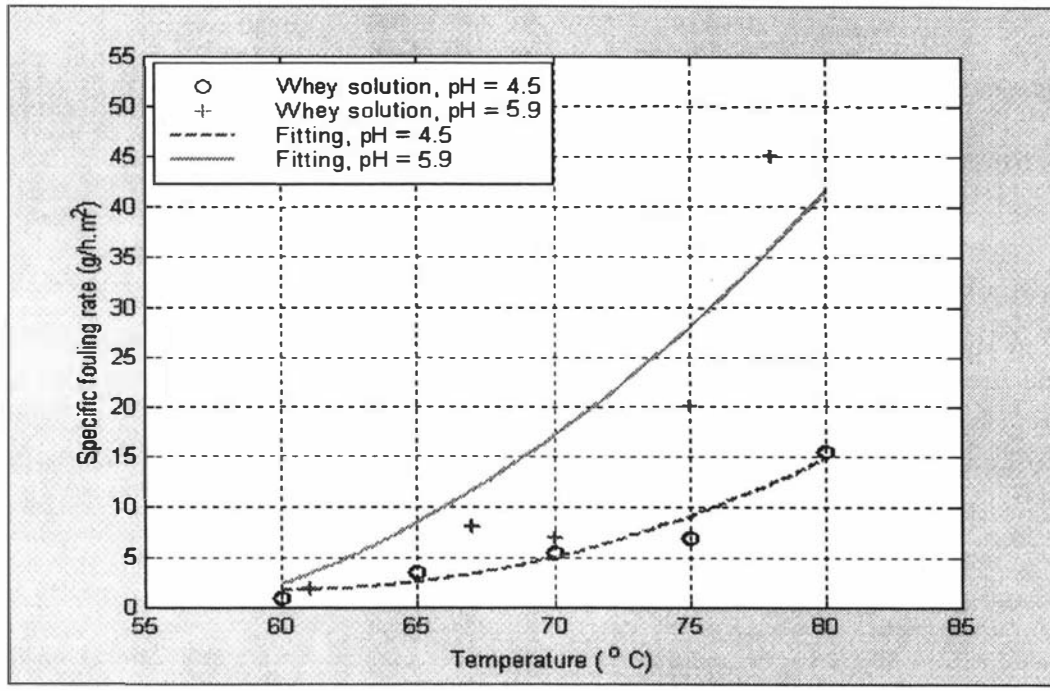

Figure 6-5 : Specific fouling rate vs evaporating temperature (Kessler, 1987) .

These results suggest that there is an optimum evaporator temperature. At low temperatures the evaporator efficiency is low but at higher temperatures the fouling becomes significant. We can model the compressor efficiency curve, but the evaporator fouling is difficult to model. Consequently, we can only determine some simple rules for the optimum evaporating temperature. At temperatures above 70 °C the fouling appears to become very serious and so the evaporator should not be run above this temperature. The fouling begins to approach zero at approximately 60 °C and the closer we operate to this temperature the less fouling should occur. Other literature sources (Fergusson, 1989) suggest that the maximum evaporation temperature is 70 °C for low milk concentrations and 58 – 60 °C for high milk concentrations. These maximum temperatures were stated with reference to a MVR/TVR evaporator plant. The low concentrations referred to the MVR evaporator section, whereas the high concentrations relate to the TVR evaporator section.

6.4.5) Concentrate Dry Matter Constraint

The milk powder quality produced from a spray dryer depends on the dry matter concentration of the spray dryer feed. Many of the milk properties have been shown to impact on the product milk powder (Chen, 1996; Neilsen *et al*, 1996; Fergusson, 1989). However, the concentrate viscosity is very strongly dependent on the dry matter concentration and so this physical property probably has the dominant impact. High viscosity milk concentrates seem to have several detrimental impacts on the operation of the spray dryer. Firstly the spray particles from the spray dryer nozzles are larger, which causes larger powder particle sizes. Secondly the spray particle evaporation mass transfer and heat transfer coefficients are low. These lower mass and heat

coefficients cause the spray particle temperatures to be higher. Overheating of the spray dryer particles then appears to cause the product milk powder to be burnt.

Middleton (1996) states that the maximum viscosity for 'good' atomisation is 100 cP. In reality this is an upper band on the viscosity to the spray dryer. Industrial plants always operate with considerably lower viscosities. Typically a viscosity of between 30 and 70 cP is used. This viscosity range can be related to a dry matter range by using Eiler's equation, from Appendix A. However, this equation is unlikely to be accurate and furthermore it does not include the non-Newtonian or age thickening nature of the milk. Milk concentrates tend to exhibit 'age thickening', where their viscosity increases as they are held. In order to overcome this problem and also to reduce the fat-globule sizes homogenisers are used. These are large variable speed positive displacement pumps, which pressurise the milk entering the spray dryer. The homogeniser operates at very high shear stresses and so the actual milk viscosity is likely to be 'shear thinned'. It is therefore difficult to determine the viscosity of the milk entering the spray dryer. There is likely to be age thickening of the milk and this increases the viscosity above that given by Eilers equation. However, the homogeniser should overcome some of this increased viscosity and provide some thinning of the milk.

Another complicating factor is the impact of the DSI preheat section conditions. In Appendix A it is shown that the specific volumes of the de-natured and natural whey proteins are significantly different. As a result the degree of whey protein de-naturation has an impact on the TVR product viscosity. The DSI preheat conditions determine the amount of whey de-naturation and consequently these have been shown to effect the viscosity (Snoeren *et al*, 1982).

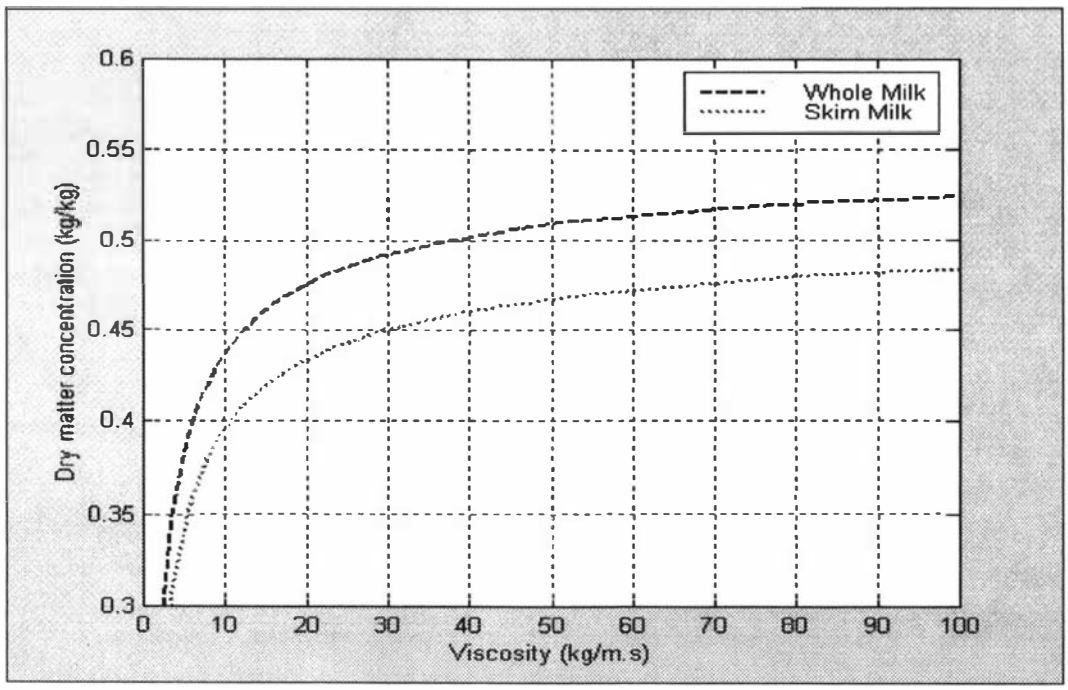

Figure 6-6 : Concentrate dry matter vs concentrate viscosity, as determined from Eilers equation.

Figure 6-6 shows the dry matter of Skim and Whole Milk, in terms of viscosity, as given by Eiler's equation. These results were calculated for a temperature of 55 °C. We can use this, with

the viscosity range of 30-70 cP, to determine the maximum dry matters from the TVR evaporator section. The dry matter range for Skim Milk is 0.45-0.475 kg/kg and for Whole Milk it is 0.49-0.52 kg/kg. However, we need to have a degree of safety to account for the potential increases in viscosity. Age thickening and preheat conditions are both likely to increase the viscosity above that given by Eiler's equations. As a result, we will have a safety margin in our dry matters of 0.04 kg/kg. This produces a critical product dry matter of 0.48 kg/kg for Whole Milk and 0.435 kg/kg for Skim Milk.

6.5) Optimum Operating Regime

6.5.1) Introduction

Here we shall consider the constrained minimisation of the plant evaporation costs. The aim is to determine the plant operating set-points that minimise the evaporation costs, whilst avoiding the process capacity, film wetting, temperature and product dry matter constraints. Therefore the six process set-points (i.e., M_f, T_{e1}, P_{sp}, N_{comp}, T_{e3} and T_{DSI}) are independent variables and we use the steady state model to determine their optimum conditions. However, a number of these set-points are constrained and they must be considered as environmental variables. For example the DSI unit temperature is determined by the degree of whey protein de-naturation that is required. Before considering the complete optimisation we consider the constraints on these set-points and thereby show that only the TVR steam pressure (P_{sp}) and the feed mass flow (or alternatively the TVR product mass flow) are truly independent.

The steady state model considered in Chapter 4 has a set of inputs (i.e., M_f, w_f, T_f, M_c, P_{sp}, m_{dsi}, N_{comp}, M_{vac} and T_{vac1}) and these determine the plant operating regime. For the process optimisation studies it is, however, advantageous to rearrange the model so that the process set-points are inputs, rather than the process manipulated variables. Therefore the model we use here includes the set-points as inputs. The only exceptions are the MVR compressor speed and the evaporator feed flow. The MVR compressor speed will be chosen so that the model produces the maximum product dry matter concentration. It is also easier to consider the TVR product mass flow as an input, rather than the evaporator feed flow, because there is a direct constraint on the product mass flow. Therefore the steady state model contains the inputs M_{p8}, P_{sp}, T_{e1}, T_{DSI}, T_{e3}, w_f, w_{p8}, T_f and T_{vac1}.

6.5.2) Environmental Process Variables

A number of the steady state model inputs can be considered as environmental variables, which will remain constant. Some of these variables are 'raw inputs' into the plant, such as the feed milk dry matter (w_f) and the cooling water inlet temperature (T_{vac1}). However, others are determined by simple optimum process conditions. Specifically the DSI unit temperature (T_{DSI}), the MVR evaporator temperature (T_{e1}), the third effect temperature (T_{e3}) and the TVR product dry matter (w_{p8}).

Feed milk dry matter
The feed milk dry matter for a given milk solution is an environmental variable. There will be variations in the feed dry matter and these can act as disturbances to the plant. However, the static feed dry matter is constant. For example, at Kiwi Co-op Dairies the feed dry matter of Whole Milk solution is approximately 0.125 kg/kg.

Cooling water temperature
The cooling water used in the vacuum condenser has an inlet temperature, which is an environmental variable. This cooling water will also vary and thereby provide disturbances to the plant. The water is supplied from the Kiwi Co-op Dairies Co-generation plant and it is approximately 24 °C.

DSI unit temperature
The DSI unit temperature has a large impact on many of the product milk powder properties. Two of the most important are the WPNI (Whey Protein Nitrogen Index) and the SI (solubility index). The controlled de-naturation of whey proteins is one of the primary purposes of the DSI preheat section. In addition the state of the proteins has a strong impact on the TVR product viscosity and this impacts on the resulting milk powder SI.

The milk whey proteins react when heated at temperatures above approximately 60 °C. These reactions are called de-naturation reactions because they change the natural state of the proteins. The reactions have been analysed relatively thoroughly (Dannerberg and Kessler, 1988; Gotham *et al*, 1992; Georgiadis *et al*, 1998). As a result it is possible to relate the amount of whey protein de-naturation to the temperature and holding tube time of the DSI preheat section. Using the whey protein reaction kinetics and given the holding tube residence time, we can determine the DSI unit temperature that is required to produce the specified WPNI.

MVR evaporator temperature
Earlier, in Section 6.3, we discussed the impact of the MVR evaporator temperature on the compressor energy efficiency and the fouling in the evaporator. It was shown that the maximum temperature for the MVR evaporator section was 70 °C and for the TVR section it was 60 °C. We will use a small safety margin of 2 °C for the MVR evaporator temperature, so a temperature of 68 °C will be used instead.

TVR final effect temperature
The TVR final effect temperature is the low pressure point for the entire Evaporator A plant. It is important that this vacuum is maintained, because milk must not be evaporated at temperatures above those that cause fouling or whey protein de-naturation. In the TVR evaporator section the second effect temperature (T_{e2}) depends on the final effect temperature. The final effect temperature must be low enough so that the second effect stays below 60 °C.

Milk solutions usually contain non-condensable gases, which will be removed during the evaporation process. In the vapour re-compression process these gases are passed to the evaporator shells, where they can significantly reduce the condensation heat transfer coefficients. This reduces the evaporating overall heat transfer coefficients and thereby reduces the evaporator capacity. As a result, it is important that the non-condensable gases are removed. This is done

using de-aeration lines, which pass the gases to the vacuum condenser. Vacuum pumps attached to the vacuum condenser then remove the gases from the condenser.

At lower final effect temperatures the possibility of fouling, protein de-naturation is reduced and non-condensable gas removal is increased. However, larger amounts of cooling water are required and the viscosity of milk solutions also increase. Generally it is considered to be difficult to maintain final effect temperatures lower than 45 °C (Trinh, 1996; Kessler. 1981). As a result, there is an optimum final effect temperature. Higher temperatures require less cooling water, but they cause whey protein de-naturation, fouling and de-aeration problems. At Kiwi Co-op Dairies, the Evaporator A plant is generally operated with a final effect temperature of 55 °C. We shall use this temperature as the set-point for the final effect temperature control loop.

TVR product dry matter

There is a very strong impact of the TVR product dry matter on the properties of the milk powder. For Whole Milk we will set the maximum product dry matter at 0.48 kg/kg and for Skim Milk at 0.43 kg/kg.

6.5.3) Film Wetting Constraint and Safety Margin

We are interested in the margins between the evaporator mass flows and the minimum required for stable falling films. Fouling will occur if this margin falls below zero. We will define the overall plant 'safety margin' as the smallest margin for the operating conditions. Strictly, each pass has a safety margin, but many of the passes will have large safety margins. Consequently, only the pass with the smallest margin is going to foul and so we are most concerned with it.

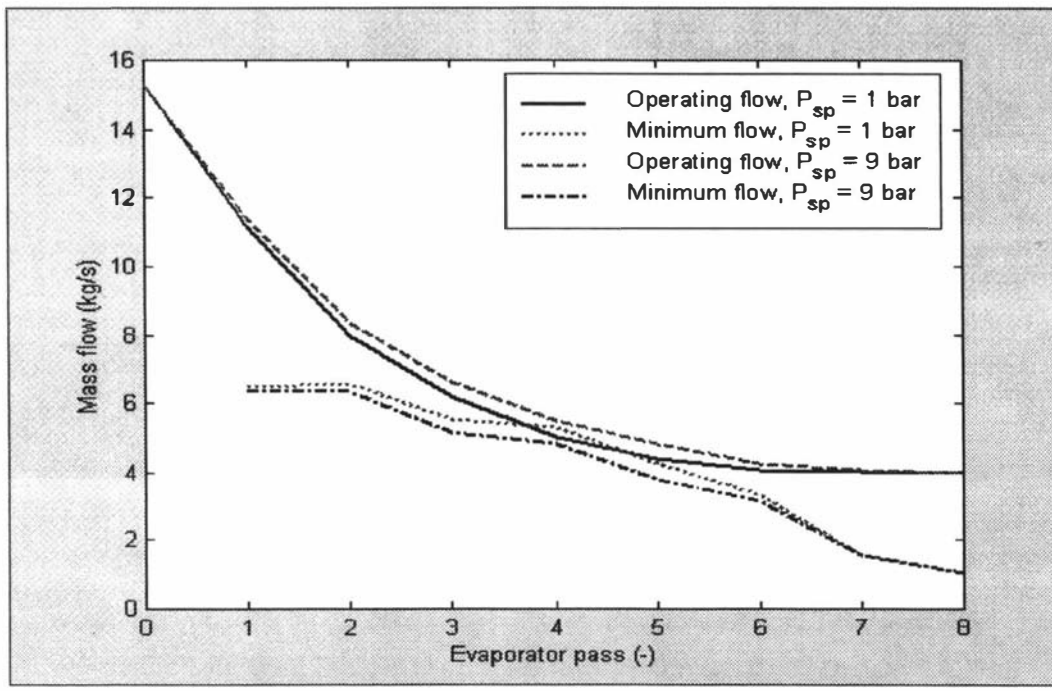

Figure 6-7 : Operating and minimum plant mass flows.

Here we consider a simple example and show how the steady state model is used to determine the plant safety margin. The steady state model, with a set of inputs (i.e., $M_{p8} = 4$ kg/s,

$w_f = 0.125\,\text{kg/kg}$, $T_f = 12°\text{C}$, $T_{vac1} = 24°\text{C}$, $w_{p8} = 0.48\,\text{kg/kg}$, $T_{DSI} = 115°\text{C}$, $T_{e3} = 55°\text{C}$ and $T_{e1} = 68°\text{C}$), can be used to calculate the operating conditions. The TVR steam pressure is also an input and we will consider two values of this variable (i.e., $P_{sp} = 1$ bar and 9 bar). Figure 6-7 shows the resulting plant mass flows and minimum mass flows required for adequate film wetting. At low TVR steam pressures the operating flow profile is low and the minimum flow profile high. This is because the MVR evaporator section must do more evaporation to produce the required TVR product mass flow. Figure 6-8 shows the calculated margins for the situation shown in Figure 6-7. Clearly the fourth pass has the smallest margin and is the most susceptible to fouling.

Until such time as the predictions of both the flow and minimum liquid loadings can be more accurately predicted, a safety margin in the region of 0.5 kg/s is recommended. The minimum liquid loading predictions could be improved through a better understanding of the physical properties of individual milk solutions. Equation (6.27) shows that the contact angle and surface tension have the most impact on the minimum flow. However, it appears that the surface tension does not vary greatly with dry matter, whereas the viscosity does (Paramalingam *et al*, 1999). Therefore the contact angle has the greatest impact on the minimum flow. As a result, accurate determination of the contact angle is required before the minimum flow can be predicted with great precision. Similarly more confidence in the flow predictions would be gained if accurate knowledge of the relationship between the heat transfer coefficients of individual milk solutions and dry matter concentration was known.

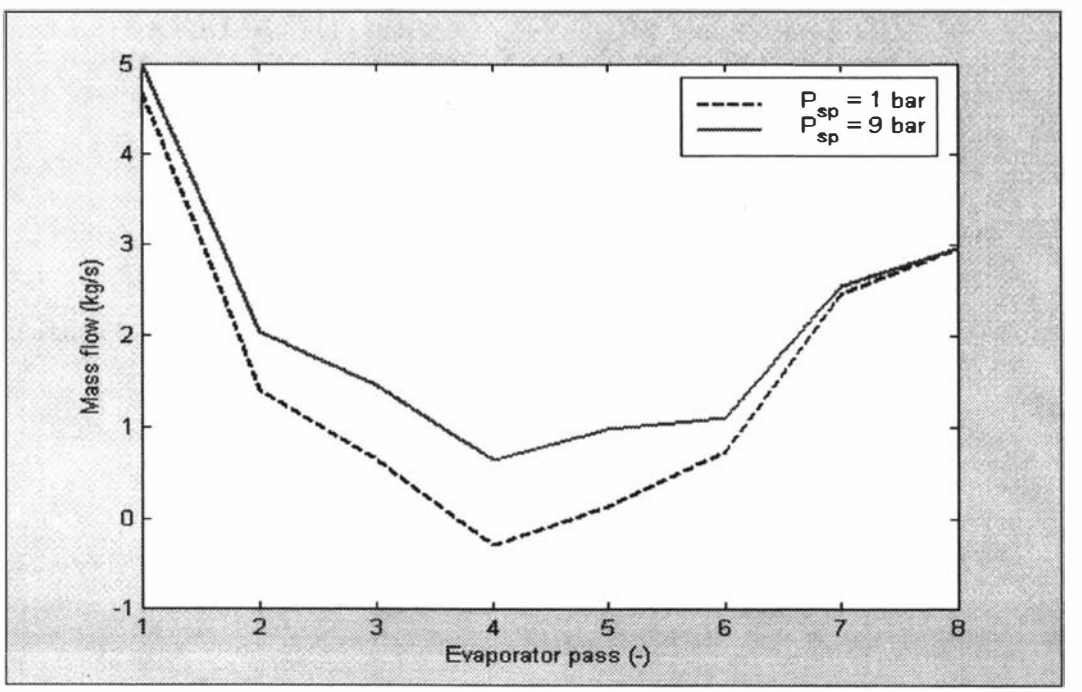

Figure 6-8 : Margins between the operating and minimum mass flows.

6.5.4) The Optimum Operating Regime

The steady state model has inputs (i.e., M_{p8}, w_f, T_f, w_{p8}, T_{DSI}, T_{e3}, T_{e1}, T_{vac1} and P_{sp}) and outputs (i.e., M_f, N_{comp}, M_c, m_{dsi} and M_{vac}). Only the TVR steam pressure (P_{sp}) and the TVR product mass flow (M_{p8}) are 'free' inputs. The other model inputs have all been set as environmental variables and these cannot be manipulated. The aim of the optimisation is therefore to determine the values for P_{sp} and M_{p8} that minimise the evaporator energy costs. Once these variables are known, the steady state model provides the evaporator feed flow (M_f) and MVR compressor speed (N_{comp}). It should, however, be remembered that some of the environment variables may actually be manipulated. Specifically, the feed dry matter (w_f) may be reduced by diluting the milk and the MVR evaporator temperature (T_{e1}) may be increased above the fouling constraint.

The optimisation proceeds in two steps :

1) Determine the plant operating constraints.

Using the steady state model the plant operating constraints are calculated. The constraints determine the allowed values of P_{sp} and M_{p8}. There are four constraints (i.e., MVR compressor power, film wetting, TVR product mass flow and TVR compressor steam supply).

2) Determine the optimum operating conditions.

Once we have determined the allowed input ranges, it is then a simple task to determine the inputs that minimise the energy costs. Since the energy costs increase with the product mass flow, the objective function uses the total evaporation cost divided by the product mass flow (i.e., $J = \frac{TC'}{M_{p8}}$, with J as the objective function and TC is the total evaporation cost). Once the optimum has been determined, then we simply use the steady state model to determine the feed mass flow and MVR compressor speed.

Whole Milk

We will now investigate the Evaporator A plant operation with Whole Milk. Typically, Whole Milk powder must have a moisture content less than 3 % and at Kiwi Co-op Dairies the feed dry matter is between 0.12 – 0.125 kg/kg. For Whole Milk the critical TVR product dry matter is approximately 0.48 kg/kg. With a spray dryer evaporative capacity of 2.475 kg/s, this means the maximum TVR product mass flow is 4.9 kg/s.

Taking the set of environment inputs ($w_f = 0.125$kg/kg, $w_{p8} = 0.48$kg/kg, $T_f = 12\,^{\circ}$C, $T_{DSI} = 115\,^{\circ}$C, $T_{vac1} = 24\,^{\circ}$C, $T_{e3} = 55\,^{\circ}$C and $T_{e1} = 68\,^{\circ}$C), we can calculate the plant operating conditions for a range of TVR steam pressures and product mass flows. Then with a film break-up safety margin of 0.5 kg/s and an MVR compressor power capacity of 500 kW, we can determine the operating constraints. The shaded triangle in Figure 6-9 shows the resulting range of allowed TVR steam pressures and product mass flows.

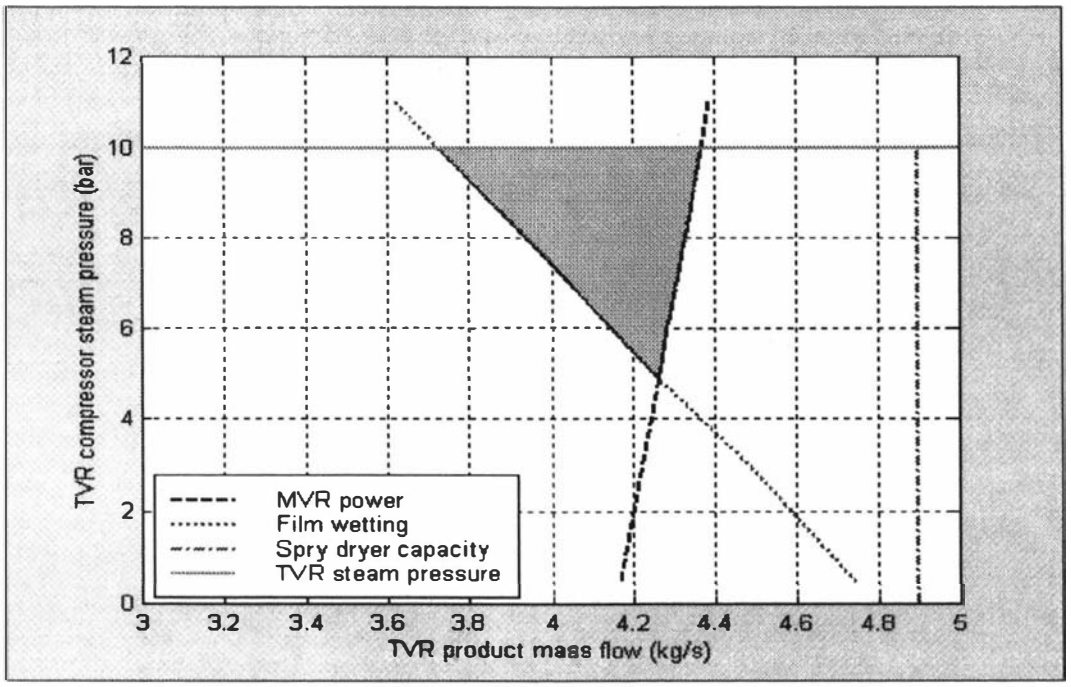

Figure 6-9 : Evaporator A plant operating constraints.

We are now interested in determining the plant energy costs. In Table 6-2 the specific energy costs where determined. Using the steady state model we can calculate the MVR power supply and the TVR steam mass flow. Then with the specific energy costs we can determine the total evaporation cost. Figure 6-10 shows a contour plot of the evaporation costs vs the TVR steam pressure and TVR product mass flow.

We determined earlier that the evaporation cost in the MVR evaporator section is lower than the TVR evaporation section. This is shown by the specific energy costs in Table 6-2. The cost of evaporation in the MVR evaporator is approximately 0.919 \$/Tonne of water evaporation, which is lower than the 3.44 \$/Tonne in the TVR evaporator. As a result we expect the total evaporation cost to reduce when the TVR steam pressure is reduced. In addition, we also showed earlier that the MVR evaporator energy efficiency reduces when it evaporates more water. Equation (6.21) shows that the MVR compressor efficiency (Eff) is lower when the flow of vapour (M_{compl}) is larger. As a result, we expect the evaporation costs to increase when the MVR evaporator is doing more evaporation, which with a specified feed and product dry matter concentration will occur with increases in the product mass flow.

Figure 6-10 shows that the evaporation cost increases with increases in TVR steam pressure and product mass flows. The minimum evaporating cost occurs at a TVR steam pressure of 9 bar and a TVR product mass flow of 3.83 kg/s. This represents an evaporating cost of just under 2.99 \$/Tonne of concentrate milk produced. It is interesting to compare this with the evaporation cost when the film safety margin is maximised. If we operate with the maximum TVR steam pressure and TVR product mass flow of 10 bar and 4.38 kg/s respectively, then we have a safety margin of 1.1 kg/s and an evaporation cost of 3.40 \$/Tonne. These are the operating conditions that the Evaporator A plant is usually run at. However, it increases the evaporation cost, while the improved safety margin may not be required.

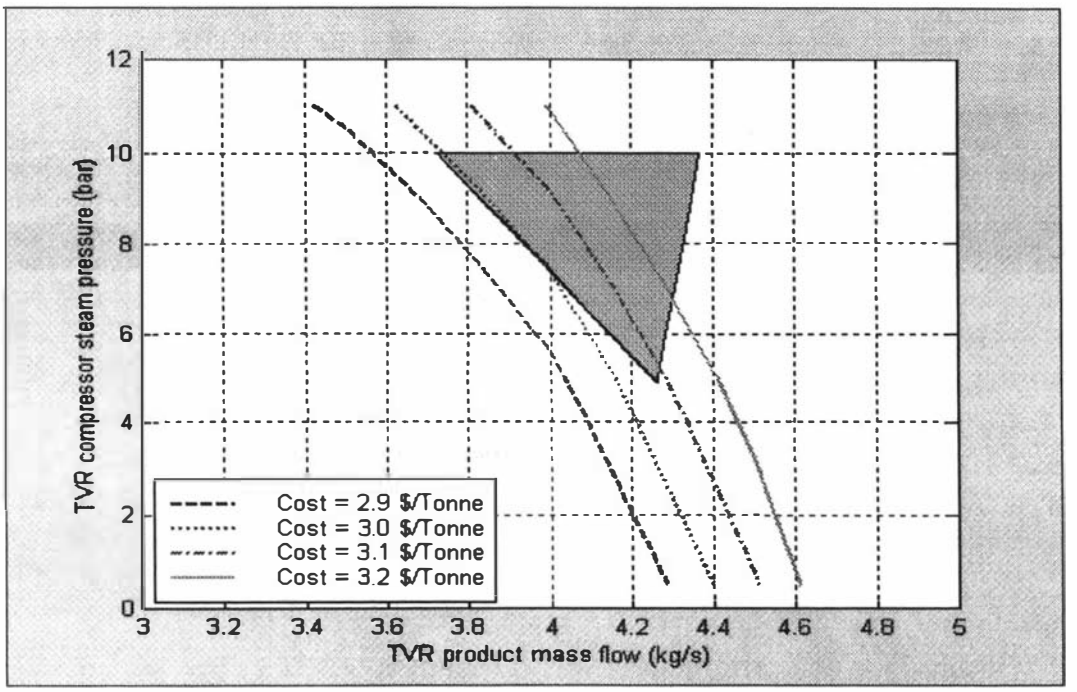

Figure 6-10 : Evaporation costs vs TVR steam pressure and product mass flow.

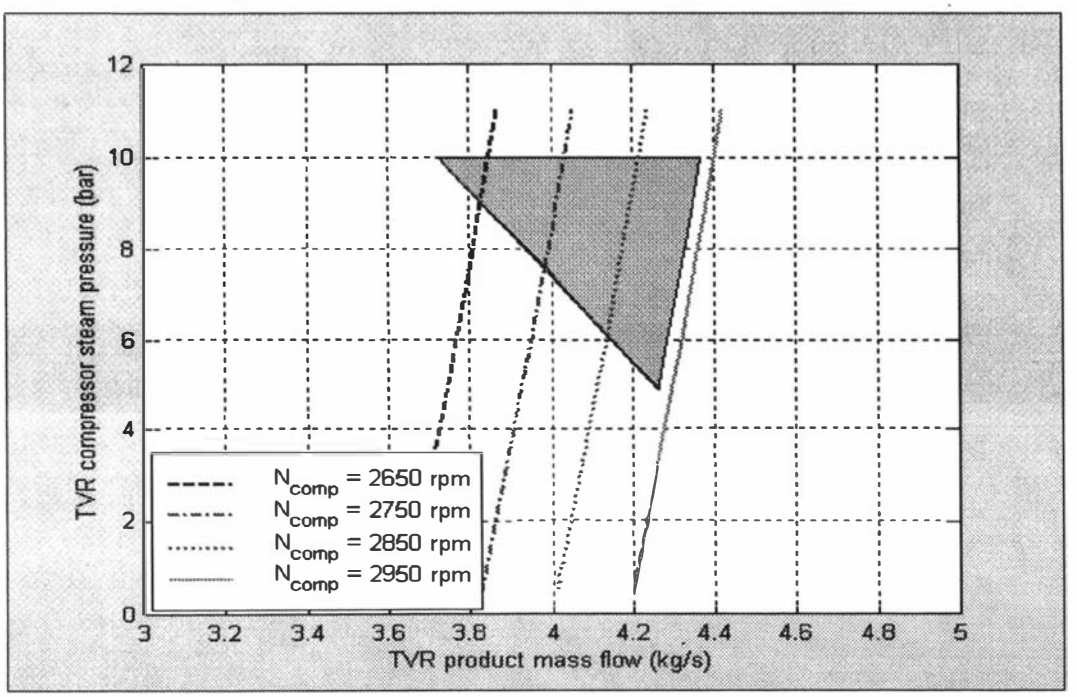

Figure 6-11 : MVR compressor speed, in terms of TVR product mass flow and TVR steam pressure.

The evaporator feed flow can be determined from the following mass balance, since the TVR product mass flow, TVR product dry matter and feed dry matter have been specified. With the

optimum operating conditions (i.e., $M_{p8} = 3.83$ kg/s, $w_{p8} = 0.48$ kg/kg and $w_f = 0.125$ kg/kg) we can determine the optimum feed flow (i.e., $M_f = 14.71$ kg/s).

$$M_f = \frac{M_{p8}.w_{p8}}{w_f} \tag{6.29}$$

The MVR compressor speed is calculated from the steady state model and is shown, in terms of the TVR product mass flow and steam pressure, by Figure 6-11. With the optimum operating conditions (i.e., $M_{p8} = 3.83$ kg/s and $P_{sp} = 9$ bar), we can determine the optimum MVR compressor speed (i.e., $N_{comp} = 2650$ rpm).

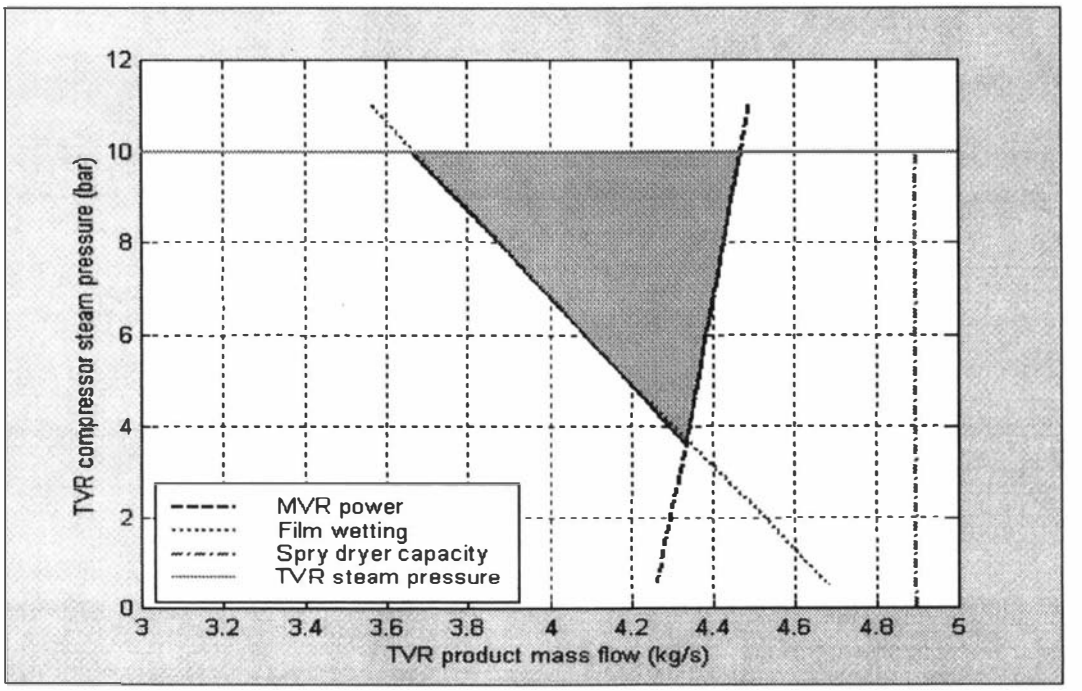

Figure 6-12 : Operating constraints for MVR evaporator plant at 70 °C.

MVR evaporating temperature

Earlier we showed that the MVR evaporating temperature has a strong impact on the compressor efficiency. Strictly there will be an optimum temperature but we cannot determine this since we do not have accurate fouling models. Here we will briefly investigate the impact of the MVR evaporating temperature on the optimisation problem. The first step is to determine the operating constraints. We start with the same inputs as from above, except the MVR evaporator temperature is now 70 °C (i.e., $w_f = 0.125$kg/kg, $T_f = 12$°C, $w_{p8} = 0.48$kg/kg, $T_{DSI} = 115$ °C, $T_{e3} = 55$ °C, $T_{vac1} = 24$ °C and $T_{e1} = 70$ °C). Figure 6-12 shows the constraints in relation to the TVR product mass flow and TVR steam pressure. Clearly, the higher temperature increases the operating range of the plant.

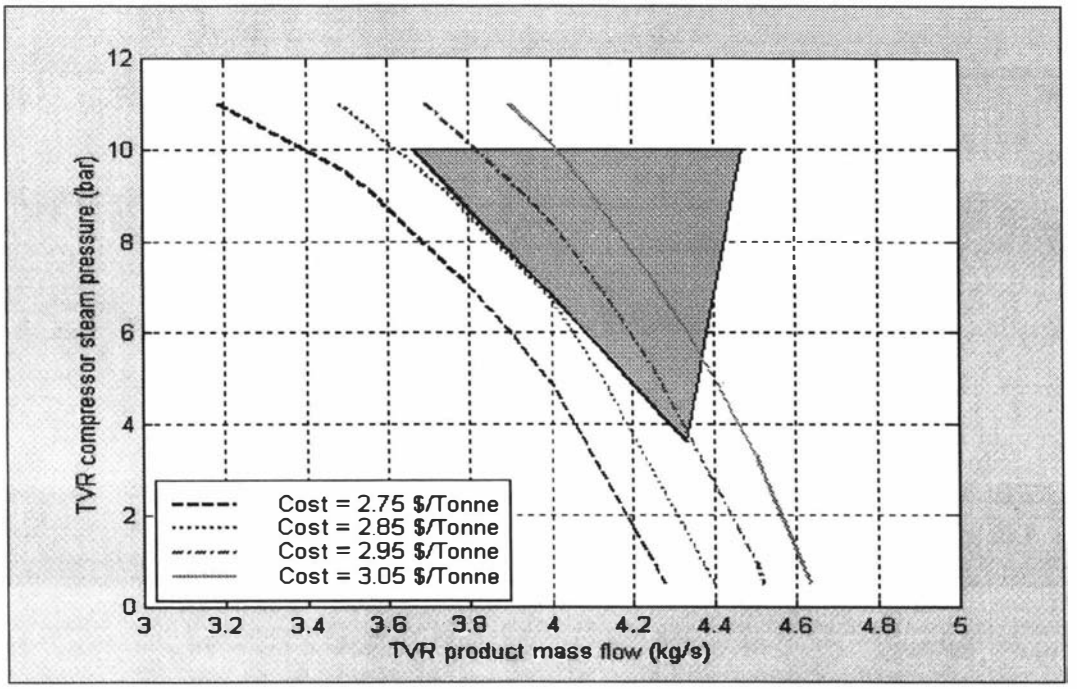

Figure 6-13 : Evaporating costs for MVR evaporator temperature of 70 °C.

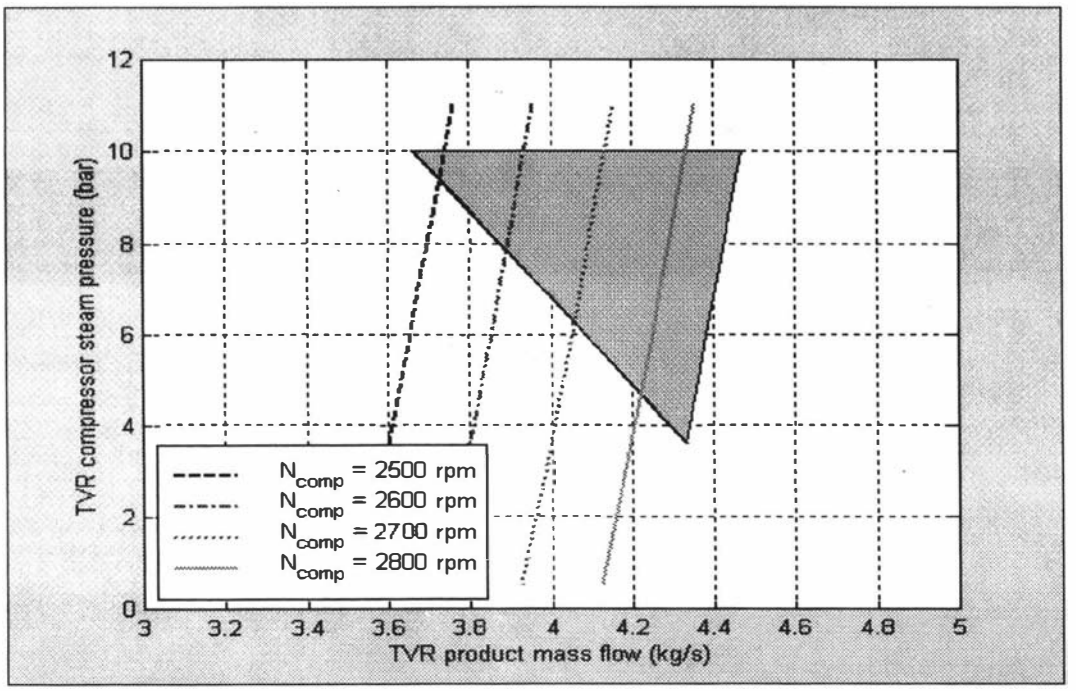

Figure 6-14 : MVR compressor speed in terms of TVR product mass flow and steam pressure.

We are now interested in determining the optimum plant operating conditions. Figure 6-13 shows the evaporation costs when the MVR evaporator temperature is 70 °C. A comparison with Figure 6-10 shows that the evaporation costs are lower at the higher MVR evaporator temperature. From Figure 6-13 we can determine that the minimum evaporating cost occurs at

the TVR product mass flow of 3.86 kg/s and the TVR steam pressure of 8.0 bar. This represents an evaporating cost of 2.94 $/Tonne of concentrate milk.

We can now determine the evaporator feed mass flow and MVR compressor speed. The mass balance shown by equation (6.29) allows us to determine the evaporator feed mass flow (i.e., $M_f = 14.82$ kg/s). Finally, the MVR compressor speed is determined from the steady state model. Figure 6-14 shows the MVR compressor speed in terms of the TVR product mass flow and TVR steam pressure. From this we can determine the optimum operating condition (i.e., $N_{comp} = 2600$ rpm).

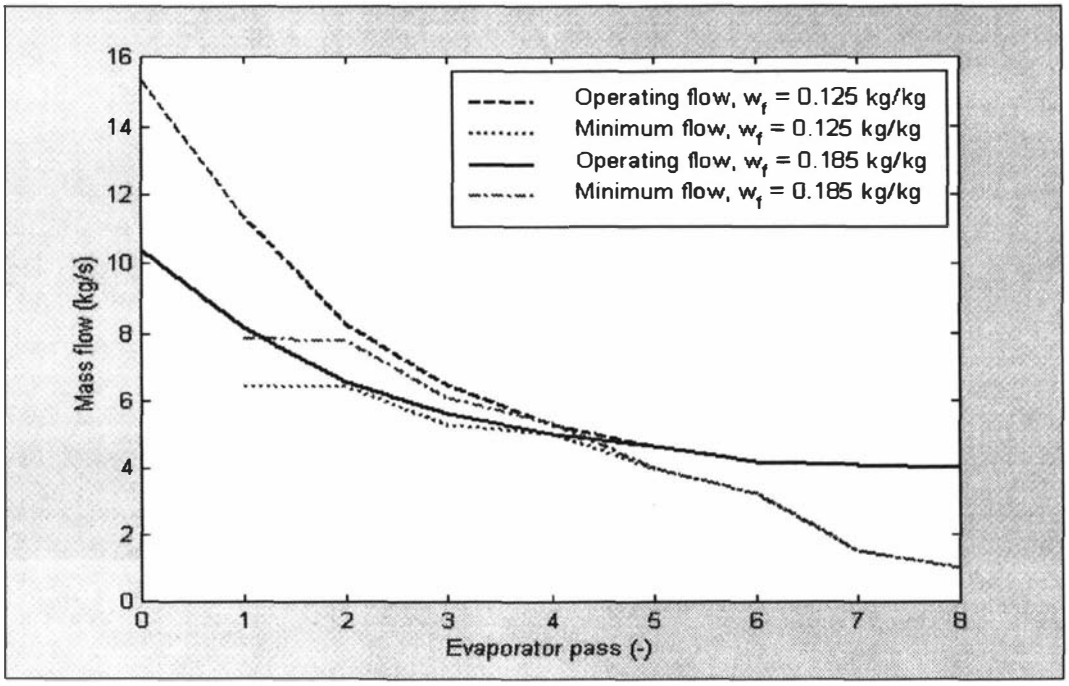

Figure 6-15 : Operating and minimum flows, with different feed dry matters.

Dilution optimisation

We are interested in the impact of the feed dry matter on the plant operating conditions. In fact, it may be necessary to dilute milk solutions with high feed dry matter concentrations. This is because low feed flows are required and this can contradict the film wetting constraint. If we consider the evaporator dry matter mass balance (i.e., $M_f = \frac{M_{p8}.w_{p8}}{w_f}$) we can see the problem with high feed dry matter milk solutions. The concentrate dry matter (w_{p8}) is set by the viscosity constraint and the maximum product flow (M_{p8}) by the spray dryer evaporation capacity. If the feed dry matter is high, then the evaporator feed flow will need to be low and this can potentially cause film wetting problems. Figure 6-15 shows the operating and minimum flow profiles for Whole Milk with different feed dry matters of 0.125 and 0.185 kg/kg (i.e., the other inputs were $T_f = 12\,°C$, $w_{p8} = 0.48$ kg/kg, $T_{DSI} = 115\,°C$, $T_{e3} = 55\,°C$, $T_{e1} = 68\,°C$, $P_{sp} = 5$ bar, $T_{vac1} = 24\,°C$ and $M_{p8} = 4$ kg/s). When the feed dry matter is 0.125 kg/kg the film wetting margin is close to zero.

However, with a feed dry matter of 0.185 kg/kg the evaporator feed flow must be reduced and this causes the lower flow profile shown in Figure 6-15. Consequently, some evaporator passes have film-wetting margins smaller than zero and they are susceptible to fouling.

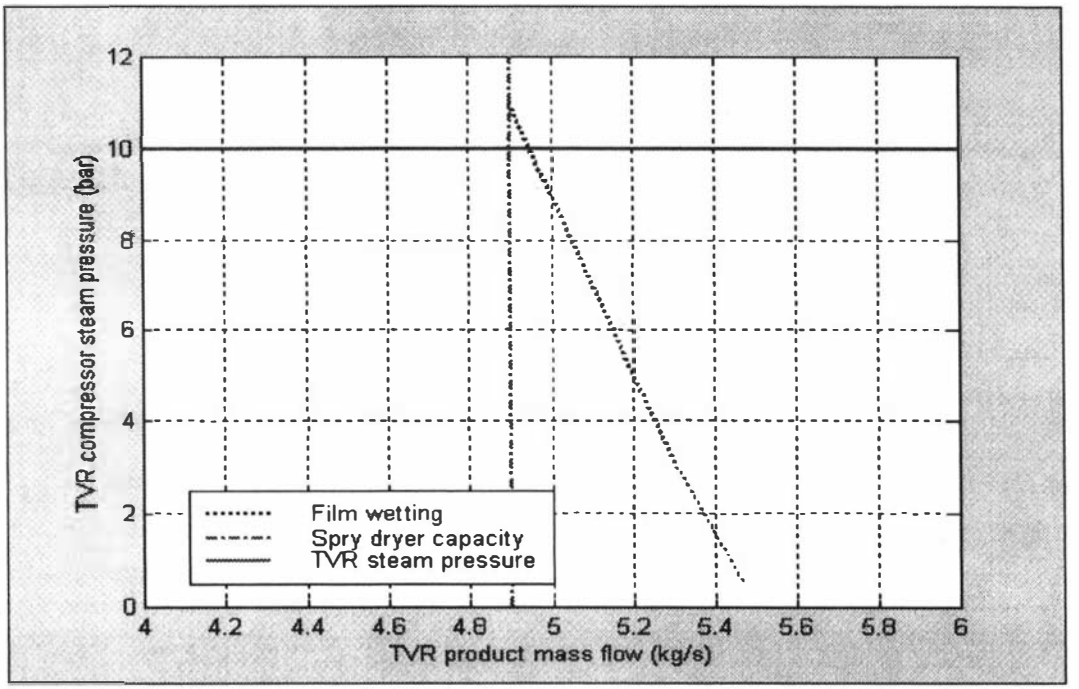

Figure 6-16 : Operating constraints with a feed dry matter of 0.185 kg/kg.

We now consider the complete optimisation problem. Figure 6-16 shows the operating constraints for a Whole Milk solution with a feed dry matter of 0.185 kg/kg. We have used the same inputs as for the previous cases (i.e., $w_{p8}=0.48\text{kg/kg}$, $T_f=12°\text{C}$, $T_{vacl}=24°\text{C}$, $T_{DSI}=115°\text{C}$, $T_{e3}=55°\text{C}$ and $T_{el}=68°\text{C}$). Clearly, the film wetting constraint and the MVR compressor power constraints have shifted. Less evaporation is required to produce the product dry matter concentration and so the compressor power constraint has shifted to high product mass flows (i.e., larger than 6 kg/s). However, the film wetting constraint has also shifted, because the dry matter concentrations are now higher in the earlier passes. The important result to notice from Figure 6-16 is that the film wetting constraint has shifted beyond the TVR product mass flow constraint. Consequently the plant has no operating range at all.

A very simple solution to this problem is to dilute the feed milk and thereby reduce its dry matter concentration. This, of course, reduces the evaporator efficiency, since more evaporation is required and thereby more power. We will not consider a complete optimisation of the plant operation with dilution, but it would be valuable to be able to determine the optimum degree of dilution. A large amount of dilution will increase the plant operational costs, since more evaporation is required, but not enough dilution may cause fouling problems. Therefore there must be an optimum amount of dilution.

6.6) Conclusions

In this Chapter we have investigated the operation of the Evaporator A DSI preheat section and the optimisation of the plant, with respect to evaporation costs. We considered three aspects of

the preheat section operation and these were the impact of air in the flash vessels, the problem of boiling in the holding tubes and flash vessel flooding. The energy cost optimisation was constrained and an important part of the investigation was the determination of these constraints.

In Section 6.2, three aspects of the DSI preheat section operation were considered. Firstly air was shown to have an important impact on the preheat operation. In Chapter 3 the DSI preheat section model was derived and it was shown that the presence of air caused a temperature difference between the top and bottom of a flash vessel. In this Chapter we have shown how this temperature difference detrimentally effects the operation of the DSI preheat section. The second operational problem with the DSI preheat section is the evaporation of milk in the preheat holding tubes. This is important because vapour bubbles form at the top of the holding tubes and thereby act as restrictions on the flow of milk. In this Chapter we showed how this problem is overcome by correctly sizing the back-pressure orifice plate and how the DSI feed pump must be correctly sized, to accommodate the back pressure orifice plate.

The remainder of this Chapter considered the optimisation of the Evaporator A plant, with respect to evaporation energy costs. The optimisation was separated into two parts : 1, the determination of the operating constraints, 2, the minimisation of the evaporation energy costs. In Sections 6.3 and 6.4 methods were developed for determining the evaporator evaporation energy costs and the operating constraints. These were then used in Section 6.5 to develop a procedure for optimising the plant operation.

The optimum operating regime is determined by the process constraints. The evaporation costs increase with the TVR steam pressure (P_{sp}) and product mass flow (M_{p8}). As a result, the optimum operating condition lies on the film wetting constraint. In fact the plant operating range is quite highly constrained, as was shown in Figure 6-10. The small plant operating range has caused the operators at Kiwi Co-op Dairies to use conservative operating conditions. They tend to run the plant with the largest possible product mass flow and TVR steam pressure, since this maximises the plant safety margin. However, the optimum plant operating condition occurs on the film wetting constraint and therefore operating with a large safety margin is effectively increasing the operating costs.

Also, it was shown in Section 6.3 that the evaporator product dry matter has a strong impact on the plant evaporation costs. With lower product dry matters, a larger amount of evaporation is required in the spray dryer, which is more expensive than the evaporators. In fact, it was shown that a 0.01 kg/kg increase in the product dry matter could produce a yearly reduction of $ 33,032 in the plant evaporation costs. This reduction is caused simply by reducing the spray dryer evaporation, whilst increasing that of the evaporator. These savings are independent of those produced with the optimisation studies of the Evaporator A plant.

The optimisation of the evaporator plant operation, with respect to evaporation energy costs can provide some savings. In this Chapter we have shown that reductions in the plant operating costs can be achieved by optimising the plant operation. The current operating conditions for the plant are determined by operating with the maximum safety margin, with respect to falling film wetting and product dry matter. In this Chapter we have shown that this causes the plant operating costs to be increased.

Chapter 7 : Controllability Studies

7.1) Introduction

Process control is very important for large industrial process plants. It provides uniform plant operation and high quality products. Both of these often lead to greater profits through lower operation costs and higher revenue. In this chapter we will investigate the control of the falling film evaporators of the Evaporator A plant at Kiwi Co-op Dairies. The aim is to determine the functional controllability of the plant. We are primarily concerned with the plant's ability to reject disturbances.

In Section 7.2, we briefly discuss the Evaporator A plant process and disturbance variables. This is done to provide some simple background to the overall plant and its control aims. Following this we discuss the methodology that will be used to investigate the plant controllability. The Evaporator A plant is a multi-variable process and it may require a multivariable controller. We discuss the Relative Gain Array (RGA), which will be used to investigate the multi-variable nature of a process. This allows us to determine if the plant can be controlled using decentralised controllers (i.e., single input/single output, SISO). Following this the methodology that will used to investigate the decentralised control loops will be discussed.

In Section 7.3, we investigate the multi-variable nature of the Evaporator A plant. The static and dynamic RGAs for the entire Evaporator A plant will be determined. We use these to determine the correct control input/output pairings and the acceptability of decentralised control. The static model developed in Chapter 4 will be used to determine the static RGA, whereas the dynamic model is used to determine the dynamic RGA.

In Section 7.4, we investigate the plant controllability using the decentralised control loop analysis methods. We firstly show that a temperature control loop on the preheat plate heat exchanger can provide adequate disturbance rejection. This result is very important because it means the dynamic feedback through the heat exchanger can be neglected. Then we consider the DSI unit temperature controllability and this will be followed by the MVR evaporator section temperature and product dry matter control loops. Finally we investigate the TVR evaporator temperature and product dry matter control loops.

7.2) Control Variables and Controllability Analysis Methodology

7.2.1) Process Control and DisturbanceVariables

The Kiwi Co-op Dairies Evaporator A plant contains many process variables, which we would like to control. In Chapter 6 the following six controller process and manipulated variables were discussed.

Table 7-1 : Process and manipulated variables for the Evaporator A plant.

	Process Variable	Manipulated Variable
1	Evaporator product mass flow (M_{p8})	Evaporator feed flow (M_f)
2	MVR evaporator temperature (T_{e1})	Heat exchanger condensate flow (M_c)
3	TVR final effect temperature (T_{e3})	Vacuum condenser water flow (M_{vac})
4	TVR product dry matter (w_{p8})	TVR steam pressure set-point (P_{sp})
5	MVR product dry matter (w_{p5})	MVR compressor speed (N_{comp})
6	DSI unit temperature (T_{DSI})	DSI unit steam mass flow (m_{dsi})

On the Evaporator A plant the product dry matters are inferred using density meters. In Appendix A it is shown that the density of a milk solution depends upon its dry matter. As a result, it is common to directly control the product densities rather than the product dry matters. We will, however, assume that the product dry matter is directly determined.

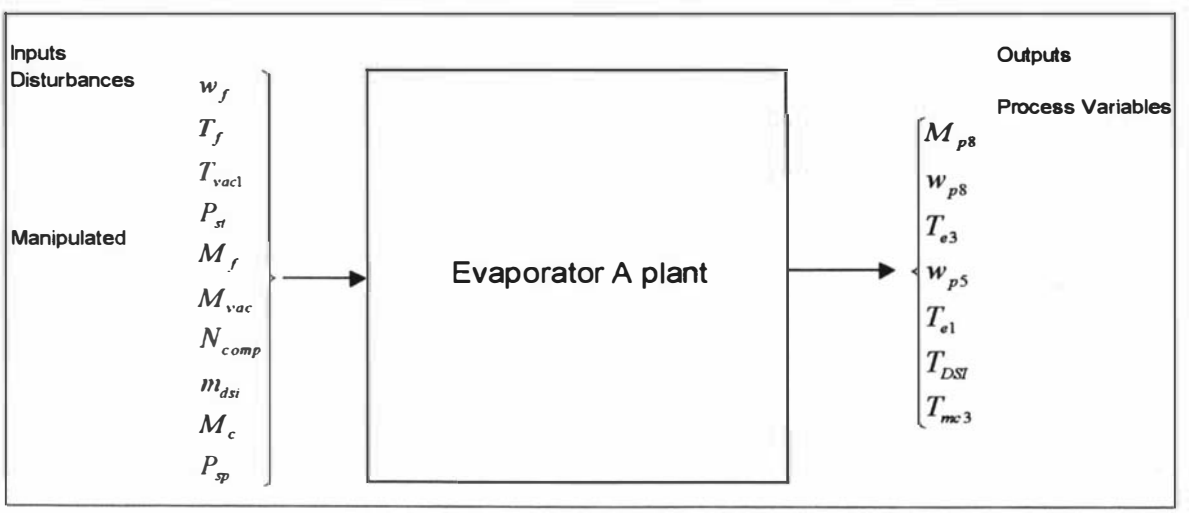

Figure 7-1 : Evaporator A manipulated, disturbances and process variables.

The Kiwi Dairy Co-operatives evaporator A plant contains four exogenous process control disturbances.

1) Feed milk dry matter (w_f).
2) Cooling water temperature (T_{vac1}).
3) Feed milk temperature (T_f).
4) Co-generation steam pressure supply (P_{st}).

7.2.2) Control Analysis Methodology

Scaling

Scaling permits meaningful analysis of the model transfer functions in the controllability analysis. Table 7-2 shows the scaling values which we shall use in the controllability analysis. The process and manipulated variable scaling values have been chosen from the allowed range of these variables. For example the TVR product dry matter (w_{p8}) has been scaled with a range of 0.01 kg/kg. This means that we seek to maintain a deviation in this variable of 0.01 kg/kg, but not more. The disturbance variable scaling values have been chosen from the expected variation in these variables. For example the cooling water inlet temperature (T_{vac1}) is expected to change by about 3 °C and so we have chosen this as the scaling value. The Evaporator A plant models have been scaled using the methods of Skogestad and Postlewaite (1996). Table 7-3 shows the static gains from Table 4-1 after they have been scaled.

Table 7-2 : Scaling parameters for controllability analysis.

Variable	Description	Type	Scaling Value	Units
w_{p5}	MVR evaporator product dry matter.	Process variable	0.01	kg/kg
w_{p8}	TVR evaporator product dry matter.	Process variable	0.01	kg/kg
w_f	Evaporator feed dry matter.	Disturbance	0.01	kg/kg
T_{DSI}	Preheat DSI temperature.	Process variable	1	°C
T_{e3}	Third effect temperature	Process variable	1	°C
T_{e1}	First effect temperature.	Process variable	1	°C
T_{mc3}	Plate heat exchanger outlet temperature.	Process variable	1	°C
T_f	Evaporator feed temperature.	Disturbance	3	°C
T_{c1}	Condensate water temperature.	Disturbance	1	°C
T_{p5}	MVR evaporator product milk temperature.	Disturbance	3	°C
T_{vac1}	Vacuum condenser cooling water.	Disturbance	3	°C
T_{vac2}	Vacuum condenser outlet temperature.	Disturbance	3	°C
T_{ph2}	Hot feed milk to the MVR evaporator section.	Disturbance	3	°C
T_{mcsp}	Plate heat exchanger control loop set-point.	Manipulation	6	°C
M_c	Plate heat exchanger condensate flow.	Manipulation	1	kg/s
M_f	Evaporator feed flow.	Manipulation	1	kg/s
M_{vac}	Vacuum condenser cooling water flow.	Manipulation	1	kg/s
M_{p8}	TVR product mass flow.	Process variable	1	kg/s
P_{st}	Raw steam pressure.	Disturbance	50000	Pa
P_{sp}	TVR steam pressure control loop set-point.	Manipulation	200000	Pa
N_{comp}	MVR compressor speed.	Manipulation	200	rpm
m_{dsi}	Mass flow of raw steam.	Manipulation	0.15	kg/s

Multivariable analysis

A large process plant will contain many potentially interacting control loops. We would like to determine whether these interactions will play an important role in the controllability of the plant. The Relative Gain Array (RGA) is an important tool that can be used to investigate control loop interactions. The properties of the RGA are rigorously proven by Grosdidier and Morari (1985) and summarised by Skogestad and Postlethwaite (1996). The RGA and the RGA_{number} of an $m \times m$ matrix, G, are defined by equation (7.1).

$$RGA = G \otimes \left(G^{-1}\right)^T, \qquad RGA_{number} = \left\| RGA - I \right\|_{sum} \tag{7.1}$$

Where the operation $\otimes$ denotes element by element multiplication (Hadamard or Schur product) and $\|G\|_{sum}$ is the sum-norm of the matrix G (Skogestad and Postlewaite, 1996). There are two important rules for the RGA :

Integrity : Avoid input-output pairings on negative steady-state RGA elements.
Stability : Prefer control loop pairings with an RGA_{number} close to 0 at crossover frequencies.

Table 7-3 : Scaled static process gains for the Evaporator A plant.

	N_{comp} = 2850 rpm	P_{sp} = 500000 Pa	M_f = 15.3 kg/s	T_f = 12 °C	w_f = 0.125 kg/kg	M_c = 9.042 kg/s	m_{dsi} = 0.35 kg/s	M_{vac} = 3.5 kg/s	T_{vacl} = 24 °C
T_{mc3} = 50.00 °C	2.0385	0.9284	-7.0553	2.7757	0.0784	5.6412	12.0718	2.3559	0.4071
T_{el} = 66.19 °C	2.9631	0.9315	-8.1040	2.7848	0.0361	5.2575	18.3718	2.3637	0.4084
T_{sl} = 69.96 °C	3.7969	1.0524	-9.2156	3.1462	0.1134	5.9396	20.7218	2.6705	0.4614
T_{DSl} = 104.38 °C	3.0277	0.9460	-10.8913	2.8284	0.0944	5.3570	33.0618	2.4007	0.4148
T_{phl} = 91.45 °C	3.0945	0.9669	-10.3280	2.8908	0.0966	5.4991	28.5231	2.4536	0.4239
T_{ph2} = 77.89 °C	3.1660	0.9893	-9.7036	2.9576	0.0990	5.6554	23.5223	2.5104	0.4337
T_{e2} = 57.48 °C	1.5577	4.2498	-3.9926	1.5185	0.5606	2.7282	10.0256	-1.8905	1.3693
T_{s2} = 63.36 °C	5.2388	6.3061	-10.2654	3.2757	1.2082	5.8757	21.4366	-0.9932	1.8406
T_{e3} =53.24 °C	-1.7551	3.1061	1.7387	-0.0594	0.1371	-0.3552	-0.2208	-3.8431	1.3600
w_{p5} = 0.408 kg/kg	13.7854	2.0021	-22.5006	5.9872	2.0453	11.3177	38.7424	5.0809	0.8778
w_{p8} = 0.469 kg/kg	18.1100	3.6971	-30.3918	8.0820	2.2069	15.2365	52.3504	7.0010	1.1334
M_{p5} = 4.68 kg/s	-1.5812	-0.2297	2.8887	-0.6864	0.1399	-1.2984	-4.4411	-0.5827	-0.1007
M_{p8} = 4.07 kg/s	-1.5702	-0.3206	2.9032	-0.7004	0.1348	-1.3215	-4.5357	-0.6069	-0.0983

The first RGA rule allows us to determine which manipulated/process variable control loop pairings should be used. This question appears trivial but with a large plant the correct choice of control loop pairings can be very important. According to this rule the RGA element corresponding to the control loop pairing should be larger than zero. The second RGA rule

determines whether decentralised control loops can be used for the plant. According to the second *RGA* this can be done if the RGA_{number} is close to zero at crossover frequencies.

Decentralised control loop analysis methodology
If the multi-variable nature of a process is not important, then we can tune the control loops independently as decentralised loops. We are interested in the ability of the control loops to reject disturbances. There are two aspects of this problem and they are investigated by considering the control loop disturbance rejection (DR) and input saturation (IS). These will be investigated using the methodology of Skogestad and Postlethwaite (pp 196–199, 1996).

1) DR : Can the scaled process variables be maintained within ± 1 for any scaled disturbance of ± 1?
2) IS : Are the scaled manipulations required for disturbance rejection within ± 1?

The Sensitivity Transfer Function ($S(s)=\frac{1}{[1+G(s)G_c(s)]}$) will be used to investigate the closed loop control performance. We will denote the process transfer function as $G(s)$, the controller transfer function as $G_c(s)$ and the disturbance transfer function as $G_d(s)$. To satisfy the disturbance rejection criterion we require $|G_d(j.\omega)S(j.\omega)|\leq 1 \forall \omega$ for each disturbance, where $S(s)$ is the Sensitivity Transfer Function and ω is the frequency. For PI control, this can be satisfied if $\omega_u \geq \omega_d$, where ω_u is the phase crossover frequency of $G(s)$ and ω_d the gain crossover frequency of $G_d(s)$. To avoid saturation of the manipulated variable, we require $|G(j.\omega)| > |G_d(j.\omega)|-1$ at frequencies where $|G_d(j.w)|>1$.

7.3) Multi-Variable Nature

7.3.1) Introduction

Here we investigate the multi-variable nature of the Evaporator A plant. We are primarily interested in determining if the plant can be controlled using decentralised control loops and the appropriate control loop pairings. The static and dynamic *RGA*s will be used to answer these questions.

7.3.2) Static *RGA* Analysis

There are six process variables that we would like to control (T_{e1}, T_{DSI}, w_{p5}, T_{e3}, M_{p8} and w_{p8}) with the manipulated variables (M_c, m_{dsi}, N_{comp}, M_{vac}, M_f and P_{sp}). The steady state model for the entire Evaporator A plant was determined in Chapter 4. We can use this model to determine the static *RGA* and this is shown by equation (7.2).

The static *RGA* shows that all of the diagonal elements are positive and so the correct control loop pairings have been chosen (i.e., w_{p5}/N_{comp}, T_{e1}/M_c, M_{p8}/M_f, T_{DSI}/m_{dsi}, w_{p8}/P_{sp} and T_{e3}/M_{vac}). However, some of the elements are large and in particular the sixth diagonal element, which corresponds to the product flow control loop (M_{p8}), is very large. The RGA_{number} for the

system is 74.06, which is very large and suggests de-centralised controllers will suffer from interaction problems.

$$RGA = \begin{array}{c} \begin{matrix} T_{e1} & T_{DSI} & T_{e3} & w_{p5} & w_{p8} & M_{p8} \end{matrix} \\ \begin{bmatrix} 3.3310 & -1.2962 & -0.0300 & -0.8803 & -0.1092 & -0.0153 \\ -1.3352 & 2.2974 & 0.0147 & 0.0203 & -0.0109 & 0.0137 \\ -0.0359 & 0.0000 & 0.9164 & 0.0001 & 0.1190 & 0.0005 \\ 6.6251 & -0.0254 & -5.1819 & 1.8509 & -2.2419 & -0.0269 \\ -6.1716 & 3.1224 & 6.0829 & 4.1182 & 3.6280 & -9.7799 \\ -1.4133 & -3.0983 & -0.8020 & -4.1092 & -0.3850 & 10.8078 \end{bmatrix} \end{array} \begin{matrix} M_c \\ m_{dsi} \\ M_{vac} \\ N_{comp} \\ P_{sp} \\ M_f \end{matrix} \quad (7.2)$$

The large RGA_{number} can be explained by considering the linearised Evaporator A mass balances. These are given by equation (7.3) and we will consider the total mass flow of evaporation (M_{tubest}) and the evaporator feed flow (M_f) as the manipulated inputs. In practice the mass flow of evaporation cannot be manipulated and industrial plants use the MVR compressor speed, or the TVR steam pressure as manipulated variables. However, these industrial manipulated variables are strongly correlated with the mass of evaporation and it is considerably simpler to assume that the mass flow of evaporation is a direct manipulation (Winchester and Marsh, 1999). The process outputs are the TVR evaporator product dry matter (w_{p8}) and flow (M_{p8}). We can then calculate the RGA and RGA_{number} for this alternative control situation and these are explicitly given by equation (7.4).

$$\begin{bmatrix} M_{p8} \\ w_{p8} \end{bmatrix} = \begin{bmatrix} 1 & -1 \\ \dfrac{w_f^0 M_{tubest}^0}{(M_f^0 - M_{tubest}^0)^2} & -\dfrac{M_f^0 . w_f^0}{(M_f^0 - M_{tubest}^0)^2} \end{bmatrix} \begin{bmatrix} M_f \\ M_{tubest} \end{bmatrix} \quad (7.3)$$

$$RGA = \begin{bmatrix} \dfrac{M_f^0}{(M_f^0 - M_{tubest}^0)} & -\dfrac{M_{tubest}^0}{(M_{tubes}^0 - M_{tubest}^0)} \\ -\dfrac{M_{tubest}^0}{(M_{tubes}^0 - M_{tubest}^0)} & \dfrac{M_{tubest}^0}{(M_f^0 - M_{tubest}^0)} \end{bmatrix}, \qquad RGA_{number} = \frac{4 M_{tubest}^0}{\left[M_f^0 - M_{tubest}^0\right]} \quad (7.4).$$

Where, M_f^0 = mass flow of feed milk to the Evaporator A plant, at steady state. (kg/s)

M_{tubest}^0 = total mass flow of evaporation in the Evaporator A plant, steady state. (kg/s)

M_{p8} = mass flow from the TVR evaporator section. (kg/s)

w_{p8} = dry matter from the TVR evaporator section. (kg/kg)

The RGA and RGA_{number} given in equation (7.4) are very dependent on M^0_{tubest}. More importantly when M^0_{tubest} is large in relation to M^0_f the RGA_{number} becomes very large. For the Evaporator A plant approximately 80 % of the water in the feed milk is evaporated and substituting this into equation (7.4) we can produce a RGA_{number} of 16. This suggests that a significant amount of the interactions are between the TVR product dry matter and flow control loops.

If we are to control the Evaporator A plant with decentralised control loops, then one of either the product dry matter or mass flow control loops will have to be sacrificed. Otherwise a multi-variable controller will be required. Of the two control loops, the product dry matter is the most important, because it has an exponential impact on viscosity. If we neglect the product flow control loop then the static RGA is given by equation (7.5).

$$RGA = \begin{array}{c} \begin{matrix} T_{e1} & T_{DSI} & T_{e3} & w_{p5} & w_{p8} \end{matrix} \\ \begin{bmatrix} 3.3281 & -1.3025 & -0.0316 & -0.8842 & -0.1098 \\ -1.3333 & 2.3051 & 0.0157 & 0.0230 & -0.0105 \\ -0.0359 & 0.0000 & 0.9168 & 0.0004 & 0.1187 \\ 6.6212 & -0.0339 & -5.1841 & 1.8393 & -2.2427 \\ -7.5802 & 0.0313 & 5.2832 & 0.0215 & 3.2442 \end{bmatrix} \end{array} \begin{matrix} M_c \\ m_{dsi} \\ M_{vac} \\ N_{comp} \\ P_{sp} \end{matrix} \qquad (7.5)$$

The RGA_{number} for this situation is 37.66 which is considerably smaller than the case with the product flow loop included. This is still a comparatively large RGA_{number} and suggests that there may still be significant controller interactions between the control loops. However, we will show in the dynamic RGA analysis that the RGA_{number} reduces at higher frequencies and it is relatively close to zero in the range of frequencies we are concerned about.

7.3.3) Dynamic RGA Analysis

The above static RGA analysis does not provide a complete investigation of the multi-variable nature of the evaporator. Static RGAs can be used to determine the control loop pairings, but they do not give a true indication of the control loop interactions. As stated in Section 4.3 the requirement for the 'Stability' of a multi-variable system is that the RGA_{number} be close to 0 at frequencies close to the cross-over.

In Chapter 4 we developed the linear dynamic model for the Evaporator A plant. The model neglected the preheat plate heat exchanger because of the difficulty of combining the dynamic heat exchanger equations with the rest of the Evaporator A plant. We can, however, combine the preheat plate heat exchanger model with the rest of the Evaporator A plant and calculate the dynamic RGA using numerical methods. This is quite simple for the RGA analysis because we only require the process gains and these are not difficult to calculate. The static RGA results suggest that there will be potential controller interactions between the control loops of the Evaporator A plant. Figure 7-2 shows the RGA_{number} across a range of frequencies, as calculated

using the numerical analysis. It should be noted that the RGA_{number} at low frequencies is different from that determined with the static model, because of the additional assumptions made in the development of the dynamic model.

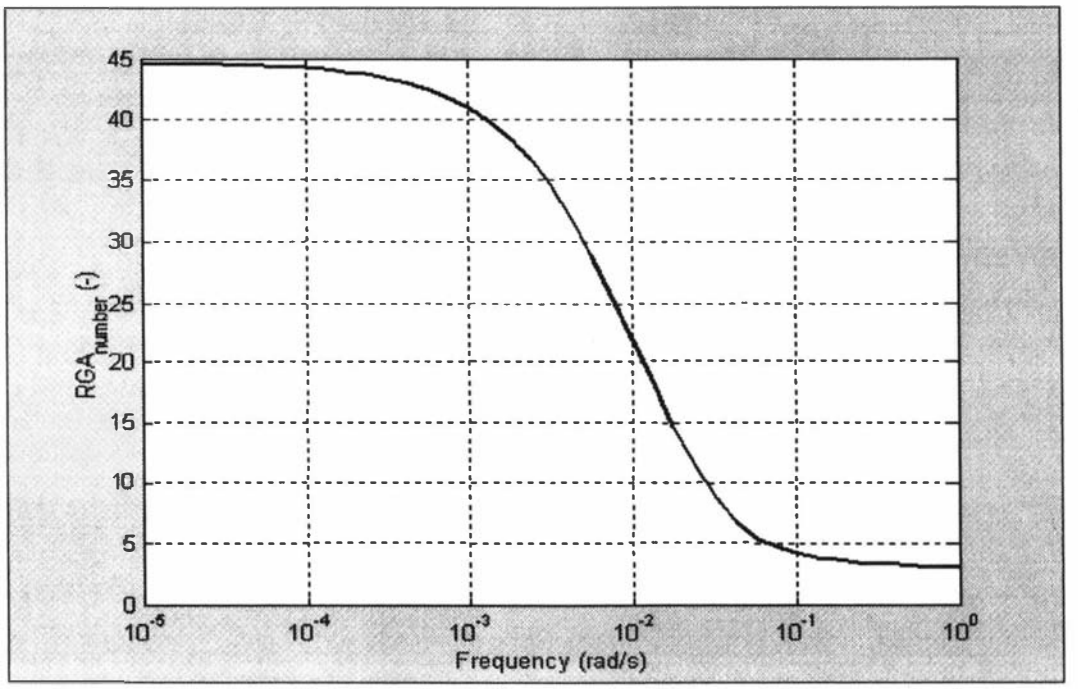

Figure 7-2 : RGA_{number} vs frequency for the complete Evaporator A plant.

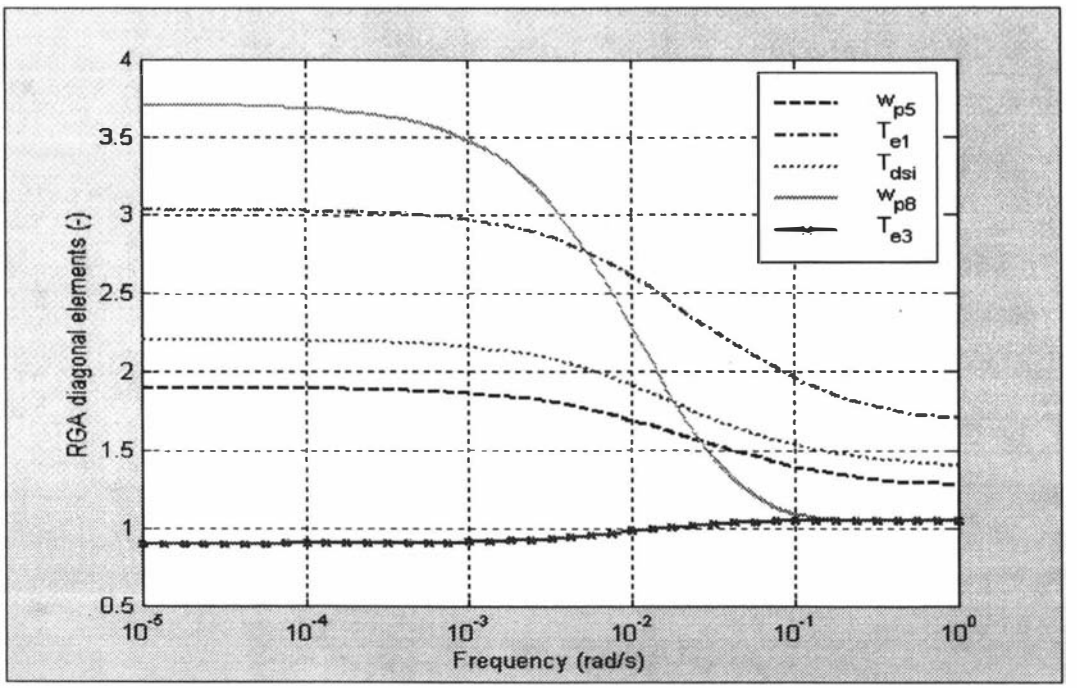

Figure 7-3 : RGA vs frequency diagonal elements for the Evaporator A plant.

The important result shown in Figure 7-2 is the reduction in the RGA_{number} at higher frequencies. At frequencies above 0.1 rad/s the RGA_{number} falls below 5 and this suggests that any controller with a cross-over frequency above this will not suffer from interaction problems. However, at frequencies below 0.01 rad/s the RGA_{number} is above 20 and this suggests that any controllers with cross-over frequencies in this range will have interaction problems. These results give a clear indication of the potential interaction problems and provide a safe frequency operating range for the plant. Provided the plant controllers operate with cross-over frequencies above 0.01 and preferably 0.1 rad/s, then no interaction problems will occur.

The RGA diagonal elements for the five control loops are shown in Figure 7-3. As expected these shift towards the ideal value at higher frequencies. In particular the temperature and product dry matter control loops for the TVR evaporator section become very close to the ideal. The elements for the MVR evaporator are not quite so close to the ideal section but they do dramatically improve. As with the RGA_{number} the RGA elements are different from those determined in the static analysis.

7.4) Decentralised Control Loops

7.4.1) Introduction

In the previous Section, we determined the applicability of de-centralised control loops. It was shown that decentralised control loops, with the exception of the product mass flow, would be adequate provided their cross-over frequencies were above 0.01 rad/s. As a result, the plant will probably not suffer from serious interaction problems when using decentralised control loops. In this section, we shall investigate the controllability of these de-centralised loops.

7.4.2) Preheat Plate Heat Exchanger

Here we will do a controllability analysis on the preheat plate heat exchanger. This is important because of the difficulty of developing the dynamic model for the complete Evaporator A plant. The dynamic model for the preheat plate heat exchanger does not represent a finite order constant coefficient linear differential equation. As a result, it is difficult to combine it with the dynamic models for the DSI preheat section, the MVR evaporator section and the TVR evaporator section. However, we show here that the plate heat exchanger exhibits good disturbance rejection. Therefore the feedback loops through the heat exchanger are removed and the Evaporator A plant dynamic model does not need to include the heat exchanger.

We are interested in the control loop for the plate heat exchanger outlet hot milk temperature. Figure 7-4 shows the temperature control loop with the process, disturbance and manipulated variables. The flow of hot condensate (M_c) is manipulated, to control the outlet milk temperature (T_{mc3}), by using a bypass control valve. There are several disturbances to the plate heat exchanger. Firstly, the vacuum condenser cooling water flow (M_{vac}) and temperature ($T_{v1} = T_{vac2}$) are disturbances to the first plate heat exchanger section. The flow of cooling water (M_{vac}) is manipulated to control the TVR final effect temperature. However, these flow variations also act as disturbances to the preheat plate heat exchanger and so we will include them here as disturbances. Secondly, the condensate flow (M_c) and temperature (T_{c1}) will vary with the MVR evaporator temperature. In Chapter 6 we showed that the MVR evaporator

temperature effects its mass flow of evaporation and hence the mass flow of condensate. Therefore both of these variables are strictly disturbances to the preheat plate heat exchanger. However, we only consider the condensate temperature as a disturbance, because the mass flow of condensate is the manipulated variable for the plate heat exchanger control loop. Thirdly the feed flow (M_f) and temperature (T_f) will disturb the heat exchanger.

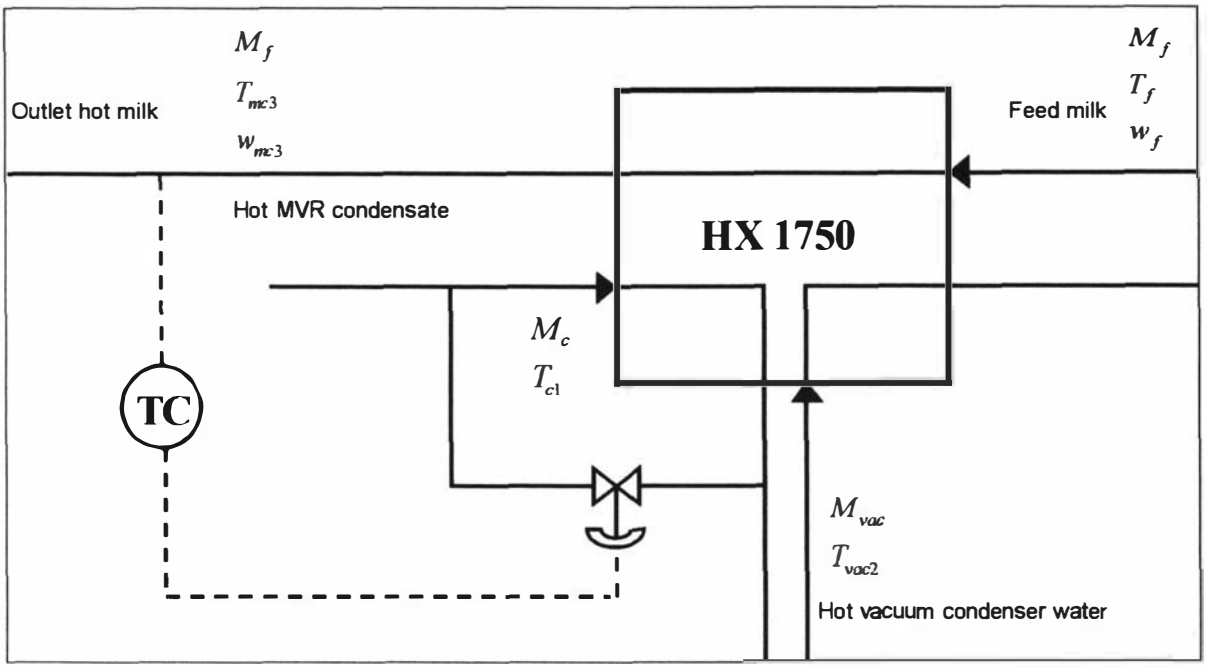

Figure 7-4 : Preheat plate heat exchanger outlet temperature control loop.

The transfer functions describing the plate heat exchanger were derived in Chapter 3. They do not represent constant coefficient linear differential equations and this presents a problem, because most dynamic analysis is based on constant coefficient equations. However, we can numerically determine the Bode and Nyquist plots for these transfer functions and thereby do a controllability analysis. The important transfer function between the condensate water flow (M_c) and the outlet hot milk temperature (T_{mc3}) is shown by equation (7.6). This transfer function is the same as that derived in Chapter 3 and is given there by equation (3.90).

$$\frac{T_{mc3}(s)}{v_c(s)} = \frac{N_2.H_2 e^{[-\beta_2.L]}}{\left[(\alpha_1-\beta_2)^2-\beta_1^2\right]}\left[\frac{(\alpha_1-\beta_2)\sinh(\beta_1.L)-\beta_1.\cosh(\beta_1.L)+\beta_1 e^{[-(\alpha_1-\beta_2)L]}}{\alpha_2.\sinh(\beta_1.L)+\beta_1.\cosh(\beta_1.L)}\right] \qquad (7.6)$$

For the steady state operating conditions determined in Chapter 4 the Bode plot for equation (7.6) has been determined and is shown in Figure 7-5. The phase cross-over frequency can be determined from Figure 7-5 as 0.9 rad/s. This is a relatively high cross-over frequency and it corresponds to a Ziegler-Nichols period of 7.9 s. The disturbance Bode plots are shown in Figure 7-5, Figure 7-6 and Figure 7-7. The gain cross-over frequency for the $\frac{T_{mc3}(s)}{T_{c1}(s)}$ transfer function is 0.09 rad/s, for the $\frac{T_{mc3}(s)}{T_{v1}(s)}$ transfer function there is no gain cross-over frequency, for the $\frac{T_{mc3}(s)}{M_{vac}(s)}$

transfer function it is 0.02 rad/s, for the $\frac{T_{mc3}(s)}{M_f(s)}$ transfer function it is 0.06 rad/s and the $\frac{T_{mc3}(s)}{T_f(s)}$ transfer function also has no gain cross-over frequency. Each of these gain cross-over frequencies is smaller than the process transfer function phase cross-over frequency. Consequently, we expect the outlet temperature control loop to provide adequate disturbance rejection.

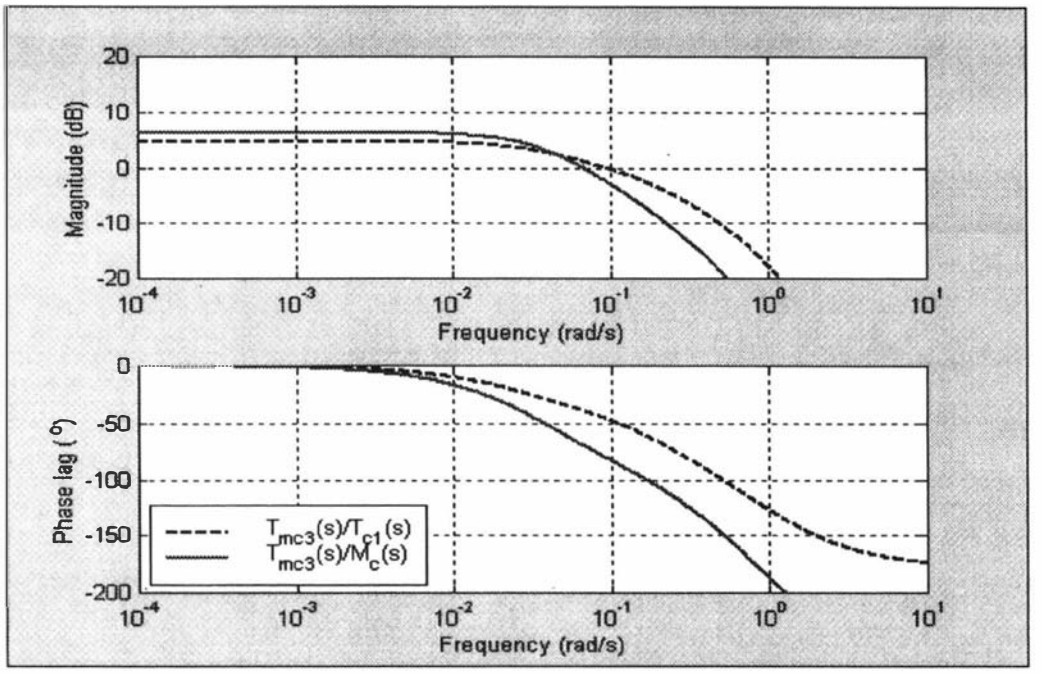

Figure 7-5 : Numerical Bode plots for the plate heat exchanger.

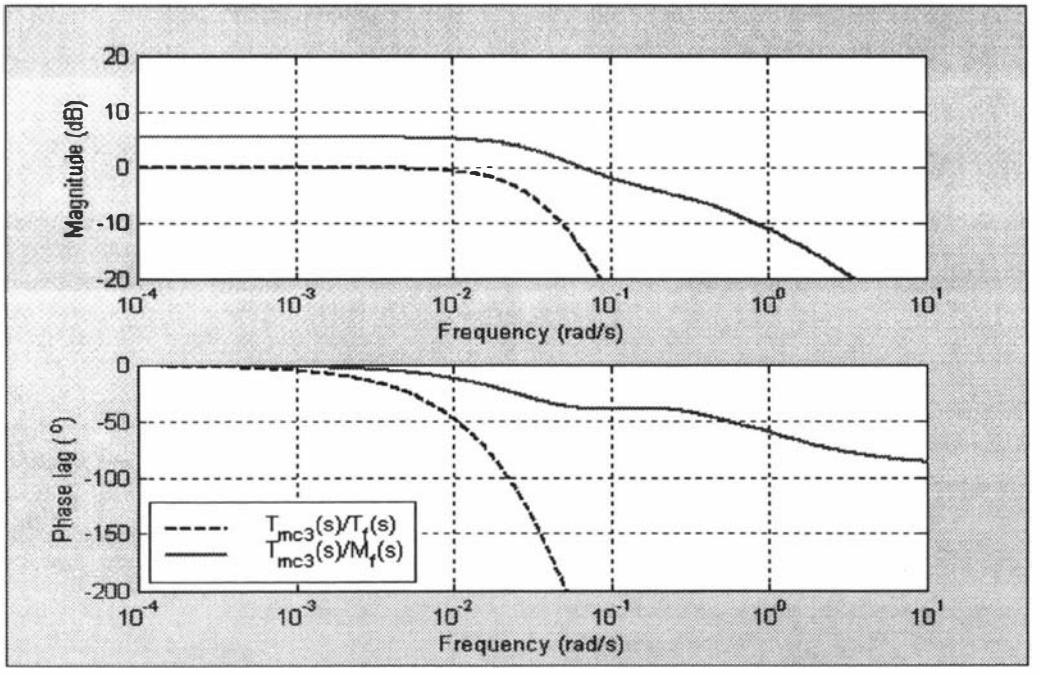

Figure 7-6 : Numerical disturbance Bode plots for the plate heat exchanger.

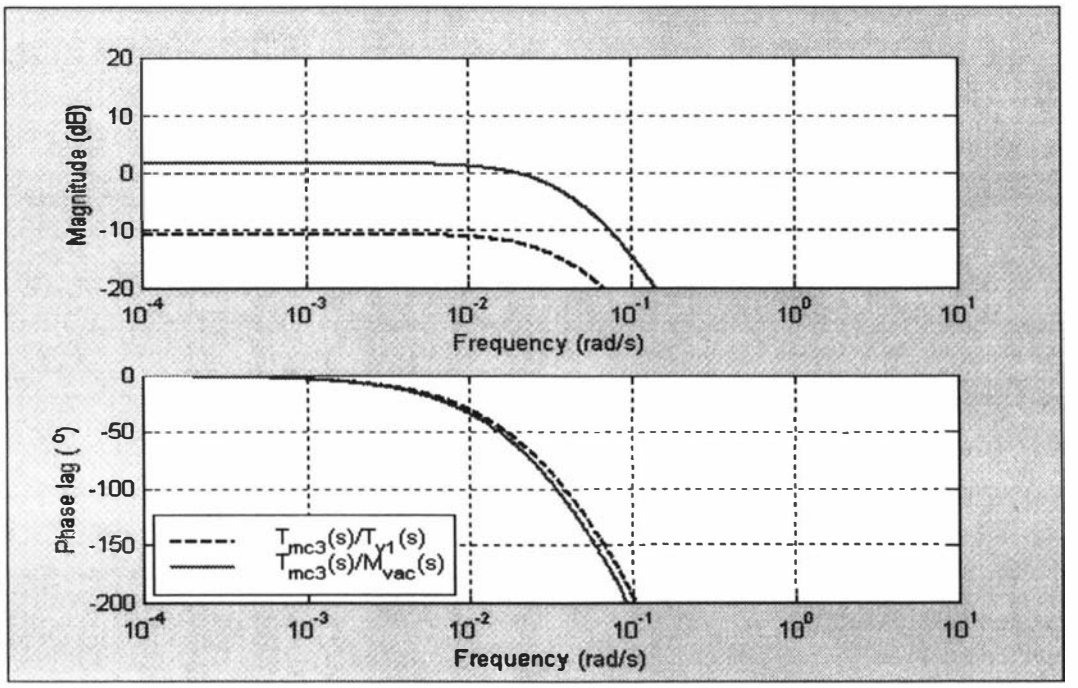

Figure 7-7 : Numerical disturbance Bode plots for the plate heat exchanger.

The above results show that the plate heat exchanger temperature control loop does have adequate disturbance rejection capabilities. This is important because it means the assumption of negligible feedback through the plate heat exchanger is valid. It also means that the plate heat exchanger outlet temperature can be assumed to be identically equal to the control loop set-point. This assumption is of some importance for the MVR evaporator temperature control loop. A cascade control loop is used with the plate heat exchanger control loop set-point as the manipulated variable for the control loop.

7.4.3) Preheat DSI temperature control

The steady state and linearised dynamic models for the preheat were developed in Chapter 4. We are interested in the control loop for the DSI unit temperature. Figure 7-8 shows the DSI unit and holding tubes, along with three different temperature control configurations. Firstly the temperature after the holding tubes is measured and the steam flow manipulated. Secondly the temperature before the holding tubes is measured and the steam flow manipulated. Thirdly the temperature after the holding tubes and the DSI unit surface temperature are measured and a cascade control loop used.

The mass flow of steam to the DSI unit depends on the raw steam pressure and the control valve. Strictly the percent opening of the control valve is the manipulated variable for the DSI unit temperature control loop and the steam pressure is a disturbance variable. However, we have taken the mass flow of steam as the manipulated variable, while still considering the raw steam pressure as a disturbance variable.

It is often found that DSI units operating with milk solutions exhibit large amounts of fouling (Trinh *et al*, 1996). Commonly, when temperature probes are placed directly after the DSI unit they become fouled and no longer give accurate temperature readings. This problem can be overcome by placing the temperature probe after the holding tubes, where no fouling is likely to

occur. However, the difficulty with measuring the temperature after the holding tubes is the large pure delay. This adds a lot of phase lag to the process transfer function, which reduces the controller's ability to reject disturbances.

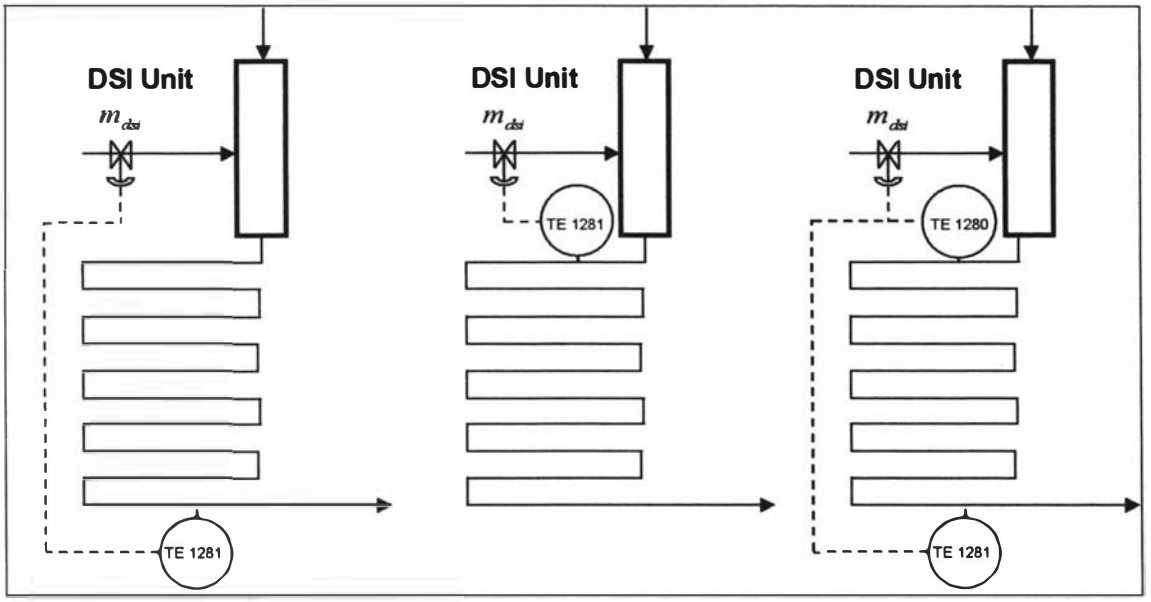

Figure 7-8 : DSI unit temperature control configurations.

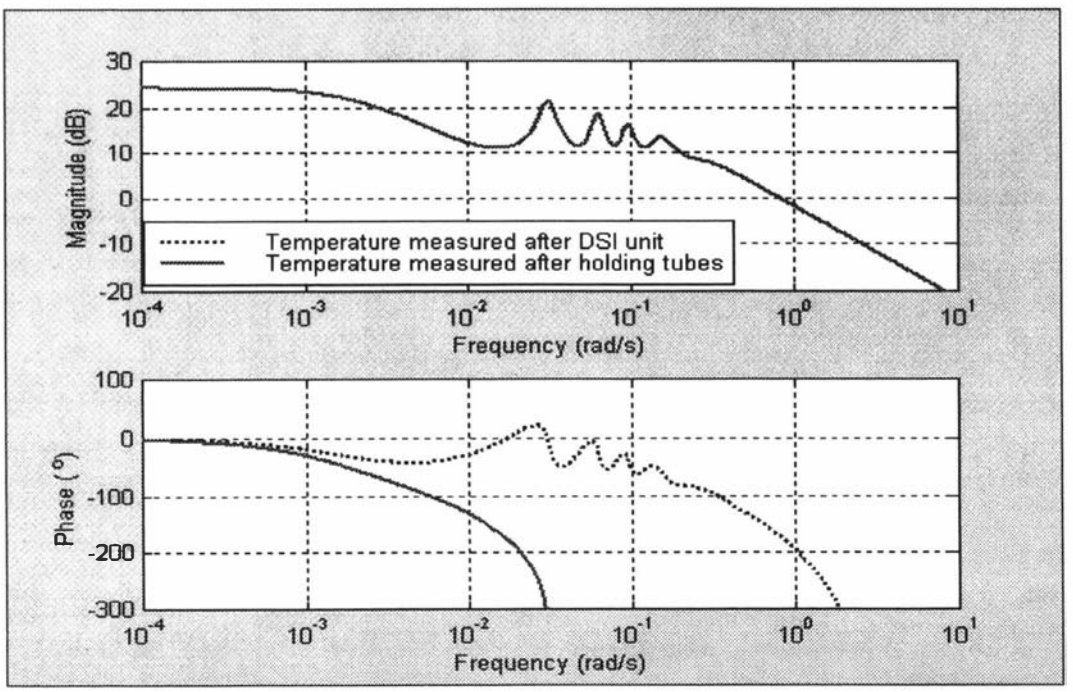

Figure 7-9 : Bode plots for the $\frac{T_{DSI}(s)}{m_{dsi}(s)}$ and $\frac{T_{fh1}(s)}{m_{dsi}(s)}$ transfer function.

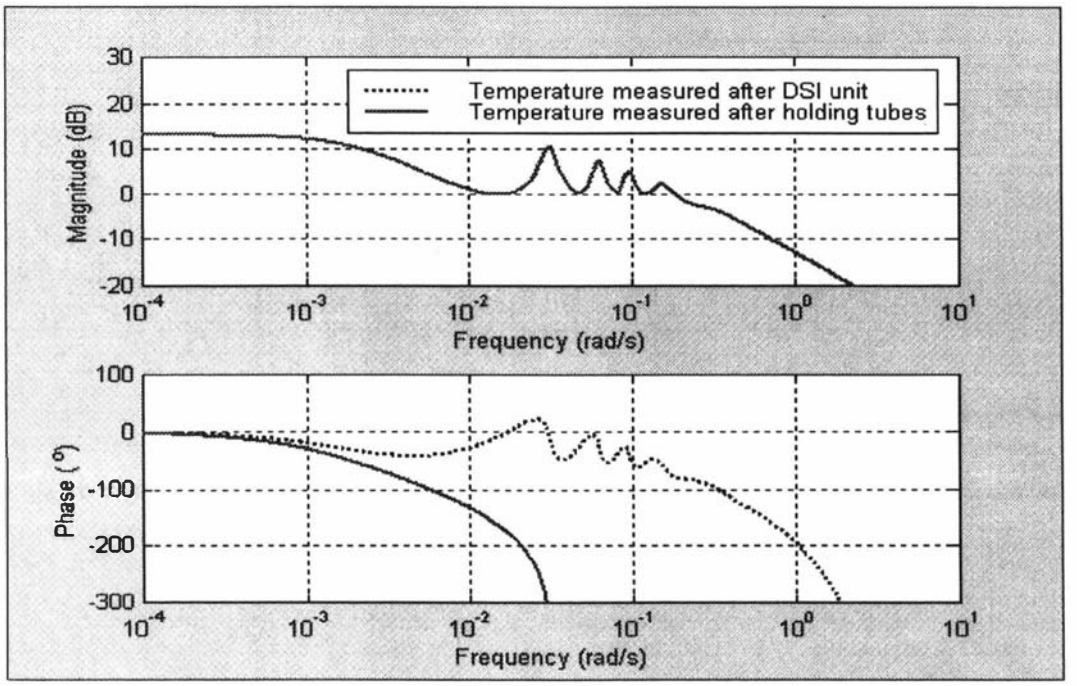

Figure 7-10 : Bode plot for the $\frac{T_{DSI}(s)}{P_{st}(s)}$ and $\frac{T_{fh1}(s)}{P_{st}(s)}$ transfer function.

Figure 7-9 shows the Bode plot for the process transfer function between the mass flow of steam and the DSI unit temperature. The transfer functions with the temperature measured before ($\frac{T_{DSI}(s)}{m_{dsi}(s)}$) and after the holding tubes ($\frac{T_{fh1}(s)}{m_{dsi}(s)}$) are both shown. Since the model neglects the heat losses from the holding tube surfaces the gains for these transfer functions are identical. Figure 7-9 shows the phase cross-over frequencies for the first and second controller configurations of Figure 7-8. When the temperature is measured directly after the DSI unit the phase cross-over frequency is 0.9 rad/s. However, the phase cross-over frequency is considerably lower, at 0.02 rad/s, when the temperature is measured after the holding tubes. The position of these cross-over frequencies depends on the model parameters. We have used a 180 s holding tube time delay and a 2 s delay between the mass flow of steam and the DSI unit. A shorter holding tube time delay would give a higher cross-over frequency, for the first controller configuration. However, 180 s is the largest holding tube time delay used at Kiwi Co-op Dairies, so it is the worst case scenario.

Figure 7-10 shows the Bode plots for the transfer function between the steam pressure disturbance (P_{st}) and the DSI unit temperature. We have used a linear gain of 0.000833 between the raw steam pressure and mass flow of steam. Figure 7-10 shows both the $\frac{T_{DSI}(s)}{P_{st}(s)}$ and the $\frac{T_{fh1}(s)}{P_{st}(s)}$ transfer functions. As with Figure 7-9 the gains in Figure 7-10 are identical for both transfer functions, since the holding tube heat losses have been neglected. The disturbance gain

cross-over frequency is 0.01 rad/s for both situations. However, the resonance nature of the preheat section means that there are several gain cross-over frequencies. The highest gain cross-over occurs at a frequency of 0.2 rad/s. This is considerably higher than the phase cross-over frequency, with the temperature measured after the holding tubes. However, it is lower than the phase cross-over frequency for the case with the temperature measured directly after the DSI unit. This clearly shows the impact of the holding tube time delay on the DSI unit temperature controllability. The controller cannot provide adequate disturbance rejection when the temperature is measured after the holding tubes.

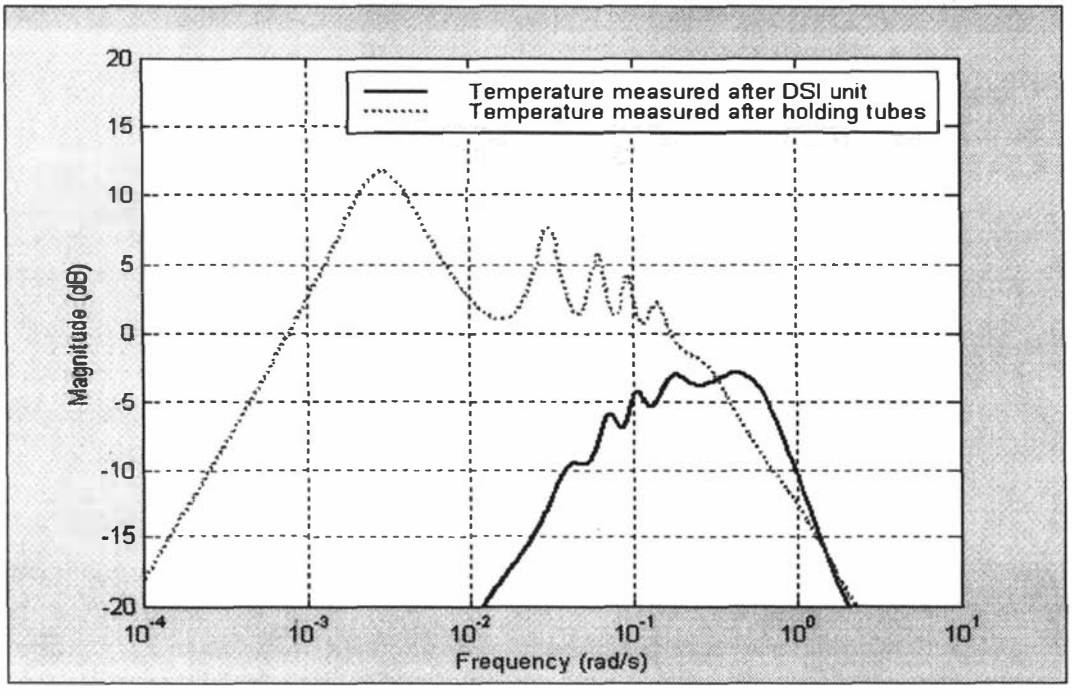

Figure 7-11 : The disturbance rejection criteria for the DSI unit temperature control loops.

We are now interested in the closed loop criteria for the DSI unit temperature control loop (i.e., $|G_d(j\omega)S(j\omega)| \leq 1 \forall \omega$). Initially we consider only the first and second control configurations shown in Figure 7-8. The third case, with the cascade controller, will be considered later. With the controller parameters $\tau_i = 20\text{s}$ and $K_c = \frac{2}{6}$, we can determine the closed loop transfer function for the second controller configuration. Figure 7-11 shows the resulting disturbance rejection criteria and there is relatively good disturbance rejection across the range of frequencies. This is consistent with the earlier results, which showed that the process phase cross-over frequency was higher than the disturbance gain cross-over frequency.

We now consider the case with the temperature measured after the holding tubes. With the controller parameters $\tau_i = 150\text{s}$ and $K_c = \frac{2}{60}$, we can determine the closed loop transfer function. We have used a larger controller integral time (τ_i) and a smaller controller gain (K_c) because of the smaller open loop phase cross-over frequency. The resulting disturbance rejection criteria is

plotted against frequency in Figure 7-11. Clearly the disturbance rejection is not very good, which is consistent with the earlier results.

The above results explain the problem with controlling the DSI unit temperature. It is better from a control perspective to measure the temperature directly after the DSI unit, but this can be susceptible to fouling. In order to overcome these problems an alternative control scheme has been developed and this is shown by the third configuration in Figure 7-8. We can measure the tube surface temperature directly after the DSI unit and also the milk temperature after the holding tubes. A cascade controller can be used with the inner loop controlling the tube surface temperature and the outer loop controlling the temperature after the holding tubes. This avoids the problems of temperature probe fouling but does not severely compromise disturbance rejection.

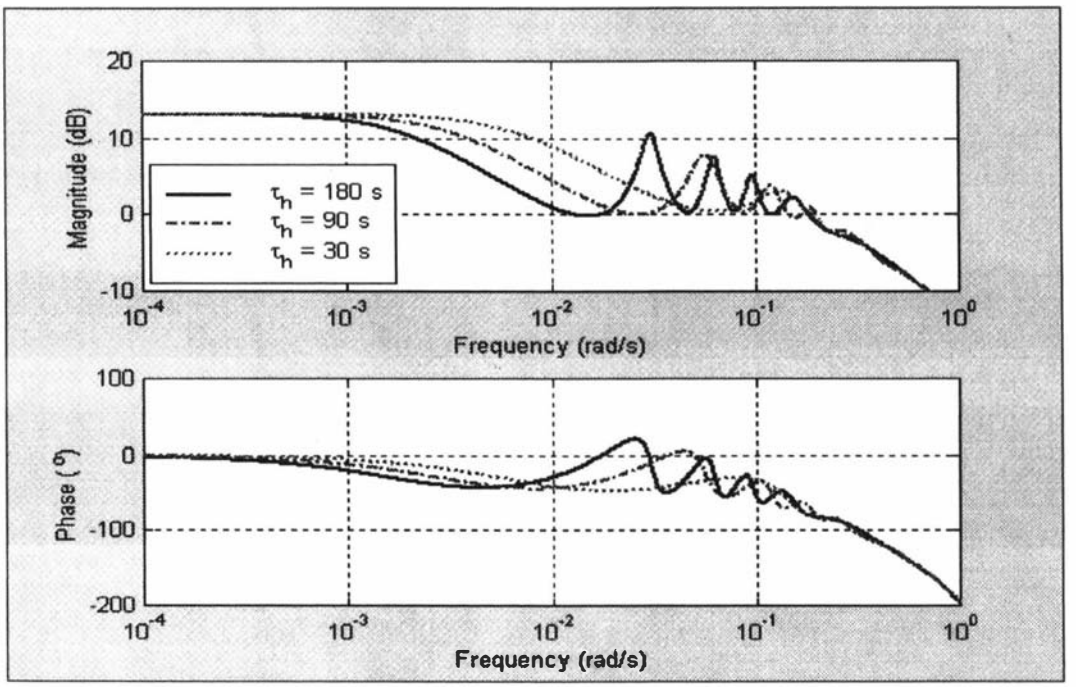

Figure 7-12 : Impact of holding tube residence time on the $\frac{T_{DSI}(s)}{P_{st}(s)}$ transfer function Bode plot.

Preheat Resonance

The DSI preheat section has a resonance effect, which can be seen from the Bode plots shown in Figure 7-12. This shows the transfer function between the steam pressure and the DSI unit temperature, for different holding tube time delays. There is clearly a resonance effect, which is indicated by the peaks in the magnitude and phase lag plots. This resonance effect is caused by the feedback through the flash vessels and the holding tube time delay. If we consider a sinusoidal variation in the steam pressure, this will cause a sinusoidal variation in the DSI unit temperature. The temperature exiting from the holding tubes will then also exhibit this sinusoidal variation but this effect will be delayed because of the holding tube time delay. This then causes a sinusoidal variation in the flash vessel temperature, which is heated by the hot liquid from the

holding tubes. The feedback through the flash vessel then interferes with the original sinusoidal steam pressure and causes the resonance effect.

The important impact of the resonance effect is the increased transfer function magnitude. This is shown in Figure 7-12, where the Bode plot magnitudes are high at the resonant frequencies. Consequently the system is sensitive to disturbances at these frequencies. In order to reject these disturbances the process transfer function phase cross-over frequency needs to be higher than the frequencies of the large resonant peaks. With the first controller configuration shown in Figure 7-8 this is impossible, because the phase cross-over frequency is very low. However, the second controller configuration has a high phase cross-over frequency and so it is able to reject disturbances that occur at the resonant frequencies.

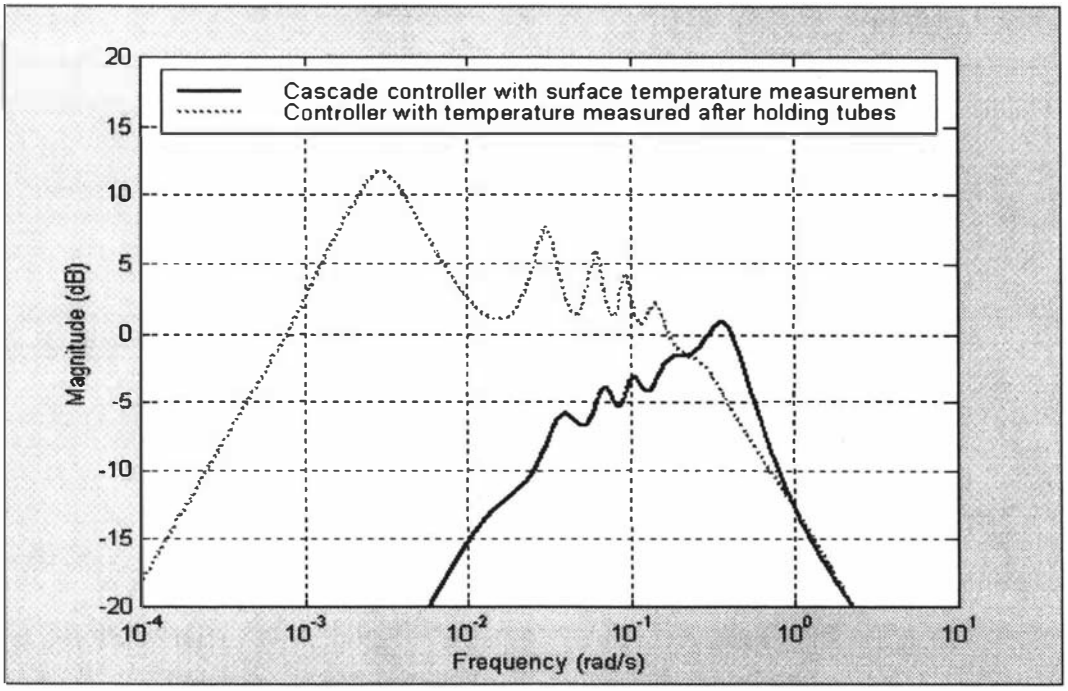

Figure 7-13 : Disturbance rejection criteria, for the third and first DSI unit controller configurations.

Cascade controller

We will now consider the third controller configuration in Figure 7-8. This is a cascade controller, which measures the tube surface temperature before the holding tubes and the milk temperature after the holding tubes. The tube surface temperature response has an additional first order dynamic, which we have modelled with a 2 second time constant. The resulting transfer functions are similar to those shown in Figure 7-9. We can now determine the closed loop transfer functions by choosing controller parameters for the cascade controller. Using the parameters $\tau_i = 20\text{s}$ and $K_c = \frac{2}{6}$ for the inner controller and $\tau_i = 150\text{s}$ and $K_c = \frac{2}{60}$ for the outer controller we can produce the disturbance rejection criteria and this is shown in Figure 7-13. Also shown is the criteria for the first controller configuration in Figure 7-8. Clearly the cascade controller provides significantly better disturbance rejection.

Finally we are interested in the controller input saturation for the DSI unit temperature control loop. The criteria for this was discussed earlier (i.e., $|G(j.\omega)| \geq |G_d(j.\omega)|-1 \forall \omega$) and we can see from Figure 7-9 and Figure 7-10 that it is satisfied. We can also determine the manipulations required for a unit disturbance and the resulting magnitude plots are shown in Figure 7-14. The magnitude is smaller than one across the entire frequency range, so there are no saturation problems.

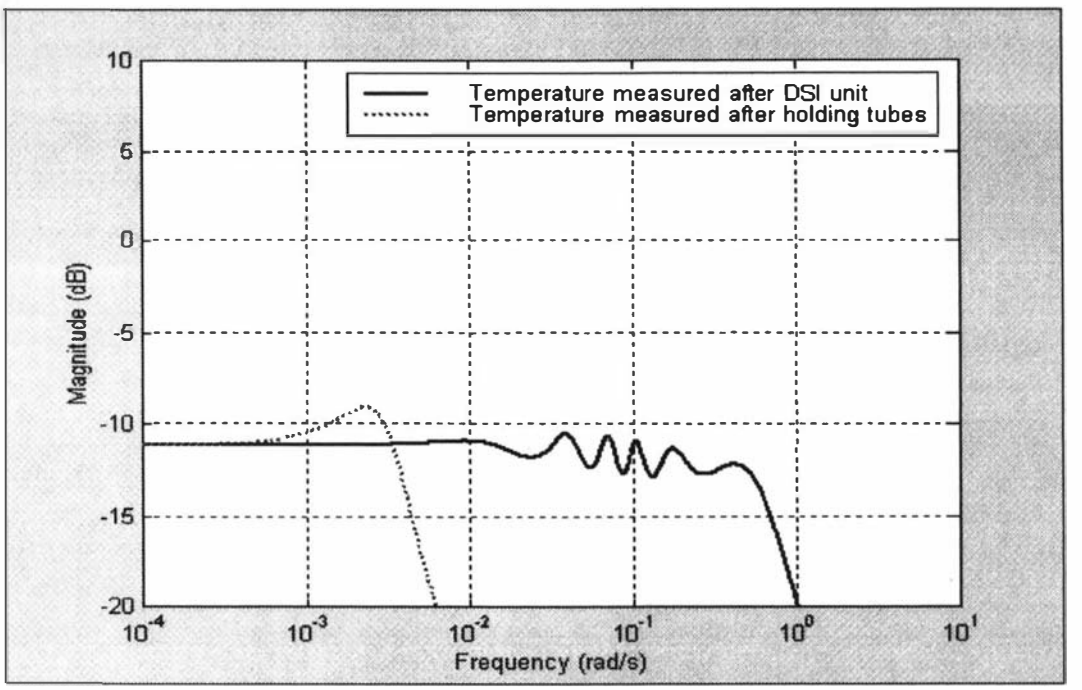

Figure 7-14 : Closed loop manipulations required for a unit disturbance.

7.4.4) MVR section control

Here we are interested in the control of the MVR evaporator section evaporation temperature (T_{e1}) and the product dry matter (w_{p5}). In the previous section we showed that decentralised controllers could be used if the process cross-over frequencies were above 0.01 rad/s. Furthermore, the results of the static *RGA* analysis shows that the correct control loop pairings are T_{e1}/M_c and w_{p5}/N_{comp}. Figure 7-15 shows the MVR evaporator section, with the temperature and product dry matter control loops.

MVR section temperature

The MVR evaporator temperature can be controlled using a cascade controller connected with the preheat plate heat exchanger. Earlier we calculated the *RGA* by considering the heat exchanger condensate flow (M_c) as the manipulated variable. However, the cascade controller in Figure 7-15 provides better disturbance rejection for the plate heat exchanger outlet temperature. The set-point for the outlet temperature controller (T_{mcsp}) is then the manipulated variable for the MVR evaporator temperature control loop. In Chapter 4 we developed the linear state space representation for the MVR evaporator section. This includes the transfer function between the preheat condenser inlet temperature (T_{mcsp}) and the evaporator temperature (T_{e1}). The resulting

Bode plot for this transfer function is shown in Figure 7-16. It should be remembered that this transfer function neglects the preheat plate heat exchanger dynamics. These have been neglected because of the disturbance rejection capabilities of the plate heat exchanger temperature control loop.

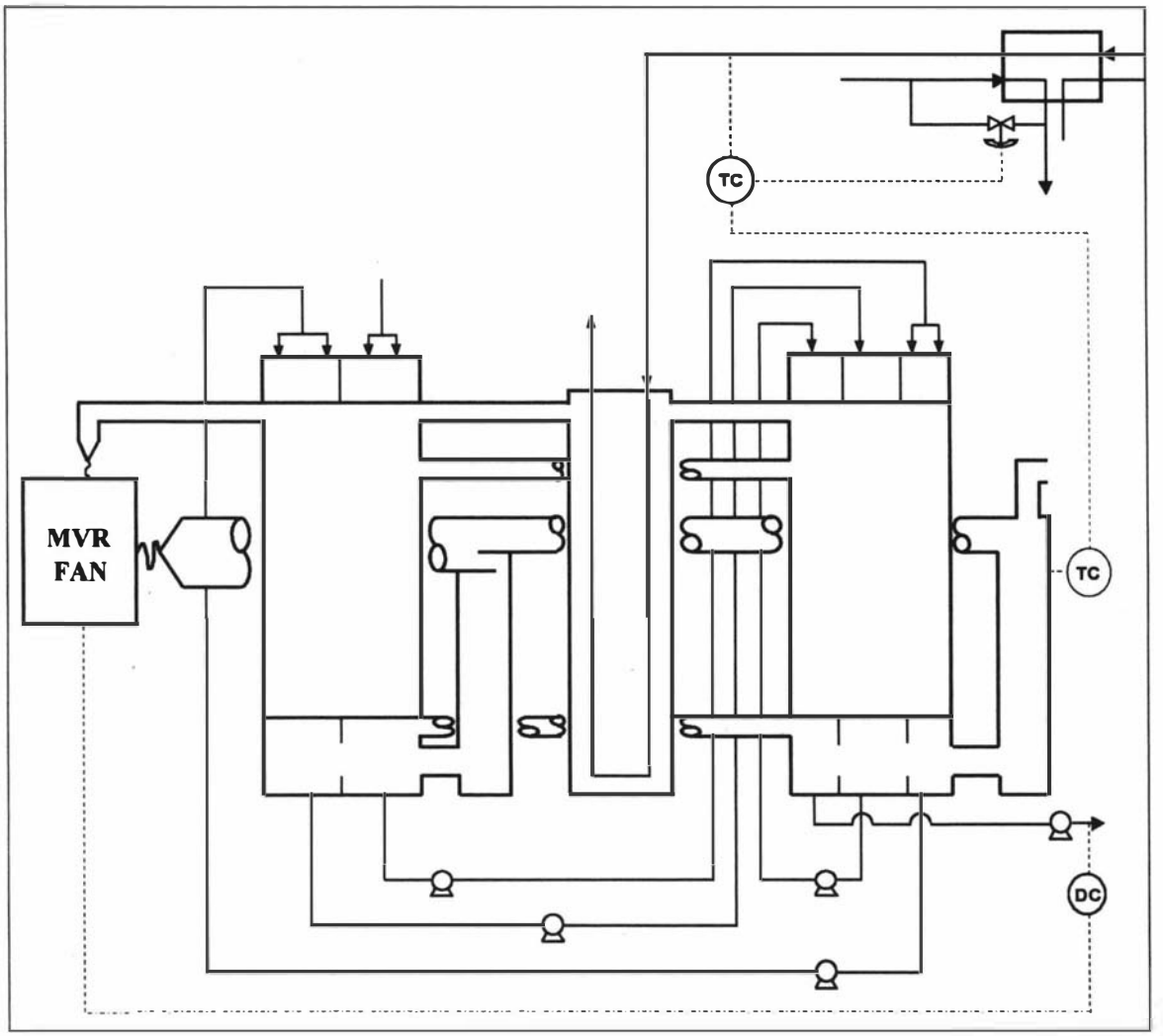

Figure 7-15 : The MVR evaporator section density (DC) and temperature (TC) control loops.

There are not many direct disturbances to the MVR evaporator section. In fact, the control loops for the preheat plate heat exchanger and DSI unit temperature would suggest that there are no disturbances. Strictly the feed temperature disturbances are removed by the heat exchanger outlet temperature control loop. In addition the potential steam pressure disturbances are removed by the DSI unit temperature control loop. However, there are many indirect disturbances which cause changes in the DSI preheat section flash vessel temperatures. For example the presence of air in the flash vessels was shown in Chapter 6 to cause changes in their temperature. As a result, the preheat section flash vessel temperatures can be a significant disturbance to the MVR evaporator section temperature.

We now consider the MVR evaporator section in isolation from the DSI preheat section. In Chapter 4 the linear dynamic model was developed by combining the DSI preheat section with the MVR evaporator section. However, for the consideration of the MVR evaporator section temperature control, we consider the MVR evaporator section in isolation. This is done to simplify the analysis and to make the flash vessel temperatures a disturbance to the evaporator. The transfer functions shown in Figure 7-16 are for the MVR evaporator section and do not include the feedback through the DSI preheat section.

The phase cross-over frequency of the $\frac{T_{e1}(s)}{T_{mcsp}(s)}$ transfer function is determined from Figure 7-16 as 0.3 rad/s. Figure 7-16 also shows the Bode plot for the $\frac{T_{e1}(s)}{T_{ph2}(s)}$ transfer function, from which we can determine a gain cross-over frequency of 0.01 rad/s. This is a very low frequency and more importantly it is considerably lower than the process transfer function phase cross-over frequency. As a result, we do not expect there to be any disturbance rejection problems with this control loop. We can confirm this by calculating the closed loop transfer function. Choosing the controller parameters $\tau_I = 100\ s$ and $K_c = 5$, we can determine the disturbance rejection criteria and this is plotted in Figure 7-18. Clearly the gain is low across the frequency range and this reflects the good disturbance rejection characteristics of the control loop.

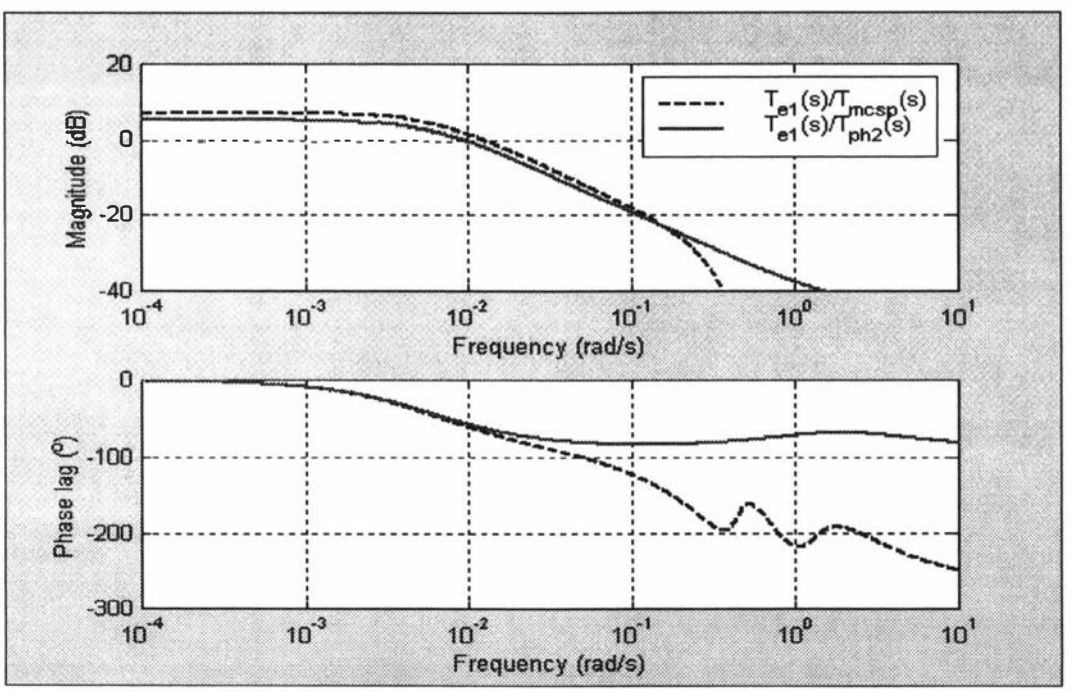

Figure 7-16 : Bode plots for the MVR evaporator temperature transfer functions.

The potential problem of controller input saturation can be investigated using the criteria of Section 7.2 (i.e., $|G(j.\omega)| \geq |G_d(j.\omega)| - 1$ at frequencies where $|G_d(j.\omega)| > 1$). Figure 7-16 shows that the process transfer function gain is larger than the disturbance gain at frequencies below 0.25 rad/s. This is consistent with the criteria and therefore we do not expect any controller saturation problems. We can confirm this result by determining the closed loop manipulations

required for a unit disturbance, which are shown in Figure 7-19. Clearly the manipulations are small and so no serious saturation problems will occur.

MVR product dry matter

For the product dry matter control loop, the disturbance is the feed dry matter (w_{fc2}) and the manipulated variable is the MVR compressor speed (N_{comp}). In Chapter 4 we developed the state space representation of the MVR evaporator. Using the linear dynamic model we can determine the Bode plots between the MVR compressor speed (N_{comp}), the feed dry matter (w_{fc2}) and the product dry matter (w_{p5}). The model combines the DSI preheat section with the MVR evaporator section, but the feedback through the plate heat exchanger is neglected. It should also be remembered that the model considers the entire MVR evaporator as a single pass, whereas it actually contains five passes. Later we show that this assumption causes some differences in the process dynamic response. However, the basic conclusion of the controllability analysis is the same when the five passes are modelled as a single pass.

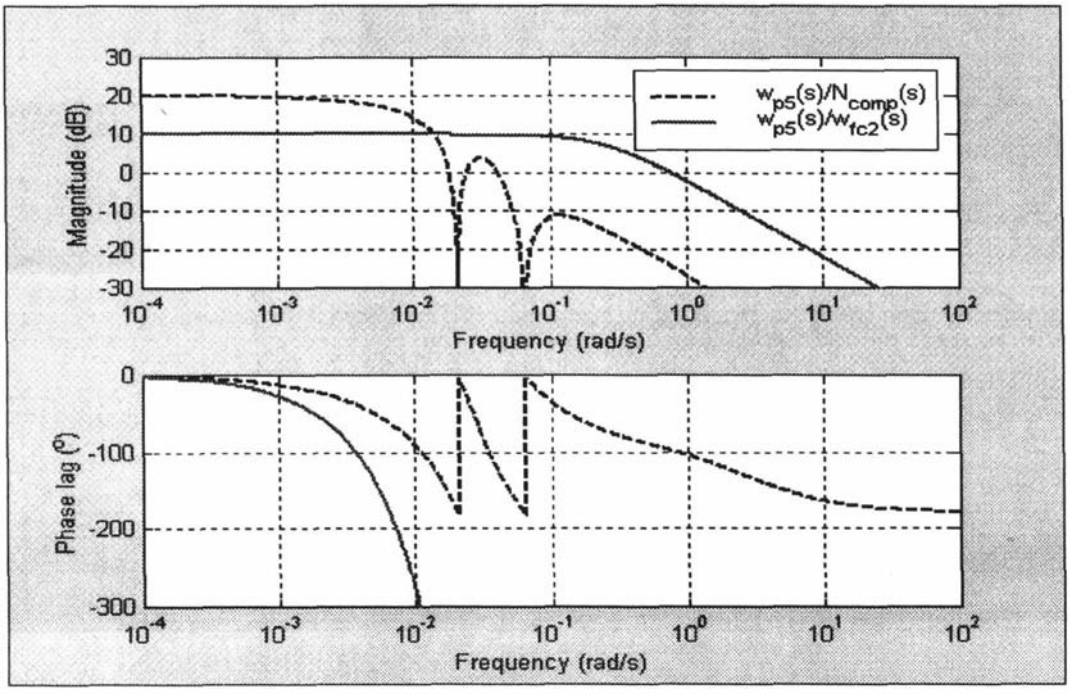

Figure 7-17 : Bode plots for the MVR evaporator product dry matter transfer functions.

The Bode plots for the process and disturbance transfer functions (i.e., $\frac{w_{p5}(s)}{N_{comp}(s)}$ and $\frac{w_{p5}(s)}{w_{fc2}(s)}$) are shown in Figure 7-17. The $\frac{w_{p5}(s)}{N_{comp}(s)}$ transfer function contains the unusual $G_{tubes}(s)$ transfer function and this is clearly seen from the Bode plot. A critically important aspect of the $G_{tubes}(s)$ transfer function is that it determines the phase crossover frequency for the dry matter control loop. It was shown in Chapter 2 that the $G_{tubes}(s)$ transfer function has explicit magnitude and phase lags given by equation (7.7).

$$|G_{tubes}(j.\omega)| = \frac{2}{\tau_e.\omega}\sin\left(\frac{\tau_e.\omega}{2}\right), \qquad \angle G_{tubes}(j.\omega) = -\frac{\tau_e.\omega}{2} \tag{7.7}$$

Where, ω = frequency. (rad/s)
τ_e = falling film residence time. (s)

Equation (7.7) shows that the phase lag increases proportionally with the falling film residence time. Consequently the MVR evaporator, with five passes and very long evaporator tubes, has a very low phase crossover frequency. From Figure 7-17 we can see that the phase crossover frequency is 0.02 rad/s. The Bode plot for the disturbance transfer function $\frac{w_{p5}(s)}{w_{fc2}(s)}$ is also shown in Figure 7-17. We can see that it has a very high gain crossover frequency of 0.8 rad/s, which is considerably larger than the open loop phase cross-over frequency. As a result, we do not expect the product dry matter control loop to provide adequate disturbance rejection. We can confirm this result by determining the closed loop transfer function. We will use the controller parameters $\tau_i = 200\ s$ and $K_c = 0.25$ and Figure 7-18 shows the disturbance rejection criteria. It is clearly large across the entire frequency range and therefore we can conclude that the dry matter control loop will not provide adequate disturbance rejection.

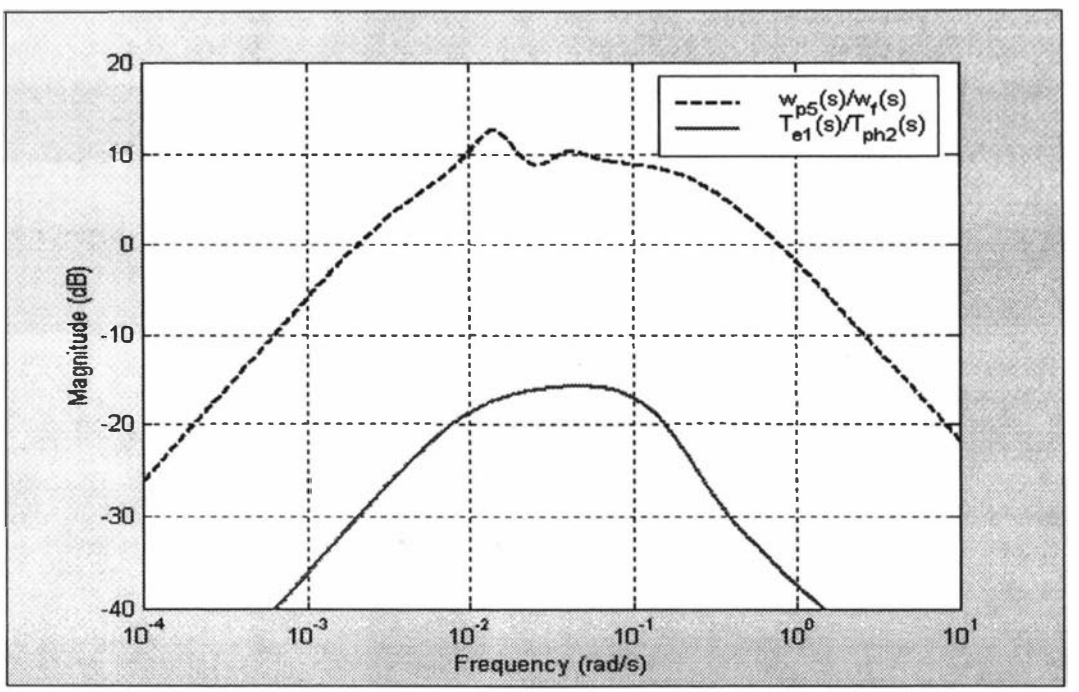

Figure 7-18 : Disturbance rejection criteria for the MVR evaporator section temperature and dry matter control loops.

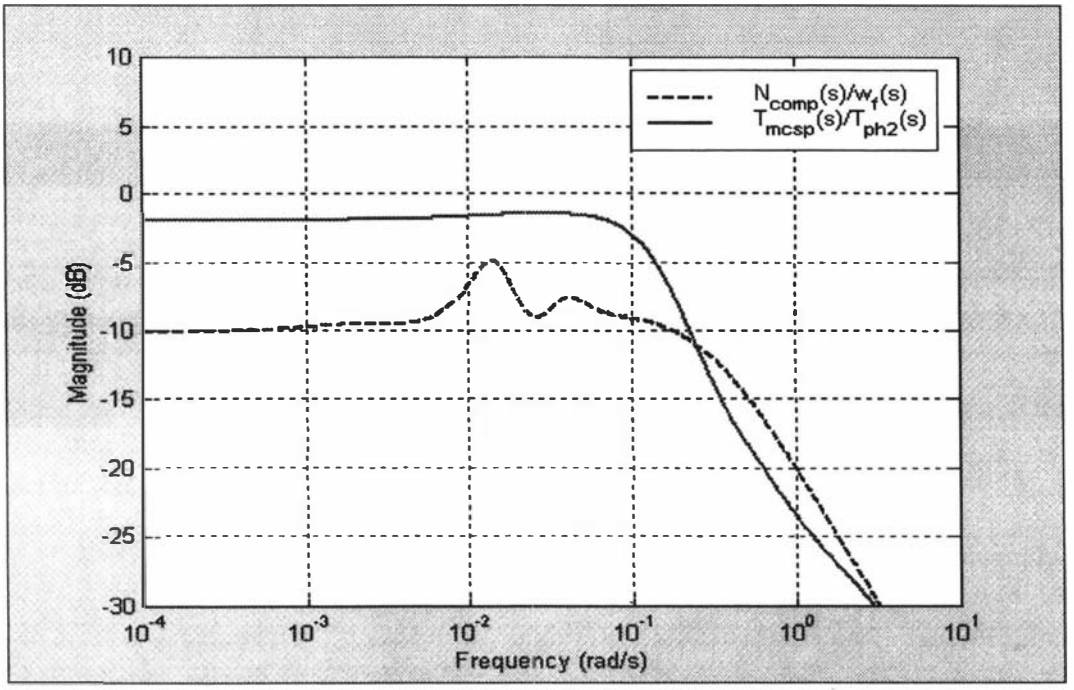

Figure 7-19 : Closed loop manipulations required for a unit disturbance.

The potential for controller input saturation can also be investigated for the dry matter control loop. From Figure 7-17 we can see that the process transfer function gain is larger than the disturbance gain at low frequencies. This suggests that there will not be any saturation problems. We can confirm this by determining the closed loop controller manipulations, for a unit dry matter disturbance. Figure 7-19 shows these results and clearly there are no saturation problems.

It is interesting to consider the cause of the dry matter disturbance rejection problem. The open loop dry matter disturbance transfer function is given by equation (7.8). This has a large gain, because the evaporation process means the product mass flow is considerably smaller than the feed flow. For the MVR evaporator section the ratio $\frac{M_f^0}{M_{p5}^0}$ is approximately 3.5. Additionally the distribution plate time constant is comparatively small because this minimises the residence time in the system. Evaporators are designed so that the milk has a narrow range of residence time, because this reduces the exposure of the milk to high temperatures (Fergusson, 1989). As a result, the disturbance transfer function has a very high gain and a high gain cross-over frequency.

$$\frac{w_{p5}(s)}{w_{fc2}(s)} = \frac{M_f^0}{M_{p5}^0} \frac{e^{[-(\tau_h+\tau_\alpha)s]}}{[\tau_{wd}.s+1]} \qquad (7.8)$$

Where, M_f^0 = feed mass flow to the evaporator plant, at steady state. (kg/s)

M_{p5}^0 = product mass flow from the MVR evaporator section, at steady state. (kg/s)

τ_h = DSI preheat section holding tube time delay. (s)

τ_{et} = total falling film residence time in the MVR evaporator section. (s)

τ_{wd} = distribution plate time constant. (s)

We showed earlier that the process transfer function for the dry matter control loop has a low phase cross-over frequency. This was caused by the large falling film residence time of the MVR evaporator section. Equation (7.7) shows that the falling film residence time directly affects the phase lag of the $\frac{w_{ps}(s)}{N_{comp}(s)}$ transfer function. Industrial evaporators in the Dairy industry tend to have large falling film residence times because of the design requirements. A primary design concern is the falling film liquid loadings. These must be larger than the minimum required for a stable falling film. This is commonly achieved by using long evaporator tubes, with the evaporator separated into multiple passes. Clearly this causes the large falling film residence times, which restricts the controller bandwidth and thereby contributes to the dry matter disturbance rejection problem.

Multiple-passes

The MVR evaporator section contains five falling film passes. In Chapter 4 we developed the linear dynamic model by assuming that the multiple passes could be modelled as a single pass. Here we shall investigate this assumption by determining the impact of multiple passes on the dynamic response. We will consider a simple two pass configuration, rather than the five passes of the Evaporator A MVR section. The impact of multiple passes can be understood with a two pass model and it is considerably simpler than the complete five pass model.

The transfer functions from the manipulated variables to the evaporating temperature (T_{e1}) and temperature difference (ΔT) are determined by the energy balances. These are the same for both the single and multiple pass cases, because we have assumed constant evaporating overall heat transfer coefficients and negligible boiling point elevation. Therefore we only need consider the transfer function from the evaporator temperature difference (ΔT) to the product mass flow (M_{p2}) and dry matter (w_{p2}).

The equations for a two pass system are given by the following.

$$M_{p1}(t)=M_{d1}(t-\tau_{e1})-M_{tube1}(t),\quad w_{p1}(t)=\frac{M_{d1}(t-\tau_{e1}).w_{d1}(t-\tau_{e1})}{[M_{d1}(t-\tau_{e1})-M_{tube1}(t)]},\quad \tau_{e1}\frac{dM_{tube1}(t)}{dt}=\frac{q_{shell1}(t)}{\lambda}-\frac{q_{shell1}(t-\tau_{e1})}{\lambda} \qquad (7.9)$$

$$M_{p2}(t)=M_{d2}(t-\tau_{e2})-M_{tube2}(t),\quad w_{p2}(t)=\frac{M_{d2}(t-\tau_{e2}).w_{d2}(t-\tau_{e2})}{[M_{d2}(t-\tau_{e2})-M_{tube2}(t)]},\quad \tau_{e2}\frac{dM_{tube2}(t)}{dt}=\frac{q_{shell2}(t)}{\lambda}-\frac{q_{shell2}(t-\tau_{e2})}{\lambda} \qquad (7.10)$$

Where $q_{shell1}(t)=U_{s1}.A_{s1}[T_s(t)-T_e(t)]$ and $q_{shell2}(t)=U_{s2}.A_{s2}[T_s(t)-T_e(t)]$ are the energy flows to the falling films in each pass. These equations can be linearised to give the following relationship between the temperature difference (ΔT), the mass flow from the distribution plate (M_{d1}), the dry matter from the distribution plate (w_{d1}) and the product dry matter (w_{p2}).

$$w_{p2}(s)=\frac{\beta_{w1}.\beta_{w2}e^{-(\tau_{e1}+\tau_{e2})s}}{[\tau_{wd2}.s+1]}w_{d1}(s)-\left[\frac{\beta_{Q2}}{\tau_{hd2}.s+1}+\frac{\beta_{Q1}.\beta_{w2}}{\tau_{wd2}.s+1}\right]e^{-(\tau_{e1}+\tau_{e2})s}M_{d1}(s)+\left[\frac{\beta_{M1}.\beta_{w2}}{\tau_{wd2}.s+1}+\frac{\beta_{Q2}}{\tau_{hd2}.s+1}\right]e^{-\tau_{e2}.s}M_{tube1}(s)+\beta_{M2}M_{tube2}(s) \quad (7.11)$$

Where, $\beta_{w1}=\frac{M^0_{d1}}{[M^0_{d1}-M^0_{tube1}]}$, $\beta_{w2}=\frac{M^0_{d2}}{[M^0_{d2}-M^0_{tube2}]}$, $\beta_{Q1}=\frac{w^0_{d1}M^0_{tubes}}{[M^0_{d2}-M^0_{tube2}]^2}$, $\beta_{Q2}=\frac{w^0_{d2}M^0_{tube2}}{[M^0_{d2}-M^0_{tube2}]^2}$,

$\beta_{M1}=\frac{M^0_{d1}.w^0_{d1}}{[M^0_{d1}-M^0_{tube1}]^2}$, and $\beta_{M2}=\frac{M^0_{d2}.w^0_{d2}}{[M^0_{d2}-M^0_{tube2}]^2}$; $\tau_{hd}=\frac{Q^0_{p1}A_{d2}}{g(C_D.A_{h2})^2}$ and $\tau_{wd}=\frac{h^0_{d2}A_{d2}}{Q^0_{p1}}$ are the time constants of the second distribution plate and $M_{tube1}(s)$ and $M_{tube2}(s)$ are related to $\Delta T(s)$ by the transfer functions $\frac{U_{s1}.A_{s1}[1-e^{-\tau_{e1}.s}]}{\tau_{e1}.s}$ and $\frac{U_{s2}.A_{s2}[1-e^{-\tau_{e}.s}]}{\tau_{e2}.s}$ respectively.

We are primarily interested in the transfer function between the evaporator temperature difference and the product dry matter. With substitution and rearrangement this is given by the following.

$$\frac{w_{p2}(s)}{\Delta T(s)}=\left[\frac{\beta_{M1}.\beta_{w2}}{\tau_{wd2}.s+1}+\frac{\beta_{Q2}}{\tau_{hd2}.s+1}\right]e^{-\tau_{e2}.s}\frac{U_s.A_{s1}[1-e^{-\tau_{e1}.s}]}{\tau_{e1}.s}+\beta_{M2}\frac{U_s.A_{s2}[1-e^{-\tau_{e2}.s}]}{\tau_{e2}.s} \quad (7.12)$$

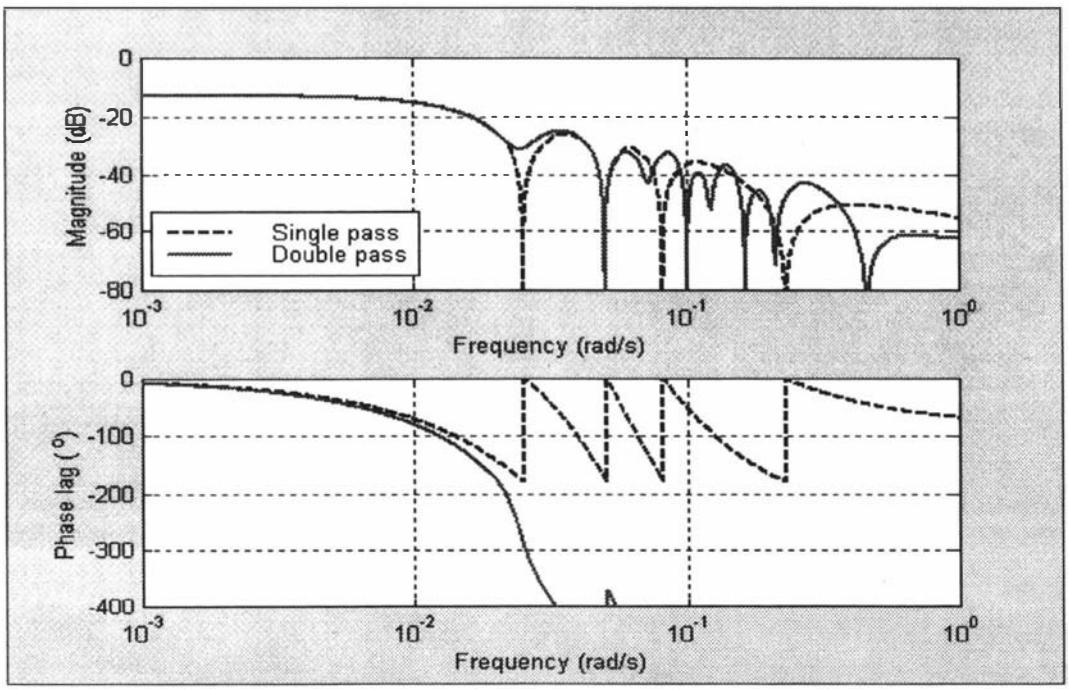

Figure 7-20 : Bode plots for single and double pass transfer functions.

Using this transfer function we can determine the Bode plots for a two pass and a single pass evaporator. We will consider a single pass configuration with a total surface area of 5055 m^2 and a double pass with 3000 m^2 in the first pass and 2055 m^2 in the second pass. The heat transfer coefficients are the same as for the single pass model and the residence times are each half of that for the single pass. The second distribution plate is assumed to have similar time constants

(τ_{hd} and τ_{wd}) to those of the single pass model. The resulting Bode plots are shown in Figure 7-20. These Bode plots were determined using a ninth order approximations to the falling film pure delays. The single pass shows the unusual impact of the $G_{tubes}(s)$ transfer function, but the double pass configuration has quite a different Bode plot. There is more phase lag in the double pass case and it does not oscillate between 0 and 180 °, as the single pass does. This suggests that there is more 'effective' delay in the double pass case.

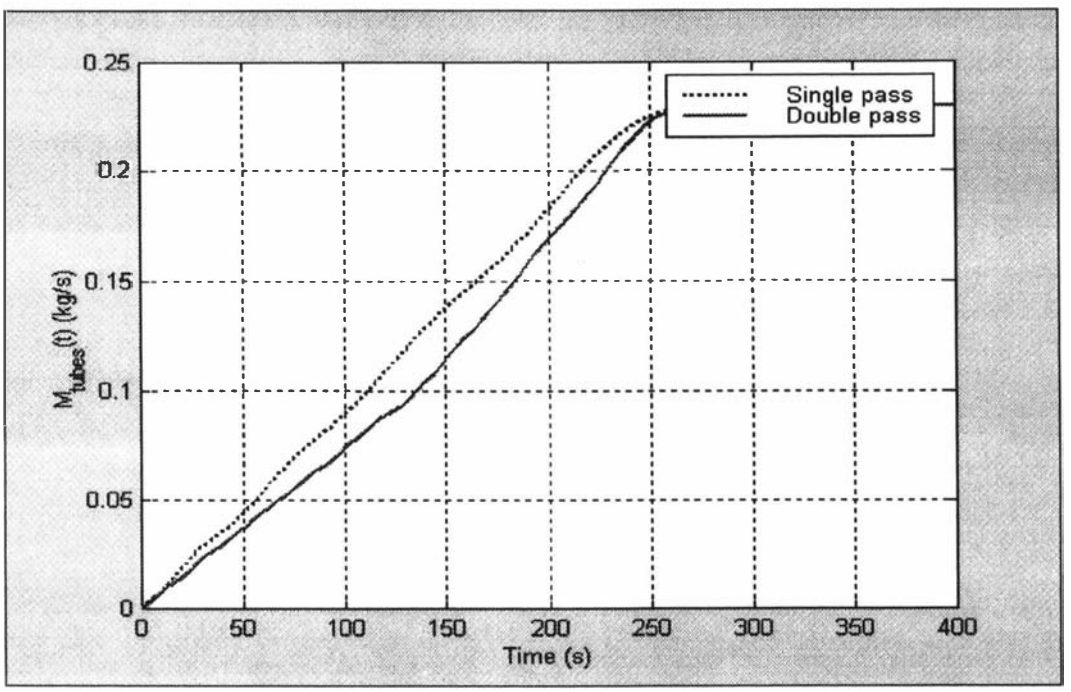

Figure 7-21 : Step responses for the single and double pass $\frac{w_{p2}(s)}{\Delta T(s)}$ transfer functions.

The longer 'effective' delay can be observed in the step response comparison in Figure 7-21. Although both configurations reach their new static equilibrium states in the same time, the double pass case initially responds less than the single pass case. This causes the increased 'effective' delay, which is shown in the Bode plot of Figure 7-20.

It was found earlier that the dry matter control loop would not provide adequate disturbance rejection. This problem was caused by the relative sizes of the process phase-crossover frequency and the disturbance gain cross-over frequency. The phase cross-over frequency was considerably smaller than the gain cross-over frequency. However, we have shown here that multiple passes will cause the phase cross-over frequency to be lower. Hence this makes the control loop disturbance rejection even worse (Winchester and Marsh, 1999).

We have considered a situation with most of the heat transfer area in the first pass. This is the typical situation with industrial evaporators, because of concerns with the falling film liquid loadings. The Evaporator A plant also follows this trend, because each succeeding evaporator pass has less heat transfer surface area than the previous one.

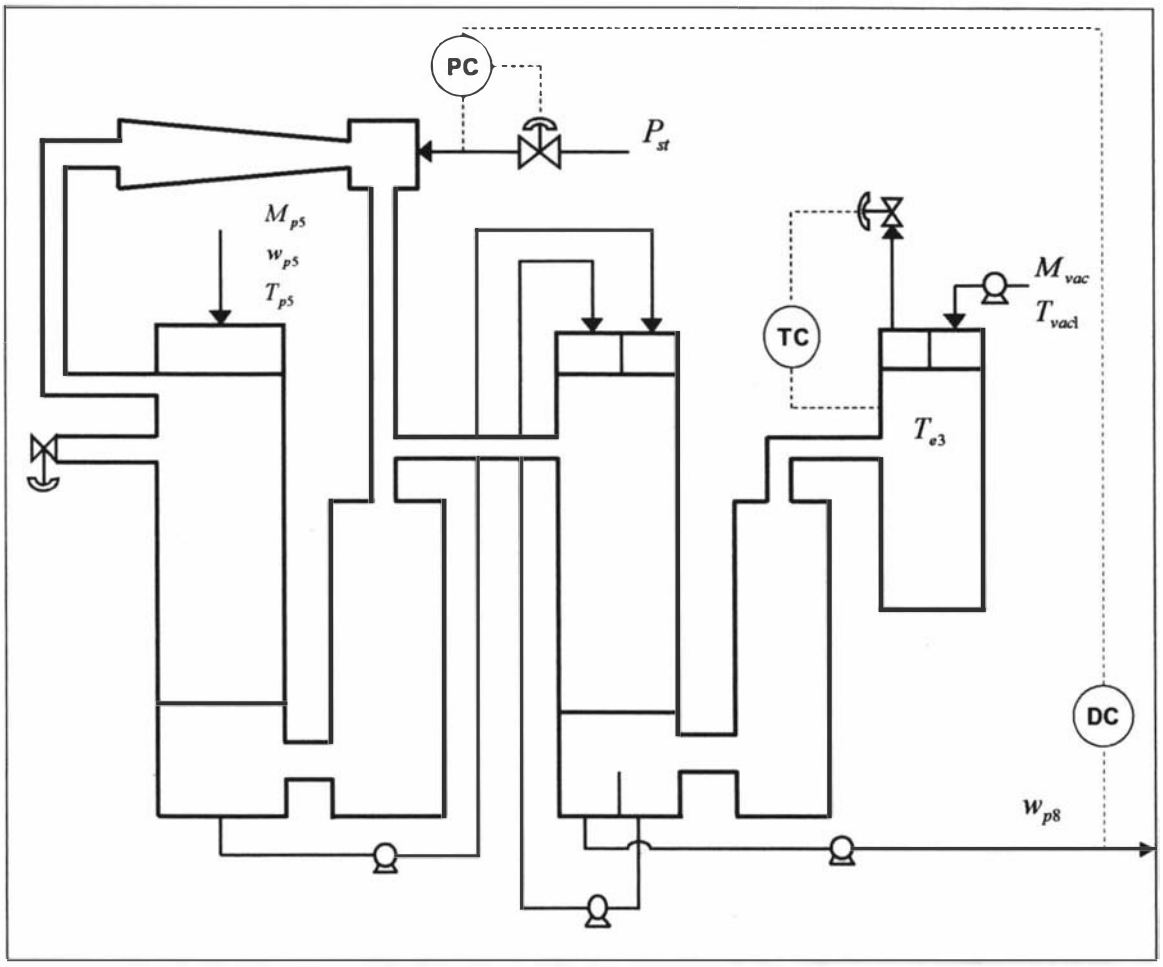

Figure 7-22 : TVR evaporator temperature (TC), density (DC) and pressure (PC) control loops.

7.4.5) TVR Section Control

Here we are interested in the control of the TVR final effect temperature (T_{e3}) and the product dry matter (w_{p8}). In Section 7.3, it was shown that these variables could be controlled with decentralised controllers if the phase cross-over frequencies were larger than 0.01 rad/s. Furthermore the static *RGA* analysis showed that the correct decentralised control loop pairings are w_{p8} / P_{sp} and T_{e3} / M_{vac}. Figure 7-22 shows the TVR evaporator section with these two decentralised control loop configurations.

TVR steam pressure

The steam supply for the TVR compressor is 9 bar saturated steam. This steam pressure supply can vary and so it is a disturbance to the Evaporator A plant. Figure 7-22 shows the TVR compressor with its steam pressure control loop. The set-point for the steam pressure control loop acts as the output for the product dry matter control loop. As a result, we need to consider the steam pressure control loop, before considering the product dry matter control loop.

The steam pressure control loop will act quickly, because the pressure responds at the speed of sound to valve changes. Consequently the process response should be very fast and a short

controller integral time can be used. We would expect the response to be in the order of seconds and that an integral time of around 5 – 20 seconds would be appropriate. This has been verified on the Evaporator A plant, when the control loop was tuned using the Ziegler-Nichols method.

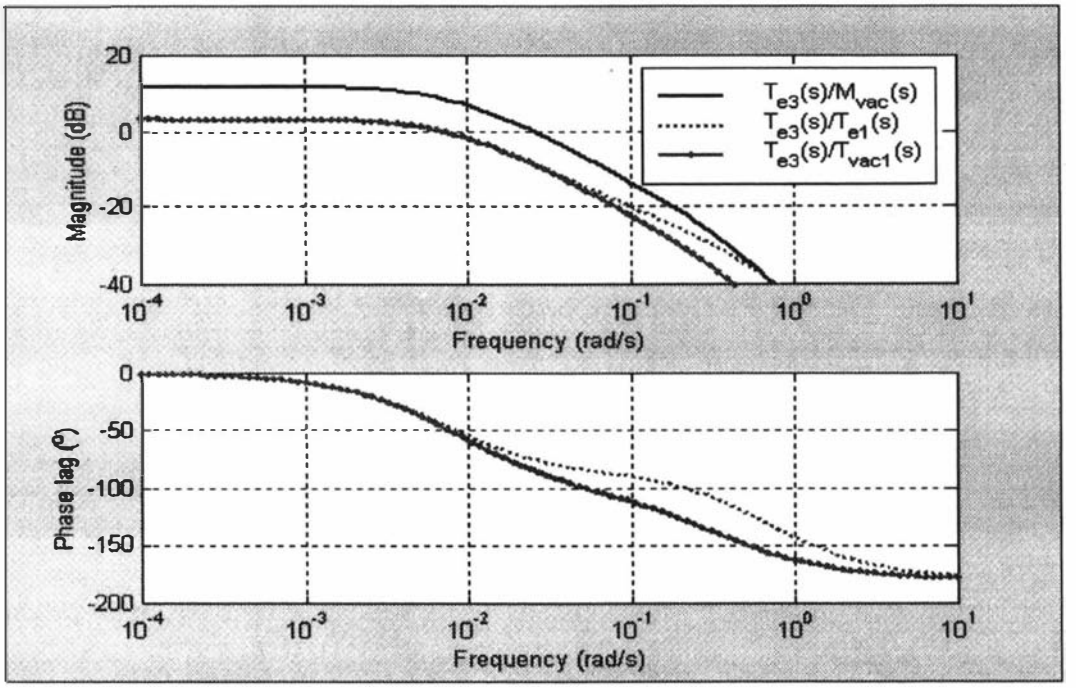

Figure 7-23 : Bode plots for the third effect temperature transfer functions.

Third effect temperature

Figure 7-22 shows the control loop for the third effect temperature (T_{e3}), by manipulation of the cooling water flow (M_{vac}). In Chapter 4 we developed the linear state space representation for the TVR evaporator section. The disturbances are the MVR evaporator section product temperature (T_{e1}) and the cooling water supply temperature (T_{vac1}). We are interested in the control loops ability to reject disturbances. The Bode plots for the transfer functions $\frac{T_{e3}(s)}{T_{e1}(s)}$ and $\frac{T_{e3}(s)}{T_{vac1}(s)}$ are shown in Figure 7-23 along with that for the $\frac{T_{e3}(s)}{M_{vac}(s)}$ transfer function. Both the $\frac{T_{e3}(s)}{T_{e1}(s)}$ and $\frac{T_{e3}(s)}{T_{vac1}(s)}$ transfer functions have very similar Bode plots, with a low gain cross-over frequency of 0.007 rad/s. The phase cross-over frequency for the $\frac{T_{e3}(s)}{M_{vac}(s)}$ transfer function is shown Figure 7-23 in to be infinity. In practice the neglected dynamics due to valves and pumping delays will cause additional phase lag at high frequencies. This means that the real crossover frequency is not infinity and so we have taken the phase cross-over frequency to be 0.7 rad/s. This is considerably larger than the gain cross-over frequencies and suggests that the controller will be able to reject disturbances.

We are also interested in the closed loop disturbance transfer function. The controller parameters will be chosen as $\tau_i = 100\text{s}$ and $K_c = 10$. From these we can determine the disturbance rejection criteria and this is shown in Figure 7-25. Clearly the gain is low across the entire frequency range and this confirms the good disturbance rejection capabilities of the control loop.

In Section 7.2 we discussed the criteria for input saturation (i.e., $|G(j.\omega)| \geq |G_d(j.\omega)|-1$ at frequencies where $|G_d(j.\omega)|>1$). From Figure 7-23 we can see that the disturbance transfer functions $\frac{T_{e3}(s)}{T_{vac1}(s)}$ and $\frac{T_{e3}(s)}{T_{e1}(s)}$ have smaller gains than the process transfer function $\frac{T_{e3}(s)}{M_{vac}(s)}$. This suggests that there will be no saturation problems. We can confirm this by determining the closed loop transfer function between the cooling water temperature disturbance (T_{vac1}) and the manipulated controller water flow (M_{vac}). With the controller parameters, used to calculate the results in Figure 7-25, we can calculate the closed loop cooling water manipulations. Figure 7-26 shows the Bode magnitude plot of the input manipulation transfer function $\frac{M_{vac}(s)}{T_{vac1}(s)}$ vs frequency. Clearly the manipulations are small and this confirms that there are no saturation problems.

Dry matter loop

A cascade controller configuration is used for the dry matter loop because of the possibility of raw steam pressure disturbances. In Chapter 4 we developed the linear state space representation for the TVR evaporator section. The disturbance is the MVR evaporator section product dry matter (w_{p5}) and the manipulated variable is the TVR compressor steam pressure set-point (P_{sp}). Therefore we are interested in the transfer functions from the TVR steam pressure set-point (P_{sp}) and the feed dry matter (w_{p5}) to the product dry matter (w_{p8}). The Bode plots for these transfer functions are shown in Figure 7-24. The $\frac{w_{p8}(s)}{P_{sp}(s)}$ transfer function neglects the dynamics of the TVR steam pressure controller because these are fast.

The phase cross-over frequency for the $\frac{w_{p8}(s)}{P_{sp}(s)}$ transfer function is quite low at 0.02 rad/s and this is caused by the large falling film residence times. A similar low phase cross-over frequency was determined for the $\frac{w_{p5}(s)}{N_{comp}(s)}$ transfer function, for the MVR evaporator section product dry matter control loop. We are also interested in the gain cross-over frequency of the $\frac{w_{p8}(s)}{w_{p5}(s)}$ transfer function and Figure 7-24 shows that this is 0.3 rad/s. This is higher than the $\frac{w_{p8}(s)}{P_{sp}(s)}$ transfer function phase cross-over frequency and therefore we expect the product dry matter

control loop to have disturbance rejection problems. We can confirm this result by choosing PI controller parameters and determining the closed loop transfer function for the product dry matter control loop. We will use $\tau_i = 200\text{s}$ and $K_c = 0.1$ for the controller parameters and the resulting disturbance rejection criteria is plotted in Figure 7-25.

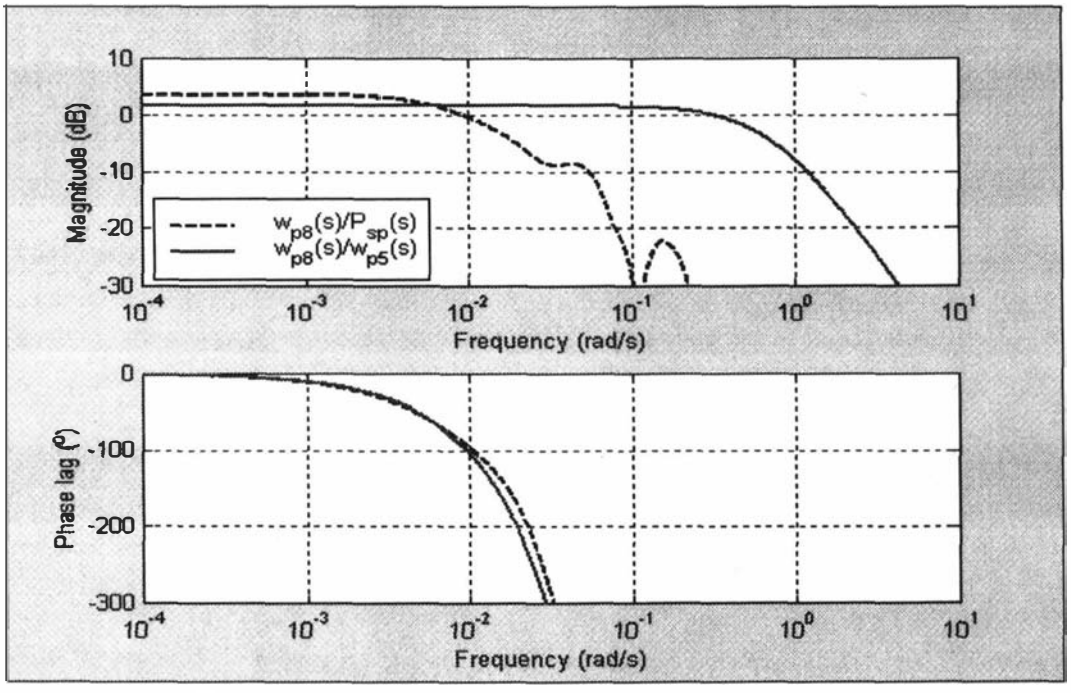

Figure 7-24 : TVR evaporator product dry matter transfer function Bode plots.

We are now interested in the controller input saturation. Figure 7-26 shows that the $\frac{w_{p8}(s)}{P_{sp}(s)}$ transfer function has larger Bode magnitudes than the $\frac{w_{p8}(s)}{w_{p5}(s)}$ transfer function, at low frequencies. Given the controller input saturation criteria (i.e., $|G(j.\omega)| \geq |G_d(j.\omega)| - 1$ for frequencies where $|G_d(j.\omega)| > 1$) this suggests that there will be no saturation problems at low frequencies. This result can be confirmed by determining the closed loop input manipulations required for a unit dry matter disturbance. Figure 7-26 shows the closed loop $\frac{P_{sp}(s)}{w_{p5}(s)}$ transfer function and clearly the magnitude is relatively low, which confirms that there will not be any input saturation problems.

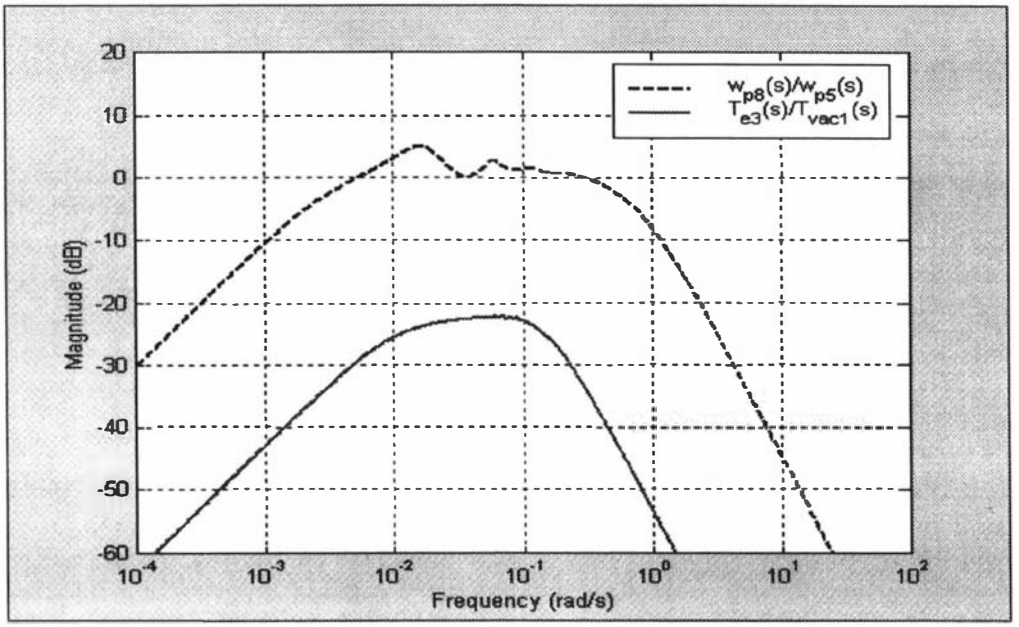

Figure 7-25 : Closed loop Bode magnitude plots for the dry matter and temperature control loops.

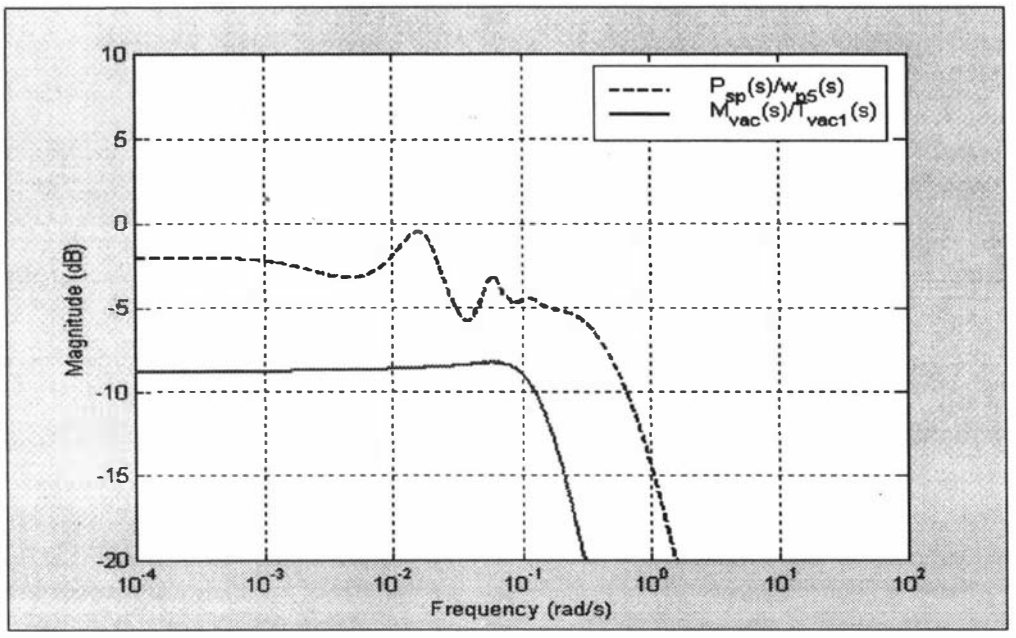

Figure 7-26 : Closed loop manipulations required for a unit increase in the disturbances.

From the above we can conclude that there are difficulties with the control of the TVR product dry matter. Specifically feed dry matter disturbances will not be adequately rejected by the control loop. The reasons for this are the same as for the MVR evaporator dry matter loop. Very little mixing occurs in the evaporator and the evaporation process amplifies the disturbances. Also the relatively long falling film residence times mean the $\frac{w_{p8}(s)}{P_{sp}(s)}$ transfer function has a low phase cross-over frequency and this restricts the controller band-width.

7.5) Conclusions

In this chapter we have investigated the controllability of the Evaporator A plant at Kiwi Co-op Dairies. We aimed to investigate the multi-variable process nature and the de-centralised controller disturbance rejection capabilities. The linear dynamic and static models, developed in Chapter 4, were used and the investigation methodology was discussed in Section 7.2.

In Section 7.3, the process multi-variable nature was investigated, with the aim of determining if decentralised controllers could be used. These are considerably simpler than multi-variable controllers and so it is valuable to know if they are applicable. The multi-variable nature was investigated using the static and dynamic *RGA*. It was found that the process multi-variable nature was not important, provided that the product mass flow was not included as a process variable and the decentralised control loop cross-over frequencies were above 0.01 rad/s.

In Section 7.4, the process disturbance rejection capabilities were investigated. Firstly we considered the preheat plate heat exchanger outlet temperature control loop. The disturbance rejection capabilities of this loop are very important because the linear dynamic model was developed by neglecting the feedback through the plate heat exchanger. Using the transfer functions derived in Chapter 3, the heat exchanger Bode plots were determined and the decentralised control loop rejection capabilities were found to be adequate. This therefore proved that the assumption of no feedback through the plate heat exchanger was reasonable.

Following the plate heat exchanger we considered the control loop for the DSI unit temperature. The controllability of the DSI unit temperature was found to depend on the position of the DSI temperature sensor. If placed directly after the DSI unit, then adequate disturbance rejection occurs, whereas the disturbance rejection was inadequate when the temperature sensor was placed after the holding tubes. The holding tube pure delay causes a significant phase lag and the preheat system resonance effect causes large peaks in the Bode magnitude plot. Both of these effects mean that the controller with the temperature sensor after the holding tubes is inadequate. However, the possibility of fouling means that it can be difficult to maintain a temperature sensor directly after the DSI unit. A new cascade controller configuration was considered, with a surface temperature sensor directly after the DSI unit and a conventional temperature sensor after the holding tubes. This cascade controller overcame the problems of fouling, large phase lag and preheat resonance.

The MVR evaporator section temperature and product dry matter control loops were considered after the DSI preheat section. It was found that the MVR evaporator temperature control loop would provide adequate disturbance rejection. However, the MVR evaporator product dry matter control loop could not provide adequate disturbance rejection. The causes of this problem were shown to be the falling film phase lag, the large concentration ratio of the MVR evaporator and the small amount of mixing in the process.

Following the MVR evaporator section the TVR evaporator section temperature and product dry matter control loops were investigated. As with the MVR evaporator section, the TVR evaporator temperature control loop was found to provide adequate disturbance rejection, whereas the product dry matter control loop could not.

Chapter 8 : Conclusions and Recommendations

8.1) Conclusions

8.1.1) Aims

In the first section of Chapter 1 the aims of this work were listed.

1) Derive, develop and identify a model for the Evaporator A plant at Kiwi Co-op Dairies.
2) Investigate the optimisation and operation of the evaporator plant using the static version of the model.
3) Investigate the controllability of the evaporator plant using the dynamic version of the model.

8.1.2) Derivation, Development and Identification of the Model

In Chapters 2 through 4 a model for the complete Evaporator A plant was derived and developed. Various assumptions in the derivation of the model were considered and the final results were a static and linear dynamic model for the Evaporator A plant at Kiwi Co-op Dairies. Following the model development Chapter 5 considered the identification of process parameters. The identification of many static process parameters and also the important falling film residence times were successfully completed.

The model was developed with the aim of specifically applying it for the optimisation/operation and controllability studies on the Evaporator A plant at Kiwi Co-op Dairies. A static model was developed for the optimisation studies and a linear dynamic model for the controllability studies. The optimisation studies require accurate predictions of the plant operating conditions and therefore attention was focused on identifying the static model. However, the controllability studies of Chapter 7 required a less accurate model and so less attention was focused on the identification of dynamic model parameters. The exception is the falling film residence times, which were shown in Chapter 7 to have an important impact on the product dry matter control loops.

8.1.3) Evaporator Optimisation and Operation

In Chapter 6 the optimisation and operation of the Evaporator A was investigated. Two areas were considered : 1) the operation of the DSI preheat section, 2) the operating regime of the Evaporator A plant, with respect to evaporation energy costs. The DSI preheat section operational problems were discussed in Section 6.2 and the optimisation studies in Section 6.5.

The DSI preheat section studies considered the impact of air in the flash vessels, the problem of milk evaporation in the preheat holding tubes and flash vessel flooding. In Chapter 3 it was shown that the presence of air causes a temperature difference between the top and bottom of a flash vessel. These results from Chapter 3 were then used in Chapter 6 to show some of the detrimental impacts of air on the preheat section operation. The presence of air caused an increase in the required mass flow of steam and increased the temperature disturbances to the DSI unit temperature and MVR evaporator section temperature control loops.

The problems of milk evaporation in the holding tubes and flash vessel flooding were considered separately, but these problems were shown to have a close link. A design equation for sizing the back-pressure orifice plate was derived and the relation between this orifice plate and the flash vessel flooding was investigated.

In Section 6.3 a simple study was made of the expected savings due to reductions in the plant evaporation costs. This was based on the lower evaporation costs of the falling film evaporators compared to the spray dryer. Increases in the evaporator product dry matter were shown to give reductions in the plant total evaporation costs. It was estimated that a 0.01 kg/kg reduction in the evaporator product dry matter would give a $ 33,032 reduction in the plant evaporating costs.

The cost of evaporation in the entire milk powder plant can be considered as an optimisation problem with constraints. There are four operating constraints and these are the evaporation capacities, the evaporator temperatures, the falling film wetting and the concentrate dry matter. In Sections 6.3 and 6.4 of Chapter 6 methods were developed for modelling the evaporation energy costs and the operating constraints of the evaporator plant. The steady state model developed and identified in Chapters 2 through 5 was then used to calculate these operating constraints and the plant evaporation energy costs.

In Section 6.5 the complete optimisation of the Evaporator A plant was considered for three cases. The plant operation with Whole Milk was first considered and an optimum operating point found. With the optimum operating conditions (i.e., $M_f = 14.71$ kg/s, $N_{comp} = 2650$ rpm, $P_{sp} = 9$ bar, $M_{p8} = 3.83$ kg/s, $w_{p8} = 0.48$ kg/kg and $w_f = 0.125$ kg/kg) the evaporation cost is 2.99 $/Tonne of product milk concentrate. The optimum operating point is on the falling film wetting constraint. This is caused by the increase in the evaporation cost with the TVR steam pressure (P_{sp}) and the TVR product mass flow (M_{p8}). However, the uncertainty in the film wetting means that a degree of danger is associated with operating near the film wetting constraint. This has been incorporated in the optimisation by using a safety margin of 0.5 kg/s in the film wetting model.

It is interesting to compare these results with the traditional plant conditions. The danger of the film wetting constraint means that the plant operators tend to operate with the maximum TVR steam pressure and TVR product mass flow. This is done to provide the plant with the maximum obtainable film wetting safety margin. However, the optimisation studies of Chapter 6 show that this causes the plant evaporation costs to increase and so there is a direct cost of using excessively large safety margins.

8.1.4) Evaporator Controllability Studies

In Chapter 7 the controllability of the Evaporator A plant was investigated. The plant is large with many process variables but we considered six important control loops in the Evaporator A plant. These were the DSI unit temperature (T_{dsi}), the MVR evaporator section temperature (T_{e1}), the MVR product dry matter (w_{p5}), the TVR evaporator section temperature (T_{e3}), the TVR product dry matter (w_{p8}) and product mass flow (M_{p8}). In Chapter 6 it was shown that

these process variables have an important impact on the plant optimisation and product milk powder quality.

Firstly the multi-variable plant nature was investigated to determine whether there would be any control loop interactions. It was found that most of the plant control loops would decouple except for the product mass flow. The static RGA analysis showed and explained the strong interaction between the TVR product dry matter and mass flow control loops. The product dry matter control loop has a very important impact on the milk powder quality, whereas the product mass flow has less impact. This was explained in Chapter 6 by the impact of the product dry matter on the concentrate milk viscosity. With the removal of the product mass flow control loop the static RGA still suggested control loop intereactions. However, the RGA_{number} was found to reduce significantly below the static result at higher frequencies. This showed the importance of considering the dynamics, when making the multi-variable analysis. Most importantly it showed that the Evaporator A plant would not suffer from serious control loop ineractions.

In Section 7.4 the control loops were investigated using decentralised control loop analysis. The disturbance rejection capabilities of the six control loops were considered. It was found that the temperature control loops could provide adequate disturbance rejection, but the product dry matter control loops could not. The temperature control loops were used for the DSI unit, the plate heat exchanger, the MVR evaporator temperature and the TVR final effect temperature. Each provided adequate disturbance rejection although the DSI preheat section temperature control loop required temperature measurements directly after the DSI unit. A control loop using only temperature measurements after the holding tubes was found to have serious disturbance rejection problems. The product dry matter control loops for the MVR evaporator and TVR evaporator sections were found to exhibit inadequate disturbance rejection. In Section 7.4 this was shown to be caused by the large falling film residence times and the process sensitivity to feed dry matter disturbances.

8.2) Recommendations for Future Work

8.2.1) Model Derivation

There are many unresolved issues with the derivation of the Evaporator A plant model. Probably the most important is the description of the falling film. This has been described by using simple transport partial differential equations, which can be transformed into differential equations with pure delays. In Chapter 7 it was shown that these falling film delays provide a very important part of the process dynamics. Therefore an important area for future work is the investigation of the falling film models.

Another major problem is with the dynamic plate heat exchanger model. This was developed by transformation and solution of the heat exchanger partial differential equations in the Laplace Domain. However, the resulting Laplace Domain transfer functions do not represent finite order linear constant coefficient differential equations and so we cannot use them to produce state space representations. This presents a problem, which can be overcome using numerical frequency analysis. In Chapter 7 these numerical methods were used to overcome the transcendental nature of the heat exchanger equations. However, it would be valuable if the heat exchanger equations could be transformed into a state space representation using Pade approximations.

8.2.2) Model Identification

The major problem with the current work is the lack of falling film evaporation heat transfer coefficient knowledge. Ideally we need a general model that can be used to determine the heat transfer coefficients for any milk solution. This is required to study the different operating conditions of alternative milk solutions. Progress has been made at determining these for some common milk solutions, such as Whole Milk and Butter Milk. However, it would be potentially very valuable to have a general model for heat transfer coefficients in terms of the milk components. Also it is probable that nucleate boiling, which has been neglected, is significant and requires greater understanding.

Another difficulty is the plate heat exchanger heat transfer coefficients. These were not identified in the model and some calculated guesses used in the final steady state model. This neglect is justified by the small role that the heat transfer coefficients have on the important model outputs. However, it may be valuable to make a better identification of the plate heat exchanger heat transfer coefficients.

Finally many of the dynamic model parameters were not identified. The thermal inertias of the preheat flash vessels, the MVR evaporator and the TVR evaporator were not identified. These were calculated from the mass of water, milk and metal in the various sections, but the accuracy of these results may not be reliable. A justification for their neglect is the limited role that they play in the controllability studies of Chapter 7, but it may be valuable to make a better identification of these parameters.

8.2.3) Model Optimisation and Operation Studies

The work on the model optimisation is quite complete. The major difficulty lies with the lack of understanding of falling film evaporating heat transfer coefficients. Without accurate models, for these in terms of the milk solution components, then the optimisation studies cannot be applied to general milk solutions. An additional problem is the assumption of convection boiling. Strictly milk solutions will boil with a combination of convection and nucleate boiling and therefore the heat transfer coefficients will also depends on the driving temperature difference.

Another problem is the falling film wetting models. A variety of sources were used to develop models for predicting the onset of film instability, but there is still some uncertainty in these predictions. The work in Chapter 6 required a safety margin of 0.5 kg/s and this reflects the uncertainty in the film wetting predictions. The importance of this uncertainty is shown by the position of the optimum operating condition. This was positioned on the film wetting constraint and therefore the film wetting constraint is a vitally important part of the optimisation.

A final problem with the optimisation studies is the MVR compressor power constraint. The power constraint was taken as 500 kW for the studies of Chapter 6. Because of the shortage of manufacturing specifications, the position of this constraint is not completely known. Although the optimum operating condition is not near the MVR compressor power constraint, it would be preferable to have a greater understanding of this constraint.

8.2.4) Model Controllability Studies

The controllability studies for the Evaporator A plant are quite complete. The controllability results were determined using the linear dynamic model developed in Chapters 2-5. The accuracy of the conclusions depends on the accuracy of the dynamic model and so further work may be required to improve the model. We have shown in Chapter 7 that the falling film residence time is a dominant part of the dynamic model. As a result, it may be worthwhile making further studies into the dynamic nature of the falling film. In Chapter 2 the partial differential equations for the falling film were derived but significant assumptions were required to simplify these into a tractable form.

We have identified the problem of product dry matter disturbance rejection and explained the nature of this problem. The large evaporator falling film residence times and the process sensitivity to feed dry matter disturbances were shown to cause the controllability problems. This controllability problem is quite serious, because the product dry matter has a strong impact on the product milk powder quality and the plant evaporation costs. As a result, improvements in the product dry matter controllability should produce significant improvements in the evaporator plant operation and milk powder products. Therefore the solution of this problem is a major area for future work.

8 Nomenclature

Here we list many of the variables used in this thesis along with their numerical values. However, the numerical values for some variables have not been included. For example, generic condenser variables do not have their numerical values included. Also the values for the individual passes of the Evaporator A plant have been excluded (i.e., A_s, A_d, A_h, d and n). These are listed with the geometries in Appendix E.

The dynamic variables of the Evaporator A plant model have been denoted with additional brackets (i.e., $M_{p5}(t)$). Also the numerical values given for these variables are those determined from the steady state model calculations of Chapter 4. The static variables are denoted with the additional superscript (i.e., M^0_{p5}).

a_{comp}	Fitting coefficient for the MVR compressor map.	(= 1.68x10^{-3} m^2/s^2.rpm^2)
A_{cond}	Heat transfer surface area for the generic condenser.	(m^2)
A_{cr}	Cross sectional flow area, liquid in the generic condenser tubes.	(m^2).
A_{cs}	Cross sectional flow area, second plate heat exchanger section.	(= 0.028 m^2).
A_d	Cross sectional area of a distribution plate.	(m^2)
A_{el1}	Surface area for energy losses from the MVR evaporator effect.	(= 134 m^2)
A_{el2}	Surface area for energy losses from a TVR evaporator effect.	(= 32 m^2)
A_{el3}	Surface area for energy losses from a TVR evaporator effect.	(= 26 m^2)
A_h	Cross sectional area of holes in the distribution plate.	(m^2)
A_{hf}	Heat transfer surface area, first plate heat exchanger section.	(= 65.65 m^2)
A_{hs}	Heat transfer surface area, second plate heat exchanger section.	(= 72.15 m^2)
A_{mf}	Cross sectional flow area, first plate heat exchanger section.	(= 0.034 m^2)
A_{pre}	Heat transfer surface area of the preheat condenser.	(= 31.67 m^2)
A_s	Surface area of the evaporator tubes.	(m^2)
A_{st}	Total heat transfer surface area of the MVR evaporator tubes.	($=\sum_{i=1}^{5} A_{si}$ = 5054.7 m^2)
A_{sl1}	Surface area for energy losses from the MVR evaporator shell.	(= 194 m^2)
A_{sl2}	Surface area for energy losses from the TVR evaporator shell.	(= 30 m^2)
A_{TVR}	TVR compressor parameter.	(= 2.129x10^{-7} m.s)
A_{water}	Fitting coefficient for Antoine saturation equation.	(= 23.1748)
A_{vac}	Heat transfer surface area of the vacuum condenser.	(= 108 m^2)
A_{vap}	Fitting coefficient for Antoine saturation equation.	(= 10.5884)

A_{vf}	Cross sectional flow area, first plate heat exchanger section.	(= 0.034 m^2)
b_{comp}	Fitting coefficient for the MVR compressor map.	(= 0.415 $m^2/s^2.rpm^2$)
b_{TS}	Parameter used in the boiling point elevation model.	()
B_{TVR}	TVR compressor parameter.	(= 47 $m^{0.03}.s^{0.06}/kg^{0.03}$)
B_{water}	Fitting coefficient for Antoine saturation equation.	(= 3806.44 K)
B_{vap}	Fitting coefficient for Antoine saturation equation.	(= 3680.109 K)
c_{comp}	Fitting coefficient for the MVR compressor map.	(= -13.7 m^{-4} *1)
C_d	Discharge coefficient for the distribution plate holes.	(= 0.611)
C_{dry}	Evaporation cost per unit mass of evaporation, in the spray dryer.	($/kg)
C_p	Heat capacity.	(J/kg.°C)
C_{pcond}	Heat capacity of the liquid in the tubes of the generic condenser.	(J/kg.°C)
C_{pfat}	Heat capacity of fat.	(J/kg.°C)
C_{plact}	Heat capacity of lactose.	(J/kg.°C)
C_{pprot}	Heat capacity of protein.	(J/kg.°C)
C_{pmilk}	Heat capacity of the liquid milk.	(J/kg.°C)
C_{psalt}	Heat capacity of salt.	(J/kg.°C)
C_{pTS}	Coefficient relating the milk heat capacity and dry mass fraction.	(J/kg.°C)
C_{pw}	Heat capacity of the metal in the generic condenser tubes.	(J/kg.°C)
C_{pwater}	Heat capacity of water.	(= 4190 J/kg.°C)
C_{mvr}	Evaporation cost per unit mass of evaporation, MVR evaporator.	($/kg)
C_{tvr}	Evaporation cost per unit mass of evaporation, TVR evaporator.	($/kg)
C_{TVR}	TVR compressor parameter.	(= 0.97)
C_{water}	Fitting coefficient for Antoine saturation equation.	(= 46.36 K)
C_{vap}	Fitting coefficient for Antoine saturation equation.	(= 41.6919 K)
d_{comp}	Fitting coefficient for the MVR compressor map.	(= 6.84x10^{-3} $m^2/s^2.rpm^2$)
d	Diameter of evaporator tubes.	(m)
D_{cond}	Diameter of the generic condenser tubes.	(m)
e_{comp}	Fitting coefficient for the MVR compressor map.	(= -0.021 l/m.s.rpm)
Eff	Energy efficiency of an evaporation process.	( )
f_{comp}	Fitting coefficient for the MVR compressor map.	(= -3.09 m^{-4})
g	Acceleration due to gravity.	(= 9.81 m/s^2)
h	Heat transfer coefficient.	($W/m^2.°C$)
h_i	Tube side heat transfer coefficient for the generic condenser.	($W/m^2.°C$)
h_{if}	Heat transfer coefficient, first plate heat exchanger section.	($W/m^2.°C$)

*1 This is the value determined from the manufacturer curves, rather than that identified in Chapter 5.

h_o	Shell side heat transfer coefficient for the generic condenser.	($W/m^2.°C$)
h_{of}	Heat transfer coefficient, first plate heat exchanger section.	($W/m^2.°C$)
h_{os}	Heat transfer coefficient, second plate heat exchanger section.	($W/m^2.°C$)
$h_d(t)$	Height of liquid above a distribution plate.	(m)
h_{steam}	Enthalpy of raw saturated steam at 10 bar .	(= 2778000 J/kg)
h_t	Height of the preheat section holding tubes.	(m)
H_k	Enthalpy of an energy balance input/output flow.	(J/kg)
H_{milk}	Enthalpy of liquid milk.	(J/kg)
I_{DSI}	Thermal inertia of the DSI unit.	(= 419000 J/°C)
$I_{effect1}$	Thermal inertia of the first evaporator effect.	(= 8380000 J/°C)
$I_{effect2}$	Thermal inertia of the second evaporator effect.	(= 1218000 J/°C)
$I_{effect3}$	Thermal inertia of the third evaporator effect.	(= 1218000 J/°C)
I_{flb}	Thermal inertia of the bottom half of a flash vessel.	(J/K)
I_{flt}	Thermal inertia of the top half of a flash vessel.	(J/K)
I_{fl1}	Thermal inertia of the first flash vessel.	(= 125700 J/°C)
I_{fl2}	Thermal inertia of the second flash vessel.	(= 125700 J/°C)
I_{shell1}	Thermal inertia of the MVR evaporator shell.	(= 8380000 J/°C)
I_{shell2}	Thermal inertia of the TVR evaporator shell.	(= 121800 J/°C)
k	Thermal conductivity.	(W/m.K)
k_{water}	Thermal conductivity of water.	(W/m.K)
k_{prot}	Thermal conductivity of protein.	(W/m.K)
k_{lact}	Thermal conductivity of lactose.	(W/m.K)
k_{salt}	Thermal conductivity of salt.	(W/m.K)
k_{fat}	Thermal conductivity of fat.	(W/m.K)
$m_{dsi}(t)$	Mass flow of steam entering the direct steam injection (DSI) unit.	(m^0_{dsi} = 0.35 kg/s)
$m_{steam}(t)$	Mass flow of raw steam entering the TVR compressor.	(m^0_{steam} = 0.107 kg/s)
M	Total mass in a control volume, used to make a mass balance.	(kg)
$M_c(t)$	Mass flow of condensate entering the preheat plate heat exchanger.	(M^0_c = 9.042 kg/s)
$M_{comp1}(t)$	Mass flow of vapour passing through the MVR compressor.	(M^0_{comp1} = 10.94 kg/s)
$M_{comp2}(t)$	Mass flow of vapour passing through the TVR compressor.	(M^0_{comp2} = 0.279 kg/s)
M_{cond}	Mass flow of liquid passing through the generic condenser tubes.	(kg/s)
$M_{cond2}(t)$	Condensate mass flow, exiting the third effect evaporator shell.	(M^0_{cond2} = 0.161 kg/s)
$M_{cond3}(t)$	Mass flow of condensate, exiting the vacuum condenser shell.	(M^0_{cond3} = 0.183 kg/s)
$M_d(t)$	Mass flow of liquid passing through a distribution plate.	(kg/s)
$M_{d1}(t)$	Mass flow passing through the first distribution plate.	($M^0_{d1} = M^0_{ph1}$)

M_{dry}	Mass flow of evaporation in the spray dryer.	(kg/s)
$M_{DSI}(t)$	Mass flow of liquid leaving the DSI unit.	(M^0_{DSI} = 16.375 kg/s)
M_{evap}	Mass flow of water evaporation in the evaporator.	(kg/s)
$M_{e5}(t)$	Mass flow from the bottom of the fifth falling film.	($M^0_{e5} = M^0_{p5}$)
$M_{e6}(t)$	Mass flow falling from the bottom of the sixth falling film.	($M^0_{e6} = M^0_{p6}$)
$M_{e8}(t)$	Mass flow falling from the bottom of the eighth falling film.	($M^0_{e8} = M^0_{p8}$)
$M_f(t)$	Mass flow of liquid milk entering the Evaporator A plant.	(M^0_f = 15.3 kg/s)
M_{fat}	Molecular mass of fat, that occurs in milk solutions.	(kg/kmol)
$M_{fc2}(t)$	Mass flow of liquid entering the DSI preheat section.	(M^0_{fc2} = 15.3 kg/s)
$M_{fh1}(t)$	Mass flow of liquid entering the bottom of the first flash vessel.	(M^0_{fh1} = 16.375 kg/s)
M_{lact}	Molecular mass of lactose, that occurs in milk solutions.	(kg/kmol)
M_k	Mass flow entering or exiting a mass balance control volume.	(kg/s)
M_{metb}	Mass of metal in the bottom section of a flash vessel.	(kg)
M_{mett}	Mass of metal in the top section of a flash vessel.	(kg)
M_{milkt}	Mass of liquid milk in the top section of a flash vessel.	(kg)
M_{milkb}	Mass of liquid milk in the bottom section of a flash vessel.	(kg)
M_{mvr}	Mass flow of evaporation in the MVR evaporator section.	(kg/s)
M_p	Mass flow of liquid exiting the evaporator.	(kg/s)
$M_{p5}(t)$	Mass flow of liquid exiting the MVR evaporator section.	(M^0_{p5} = 4.68 kg/s)
$M_{p8}(t)$	Mass flow of liquid exiting the TVR evaporator section.	(M^0_{p8} = 4.07 kg/s)
$M_{pc1}(t)$	Mass flow of liquid entering the DSI from the first flash vessel.	(M^0_{pc1} = 16.025 kg/s)
$M_{pc2}(t)$	Mass flow of liquid exiting the top of the second flash vessel.	(M^0_{pc2} = 15.667 kg/s)
$M_{ph1}(t)$	Mass flow of liquid exiting the bottom of the first flash vessel.	(M^0_{ph1} = 16.017 kg/s)
$M_{ph2}(t)$	Mass flow of liquid entering the MVR evaporator section.	(M^0_{ph2} = 15.65 kg/s)
M_{prot}	Molecular mass of protein, that occurs in milk solution.	(kg/kmol)
M_{salt}	Molecular mass of salt, that occurs in milk solutions.	(kg/kmol)
$M_{scond1}(t)$	Mass flow of condensate leaving the MVR evaporator shell.	(M^0_{scond1} = 10.66 kg/s)
$M_{scond2}(t)$	Mass flow of condensate leaving the TVR evaporator shell.	(M^0_{scond2} = 0.366 kg/s)
$M_{tubes}(t)$	Mass of evaporation during one falling film residence time.	(kg/s)
$M_{tubest}(t)$	Mass of evaporation during the MVR evaporator five passes.	(kg/s)
M_{tvr}	Mass flow of evaporation in the TVR evaporator section.	(kg/s)
$M_{vac}(t)$	Mass flow of cooling water entering the vacuum condenser.	(M^0_{vac} = 3.5 kg/s)
M_{water}	Molecular mass of water.	(kg/kmol)
n	Number of evaporator tubes.	(-)

n_{cond}	Number of condenser tubes.	(-)
$N_{comp}(t)$	MVR compressor speed.	(N^0_{comp} = 2850 rpm)
Nu	Nusselt dimensionless number.	(-)
P_h	Pressure at the top of the preheat holding tubes.	(Pa)
P_k	Pressure of the energy balance input/output flows.	(Pa)
$P_{e1}(t)$	Pressure of the MVR evaporator effect.	(P^0_{e1} = 26435 Pa)
$P_{ph1}(t)$	Pressure of the first flash vessel.	(Pa)
Pr	Prandlt dimensionless number.	(-)
$P_{s2}(t)$	Pressure of the MVR evaporator shell.	(P^0_{s1} = 31184 Pa)
$P_{sp}(t)$	Set-point for the TVR compressor pressure control loop.	(P^0_{sp} = 500,000 Pa)
$P_{st}(t)$	Raw steam pressure to the TVR compressor and DSI unit.	(= 10,000,000 Pa)
P_{vap}	Vapour pressure of a liquid.	(Pa)
ΔP_{flood}	Hydrostatic pressure due to the liquid height above the DSI pump.	(Pa)
ΔP_{head}	Pressure drop caused by the height of the DSI holding tubes.	(Pa)
ΔP_{loss}	Pressure drop caused by frictional losses in the holding tubes.	(Pa)
ΔP_{orif}	Pressure drop due to the preheat section back-pressure orifice plate.	(Pa)
ΔP_{pump}	Pressure gain caused by the DSI pump.	(Pa)
q	Net heat flow into an energy balance control volume.	(W)
q_{cond}	Heat flow through the tubes of the generic condenser.	(W)
q_{condi}	Heat flow between condensing steam/tubes of generic condenser.	(W)
q_{condo}	Heat flow between tube/condenser liquid of generic condenser.	(W)
$q_{comp1}(t)$	Latent enthalpy, vapour passing through the MVR compressor.	(q^0_{comp1} = 25,603,000 W)
$q_{comp2}(t)$	Latent enthalpy, vapour entering the TVR compressor.	(q^0_{comp2} = 653,240 W)
$q_{eloss1}(t)$	Surface energy loss heat flow for the MVR evaporator effect.	(q^0_{eloss1} = 58,186 W)
$q_{eloss2}(t)$	Surface energy loss heat flow for a TVR evaporator section.	(q^0_{eloss2} = 10,553 W)
$q_{eloss3}(t)$	Surface energy loss heat flow for a TVR evaporator section.	(q^0_{eloss3} = 7,251 W)
$q_{feed1}(t)$	Net enthalpy of the feed entering the MVR evaporator section.	(q^0_{feed1} = 723,638W)
$q_{feed6}(t)$	Net enthalpy of the feed entering the TVR evaporator section.	(q^0_{feed6} = 127,777W)
$q_{pcond}(t)$	Heat flow passing through the preheat condenser tubes.	(q^0_{pcond} = 824,591W)
$q_{sloss1}(t)$	Surface energy loss heat flow for the MVR evaporator shell.	(q^0_{sloss1} = 93,024 W)
$q_{sloss2}(t)$	Surface energy loss heat flow for the TVR evaporator shell.	(q^0_{sloss2} = 12,011W)
$q_{shell}(t)$	Heat flow passing through the evaporator tubes.	(W)
$q_{shellt}(t)$	Total heat flow passing through the MVR evaporator tubes.	($= \sum_{i=1}^{5} q_{shelli}$ W)

$q_{vac}(t)$	Heat flow passing through the vacuum condenser tubes.	(q^0_{vac} = 428,570 W)
$Q_d(t)$	Volumetric flow of liquid passing through a distribution plate.	(m^3/s)
$Q_{DSI}(t)$	Volumetric flow of liquid passing through the DSI unit.	(m^3/s)
Re	Reynolds dimensionless number.	(-)
T_a	Ambient temperature.	(= 30 °C)
$T_{c1}(t)$	Temperature of hot condensate entering the plate heat exchanger.	(T^0_{c1} = 69.959 °C)
$T_{c2}(t)$	Temperature of hot condensate exiting the plate heat exchanger.	(T^0_{c2} = 25.421 °C)
T_{cs}	Condensate temperature, second plate heat exchanger section.	(°C)
$T_{cond}(t)$	Temperature of liquid in the generic condenser tubes.	(°C)
$T_{cond1}(t)$	Inlet temperature to the generic condenser tubes.	(°C)
$T_{cond2}(t)$	Outlet temperature from the generic condenser tubes.	(°C)
$T_{dum}(t)$	Dummy variable used in the generic condenser model.	(°C)
$T_{DSI}(t)$	Temperature of the direct steam injection (DSI) unit.	(T^0_{DSI} = 104.383 °C)
$T_{e1}(t)$	Temperature of the MVR evaporator effect.	(T^0_{e1} = 66.186 °C)
$T_{e2}(t)$	Temperature of the second evaporator effect.	(T^0_{e2} = 57.482 °C)
$T_{e3}(t)$	Temperature of the third evaporator effect.	(T^0_{e3} = 53.243 °C)
$T_f(t)$	Temperature of the evaporator feed.	(T^0_f = 12 °C)
$T_{fc2}(t)$	Temperature of feed liquid to the DSI preheat section.	(T^0_{fc2} = 63.672 °C)
$T_{fh1}(t)$	Temperature to the bottom of the first flash vessel.	($T^0_{fh1} = T^0_{DSI}$)
T_{mcf}	Milk temperature, cold side, first plate heat exchanger section.	(°C)
T_{mcs}	Milk temperature, cold side, second plate heat exchanger section.	(°C)
T_{pc}	Temperature of the top of a flash vessel.	(°C)
T_{ph}	Temperature of the bottom of a flash vessel.	(°C)
$T_{pc1}(t)$	Temperature of the liquid to the DSI from the first flash vessel.	($T^0_{pc1} = T^0_{ph1}$)
$T_{pc2}(t)$	Temperature of the liquid from the top of the second flash vessel.	($T^0_{pc2} = T^0_{ph2}$)
$T_{ph1}(t)$	Temperature of the liquid from the bottom of the first flash vessel.	(T^0_{ph1} = 91.451 °C)
$T_{ph2}(t)$	Temperature of the liquid entering the MVR evaporator section.	(T^0_{ph2} = 77.899 °C)
T_{mcf}	Milk temperature, first section of the plate heat exchanger.	(°C)
$T_{mc1}(t)$	Temperature of cold milk entering the plate heat exchanger.	($T^0_{mc1} = T^0_f$)
$T_{mc2}(t)$	Milk temperature between first/second heat exchanger sections.	(T^0_{mc2} = 22.02 °C)
$T_{mc3}(t)$	Temperature of the hot milk exiting the plate heat exchanger.	(T^0_{mc3} = 50.00 °C)
T_{sat}	Boiling temperature of a liquid, in degrees Kelvin.	(K)
$T_{s1}(t)$	Temperature of the MVR evaporator shell.	(T^0_{s1} = 69.959 °C)
$T_{s2}(t)$	Temperature of the TVR evaporator shell.	(T^0_{s2} = 63.362 °C)

T_{sh}	Temperature of the generic condenser shell.	(°C)
$T_{v1}(t)$	Temperature of hot cooling water entering the plate heat exchanger.	($T_{v1}^0 = T_{vac2}^0$)
$T_{v2}(t)$	Temperature of hot cooling water exiting the plate heat exchanger.	($T_{v2}^0 = 12.007$ °C)
$T_{vac1}(t)$	Vacuum condenser cooling water inlet temperature.	($T_{vac1}^0 = 24.00$ °C)
$T_{vac2}(t)$	Vacuum condenser cooling water outlet temperature.	($T_{vac2}^0 = 55.32$ °C)
T_{vf}	Hot water temperature, first plate heat exchanger section.	(°C)
T_w	Wall temperature of the generic condenser tubes.	(°C)
T_{wf}	Wall temperature of the first section of the plate heat exchanger.	(°C)
T_{ws}	Wall temperature of the second section of the plate heat exchanger.	(°C)
U	Internal energy of a control volume, used for an energy balance.	(J/kg)
U_{cond}	Overall heat transfer coefficient for the generic condenser.	(W/m^2.°C)
U_{eo}	Coefficient for the evaporating falling film heat transfer model.	(W/m^2.°C)
U_{ew}	Coefficient for the evaporating falling film heat transfer model.	(W/m^2.°C)
U_{hf}	Overall transfer coefficient, first plate heat exchanger section.	(= 2500 W/m^2.°C)
U_{hs}	Overall transfer coefficient, second plate heat exchanger section.	(= 2500 W/m^2.°C)
U_k	Internal energy of a flow input/output of the energy balance.	(J/kg)
U_l	Overall heat transfer coefficient for the surface energy losses.	(= 12 W/m^2.°C)
U_{lo}	Coefficient used in the linear falling film heat transfer model.	(W/m^2.°C)
U_{lw}	Coefficient used in the linear falling film heat transfer model.	(W/m^2.°C)
U_{pre}	Overall heat transfer coefficient for the preheat condenser.	(= 2260 W/m^2.°C)
U_s	Overall heat transfer coefficient for evaporator falling film.	(W/m^2.°C)
U_{so}	Coefficient used in the simple falling film heat transfer model.	(W/m^2.°C)
U_{sw}	Coefficient used in the simple falling film heat transfer model.	(W/m^2.°C)
U_{sw}	Coefficient for simple linear evaporating falling film heat transfer.	(W/m^2.°C)
U_{vac}	Overall heat transfer coefficient for the vacuum condenser.	(= 2000 W/m^2.°C)
v_{cond}	Velocity of the cooling water in the generic condenser.	(m/s)
v_{cs}	Hot water velocity, second section of the plate heat exchanger.	(= 0.3071 m/s)
v_e	Velocity of the evaporating falling film.	(m/s)
v_{mf}	Cold milk velocity, first section of the plate heat exchanger.	(= 0.4500 m/s)
v_{ms}	Cold milk velocity, second section of the plate heat exchanger.	(= 0.5464 m/s)
v_{vf}	Water velocity, first section of the plate heat exchanger.	(= 0.1029 m/s)
V_T	Total volume of an energy balance control volume.	(m^3)
V_k	Specific volume of the energy balance input/output flows.	(m^3/kg)
V_{cond}	Volume of liquid in the tubes of the generic condenser.	(m^3)
$V_{dum}(t)$	Dummy variable used in the generic condenser model.	(m^3)

V_{cs}	Volume of condensate water, second plate heat exchanger section.	(m^3)
V_{mf}	Volume of liquid milk, first plate heat exchanger section.	(m^3)
V_{ms}	Volume of liquid milk, second plate heat exchanger section.	(m^3)
V_{vf}	Volume of liquid hot water, first plate heat exchanger section.	(m^3)
V_{pre}	Internal volume of the preheat condenser tubes.	(= 0.237 m^3)
V_{vac}	Internal volume of the vacuum condenser tubes.	(= 0.43 m^3)
V_w	Volume of metal in the generic condenser tubes.	(m^3)
V_{wf}	Volume of metal, first plate heat exchanger section.	(m^3)
V_{ws}	Volume of metal, second plate heat exchanger section.	(m^3)
$w_d(t)$	Dry mass fraction of liquid passing through the distribution plate.	(kg/kg)
$w_{d1}(t)$	Dry mass fraction of liquid, first distribution plate.	($w_{d1}^0 = w_{ph1}^0$)
$w_e(t)$	Dry mass fraction of liquid falling from the evaporator film.	(kg/kg)
$w_{e5}(t)$	Dry mass fraction of liquid falling from the fifth evaporator film.	($w_{e5}^0 = w_{p5}^0$)
$w_{e6}(t)$	Dry mass fraction of liquid falling from the sixth evaporator film.	($w_{e6}^0 = w_{p6}^0$)
$w_{e8}(t)$	Dry mass fraction of liquid falling from the eighth evaporator film.	($w_{e8}^0 = w_{p8}^0$)
$w_f(t)$	Dry mass fraction of liquid entering the evaporator plant.	(w_f^0 = 0.125 kg/kg)
$w_{fc2}(t)$	Dry mass fraction of liquid entering the DSI preheat section.	($w_{fc2}^0 = w_f^0$)
$w_p(t)$	Dry mass fraction of liquid exiting an evaporator pass.	(kg/kg)
$w_{p5}(t)$	Dry mass fraction of liquid exiting the MVR evaporator section.	(w_{p5}^0 = 0.408 kg/kg)
$w_{p8}(t)$	Dry mass fraction of milk exiting the TVR evaporator section.	(w_{p8}^0 = 0.470 kg/kg)
$w_{ph2}(t)$	Dry mass fraction of milk entering the MVR evaporator section.	(w_{ph2}^0 = 0.122 kg/kg)
W_s	Net work acting on a energy balance control volume.	(W)
W_{comp}	Driving energy flow, or power supplied, to the evaporation process.	(W)
$W_{comp1}(t)$	Electric Powder supply to the MVR compressor.	(W_{comp1}^0 = 425,145 W)
$W_{comp2}(t)$	Net raw steam enthalpy to the TVR compressor.	(W_{comp2}^0 = 267,457 W)
y_{air}	Molar concentration of non-condensable gases in a flash vessel.	(mol/mol)

Greek Symbols

β	Ratio between the areas of a distribution plate hole and calandria.	(-)
δ	Thickness of a falling film.	(m)
δ^+	Dimensionless falling film thickness.	(-)
σ	Surface tension.	(N/m)
ΔT_{bpe}	Boiling point elevation.	(°C)
Γ	Falling film liquid loading, or mass flow per unit perimeter.	(kg/m.s)
μ	Viscosity.	(kg/m.s)

ρ	Density.	(kg/m^3)
ρ_{cond}	Density of the liquid in the generic condenser.	(kg/m^3)
ρ_{water}	Density of water.	(kg/m^3)
ρ_{lact}	Density of lactose.	(kg/m^3)
ρ_{prot}	Density of protein.	(kg/m^3)
ρ_{salt}	Density of salt.	(kg/m^3)
ρ_{fat}	Density of fat.	(kg/m^3)
$\rho_{p5}(t)$	Density of the product milk from the fifth pass.	(kg/m^3)
$\rho_{p8}(t)$	Density of the product milk from the eighth pass.	(kg/m^3)
$\rho_{vel}(t)$	Density of the MVR evaporator effect vapour.	(ρ^0_{vel} = 0.1694 kg/m^3)
ρ_w	Density of the metal in the generic condenser tubes.	(kg/m^3)
λ	Latent heat of vaporisation.	(= 2340000 J/kg)
τ_c	Residence time of the generic condenser tubes.	(s)
τ_{cis}	Time dimensioned variable associated with plate heat exchanger.	(s)
τ_{DSI}	Time constant, DSI unit temperature differential equation.	(s)
τ_e	Residence time of a falling film.	(= 50 s)
τ_{et}	Total residence time of all five passes of the MVR evaporator.	(= 300 s)
τ_{fl1}	Time constant, first flash vessel temperature differential equation.	(s)
τ_{fl2}	Time constant, second flash vessel differential equation.	(s)
τ_i	Time dimensioned variable associated with the generic condenser.	(s)
τ_{mof}	Time dimensioned variable associated with plate heat exchanger.	(s)
τ_{mos}	Time dimensioned variable associated with plate heat exchanger.	(s)
τ_o	Time dimensioned variable associated with the generic condenser.	(s)
τ_{Tvf}	Residence time, first section of the plate heat exchanger.	(= 42.2571 s)
τ_{Tvs}	Residence time, second section of the plate heat exchanger.	(= 18.8837 s)
τ_{pre}	Residence time of the liquid in the tubes of the preheat condenser.	(= 15.4902 s)
τ_{Tc}	Time dimensioned variable associated with the generic condenser.	(s)
τ_{Tc0}	Time dimensioned variable associated with the generic condenser.	(s)
τ_{Tvac}	Time dimensioned variable associated with the vacuum condenser.	(=16.6824 s)
τ_{Tel}	Time constant, MVR evaporator temperature differential equation.	(s)
τ_{Te2}	Time constant, TVR evaporator temperature differential equation.	(s)
τ_{Te3}	Time constant, TVR evaporator temperature differential equation.	(s)
τ_{Tif}	Time dimensioned variable, first plate heat exchanger section.	(= 3.7758 s)
τ_{Tmf}	Residence time, first plate heat exchanger section.	(= 9.6666s)
τ_{Tis}	Time dimensioned variable, second plate heat exchanger section.	(= 3.7725 s)

τ_{Tms}	Residence time, second section of the plate heat exchanger.	(= 10.6142s)
τ_{Tof}	Time dimensioned variable, first plate heat exchanger section.	(= 3.7758 s)
τ_{Tos}	Time dimensioned variable, second plate heat exchanger section.	(= 3.7725 s)
τ_{Tpre}	Time dimensioned variable associated with the preheat condenser.	(= 13.4021 s)
τ_{Ts1}	Time constant, MVR evaporator shell differential equation.	(s)
τ_{Ts2}	Time constant , TVR evaporator shell differential equation.	(s)
τ_{vac}	Residence time of the vacuum condenser.	(= 122.8571 s)
τ_{vif}	Time dimensioned variable associated with plate heat exchanger.	(s)
τ_{wif}	Time dimensioned variable associated with plate heat exchanger.	(s)
τ_{wof}	Time dimensioned variable associated with plate heat exchanger.	(s)
τ_{wis}	Time dimensioned variable associated with plate heat exchanger.	(s)
τ_{wos}	Time dimensioned variable associated with plate heat exchanger.	(s)
ψ	Potential energy of the energy balance control volume.	(J/kg)
ψ_k	Potential energy of the energy balance input/output flows.	(J/kg)

9 References

Alhusseini A N, Tuzla K and Chen J C (1998). "Falling film evaporation of single component liquids", Journal of Heat and Mass Transfer, 41, 12, 1623 - 1632.

Angeletti S and Moresi M (1983). "Modelling of multiple-effect falling-film evaporators", Journal of Food Technology, 18, 539-563.

Benjamin B T (1957). "Wave formation in laminar flow down an inclined plane", Journal of Fluid Mechanics, 2, 554-574.

Bouman S and Waalewijn R (1994). "Concentration of dairy products with rotating evaporators. 2 Results and conclusions', Milchwissenschaft, 49, 253-255.

Bouman S, Waalewijn R, de Jong R and van der Linden H J (1993). "Design of falling film evaporators in the dairy industry", Journal of the Society of Dairy Technology, 46, 3, 100-106.

Burdett J W and Holland C D (1971). "Dynamics of a multiple effect evaporator system", AIChE Journal, 17, 5, 1080-1089.

Chen H (1992). "Factors Affecting the Heat Transfer in the Falling Film Evaporator", M.Tech Thesis, Department of Food Technology, Massey University, Palmerston North.

Chen X D (1996). "Selected fundamental aspects of the drying of milk", Milk Powders for the Future, New Zealand Dairy Research Institute, Palmerston North, New Zealand.

Chun K R and Seban R A (1971). "Heat transfer to evaporating liquid films", ASME Journal of Heat Transfer, 93, 391.

Chun M H and Kim K T (1990). "Assessment of the new and existing correlations for laminar and turbulent film condensation on a vertical wall", International Communications in Heat and Mass Transfer, 17, 421-441.

Chung J C and Bankoff S G (1980). "Initial breakdown of a heated liquid film in co-current two component annular flow: i small perturbation model", Chemical Engineering Communications, 4, 433-453.

Chung J C and Bankoff S G (1980). "Initial breakdown of a heated liquid film in co-current two component annular flow: ii rivulet and dry patch models", Chemical Engineering Communications, 4, 455-470.

Dannenberg F and Kessler H G (1988). "Reaction kinetics of the de-naturation of whey proteins in milk", Journal of Food Science, 53, 1, 258-263.

Dotterweich F H and Mooney C V (1955). "How to design and operate gas jet compressors", Petroleum Refiner, 34(10), pp 104-109.

Dukler A E and Bergelin O P (1952). "Characteristics of flow in falling liquid films", Chemical Engineering Progress, 48, 11, 557-563.

Fergusson P H (1989). "Developments in the evaporation and drying of dairy products", Journal of the Society of Dairy Technology, 42, 4, 94-101.

Fernandez-Martin F (1972). "Influence of temperature and composition on some physical properties of milk and milk concentrates. I. Heat Capacity", Journal of Dairy Research, 39, 65-73.

Fernandez-Martin F and Montes F (1977). "Thermal conductivity of creams", Journal of Dairy Research, 44, 103-109.

Fox J A (1977). "An Introduction to Engineering Fluid Mechanics", Mac-Millian, London, England.

Fulford G D (1964). "The flow of liquids in thin films", Advances in Chemical Engineering, Vol 5, Academic Press, New York.

Geordiadis M C, Rotstein G E and Macchietto S (1998). "Modeling and simulation of shell and tube heat exchangers under milk fouling", AIChE Journal, 44, 4, 959-971.

Gotham S M, Fryer P J and Pritchard A M (1992). "β-lactoglobulin denaturation aggregation reactions and fouling deposit formation : a DSC study", International Journal of Food Science and Technology, 27, 313-327.

Grosdidier P and Morari M (1986). "Interaction measures for systems under decentralized control", Automatica, 22, 309-319.

Hansen H (1985). "Evaporation, Membrane Filtration and Spray Drying", Vanlose, Denmark : North European Dairy Journal.

Holland C D and Liapsis A I (1985). "Computer Methods for Solving Dynamic Separation Problems", McGraw-Hill, New York.

Hartley D E and Murgatroyd W (1964). "Criteria for the break-up of thin liquid layers flowing isothermally over solid surfaces", Journal of Heat and Mass Transfer, 7, 1003-1015.

Holman J P (1989). "Heat Transfer", McGraw-Hill, Singapore.

Hoke B C and Chen J C (1992). "Thermocapillary breakdown of subcooled falling liquid films", Industrial Engineering and Chemistry Research, 31, 688-694.

Hori T (1983). "Effets of rennet treatment and water content on the thermal conductivity of Skim Milk", Journal of Food Science, 48, 1492-1496.

Hovd M and Skogestad S (1994). "Sequential design of decentralised controllers", Automatica, Vol. 30, No. 10, pp. 1601-1607.

Jebson R S and Iyer M (1991). "Performances of falling film evaporators", Journal of Dairy Research, 58, 29-38.

Kessler H G (1981). "Food Engineering and Dairy Technology", Verlag A Kessler, Freising, Germany.

Kessler H G (1987). "Multistage evaporation and water vapour recompression with special emphasis on high dry matter content, product losses, cleaning and energy savings", In "Milk – The Vital Force. Proceedings of the 22nd International Dairy Congress" The Hague, Sept 29 – Oct 3 1986, pp 545-558. D Reidel Publishing. Co., Dordrecht.

Koppel L B (1962). "Dynamics of a flow forced heat exchanger", Industrial and Engineering Chemistry Fundementals, 1, 2, 131-134.

Lee P L, Newell R B and Sullivan G R (1989). "Generic model control - A case study", The Canadian Journal of Chemical Engineering, 67, June.

Lim H C (1970). "Time-optimal output control computations for a class of linear tubular processes", The Canadian Journal of Chemical Engineering, 48, 301-307.

Mackereth A R (1995). "Thermal and Hydraulic Aspects of Falling Film Evaporation", Ph.D thesis, Department of Chemical and Process Engineering, University of Canterbury, Christchurch, New Zealand.

Middleton J (1996). "Physical Properties of Dairy Products", MAF Quality Management, Ministry of Agriculture, New Zealand.

Montgomery D C (1991). "Design and Analysis of Experiments", John Wiley and Sons, New York, USA.

More G R and Prasad S (1988). "Thermal conductivity of concentrated Whole Milk", Journal of Food Process Engineering, 10, 105-112.

Moresi M (1985). "Design and Optimisation of Falling Film Evaporators", in Developments in Food Preservations, ed Thorne S, Elsevier.

Mozley J M (1956). "Predicting dynamics of concentric pipe heat exchangers", Industrial and Engineering Chemistry, Engineering, Design and Process Developments, 48 , 6, 1035-1041.

Munday J T and Bagster D F (1977). "A new ejector theory applied to steam jet refrigeration", Ind Eng Chem, Process Des Dev, 16 (4), 442-448.

Murakami E G and Okos M R (1989). "Measurement and prediction of thermal properties of foods", in Food Properties and Computer-Aided Engineering of Food Processing Systems, ed Singh R P and Medina A G, Klumer Academic Publishers.

de Nevers N (1991). "Fluid Mechanics for Chemical Engineers", McGraw-Hill International, New York, USA.

Nielsen L S, Fee C J and Chen X D (1996). "The effects of temperature and holding time of external heating on solubility deterioration of a skim milk powder", Transactions of the Institute of Chemical Engineers, 74, 159-162.

Nusselt W (1916). "The condensation of steam on cooled surfaces", Chemical Engineering Fundamentals, 1, 2, 6-19, 1982. (trans Fullarton, D) from Zeitachrift des Vereins Deutscher Ingenieure, 60, 27, 541-546 (1916).

Paramalingam S, Winchester J and Marsh C (1999). "On the fouling of falling-film evaporators due to film break-up", Transactions of the Institute of Chemical Engineers, Vol 78, 79-84.

Perry R H and Green D (1984). "Perry's Chemical Engineers' Handbook", McGraw-Hill, New York, USA.

Quaak P and Gerritsen J B M (1990). "Modelling dynamic behaviour of multi-effect falling-film evaporators", Computer Applications in Chemical Engineering (Bussemaker H T and Iedema P D eds.), Elsevier, Amsterdam.

Quaak P, van Wijck M P C M and van Haren J J (1994). "Comparision of process identification and physical modelling for falling-film evaporators", Food Control, 5, 2, 73-82.

Rogers G F C and Mayhew Y R (1988)."Thermodynamic and Transport Properties of Fluids", Blackwell Publishers, Oxford, Great Britain.

Sandler S I (1989). "Chemical Engineering Thermodynamics", Wiley and Sons, New York.

Schwartzberg H G (1989). "Food Property Effects in Evaporation", in Food Properties and Computer-Aided Engineering of Food Processing Systems, eds Singh R P and Medina A G, 443-470.

Skogestad S and Postlethwaite I (1996). "Multivariable Feedback Control : Analysis and Design", Wiley and Sons, New York.

Smith J M and van Ness H C (1987). "Introduction to Chemical Engineering Thermodynamics", McGraw-Hill International, New York.

Snoeren T H M, Damman A J and Klok H J (1982). "The viscosity of skim milk concentrates", Netherlands Milk Dairy Journal, 36, 305-316.

Stermole F J and Larson M A (1964). "The dynamics of flow forced distributed parameter heat exchangers", A.I.Ch.E.Journal, 10, 5, 688-694.

Sun D and Eames IW (1995). "Recent developments in the design theories and applications of ejectors", Journal of the Institute of Energy, 68, 65-79.

Tonelli S M, Romagnoli J A and Porras J A (1994). "Computer package for transient analysis of industrial multiple effect evaporators", Journal of Food Engineering, 4, 2, 59-75.

Trinh KT, Mackereth A R and Woodhall M C (1996). "Milk Powder Technology : Principles and Process Applications", New Zealand Dairy Research Institute.

van Wijck M P C M, Quaak P and van Haren J J (1994). "Multivariable supervisory control of a four-effect falling-film evaporator", Food Control, 5, 2, 83-89.

Wang F Y and Cameron I T (1994). "Control studies on a model evaporation process constrained state driving with conventional and higher relative degree systems", Journal of Process Control, 4, 2, 59-75.

Walstra P and Jenness R (1984). "Dairy Chemistry and Physics", John Wiley and Sons, Toronto, Ontario.

Winchester J and Marsh C (1998). "Dynamics and control of falling film evaporators with mechanical vapour recompression", Transactions of the Institute of Chemical Engineers, Part A, Vol.77, pp 357-371.

Van Wylen G J, Sonntag R E and Borgnakke C (1994). "Fundamentals of Classical Thermodynamics", John Wiley and Sons, Inc.

Yeates R J (1996). "The Modelling of Falling Film Evaporators in the Dairy Industry", B.E. Research Project, Department of Chemical and Process Engineering, University of Canterbury, New Zealand.

Zuber N and Staub F W (1965). "Stability of dry patches forming in liquid films flowing over heated surfaces", International Journal of Heat and Mass Transfer, 9, 897-905.

Appendix A : Properties of Milk

A.1) Introduction

Here we examine models for predicting the physical properties and thermodynamic equilibrium relationships of milk solutions. The physical properties we will investigate are the density, heat capacity, thermal conductivity and viscosity. The thermodynamic equilibrium relationships are the liquid/vapour saturation equations for water and also the boiling point elevation due to dissolved milk components.

The models discussed here are mostly based on the assumption of an ideal mixture. An ideal mixture is one where the properties of the mixture are considered to be the algebraic sum of the components making up the mixture. This assumption is strictly only true for mixtures of similar components, since the intermolecular forces do not change much upon mixing. The components in milk solutions are not similar and so we would not expect the ideal mixture assumption to be correct. However, the ideal mixture models are comparatively simple and their accuracy can be improved by model identification.

A.2) Density of Milk

The density is the reciprocal of the specific volume and this is modelled in the ideal mixture using the following. This is rearranged in terms of the density to produce equation (A.2).

$$V_{milk} = \sum_i V_i . w_i \qquad \text{(A.1)}$$

$$\frac{1}{\rho} = \sum_i \frac{w_i}{\rho_i} \qquad \text{(A.2)}$$

Where, w_i	=	mass fraction of component in the milk mixture.	(kg/kg)
ρ_i	=	density of component in the milk mixture.	(kg/m^3)
ρ	=	density of the milk mixture.	(kg/m^3)
V_{milk}	=	milk specific volume, volume that a unit mass occupies.	(m^3/kg)
V_i	=	specific volume of a milk component.	(m^3/kg)

The following specific densities have been given by Murakami and Okos (1989).

$$\rho_{water} = 997.18 + 3.1439x10^{-1}T - 3.7574x10^{-3}T^2, \quad \rho_{fat} = 925.59 - 0.31046T, \qquad \text{(A.3)}$$

$$\rho_{lact} = 1599.1 - 0.31046T, \quad \rho_{salt} = 2423.8 - 0.28063T, \quad \rho_{prot} = 1329.9 - 0.5184T \qquad \text{(A.4)}$$

We can rearrange the above density equation to produce equation (A.5) for the milk density. The total solids dry matter concentration is the mass concentration of all the non-water milk components. This includes lactose, protein, fat and mineral salts.

$$\rho = \frac{\rho_{water}}{[1 - a_{TS}.w_{TS}]}, \quad a_{TS} = 1 - \frac{\rho_{water}}{\rho_{lact}} x_{lact} - \frac{\rho_{water}}{\rho_{prot}} x_{prot} - \frac{\rho_{water}}{\rho_{fat}} x_{fat} - \frac{\rho_{water}}{\rho_{salt}} x_{salt}, \quad x_i = \frac{w_i}{w_{TS}} \qquad \text{(A.5)}$$

Where, w_{TS} = mass fraction of the total solids in the milk solution. (kg/kg)

ρ_{water} = density of water. (kg/m^3)

x_i = fraction of component i in total solids. (kg/kg)

w_i = mass fraction of the component i in the mixture. (kg/kg)

The coefficient a_{TS} has been determined for various milk mixtures using historical data from the Kiwi Co-op Dairies, Evaporator A plant. These coefficients are shown in Table A-1 along with those calculated using the specific densities from above. The predicted coefficients shows the required trends, such as lower densities with high fat content milk solutions. However, there are some significant deviations between the experimental and predicted results.

Table A-1 : Density model coefficients.

Milk	Milkfat (%)	Lactose (%)	Protein (%)	Salt (%)	Experimental a_{TS} (kg/kg)	Murakami a_{TS} (kg/kg)
Whole	27.7	38.4	27.9	6	0.24187	0.20886
Skim	0.8	53.1	37.9	8.1	0.34394	0.32781
Butter	9.3	47.4	35.9	7.5	0.30364	0.29611
Freya	26.7	55.1	12.3	6	0.26814	0.23662
Sophie-Lo	24.6	52	17.4	6	0.26518	0.23924
MPC56	0	39.1	57.7	5.2	0.29871	0.29366

The density coefficient (a_{TS}) in equation (A.5) is linear in terms of the water and component specific densities (i.e., $\frac{\rho_{water}}{\rho_i}$). As a result we can determine the specific densities that produce a best fit of the experimental data by using standard regression analysis (Montgomery, 1991). The water density was assumed to be constant during the mixture process. The resulting specific densities are given by the following.

$$\rho_{water} = 997.18 + 3.1439x10^{-1}T - 3.7574x10^{-3}T^2, \qquad \rho_{prot} = 1275.92 \qquad \text{(A.6)}$$

$$\rho_{lact} = 1585.59, \qquad \rho_{salt} = 2655.801, \qquad \rho_{fat} = 962.54 \qquad \text{(A.7)}$$

A.3) Thermal Conductivity

The thermal conductivity can be estimated using the following equations (Murakami and Okos, 1989). We have further assumed that the component specific volumes are the inverse of the specific densities.

$$k = \sum \phi_i . k_i \,, \qquad \phi_i = \frac{w_i}{\rho_i \sum \frac{w_i}{\rho_i}} = \frac{w_i . \rho}{\rho_i} \tag{A.8}$$

Where, k	=	thermal conductivity of the milk mixture.	(W/m.K)
k_i	=	thermal conductivity of component i in the milk mixture.	(W/m.K)
ϕ_i	=	volume fraction of the component in mixture.	(kg/kg)
ρ_i	=	density of component in mixture.	(kg/m^3).
ρ	=	density of the milk mixture.	(kg/m^3)

The density of the milk mixture is determined using the equations shown earlier. The specific thermal conductivities are given by the following equations (Murakami and Okos, 1989).

$$k_{water} = 0.5711 + 1.73x10^{-3}T - 6.704x10^{-6}T^2,\ k_{fat} = 0.1807 + 2.7604x10^{-4}T - 1.7749x10^{-7}T^2 \tag{A.10}$$

$$k_{prot} = 0.1788 + 1.958x10^{-3}T - 2.718x10^{-6}T^2,\ k_{lact} = 0.2014 + 1.3874x10^{-3}T - 4.3312x10^{-6}T^2 \tag{A.12}$$

$$k_{salt} = 0.3296 + 1.4011x10^{-3}T - 2.9069x10^{-6}T^2 \tag{A.13}$$

We can rearrange the above equation to produce the following linear model, between the mixture thermal conductivity and milk dry matter concentration.

$$\frac{k}{\rho} = \frac{k_{water}}{\rho_{water}} + k_{TS} . w_{TS} \tag{A.14}$$

Where, the linear coefficient k_{TS} is given by equation (A.15)

$$k_{TS} = \frac{k_{prot}}{\rho_{prot}} x_{prot} + \frac{k_{lact}}{\rho_{lact}} x_{lact} + \frac{k_{salt}}{\rho_{salt}} x_{salt} + \frac{k_{fat}}{\rho_{fat}} x_{fat} - \frac{k_{water}}{\rho_{water}} \tag{A.15}$$

Using the Murakina thermal conductivity equations we can calculate the k_{TS} parameter for Whole Milk, Skim Milk and Cream. These can be compared to values determined from experimental results given in the literature (More and Prasad, 1988; Hori, 1983; Fernandez-Martin and Montes, 1977) and the results are shown in Table A-2. The results for Skim Milk are quite good, but those for Whole Milk and Cream show significant deviations. The cause of these deviations is unknown, but it is interesting to note that the predictions improve dramatically

when the fat specific thermal conductivity is assumed to be zero. The predicted milk thermal conductivity coefficients, when fat is assumed to have a specific thermal conductivity of zero, are shown in the final column of Table A-2.

Table A-2 : Themal conductivity model coefficients.

Milk	Milkfat (%)	Lactose (%)	Protein (%)	Salt (%)	a_{TS} (-)	Murakami k_{TS} ($m^4/s^3.K$)	Literature k_{TS} ($m^4/s^3.K$)	No fat k_{TS} ($m^4/s^3.K$)
Whole	27.7	38.4	27.9	6	0.24187	$-4.484x10^{-4}$	$-5.535x10^{-4}$	$-5.0252x10^{-4}$
Skim	0.8	53.1	37.9	8.1	0.34394	$-4.572x10^{-4}$	$-4.857x10^{-4}$	$-4.5874x10^{-4}$
Cream	100	0	0	0	-0.03438	$-4.254x10^{-4}$	$-6.286x10^{-4}$	$-6.2089x10^{-4}$

A.4) Specific Heat Capacity

The heat capacity of an ideal mixture is given by equation (A.16) (Murakina and Okos, 1989).

$$C_p = \sum w_i . C_{p,i} \qquad \text{(A.16)}$$

The specific heat capacities of the milk components are given by the following equations.

$$C_{pwater} = 4.21660729 - 2.35427x10^{-3}T + 3.9274488x10^{-5}.T^2 - 1.994188x10^{-7}T^3 + 4.8844x10^{-10}T^4 \qquad \text{(A.17)}$$

$$C_{pfat} = 1.848533088 + 8.258845x10^{-3}T - 4.97689x10^{-5}T^2, \qquad C_{pprot} = 2.219 \qquad \text{(A.18)}$$

$$C_{plact} = 1.256, \qquad C_{psalt} = 2.9301 \qquad \text{(A.19)}$$

Table A-3 : Linear heat capacity model coefficients.

Milk	Milkfat (%)	Lactose (%)	Protein (%)	Salt (%)	Murakami C_{pTS} (kJ/kg.K)	Literature C_{pTS} (kJ/kg.K)
Whole	27.7	38.4	27.9	6	2.1389	1.98454
Skim	0.8	53.1	37.9	8.1	2.4693	2.08921

Equations (A.17) – (A.19) give the true heat capacities. The effective heat capacity for milk is often different from these due to the melting, solidification and crystallisation of milk components. This causes the effective heat capacity to have a latent heat contribution that is neglected in these equations (Middleton, 1996). The above equation can be rearranged to produce the following linear model for the mixture heat capacity.

$$C_p = C_{pwater} - C_{pTS}.w_{TS} \tag{A.20}$$

$$C_{pTS} = C_{pwater} - C_{plact}.x_{lact} - C_{pprot}.x_{prot} - C_{pfat}.x_{fat} - C_{psalt}.x_{salt} \tag{A.21}$$

Where, C_{pwater} = heat capacity of water. (J/kg.°C)

C_{pTS} = linear heat capacity coefficient. (J/kg.°C)

Using this model the linear heat capacity coefficients for Whole and Skim Milk were determined. Literature sources were also found for these coefficients (Fernandez-Martin, 1972). The comparison between the experimental and model predictions are shown in Table A-3.

A.5) Viscosity

The viscosity of milk solutions at low shear rates has been calculated by the Eiler equation (Snoeren *et al*, 1982). This equation relates the viscosity to the volume fraction of the dissolved solute particles. Eiler's equation assumes that the dissolved solute particles are compact spheres and it has been shown that the protein component of milk can be described by this assumption. The equation also neglects the non-Newtonian nature of the milk. However, the shear rates of falling films are usually low and it is therefore possible to assume that the fluid is Newtonian. The maximum volume fraction of the solute components has been given as 0.79 for Skim Milk (Snoeren *et al*, 1982).

$$\mu = \mu_{water}\left[1 + \frac{1.25\Phi}{1 - \Phi/\Phi_{max}}\right]^2 \tag{A.22}$$

Where, μ = viscosity of milk solution. (kg/m.s)

μ_{water} = viscosity of water. (kg/m.s)

Φ = volume fraction of dissolved solute particles. (-)

Φ_{max} = maximum volume fraction dissolved solute particles. (= 0.79)

The volume fraction of the dissolved solute particles can be determined from the following. When used to descibe the viscosity of milk, only the protein and fat components are used to calculate the volume fraction. The lactose and mineral salt components do not behave as compact spheres and so their impact on the viscosity is not accurately described by Eiler's equation. In the paper of Snoeren *et al* (1982), the lactose and mineral salts contribution to the viscosity is modelled using an empirical linear relationship (i.e., $\frac{\mu_{lactose+salt}}{\mu_{water}} = [1 + d_1.w_{TS}]$). The resulting equation is given by (A.24).

$$\Phi = \mu_{TS}.w_{TS}.\rho, \qquad \mu_{TS} = v_{cas}.x_{cas} + v_{whey}.x_{whey} + v_{fat}.x_{fat} \tag{A.23}$$

$$\mu = \mu_{water}\left[1 + d_1 . w_{TS}\left[1 + \frac{1.25\mu_{TS} . w_{TS} \cdot \rho_{water}}{1-(a_{TS} + \mu_{TS} \cdot \rho_{water} / \Phi_{max})w_{TS}}\right]^2\right] \quad (A.24)$$

Where, w_{TS} = total solids content of the milk. (kg/kg)
μ_{TS} = viscosity parameter. (kg/m.s)
ρ = milk solution density. (kg/m^3)
v = specific volume of mixture component. (m^3/kg)
d_1 = linear coefficient for lactose and salt contribution to viscosity. (-)
a_{TS} = density dry matter parameter. (-)

The viscosity temperature dependence is determined by the viscosity of water and the component specific volumes. It is well known that the viscosity of water varies greatly with temperature, but the component specific volumes also vary. In addition, changes in the milk composition can cause a change in the viscosity temperature dependence. For example, the specific volumes of natural and de-natured whey proteins are substantially different. Since the whey de-naturation reactions are temperature dependent, this causes an additional viscosity temperature dependence.

Table A-4 : Specific volumes of milk components.

	Inverse of specific density (l/kg)	**Experimental specific volume (l/kg)**
Milkfat	1.039	- *1
Casein protein	0.784	3.57
Whey protein	0.784	1.07
Denatured whey protein	0.784	3.09

Table A-5 : Viscosity model parameters.

Milk	**Milkfat (%)**	**Lactose (%)**	**Protein (%)**	**Salt (%)**	**Snoeren μ_{TS} (m^3/kg)**
Whole	27.7	38.4	27.9	6	0.001144
Skim	0.8	53.1	37.9	8.1	0.001172

The specific volumes (v) for the components are strictly the inverse of the densities. However, it has been found experimentally that the protein specific volumes are considerably larger than the inverse densities (Snoeren *et al*, 1982). Additionally it has been found that the specific volumes for natural and de-natured whey proteins are very different. This means that the viscosity dry

*1 No experimental results appear to be available for the specific volumes of milk fat.

matter relationship depends on the preheat conditions since these determine the amount of whey protein denaturation.

Using these specific volumes we can calculate the viscosity parameter (μ_{TS}) for Whole and Skim Milk solutions, as shown in Table A-5. These results were calculated by assuming that 20 % of the milk protein exists as whey protein and that the proteins have not been de-natured.

A.6) Pure fluid saturation relationships

The prediction of water liquid/vapour saturation relationships is very important. We are interested in the relationships between the pressure, density and temperature. The thermodynamic criteria for liquid/vapour coexistence is the equality of the Gibbs free energies.

$$G_l = G_v \tag{A.25}$$

Where, G_l = Gibbs free energy of the liquid. (J)

G_v = Gibbs free energy of the vapour. (J)

With some suitable assumptions this equation can be rearranged into the Clasius-Clapeyron equation (Sandler, 1989, p 238). Notice that the temperature is required in degrees Kelvin for this equation.

$$\left(\frac{\partial \ln(P_{sat})}{\partial T_{sat}}\right) = \frac{\lambda}{R.T_{sat}^2} \tag{A.26}$$

Where, λ = latent heat of vapourisation. (J/kg)

R = universal gas constant. (J/kg.K)

T_{sat} = boiling temperature, in degrees Kelvin. (K)

P_{sat} = saturation temperature. (Pa)

With the assumption of constant latent heat this is integrated to produce equation (A.27).

$$\ln[P_{sat}] = A - \frac{\lambda}{R.T_{sat}} \tag{A.27}$$

In practice the assumptions made in the derivation of this equation are not very accurate and a semi-empirical version, the Antoine equation, is used. As for the above the temperature is required in degrees Kelvin.

$$\ln[P_{sat}] = A_{water} - \frac{B_{water}}{[T_{sat} - C_{water}]} \tag{A.28}$$

Where, A_{water} = fitting coefficient used in the Antoine equation. (-)

B_{water} = fitting coefficient used in the Antoine equation. (K)

C_{water} = fitting coefficient used in the Antoine equation. (K)

The density of the vapour is strictly given by the combination of the above Antoine equation with an Equation of State. However, the relationship between the saturation temperature and vapour density can also be accomodated using the Antoine equation. Once again, the temperature used in this equation is in degrees Kelvin.

$$\ln[\rho_{ve}] = A_{vap} - \frac{B_{vap}}{[T_{sat} - C_{vap}]} \tag{A.29}$$

Where, A_{vap} = fitting coefficient used in the vapour density Antoine equation. (-)

B_{vap} = fitting coefficient used in the vapour density Antoine equation. (K)

C_{vap} = fitting coefficient used in the vapour density Antoine equation. (K)

The parameters in the above Antoine equations can be identified from a set of saturation data for water (Rogers and Mayhew, 1988). The resulting parameters are $A_{water} = 23.1748$, $B_{water} = 3806.44$, $C_{water} = 46.36$, $A_{vap} = 10.5884$, $B_{vap} = 3680.109$ and $C_{vap} = 41.6919$.

A.7) Mixture saturation relationships

When additional components are dissolved in water the mixture will boil at a different temperature to that given by the Antoine equation. This difference between the boiling temperature of pure water and the mixture is called the boiling point elevation. Starting from the equality of Gibbs free energies and using the assumption of an ideal mixture we can produce the classical equation for the boiling point elevation.

$$\Delta T_{BPE} = \left[\frac{1}{\frac{1}{T_{sat}} + \frac{R.\ln(1-x_{sol})}{\lambda}} \right] - T_{sat} \tag{A.30}$$

Where, ΔT_{BPE} = boiling point elevation. (°C)

T_{sat} = boiling temperature of water, in degrees Kelvin. (K)

R = universal gas constant. (J/kg.K)

x_{sol} = molar concentration of dissolved solute particles. (mol/mol)

This equation can be expanded to produce the following series, which can be further approximated by equation (A.32). The first approximation in equation (A.32) uses is a simple first term approximation of equation (A.31). The second approximation uses a first term Taylor series approximation of the natural logarithm.

$$\Delta T_{BPE} = T_{sat}\left[1+\frac{R.T_{sat}}{\lambda}\ln\left[\frac{1}{(1-x_{sol})}\right]+\frac{R^2.T_{sat}^2}{\lambda^2}\ln^2\left[\frac{1}{(1-x_{sol})}\right]+\frac{R^3.T_{sat}^3}{\lambda^3}\ln^3\left[\frac{1}{(1-x_{sol})}\right]+\ldots\right]-T_{sat} \quad \text{(A.31)}$$

$$\Delta T_{BPE} = \frac{R.T_{sat}^2}{\lambda}\ln\left[\frac{1}{(1-x_{sol})}\right], \qquad \Delta T_{BPE} = \frac{R.T_{sat}^2.x_{sol}}{\lambda} \quad \text{(A.32)}$$

An important consequence of these equations is that the boiling point elevation is related to the molar concentration rather than the mass concentration. Milk mixtures tend to have small boiling point elevations since the protein and fat components have very large molecular masses. This means that even with high mass concentrations these components have very small molar concentrations. However, the molecular mass of the lactose and the mineral salt components is relatively small. These components essentially determine the milk boiling point elevation. The total solute mole fraction in the milk mixture is given by equation (A.33), where the summation is made over the solute dry matter components ($w_{water} = 1 - \sum w$). This can be rearranged into equation (A.34) for x_{sol}.

$$x_{sol} = \frac{\sum_{i=1}^{n}\left(\frac{w_i}{M_i}\right)}{\left[\frac{w_{water}}{M_{water}}+\sum_{i=1}^{n}\left(\frac{w_i}{M_i}\right)\right]}, \qquad x_{sol} = \frac{M_{water}\sum_{i=1}^{n}\left(\frac{w_i}{M_i}\right)}{\left[1+\sum_{i=1}^{n}\left(\frac{w_i.M_{water}}{M_i}-w_i\right)\right]} \quad \text{(A.33)}$$

$$x_{sol} = \frac{b_{TS}.w_{TS}}{\left[1+(b_{TS}-1)w_{TS}\right]}, \qquad b_{TS} = \frac{M_{water}}{M_{fat}}x_{fat}+\frac{M_{water}}{M_{prot}}x_{prot}+\frac{M_{water}}{M_{lact}}x_{lact}+\frac{M_{water}}{M_{salt}}x_{salt} \quad \text{(A.34)}$$

Where, b_{TS}	=	parameter used in the boiling point elevation model.	(-)
M_{water}	=	molecular mass of water.	(kg/kmol)
M_{fat}	=	molecular mass of fat, that occurs in milk solutions.	(kg/kmol)
M_{prot}	=	molecular mass of protein, that occurs in milk solutions.	(kg/kmol)
M_{lact}	=	molecular mass of lactose, that occurs in milk solutions.	(kg/kmol)
M_{salt}	=	molecular mass of salt, that occurs in milk solutions.	(kg/kmol)

The molecular masses of the mixture components are shown in Table A-6. Using these values we can determine numerical values for the b_{TS} parameter. Table A-7 shows the calculated b_{TS} coefficients for Whole Milk and Skim Milk. Figure A-1 shows the boiling point elevation calculated using equation (A.30) and some experimental boiling point data for Skim Milk (Trinh *et al*, 1996).

Table A-6 : Molecular mass of milk components.

	Molecular Mass (kg/kmol)
Milk fat	30000
Lactose	300
Protein	24000
Salt	100
Water	18

Table A-7 : Boiling point elevation coefficients for Whole and Skim Milk.

Milk	Milkfat (%)	Lactose (%)	Protein (%)	Salt (%)	b_{TS} (-)
Whole	27.7	38.4	27.9	6	0.03422
Skim	0.8	53.1	37.9	8.1	0.04673

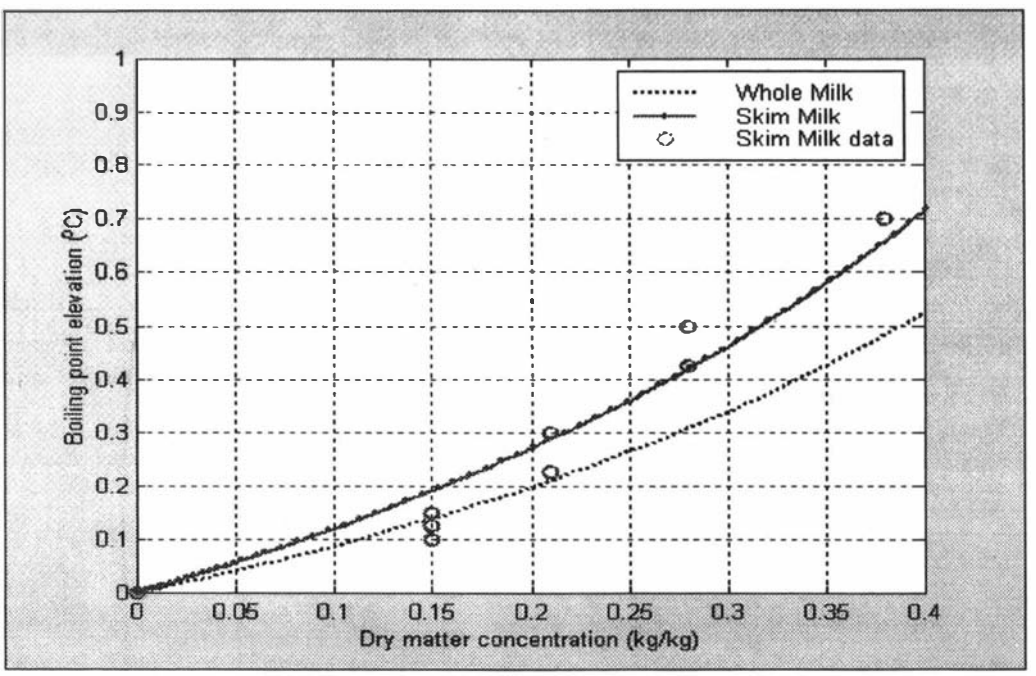

Figure A-1 : Boiling point elevation vs dry matter concentration.

Appendix B I : Falling Film Models and Heat Transfer Coefficients

BI.1) Introduction

Here we investigate some models for the average velocities and heat transfer coefficients of falling films. The simplest model is the Nusselt model and it shall be considered first. This produces a simple, but important result, for the falling film velocity and heat transfer coefficient. However, the Nusselt solution is limited to Laminar flow and so it cannot be applied to general falling films. As a result, the general velocity model of Dukler and some empirical heat transfer models will also be considered.

BI.2) The Nusselt Laminar Model

An exact solution to the falling film transport equations was originally derived by Nusselt (1916). The solution requires a number of simplifications and is only accurate for laminar flow. However, it provides a simple starting point for understanding the nature of a falling film. Nusselt derived his classic parabolic velocity profile.

$$u = \frac{\rho.g}{\mu}\left(\delta.y - \frac{1}{2}y^2\right), \qquad \rho.g = \mu\frac{d^2u}{dy^2}, \qquad \left.\frac{du}{dy}\right|_{y=\delta} = 0, \qquad u|_{y=0} = 0 \qquad \text{(BI.1)}$$

Where, u	=	velocity of the falling film.	(m/s)
y	=	distance from wall.	(m)
ρ	=	density of liquid.	(kg/m^3)
μ	=	Newtonian viscosity of liquid.	(kg/m.s)
δ	=	falling film thickness.	(m)
g	=	acceleration due to gravity.	(m/s^2)

This can be integrated to produce the average film velocity and the mass flow per unit perimeter.

$$u_{aver} = \frac{1}{\delta}\int_0^{\delta} u(y)dy = \frac{\rho.g.\delta^2}{3.\mu}, \qquad \Gamma = \rho.u_{aver}.\delta = \frac{\rho^2.g.\delta^3}{3.\mu} \qquad \text{(BI.2)}$$

Where, u_{aver}	=	average falling film velocity.	(m/s)
Γ	=	mass flow per unit perimeter, or falling film liquid loading.	(kg/m.s)

Nusselt then assumed that the heat transfer was due to conduction and therefore a linear temperature profile could be used. Integration of Fourier's Law produces the following explicit equation for the heat transfer coefficient.

$$h=\frac{k}{\delta}=k\sqrt[3]{\frac{\rho^2.g}{3.\mu.\Gamma}} \qquad \text{(BI.3)}$$

Where, h = falling film heat transfer coefficient. ($W/m^2.°C$)
k = thermal conductivity. ($W/m.°C$)

Using Nusselt's definition for the falling film Nusselt number ($Nu=\frac{h}{k}\left(\frac{\mu^2}{\rho^2.g}\right)^{\frac{1}{3}}$), he produced his classic correlation with the Reynolds number ($Re=\frac{4.\Gamma}{\mu}$). This definition for the Reynolds number is derived from the classic definition ($Re=\frac{\rho.u_{aver}.d_h}{\mu}$), the hydraulic diameter ($d_h=\frac{4.A}{P}$) and the liquid loading ($\Gamma=\frac{m}{P}=\frac{\rho.u_{aver}.A}{P}$).

$$Nu=\left(\frac{4}{3}\right)^{\frac{1}{3}}Re^{-\frac{1}{3}} \qquad \text{(BI.4)}$$

Where, d_h = hydraulic diameter. (m)
A = cross sectional area of falling film. (m)
P = falling film tube perimeter. (m)

A second equation, that is often quoted, is the integrated version of this along the length of the tubes ($h=\frac{1}{L}\int_0^L h_x dx$)(Holman, 1989; p 494).

$$h=\frac{4}{3}h_x, \quad Nu=\left(\frac{4}{3}\right)^{\frac{4}{3}}Re^{-\frac{1}{3}}=1.47Re^{-\frac{1}{3}} \qquad \text{(BI.5)}$$

The Nusselt equations are exact for laminar flow with no surface waves. However, it has been shown theoretically that vertical falling films always contain surface waves (Benjamin, 1957). In addition the falling film changes from laminar to turbulent flow at Reynolds numbers above approximately 1000. As a result, the Nusselt falling film equations cannot be used to describe general falling films.

BI.3) Semi-empirical Dukler Model

A simple semi-empirical method for describing a falling film under turbulent conditions has been developed by Dukler (1952) using the Nikuradse universal velocity profile.

$$
\begin{aligned}
u^+ &= y^+ && 0 < y^+ < 5 \\
u^+ &= -3.05 + 5\ln\left(y^+\right) && 5 < y^+ < 30 \\
u^+ &= 5.5 + 2.5\ln\left(y^+\right) && 30 < y^+ < \delta^+
\end{aligned}
\qquad \text{(BI.6)}
$$

Where, $u^+\left(=\dfrac{u}{\sqrt{g.\delta}}\right)$ = dimensionless film velocity. (-)

$y^+\left(=\dfrac{\rho\sqrt{g.\delta}\,y}{\mu}\right)$ = dimensionless distance from wall surface. (-)

With these dimensionless variables we can produce the following integral equation for the liquid loading.

$$
\Gamma = \mu\int_0^{\delta^+} u^+ dy^+ , \qquad Re = 4\int_0^{\delta^+} u^+ dy^+ \qquad \text{(BI.7)}
$$

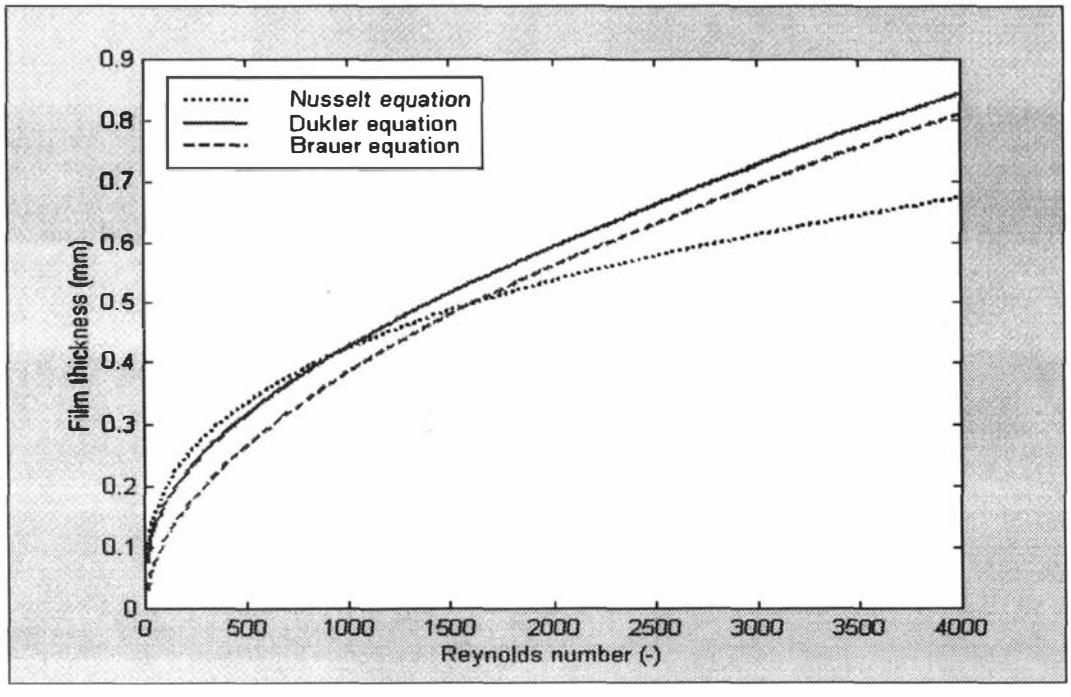

Figure B-1 : Film thickness vs Reynolds number, using Nusselt, Dukler and Brauer models.

Substituting the Nikuradse velocity profile, we then produce the following piece-wise equation.

$$
\begin{aligned}
Re &= 2\left(\delta^+\right)^2 && 0 < Re < 50 \\
Re &= 50.04 - 32.2\delta^+ + 20\delta^+ \ln\left(\delta^+\right) && 50 < Re < 1124.8 \\
Re &= -255.6 + 12\delta^+ + 10\delta^+ \ln\left(\delta^+\right) && 1124.8 < Re < \infty
\end{aligned}
\qquad \text{(BI.8)}
$$

Where, $\delta^+ \left(= \frac{\rho\sqrt{g.\delta}\delta}{\mu} \right)$ = dimensionless film thickness. (-)

The above film model can be compared with the Nusselt correlation ($\delta = \sqrt[3]{\frac{3.\mu.\Gamma}{\rho^2.g}}$) and other empirical turbulent models (Yeates, 1996). For example the turbulent film thickness model of Brauer is given by the following equation.

$$\delta^+ = 0.0947 Re^{0.8} \qquad \text{(BI.9)}$$

Figure B-1 shows the calculated film thickness for a liquid with a density of 1000 kg/m3 and a viscosity of 0.001 kg/m.s from the Dukler, Nusselt and Brauer models. The Dukler model provides a good description for both the Laminar and Turbulent regions. This result is important because we can use it to calculate the falling film velocity for a given Reynolds number. If we then assume that the falling film properties are constant along its length, we can determine its residence time. The Reynolds number is given by the following.

$$Re = \frac{4.\Gamma}{\mu} \qquad \text{(BI.10)}$$

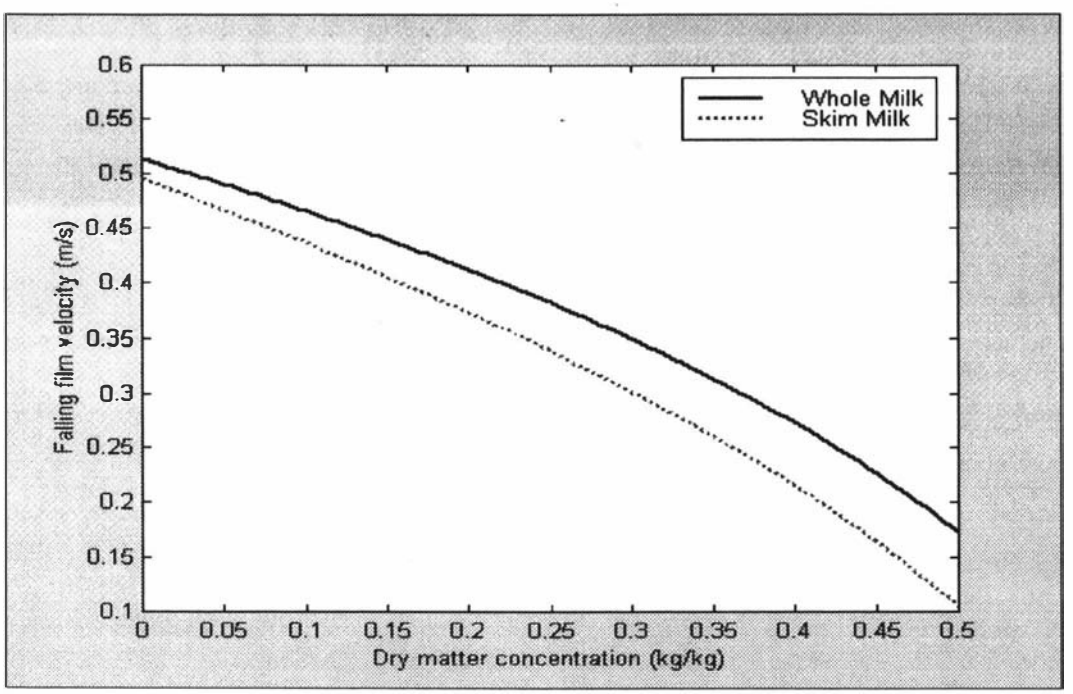

Figure B-2 : Falling film velocity vs Skim Milk and Whole Milk dry matters.

Given the falling film Reynolds number we can calculate the film thickness from the Dukler correlation and then the average film velocity. The residence time is then simply determined from the length of the evaporator tubes and the average film velocity. By assuming that the falling film liquid loading is 0.14 kg/m.s and given the physical property correlations of

Appendix A, we can calculate the average falling film velocities for Whole Milk and Skim Milk. Figure B-2 shows the resulting falling film velocities vs the milk solution dry mass fractions.

BI.4) Empirical Falling Film Heat Transfer Models

There are three empirical models for falling film heat transfer coefficients. The model of Chun and Seban (1971) is very commonly quoted. It describes the Nusselt number in the Laminar region by the following modification of Nusselt's classic equation :

$$Nu = 0.822 Re^{-0.22} \qquad \text{(BI.11)}$$

and in the turbulent region :

$$Nu = 0.0038 Re^{0.4} Pr^{0.65} \qquad \text{(BI.12)}$$

Where, Nu	=	falling film Nusselt number ($Nu = \frac{h}{k}\left(\frac{\mu^2}{\rho^2.g}\right)^{\frac{1}{3}}$).	(-)
Re	=	falling film Reynolds number ($Re = \frac{4.\Gamma}{\mu}$).	(-)
Pr	=	falling film Prandlt number ($Pr = \frac{C_p.\mu}{k}$).	(-)
h	=	heat transfer coefficient.	($W/m^2.K$)
k	=	thermal conductivity.	(W/m.K)
μ	=	viscosity.	(kg/m.s)
ρ	=	density.	(kg/m^3)
C_p	=	heat capacity.	(J/kg.K)
Γ	=	falling film liquid loading.	(kg/m.s)

Chun and Seban also showed that the transition from laminar to turbulent flow depends on the Prandtl number by the following equation.

$$Re = 2460 Pr^{-0.65} \qquad \text{(BI.13)}$$

The Chun and Kim (1990) model does not separate the flow into Laminar and Turbulent regions but uses a single equation that is applicable to both.

$$Nu = 1.33 Re^{-\frac{1}{3}} + 9.56x10^{-6} Re^{0.89} Pr^{0.94} + 0.00822 \qquad \text{(BI.14)}$$

A considerably more advanced model is that of Alhusseini *et al* (1998). This model potentially accounts for the presence of surface waves and turbulence. The heat transfer coefficient is given by the combination of the laminar and turbulent Nusselt numbers.

$$Nu = \left(Nu_l^5 + Nu_t^5\right)^{\frac{1}{5}} \qquad \text{(BI.15)}$$

The Laminar flow Nusselt number is given by the following equation.

$$Nu_l = 2.65\,\mathrm{Re}^{-0.158}.Ka^{0.0563} \qquad \text{(BI.16)}$$

The turbulent flow Nusselt number is given by the following equation.

$$Nu_t = \frac{Pr.\delta^{\frac{1}{3}}}{\left[9.17.Pr^{\frac{3}{4}} + A_2.Pr^{\frac{1}{2}} + A_3.Pr^{\frac{1}{4}} + C_t + B.Ka^{\frac{1}{2}}.Pr^{\frac{1}{2}}\right]} \qquad \text{(BI.17)}$$

$$A_2 = 0.328\pi\frac{\left(130+\delta^+\right)}{\delta^+}, \qquad A_3 = 0.0289\frac{\left(152100+2340\delta^+ + 7\left(\delta^+\right)^2\right)}{\left(\delta^+\right)^2} \qquad \text{(BI.18)}$$

$$B = 2.51x10^6\left(\delta^+\right)^{\frac{1}{3}}\frac{Ka^{-0.173}}{Re^{0.349.Ka^{0.0675}}}, \qquad C_t = 8.82 + 0.0003Re, \qquad \delta^+ = 0.0946Re^{0.8} \qquad \text{(BI.19)}$$

Where, $Ka\left(\frac{g.\mu^4}{\rho.\sigma^3}\right)$	=	Kapitsa dimensionless number.	(-)
σ	=	Surface tension.	()
μ	=	Viscosity.	(kg/m.s)
ρ	=	Density.	(kg/m^3)

Appendix B II : Falling Film Models and Heat Transfer Coefficients

BII.1) Introduction

In this Appendix we investigate some simple falling film heat transfer models for milk and also some heat transfer models for forced/natural convection. In Appendix BI some empirical correlations for the evaporating heat transfer coefficients were represented. However, the correlations are very complex and it would be valuable if simpler equations could be determined. Here we shall be primarily concerned with determining these 'simpler' models for evaporating falling films, working with milk solution. An important part of this is the integration of the falling film static equations, to account for the variation in the milk dry matter down the length of the falling film. The final part of this Appendix will consider some empirical correlations for forced and natural convection.

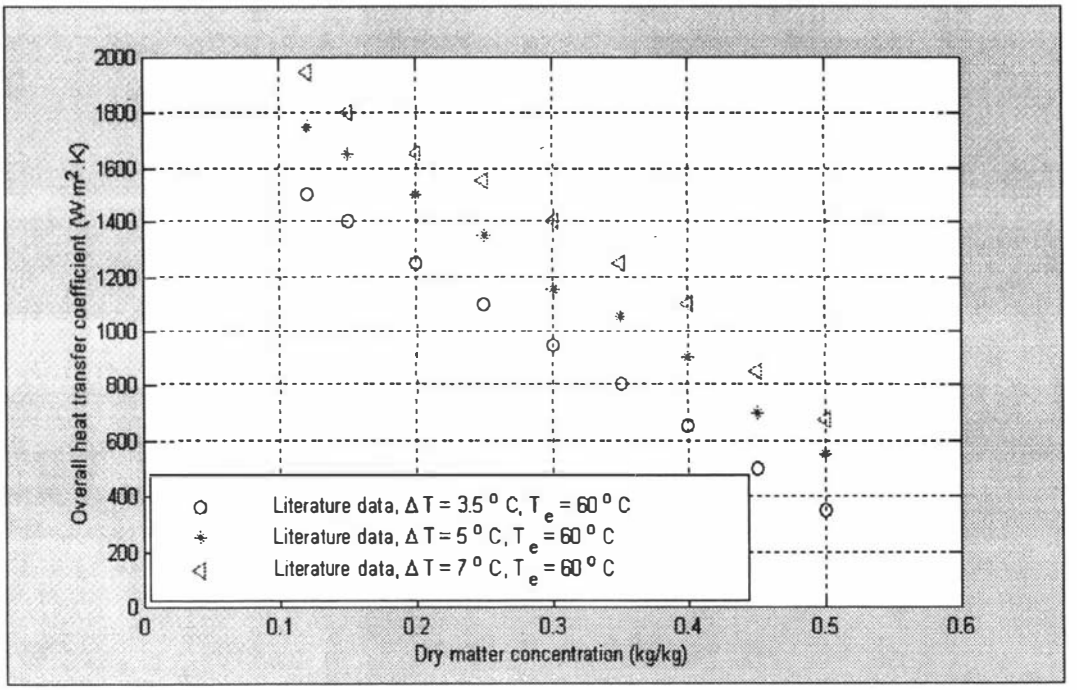

Figure B-1 : Experimental Whole Milk falling film overall heat transfer coefficient vs dry matter.

BII.2) Heat Transfer Coefficients for Milk

In the previous Appendix we investigated some models for the heat transfer coefficients of falling films. The models show that the coefficients depend on the Reynolds and Prandlt numbers. This means that the heat transfer coefficients depend on the falling film mass flow and the physical properties. However, for milk solutions the physical properties have the most

important impact, because they are strong functions of the dry matter concentration. This is shown by the results in Figure B-1 for the Whole Milk overall heat transfer coefficient vs dry matter concentration (Trinh *et al*, 1996). Clearly the overall heat transfer coefficient reduces dramatically as the milk dry matter increases.

An additionally important effect is the occurrence of nucleate boiling. The correlations of the previous Appendix assume that the heat transfer occurs by convection only and that there is no nucleate boiling. For milk solutions, which have lower surface tensions than water, nucleate boiling is likely to have some impact on the heat transfer coefficients. This is the probable cause of the impact of the temperature difference shown in Figure B-1. However, we shall neglect the impact of nucleate boiling and only consider the relationship between dry matter and heat transfer coefficient.

A simple method for accommodating the impact of dry matter on the heat transfer coefficient is to use a linear model.

$$U = U_{lo} - U_{lw}.w \tag{BII.1}$$

This equation is simple but it can only be applied for a specific dry matter concentration range. A model that can potentially be applied for a larger dry matter range is given by the following.

$$U = \frac{U_{eo}}{\left[1 + U_{ew} e^{\beta.w}\right]} \tag{BII.2}$$

This can also be derived from Nusselt's correlation which is given by the following.

$$h = \left(\frac{1}{3}\right)^{\frac{1}{3}} \left(\frac{k^3.\rho^2.g}{\mu.\Gamma}\right)^{\frac{1}{3}} \tag{BII.3}$$

The milk viscosity can be approximated by an exponential equation ($\mu = \mu_o e^{\beta_1.w}$), which varies greatly with dry matter. However, the density, thermal conductivity and liquid loading are comparatively constant. If we neglect the variation in density, thermal conductivity and liquid loading and only include the viscosity effect then the following equation is produced.

$$h = \left(\frac{1}{3}\right)^{\frac{1}{3}} \left(\frac{k^3.\rho^2.g}{\mu_o.\Gamma}\right)^{\frac{1}{3}} e^{-\frac{\beta_1.w}{3}} = h_w e^{-\frac{\beta_1.w}{3}} \tag{BII.4}$$

$$U = \frac{h_w e^{-\frac{\beta_1.w}{3}} h_o}{\left[h_w e^{-\frac{\beta_1.w}{3}} + h_o\right]} = \frac{h_o}{\left[1 + \frac{h_o}{h_w} e^{\frac{\beta_1.w}{3}}\right]} = \frac{U_{eo}}{\left[1 + U_{ew} e^{\beta.w}\right]} \tag{BII.5}$$

Where, h_w = heat transfer coefficient of falling film with water. ($W/m^2.K$)

h_o = heat transfer coefficient of condensing falling film. ($W/m^2.K$)

U = overall heat transfer coefficient. ($W/m^2.K$)

The falling film is a distributed parameter system so the heat transfer coefficient varies along the length of the falling film. We could take the average falling film dry matter and use this to determine the overall heat transfer coefficient. However, a better method is to integrate the static falling film partial differential equations which are derived in Chapter 2.

Linear overall heat transfer coefficient model

The steady flow profile is given by the following.

$$\frac{dM}{dx}+U(w)\frac{\pi.d.n}{\lambda}\left[T_s-T_e-\Delta T_{bpe}(w)\right]=0, \qquad \frac{d[M.w]}{dx}=0 \tag{BII.6}$$

The dry matter differential equation can be easily solved.

$$w(x)=\frac{M_d.w_d}{M(x)} \tag{BII.7}$$

Now if we assume linear relationships between the boiling point elevation/heat transfer coefficients and dry matter (i.e., $\Delta T_{bpe}=\alpha.w$ and $U=U_{lo}-U_{lw}.w$) we can substitute these into equation (BII.6) and produce a differential equation for the flow down the film. This equation can be integrated to produce the following implicit equation for the mass flow of evaporation in the falling film (i.e., $M_{tubes}=M_d-M_e$).

$$M_{tubes}-\frac{\alpha^2 M_d.w_d}{\Delta T^2\left[\frac{\alpha}{\Delta T}-\frac{U_{lw}}{U_{lo}}\right]}\ln\left[1-\frac{M_{tubes}.\Delta T}{M_d(\Delta T-\alpha.w_d)}\right]-\frac{U_{lw}^2 M_d.w_d}{U_{lo}^2\left[\frac{U_{lw}}{U_{lo}}-\frac{\alpha}{\Delta T}\right]}\ln\left[1-\frac{U_{lo}.M_{tubes}}{M_d(U_{lo}-U_{lw}.w_d)}\right]=\frac{U_{lo}.\pi.d.n.L.\Delta T}{\lambda} \tag{BII.8}$$

The heat flow through the evaporator tubes is given by the following integral equation.

$$q_{shell}=\int_0^L\left[U_{lo}-U_{lw}.w\right]\pi.d.n\left[\Delta T-\alpha.w\right]dx \tag{BII.9}$$

This integral equation can be solved by substitution of the differential equation $\frac{dw}{dx}=\frac{w^2\left[U_{lo}-U_{lw}\right]\pi.d.n\left[\Delta T-\alpha.w\right]}{\lambda M_d.w_d}$.

$$q_{shell}=\lambda M_d.w_d\left[\frac{1}{w_d}-\frac{1}{w_e}\right]=\lambda M_{tubes} \tag{BII.10}$$

If we neglect the boiling point elevation, then equation (BII.8) simplifies to the following.

$$M_{tubes} - \frac{U_{lw}.M_d.w_d}{U_{lo}} \ln\left[1 - \frac{U_{lo}.M_{tubes}}{M_d(U_{lo} - U_{lw}.w_d)}\right] = \frac{U_{lo}.\pi.d.n.L.\Delta T}{\lambda} \qquad \text{(BII.11)}$$

This is an implicit equation for the mass of evaporation in the falling film. However, if we use a first term MacLaurin series approximation for the logarithm of 1-x (i.e., $\ln(1-x) \approx -x$) we can produce the following equation. This is explicit for the mass flow of evaporation and it is also linear in terms of the heat transfer parameters. However, because this equation is only an approximation of (BII.11) the model parameters are not exactly the same and they are given different definitions (i.e., $U_{lo} \neq U_{so}$, $U_{lw} \neq U_{sw}$).

$$M_{tubes} = [U_{so} - U_{sw}.w_d]\frac{\pi.d.n.L.\Delta T}{\lambda} \qquad \text{(BII.12)}$$

Exponential heat transfer coefficient model

The overall heat transfer coefficient and the boiling point elevation are given by the following functions.

$$U = \frac{U_{e0}}{\left[1 + U_{ew}.e^{\beta.w}\right]}, \quad \Delta T_{bpe} = \alpha.w \qquad \text{(BII.13)}$$

The steady state mass balances produces the following differential equations.

$$\frac{dM}{dx} + \frac{U_{e0}.\pi.d.n[\Delta T - \alpha.w]}{\left[1 + U_{ew}e^{\beta.w}\right]\lambda} = 0, \qquad \frac{d[M.w]}{dx} = 0 \qquad \text{(BII.14)}$$

The second of these can be solved and substituted to produce the following differential equation for the dry matter down the falling film length.

$$\frac{dw}{dx} = \frac{w^2.U_{e0}.\pi.d.n[\Delta T - \alpha.w]}{M_d.w_d\left[1 + U_{ew}.e^{\beta.w}\right]\lambda} \qquad \text{(BII.15)}$$

This differential equation is difficult to solve. However, it is simplified quite considerably if the boiling point elevation is neglected.

$$\left[\frac{1}{w_d} - \frac{1}{w_e}\right] + U_{ew}\int_{w_d}^{w_e}\frac{e^{\beta.w}}{w^2}dw = \frac{U_{e0}.A.\Delta T}{\lambda M_d.w_d} \qquad \text{(BII.16)}$$

The solution of this is given by the following, which uses the exponential integral function ($Ei(x) = \int_{-\infty}^{x}\frac{e^t}{t}dt$).

$$M_{tubes}+U_{ew}\left[M_d.e^{\beta.w_d}-M_e.e^{\beta.w_e}\right]+U_{ew}.\beta M_d.w_d\left[Ei(\beta.w_e)-Ei(\beta.w_d)\right]=\frac{U_{eo}.A.\Delta T}{\lambda} \quad \text{(B11.17)}$$

BII.3) Forced Convection Heat Transfer Coefficients

The heat transfer coefficients between a tube surface and a flowing liquid can be predicted using the Dittus and Boelter correlation (Holman, 1989; pp 274-275). This heat transfer occurs in the shell and tube condensers of the Evaporator A plant.

$$Nu=0.023Re^{0.8}.Pr^{0.4} \quad \text{(BII.18)}$$

Where, $Nu\left(=\frac{h.d}{k}\right)$ = Nusselt number.

$Re\left(=\frac{\rho.u.d}{\mu}\right)$ = Reynolds number.

$Pr\left(=\frac{C_p.\mu}{k}\right)$ = Prandlt number.

BII.4) Natural Convection Heat Transfer Coefficient

The heat transfer from the evaporator surfaces is due to natural convection and radiation. For natural convection the heat transfer coefficient can be determined from the following correlations (Holman, 1989; pp 332-339).

$$Nu^{\frac{1}{2}}=0.825+\frac{0.387(Gr.Pr)^{\frac{1}{6}}}{\left[1+\left(\frac{0.492}{Pr}\right)^{\frac{9}{16}}\right]^{\frac{8}{27}}} \quad \text{(BII.19)}$$

$$Nu=0.1(Gr.Pr)^{\frac{1}{3}} \quad \text{(BII.20)}$$

Where, Pr = Prandlt number. $\left(Pr=\frac{C_p.\mu}{k}\right)$

Gr = Grashof number. $\left(Gr=\frac{g.\beta.(T_w-T_{amb})L^3}{\upsilon^2}\right)$

Nu = Nusselt number. $\left(Nu=\frac{h.L}{k}\right)$

It must be remembered that these correlations only apply for natural convection and so they are likely to underestimate the actual heat transfer coefficient. In reality the effect of radiation will cause the coefficient to be larger. The evaporator surfaces are at approximately 60 °C and the ambient temperature around the evaporators is approximately 30 °C. Using these numbers we

can determine that natural convection film temperature ($T_f = \frac{(60+30)}{2} = 318.16K$) and the properties of the air ($\beta = \frac{1}{T_f} = 3.143x10^{-3}\ \frac{1}{K}$, $k = 0.0272$ W/m.K, $Pr = 0.704$ (–), $\nu = 1.683x10^{-5}$ m^2/s). The length of the evaporator surfaces is approximately 16 meters. With this we can determine the Grashof number ($Gr = 9.416x10^{12}$) and hence the Nusselt number ($Nu = 2298.05$). From this the natural convection heat transfer coefficient can be determined ($h = 3.907$ W/m^2.K).

Appendix C : Film Breakdown

C.1) Introduction

Here we investigate some models and experimental data for the breakdown of falling films. This occurs when the falling film flows in rivulets, rather than as a uniform film. The prediction of the mass flow at which breakdown occurs is important for the avoidance of fouling. In this Appendix we describe some models for predicting film breakdown and also make comparisons between the models and some experimental results.

C.2) Hartley and Murgatroyd Model

The simplest film breakdown model is that of Hartley and Murgatroyd (1964). The criteria for film break-up is when the surface tension force is equal to the falling film momentum.

$$\sigma[1-\cos(\theta)]=\frac{\rho}{2}\int_0^{\delta}u^2(y)dy \qquad (C.1)$$

Where, ρ	=	density of falling film liquid.	(kg/m^3)
σ	=	surface tension of falling film liquid.	(N/m)
θ	=	contact angle of liquid with wall surface.	(^{o})
u	=	falling film velocity.	(m/s)
y	=	distance from wall surface.	(m)

Nusselt's classic parabolic film velocity equation is used.

$$u(y)=\frac{\rho.g}{\mu}\left[\delta.y-\frac{1}{2}y^2\right] \qquad (C.2)$$

Where, μ	=	viscosity of falling film liquid.	(kg/m.s)
δ	=	falling film thickness.	(m)
g	=	gravitional acceleration.	(m/s^2)

Substituting the film velocity into the force balance produces the following equation. This gives the critical falling film thickness for film breakdown. Nusselt's falling film model shows that the liquid loading depends on the falling film thickness.

$$\sigma[1-\cos(\theta)]=\frac{\rho}{15}\left(\frac{\rho.g}{\mu}\right)^2\delta^5, \qquad \Gamma=\rho.u_{aver}.\delta=\rho\int_0^{\delta}u(y)dy=\frac{\rho^2.g.\delta^3}{3.\mu} \qquad (C.3)$$

This allows us to determine the critical liquid loading for film break-up. The result is the famous Hartley and Murgatroyd equation.

$$\Gamma_{min} = \frac{1}{3}(15)^{\frac{3}{5}}\left[\frac{\mu.\rho}{g}\right]^{\frac{1}{5}}[\sigma(1-\cos(\theta))]^{\frac{3}{5}} \qquad \text{(C.4)}$$

C.3) Zuber and Staub model

The Hartley and Murgatroyd film breakdown model is strictly only correct for isothermal falling films. When the falling film is being heated additional force terms must be included. Zuber and Staub (1966) included two extra terms.

$$\sigma[1-\cos(\theta)]+\left(\frac{\partial\sigma}{\partial T}\right)\frac{q.\delta_c.\cos(\theta)}{A.k}+\rho_v\left[\frac{q.\cos(\theta)}{A.\rho_v.\lambda}\right]^2\frac{\Delta\rho.\delta_c}{\rho}=\frac{\rho}{2}\int_0^{\delta}u(y)dy \qquad \text{(C.5)}$$

Where, q = heat flow through the film. (W)
A = area of heat flow through the film. (m^2)
k = thermal conductivity of fluid. (W/m.K)

This equation shows that the extra terms depend upon the heat flow per unit area ($\frac{q}{A}=U.\Delta T$), which depends on the temperature difference. For MVR evaporator plants this temperature difference is designed to be small because this improves the energy efficiency. Consequently, for these MVR evaporator plants these terms do not have much impact on the falling film stability.

C.4) Hoke and Chen model

The Hartley and Murgatroyd model assumes that the weight of the liquid above the dry patch is cancelled by the wall shear force. This assumption is relaxed by Hoke and Chen (1992) and they add an additional term to the balance equation. This equation is implicit for the falling film thickness, which is substituted into equation (C.3) to calculate the liquid loading.

$$\sigma[1-\cos(\theta)]=\frac{\rho.g}{4}\left[\frac{\delta}{1-\cos(\theta)}\right]^2[2.\theta-\sin(2.\theta)]+\frac{\rho^3.g^2.\delta^5}{15.\mu^2} \qquad \text{(C.6)}$$

C.5) Chung and Bankoff model

The models of Hartley/Murgatroyd, Zuber/Staub and Hoke/Chen don't consider all of the forces acting on the falling film. Two large papers by Chung and Bankoff (1980) include the forces due to vapour shear, hydrostatic head, wall shear, thermocapillary, evaporative thrust etc. The resulting balance is, however, not as simple as the above and we will not be consider it here.

C.6) Contact Angles

An important part of the determination of the liquid loading for film breakdown is the contact angle. This has been determined for Whole Milk at 20 °C (Paramalingam *et al*, 1999). Table C-1

shows the resulting contact angles and surface tensions. In addition Whole Milk was observed flowing down a vertical surface. The minimum flow for a stable film was determined and the corresponding liquid loading determined. Figure C-1 shows the experimental minimum falling film flows determined along with the Hartley/Murgatroyd and Hoke/Chen model predictions.

Table C-1 : Whole film breakdown parameters.

Dry matter (kg/kg)	Contact Angle (°)	Surface Tension (N/m)	Density (kg/m^3)	Viscosity (kg/m.s)	Observed minimum flow (kg/m.s)
0	93.0	0.0727	998	0.00109	0.222
0.05	67.8	0.0471	1010	0.00187	0.135
0.10	64.0	0.0476	1022	0.00189	
0.20	60.6	0.0498	1048	0.00401	0.151
0.30	58.3	0.0532	1075	0.01040	0.143
0.40	54.2	0.0580	1103	0.03540	0.123

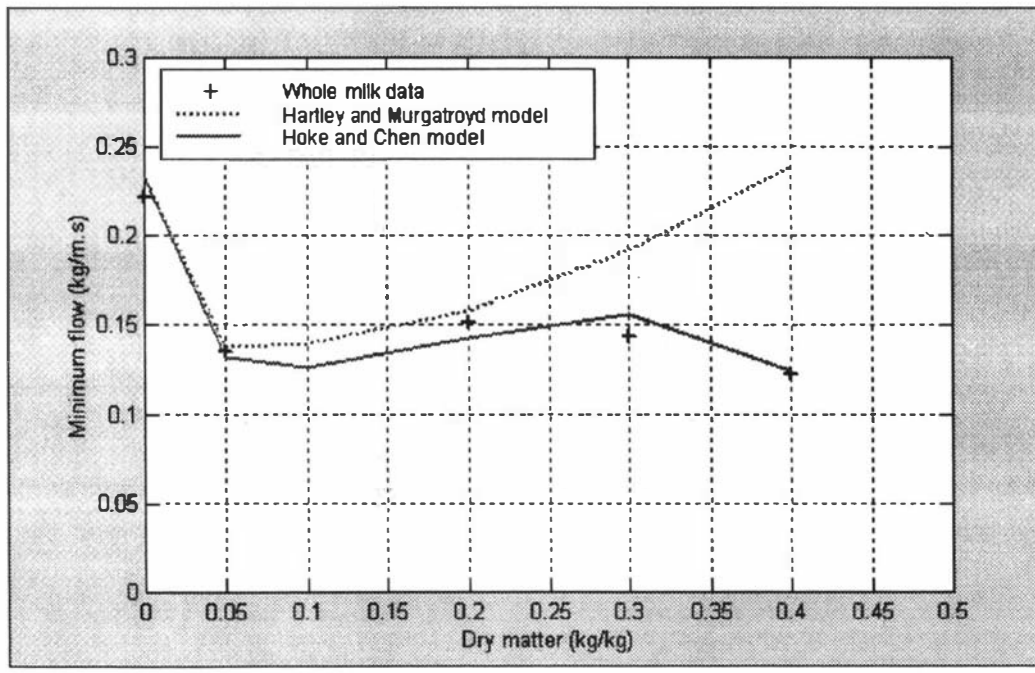

Figure C-1 : Experimental minimum flows, for Whole milk.

Some falling film wetting literature results for Skim Milk in falling film evaporators are also known (Trinh *et al*, 1996). These can also be compared to the Hartley/Murgatroyd and Hoke/Chen models and the results are shown in Figure C-2. Interestingly the model predictions are higher than the literature results. This is probably due to the contact angles of the falling film evaporator tubes. Presumably the tubes are polished and carefully maintained so that the contact angles are lower. The Skim Milk literature data can be fitted to a polynomial function in terms of the dry matter concentration. This is shown in Figure C-2 along with the model predictions and literature data.

C.6) Experimental Water film Break-up

In Chapter 5 the TVR parameter identification neglected some data points. Here we show that these data points correspond to film break-up in the seventh pass of the Evaporator A plant. When falling film break-up occurs the measured heat transfer coefficient is smaller than expected because the heat transfer area is reduced. As a result, the heat transfer coefficients cannot be identified with data that includes film breakdown.

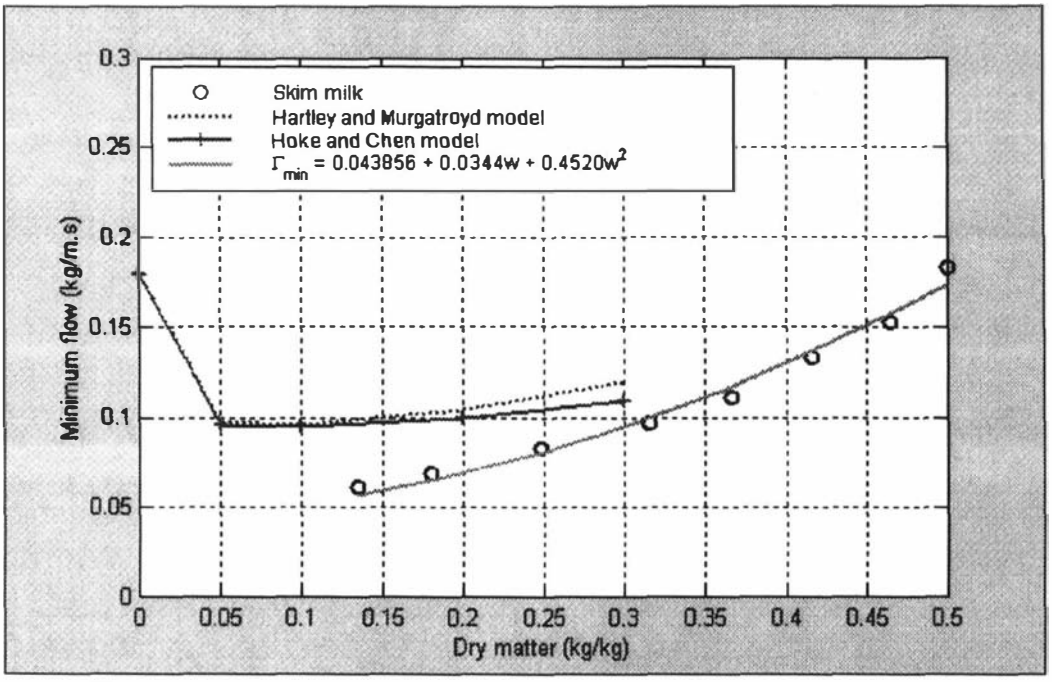

Figure C-2 : Skim milk minimum liquid loadings vs dry matter.

Using historical data from the Evaporator A plant we can calculate the overall heat transfer coefficient in the third evaporator effect. The second effect overall energy balance is given by equation (C.7). This equation is also shown by equation (5.24) and it is derived by the addition of equations (2.30) and (2.63).

$$q_{feed6} + W_{comp2} = q_{shell7} + q_{shell8} + q_{eloss2} + q_{sloss2} + q_{condensate2} \tag{C.7}$$

This can be rearranged into an explicit equation for the overall heat transfer coefficient in the third evaporator effect.

$$\frac{\left[q_{feed6} + W_{comp2} - q_{eloss2} - q_{sloss2} - q_{condensate2}\right]}{\left[A_{s7} + A_{s8}\right]\left[T_{e2} - T_{e3}\right]} = \left[U_{s7} + U_{s8}\right] \tag{C.9}$$

Figure C-3 shows the calculated overall heat transfer coefficients vs the mass flow from the bottom of the evaporator tubes. As expected the heat transfer coefficients dramatically reduce at low flow rates. This is consistent with the expectation that heat transfer coefficients are lower when falling film breakdown occurs. We can test whether the results in Figure C-3 represent film break-up by using the Hartley and Murgatroyd equation. With a contact angle of 93 ° and the

physical properties of water at 55 °C we can calculate the mass flow required for a wetted film. The thick lines in Figure C-3 show the calculated mass flows required for film breakdown in the seventh and eighth evaporator passes. It appears that the reduction in heat transfer coefficients at low flows is due to film breakdown in the seventh pass.

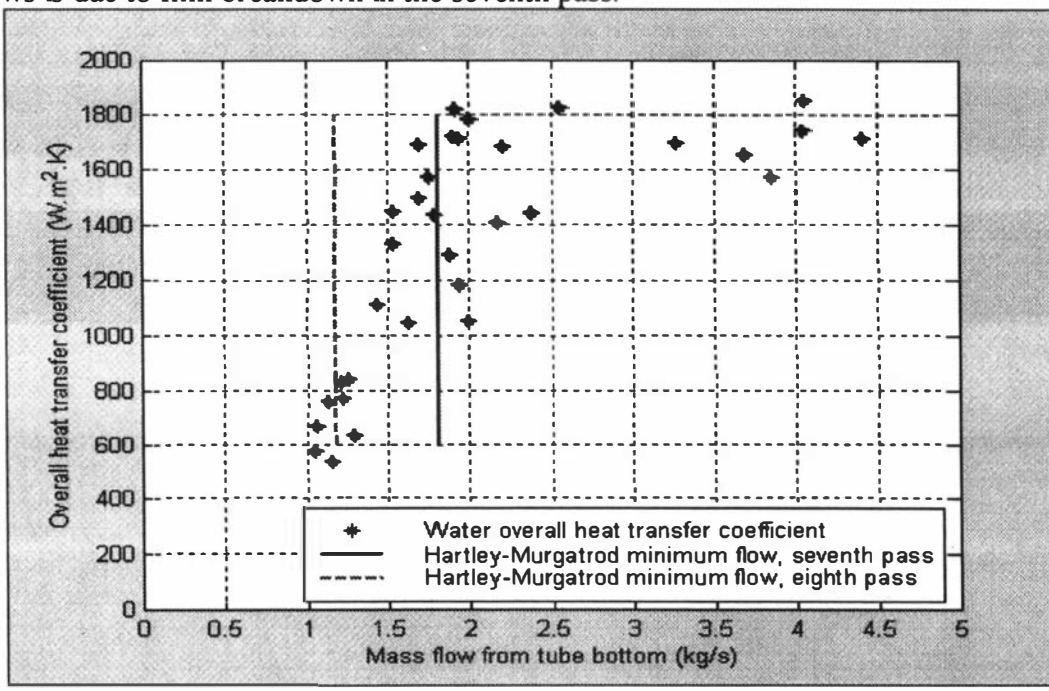

Figure C-3 : Overall heat transfer coefficients vs mass flow from tube bottom.

Appendix D : TVR Compressor Models

D.1) Introduction

A thermal compressor uses high pressure steam to compress a low pressure vapour. These compressors are also called jet ejectors and they are sometimes used as vacuum pumps. Figure D-1 shows a TVR (Thermal Vapour Recompression) compressor.

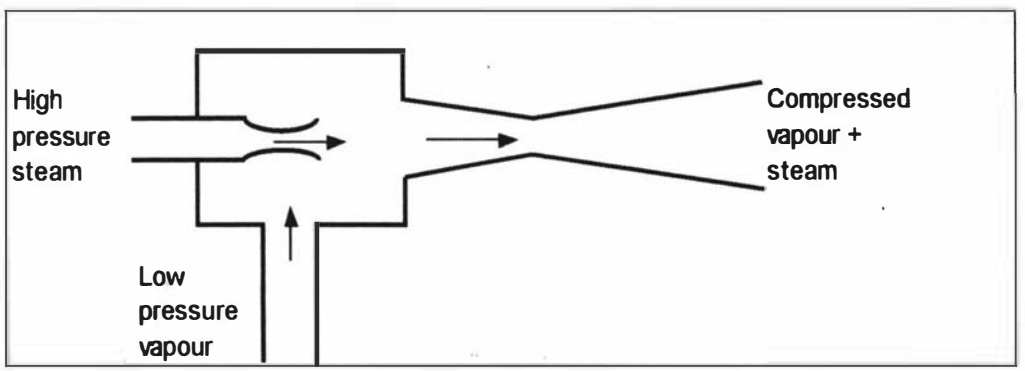

Figure D-1 : A TVR compressor.

The description of the TVR compressor, by all models, will be separated into two sections. Firstly the determination of the mass flow of high pressure steam and secondly the determination of the entrainment ratio of high pressure steam to low pressure vapour.

D.2) The Sonic Orifice Equation

The flow of a high pressure steam through a nozzle can be given by equation (D.1) (van Wylen, 1994). This applies for sonic flow through the nozzle, which commonly occurs in the high pressure steam nozzle of a TVR compressor.

$$m_{steam} = A_{throat} . P_{steam} \sqrt{\frac{2}{R.T}\left(\frac{2}{\gamma+1}\right)^{\frac{(\gamma+1)}{(\gamma-1)}}} = A_{TVR} . P_{steam} \qquad \text{(D.1)}$$

Where, m_{steam} = mass flow of steam through the TVR compressor nozzle. (kg/s)

P_{steam} = high pressure steam supply pressure. (Pa)

R = universal gas constant. (kJ/kg.K)

T = temperature of high pressure steam. (K)

γ = ratio of constant pressure and volume heat capacities. $\left(=\frac{C_p}{C_v}\right)$ (-)

A_{throat} = cross sectional area of TVR compressor nozzle throat. (m^2)

Equation (D.1) shows that the mass flow of steam through the TVR compressor nozzle is directly proportional to the pressure of the steam. Using the design specifications of the Evaporator A plant TVR compressor, we can calculate the A_{TVR} parameter. This result can then be compared with the value determined from equation (D.1). The compressor contains four raw steam nozzles each with a diameter of 6.6 mm and this allows us to calculate the nozzle surface area (i.e., $A_{throat} = 0.00013685$ m^2). We can determine the physical properties of the raw steam at the saturated pressure of 10 bar (i.e., $T = 179.9$ °C, $R = 461.88$ J/kg.K, $C_p = 2620$ J/kg.K, $\gamma = 1.214$ (-)) and thereby determine the value for A_{TVR} from equation (D.1) (i.e., $A_{TVR} = 2.5006x10^{-7}$ kg/s.Pa). The design specifications can also be used to determine this parameter (i.e, $m_{steam} = 690$ kg/hr @ $P_{st} = 9$ bar, $A_{TVR} = 2.129x10^{-7}$ kg/s.Pa).

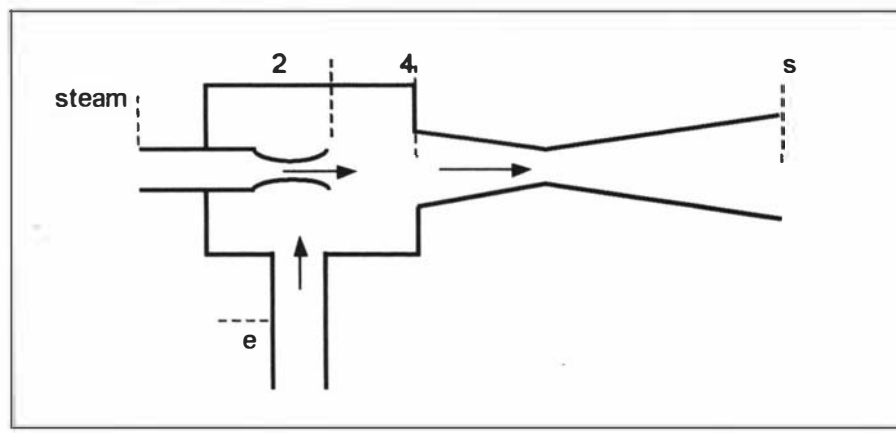

Figure D-2 : TVR compressor balances.

D.3) Kessler TVR Compressor model

The Kessler (1981) model is the simplest TVR compressor entrainment model. It is not very accurate, but it provides a simple starting point for modelling the compressor suction mass flow. Making a momentum and enthalpy balances around the mixing, raw steam entry and diffuser sections produces equation (D.2).

$$m_{steam}.v_2 = (m_{steam} + m_{comp})v_4, \qquad h_4 + \frac{1}{2}v_4^2 = h_s, \quad h_2 + \frac{1}{2}v_2^2 = h_{steam} \tag{D.2}$$

Where, m_{steam} = mass flow of high pressure steam. (kg/s)

m_{comp} = mass flow of the entrained vapour. (kg/s)

v_4 = velocity of the vapour/steam mixture at point 4. (m/s)

v_2 = velocity of the steam at point 2. (m/s)

h_2 = enthalpy of the steam at point 2. (J/kg)

h_4 = enthalpy of the steam at point 4. (J/kg)
h_{steam} = enthalpy of the steam before entering the compressor. (J/kg)
h_s = enthalpy of the vapour/steam mixture exiting the compressor. (J/kg)

Combining these we produce the following equation for the compressor entrainment ratio.

$$m_{steam}\sqrt{2(h_{steam}-h_2)}=(m_{steam}+m_{comp})\sqrt{2(h_s-h_4)}, \qquad w=\frac{m_{comp}}{m_{steam}}=\sqrt{\frac{(h_{steam}-h_2)}{(h_s-h_4)}}-1 \qquad \text{(D.3)}$$

Where, w = entrainment ratio of the compressor. (-)

D.4) DM TVR Compressor Model

A second TVR compressor model has been developed by Dotterweich and Mooney (1955). This model is also simple and is really just a modification of the Kessler model. The end result is equation (D.4) for the entrainment ratio.

$$w=\frac{1}{2}\left[\left(\frac{T_{steam}}{T_e}-1\right)^2+\frac{4.T_{steam}}{T_e}\frac{\left(1-\left(\frac{P_2}{P_{steam}}\right)^{\frac{k-1}{k}}\right)}{\left(1-\left(\frac{P_4}{P_s}\right)^{\frac{k-1}{k}}\right)}\right]^{\frac{1}{2}}-\frac{1}{2}\left(\frac{T_{steam}}{T_e}+1\right) \qquad \text{(D.4)}$$

Where, T_e = temperature of the vapour entering the compressor suction section. (°C)
T_{steam} = temperature of raw high pressure steam. (°C)
P_s = pressure of the exiting vapour/steam mixture. (Pa)
P_{steam} = pressure of raw high pressure steam. (Pa)
P_4 = pressure of the vapour and steam before passing through exit diffuser. (Pa)

D.5) Empirical TVR Compressor Model

Neither of the above models are found to accurately describe the entrainment characteristics of TVR compressors. There are many characteristics of TVR compressors which they do not include. The most important is the constant suction capacity of the compressor. It is often found (Munday and Bagster, 1977) that the flow of suction vapour is independent of the raw steam and compressed vapour properties.

While there have been many models published in the literature that claim to provide a complete description of TVR compressors (Sun and Eames, 1995) none appear to be completely reliable. Consequently we will use a simple empirical model to describe the TVR compressor entrainment characteristics. Equation (D.5) shows the model for the mass flow of suction vapour that we shall use. The basis for this model is taken from the above literature models. The mass flow of suction

vapour is shown to depend on the suction vapour conditions and the high pressure steam condition.

$$M_{comp} = \frac{A_{TVR}.B_{TVR}.P_e.P_{sp}}{(P_{st})^{C_{TVR}}} \qquad (D.5)$$

Where, B_{TVR} = TVR compressor parameter. ($m^{0.03}.s^{0.06}/kg^{0.03}$)

P_e = pressure of the suction vapour to the compressor. (Pa)

P_{st} = raw steam pressure to the TVR compressor. (Pa)

From the design specifications we can deteremine the TVR compressor parameter B_{TVR}. The A_{TVR} parameter was earlier determined to be 2.129×10^{-7} m.s. The design specifications give M_{comp} as 1210 kg/hr, P_{st} as 9 bar and P_e as 0.1815 bar. Using these values we can determine that B_{TVR} is 58.44 $m^{0.03}.s^{0.06}/kg^{0.03}$.

Appendix E : Evaporator Geometries and Computer Tagnames

Powder 3			Powder 4			Powder 5			
First Evaporator Pass			**First Evaporator Pass**			**First Evaporator Pass**			
L_1 =	16	m	L_1 =	16	m	L_1 =	16	m	Length of evaporator tubes.
D_1 =	0.0385	m	D_1 =	0.0385	m	D_1 =	0.0463	m	Diameter of evaporator tubes.
n_1 =	846		n_1 =	846		n_1 =	659		Number of evaporator tubes.
np_1 =	1783		np_1 =	1783		np_1 =	1318		Number of distribution plate holes
dp_1 =	0.0045	m	dp_1 =	0.0045	m	dp_1 =	0.0055	m	Diameter of distribution plate holes
nr_1 =	815		nr_1 =	817		nr_1 =			Number of rising tubes
hr_1 =	45	mm	hr_1 =	45	mm	hr_1 =	45	mm	Height of rising tubes
P_1 =	102.32	m	P_1 =	102.32	m	P_1 =	95.86	m	Perimeter of evaporator tubes
As_1 =	1637.2	m^2	As_1 =	1637.2	m^2	As_1 =	1533.7	m^2	Surface area of evaporator tubes
Ah_1 =	0.0284	m^2	Ah_1 =	0.0284	m^2	Ah_1 =	0.0313	m^2	Surface area of distribution plate holes
Ad_1 =	1.6849	m^2	Ad_1 =	1.6844	m^2	Ad_1 =		m^2	Surface area of distribution plate
Second Evaporator Pass.			**Second Evaporator Pass.**			**Second Evaporator Pass.**			
L_2 =	16	m	L_2 =	16	m	L_2 =	16	m	
D_2 =	0.0385	m	D_2 =	0.0385	m	D_2 =	0.0463	m	
n_2 =	697		n_2 =	697		n_2 =	434		
np_2 =	1470		np_2 =	1470		np_2 =	868		
dp_2 =	0.0045	m	dp_2 =	0.0045	m	dp_2 =	0.0055	m	
nr_2 =	667		nr_2 =	670		nr_2 =			
hr_2 =	45	mm	hr_2 =	45	mm	hr_2 =	45	mm	
P_2 =	84.30	m	P_2 =	84.30	m	P_2 =	63.13	m	
As_2 =	1348.8	m^2	As_2 =	1348.8	m^2	As_2 =	1010.0	m^2	
Ah_2 =	0.0234	m^2	Ah_2 =	0.0234	m^2	Ah_2 =	0.0206	m^2	
Ad_2 =	1.4037	m^2	Ad_2 =	1.4053	m^2	Ad_2 =		m^2	
Third Evaporator Pass			**Third Evaporator Pass**			**Third Evaporator Pass**			
L_3 =	16	m	L_3 =	16	m	L_3 =	16	m	
D_3 =	0.0385	m	D_3 =	0.0385	m	D_3 =	0.0463	m	
n_3 =	466		n_3 =	466		n_3 =	312		
np_3 =	1007		np_3 =	1007		np_3 =	624		
dp_2 =	0.0045	m	dp_3 =	0.0045	m	dp_3 =	0.0055	m	
nr_3 =	447		nr_3 =	445		nr_3 =			
hr_3 =	45	mm	hr_3 =	45	mm	hr_3 =	45	mm	
P_3 =	56.36	m	P_3 =	56.36	m	P_3 =	45.38	m	
As_3 =	901.8	m^2	As_3 =	901.8	m^2	As_3 =	726.1	m^2	
Ah_3 =	0.0160	m^2	Ah_3 =	0.0160	m^2	Ah_3 =	0.0148	m^2	
Ad_3 =	0.9286	m^2	Ad_3 =	0.9291	m^2	Ad_3 =		m^2	
Fourth Evaporator Pass			**Fourth Evaporator Pass**			**Fourth Evaporator Pass**			
L_4 =	16	m	L_4 =	16	m	L_4 =	16	m	
D_4 =	0.0385	m	D_4 =	0.0385	m	D_4 =	0.0463	m	
n_4 =	358		n_4 =	358		n_4 =	247		
np_4 =	777		np_4 =	777		np_4 =	494		
dp_4 =	0.0045	m	dp_4 =	0.0055	m	dp_4 =	0.0055	m	
nr_4 =	330		nr_4 =	341		nr_4 =			
hr_4 =	45	mm	hr_4 =	45	mm	hr_4 =	45	mm	
P_4 =	43.30	m	P_4 =	43.30	m	P_4 =	35.93	m	
As_4 =	692.8	m^2	As_4 =	692.8	m^2	As_4 =	574.8	m^2	
Ah_4 =	0.0124	m^2	Ah_4 =	0.0185	m^2	Ah_4 =	0.0117	m^2	
Ad_4 =	0.7242	m^2	Ad_4 =	0.7226	m^2	Ad_4 =		m^2	
Fifth Evaporator Pass			**Fifth Evaporator Pass**			**Fifth Evaporator Pass**			
L_5 =	16	m	L_5 =	16	m	L_5 =	16	m	
D_5 =	0.0385	m	D_5 =	0.0385	m	D_5 =	0.0463	m	
n_5 =	245		n_5 =	243		n_5 =	170		
np_5 =	538		np_5 =	538		np_5 =	340		
dp_5 =	0.0045	m	dp_5 =	0.0045	m	dp_5 =	0.0055	m	
nr_5 =	232		nr_5 =	232		nr_5 =			
hr_5 =	45	mm	hr_5 =	45	mm	hr_5 =	45	mm	
P_5 =	29.63	m	P_5 =	29.39	m	P_5 =	24.73	m	
As_5 =	474.1	m^2	As_5 =	470.3	m^2	As_5 =	395.6	m^2	
Ah_5 =	0.0086	m^2	Ah_5 =	0.0086	m^2	Ah_5 =	0.0081	m^2	
Ad_5 =	0.5416	m^2	Ad_5 =	0.5379	m^2	Ad_5 =		m^2	

Sixth Evaporator Pass			Sixth Evaporator Pass			Sixth Evaporator Pass			
L_6 =	10	m	L_6 =	10	m	L_6 =	10	m	Length of evaporator tubes.
D_6 =	0.0463	m	D_6 =	0.0463	m	D_6 =	0.0463	m	Diameter of evaporator tubes.
n_6 =	144		n_6 =	144		n_6 =	135		Number of evaporator tubes.
np_6 =	328		np_6 =	328		np_6 =	280		Number of distribution plate holes
dp_6 =	0.006	m	dp_6 =	0.006	m	dp_6 =	0.006	m	Diameter of distribution plate holes
nr_6 =	144		nr_6 =	146		nr_6 =			Number of rising tubes
hr_6 =	75	mm	hr_6 =	75	mm	hr_6 =	75	mm	Height of rising tubes
P_6 =	20.95	m	P_6 =	20.95	m	P_6 =	19.64	m	Perimeter of evaporator tubes
As_6 =	209.5	m^2	As_6 =	209.5	m^2	As_6 =	196.4	m^2	Surface area of evaporator tubes
Ah_6 =	0.0093	m^2	Ah_6 =	0.0093	m^2	Ah_6 =	0.0082	m^2	Surface area of distribution plate holes
Ad_6 =	0.5743	m^2	Ad_6 =	0.5738	m^2	Ad_6 =		m^2	Surface area of distribution plate
Seventh Evaporator Pass			**Seventh Evaporator Pass**			**Seventh Evaporator Pass**			
L_7 =	10	m	L_7 =	10	m	L_7 =	10	m	
D_7 =	0.0463	m	D_7 =	0.0463	m	D_7 =	0.0463	m	
n_7 =	66		n_7 =	66		n_7 =	66		
np_7 =	156		np_7 =	156		np_7 =	156		
dp_7 =	0.007	m	dp_7 =	0.007	m	dp_7 =	0.008	m	
nr_7 =	66		nr_7 =	68		nr_7 =	51		
hr_7 =	75	mm	hr_7 =	75	mm	hr_7 =	75	mm	
P_7 =	9.60	m	P_7 =	9.60	m	P_7 =	9.60	m	
As_7 =	96.0	m^2	As_7 =	96.0	m^2	As_7 =	96.0	m^2	
Ah_7 =	0.0060	m^2	Ah_7 =	0.0060	m^2	Ah_7 =	0.0078	m^2	
Ad_7 =	0.2250	m^2	Ad_7 =	0.2245	m^2	Ad_7 =		m^2	
Eighth Evaporator Pass			**Eighth Evaporator Pass**			**Eighth Evaporator Pass**			
L_8 =	10	m	L_8 =	10	m	L_8 =	10	m	
D_8 =	0.0463	m	D_8 =	0.0463	m	D_8 =	0.0463	m	
n_8 =	43		n_8 =	43		n_8 =	44		
np_8 =	101		np_8 =	101		np_8 =	109		
dp_8 =	0.008	m	dp_8 =	0.008	m	dp_8 =	0.009	m	
nr_8 =	43		nr_8 =	43		nr_8 =	30		
hr_8 =	75	mm	hr_8 =	75	mm	hr_8 =	75	mm	
P_8 =	6.25	m	P_8 =	6.25	m	P_8 =	6.40	m	
As_8 =	62.5	m^2	As_8 =	62.5	m^2	As_8 =	64.0	m^2	
Ah_8 =	0.0051	m^2	Ah_8 =	0.0051	m^2	Ah_8 =	0.0069	m^2	
Ad_8 =	0.1466	m^2	Ad_8 =	0.1466	m^2	Ad_8 =		m^2	
Vacuum Condenser			**Vacuum Condenser**			**TVR Vacuum Condenser**			
L_c =	12	m	L_c =	12	m	L_c =	24	m	Length of condenser tubes.
n_c =	144		n_c =	144		n_c =	30		Number of condenser tubes.
D_c =	0.020	m	D_c =	0.020	m	D_c =	0.020	m	Diameter of condenser tubes.
Preheat condenser			**Preheat condenser**			**MVR Vacuum Condenser**			
L_c =	12	m	L_c =	12	m	L_c =	24	m	
n_c =	28		n_c =	28		n_c =	14		
D_c =	0.030	m	D_c =	0.030	m	D_c =	0.030	m	
Calandrias			**Calandrias**						
DE01 =	1.933	m	DE01 =	1.933	m				
DE02 =	1.933	m	DE02 =	1.933	m				
DE03 =	0.882	m	DE03 =	0.882	m				
DE04 =	0.713	m	DE04 =	0.713	m				
A_{tvrfe}	131	m^2							
A_{tvrfs}	194	m^2							

Inner Diameter of Rising tubes = 18 mm

Plate Heat Exchanger			
A_{mf} =	65.65	m^2	Heat transfer surface area for the first section.
A_{ms} =	72.15	m^2	Heat transfer surface area for the second section.
A_{mf} =	0.034	m^2	Cross sectional area of fluid flow, for milk in the first section.
A_{ms} =	0.034	m^2	Cross sectional area of fluid flow, for milk in the second section.
A_{cs} =	0.028	m^2	Cross sectional area of fluid flow, for condensate in the second section.
A_{wf} =	0.028	m^2	Cross sectional area of fluid flow, for water in the first section.
V_{mf} =	0.1479	m^3	Volume of milk in the first section.
V_{wf} =	0.1479	m^3	Volume of hot water in the first section.
V_{cs} =	0.1624	m^3	Volume of condensate in the second section.
V_{ms} =	0.1624	m^3	Volume of milk in the second section.

Powder 3 Evaporator A Online Computer Tagnames

Tag	Units	Description
P3PT1581	bar	TVR steam pressure,
P3PC1581SP	bar	TVR steam pressure setpoint,
P3PT1584	Bar	Preheat backpressure
P3PT1782		TVR vacuum condenser pressure
P3PC1584SP	Bar	Preheat backpressure setpoint,
P3PC1584OT	%	Preheat backpressure valve position,
P3FT1787FL	l/h	TVR filtered product flow.
P3FT1777	l/h	MVR product flow.
P3TE1381	DegC	MVR evaporator shell temperature.
P3TE1382	DegC	MVR evaporator effect temperature.
P3ST1339	rpm	MVR compressor speed.
P3VC1321DO	rpm	MVR turbine speed setpoint.
P3TE1283	DegC	First flash vessel temperature.
P3TE1781	DegC	TVR third effect temperature.
P3TE1785	DegC	Plate HX outlet condensate temperature.
P3DT1778	kg/m	MVR product density.
P3AV2851	B	Inlet air from 2850 damper.
P3PT2681	mmWC	Fines return system pressure.
P3TCA1781O	%	
P3TE1784	DegC	Plate HX outlet temperature.
P3TE1294	DegC	Second flash vessel temperature.
P3TE1295	DegC	Preheat condenser outlet temperature.
P3TE1296	DegC	MVR evaporator feed temperature.
P3TE2782	DegC	Shaking bed well mixed section inlet air temperature.
P3TE2784	DegC	Shaking bed drying section inlet air temperature.
P3DT1788	kg/m	TVR product density.
P3LT1181		Evaporator feed tank level.
P3TE1334	DegC	MVR compressor temperatures.
P3TE1335	DegC	MVR compressor temperatures.
P3TE1336	DegC	MVR compressor temperatures.
P3TE1337	DegC	MVR compressor temperatures.
P3FT1182	l/h	Evaporator feed flow.
P3FT2180F		
P3TE1284	DegC	First flash vessel temperature.
P3FT2781	m/s	Shaking bed well mixed section airflow.
P3FT2783	m/s	Shaking bed drying section airflow.
P3TE1482	DegC	MVR evaporator effect temperature.
P3TE1582	DegC	TVR second effect temperature.
P3TE1682	DegC	TVR third effect temperature.
P3PT2147	bar	Homo PLC homgenizer pressure.
P3PT2149	bar	Homo PLC homgenizer pressure.
P3PT2181	bar	
P3LT1881		Concentrate tank level
P3TE2786	DegC	Shaking bed cooling section inlet air temperature.
P3PT2183	bar	Dryer nozzle pressure.
P3TE2481	DegC	Dryer chamber outlet air temperature.
P3TC1785SPC		
P3TC1784SPC		Plate HX outlet temperature control setpoint.
P3TC1281SPC		DSI outer loop temperature setpoint.
P3TC1281OTC		DSI temperature controller setpoint.
P3TC1784OT		Plate HX outlet temperature control loop valve position.
P3TC1785OT		
P3FT1787	l/h	TVR product flow.
P3FT1777FL	l/h	MVR filtered product flow.
P3TC1482SP		MVR evaporator effect temperature control loop setpoint.
P3TC1482OT		MVR evaporator effect temperature control loop valve position.
P3TCA1781SC		TVR third effect temperature control loop setpoint.
P3FT1970	l/hr	
P3FT1971	l/hr	
P3TE2880	DegC	Dryer chamber inlet air temperature.
P3FT2785	m/s	Shaking bed cooling section airflow.
P3TE2182	DegC	
P3VS1249OP	EB	
P3FT0580	l/m	
P3FT0580Acl		
P3FT0580	Ydl	
P3TE1281	DegC	DSI temperature, after holding tubes, for outer control loop.
P3TE1280	DegC	DSI temperature, surface temperature, for inner control loop.
P3TC1280OTC		DSI temperature control valve position.
PC1581OT		
P3PC1581OP	%	TVR steam pressure valve position.
P3EI1321	amps	MVR compressor current drawn.